Abstract

This study investigates the effects of Z-pinning on the delamination performance in opening and shear loading modes in woven fabric reinforced / epoxy composite materials, as well as the effects of friction between specimen crack faces and the Z-pin failure mechanisms involved in mode II delamination.

Mode I and mode II delamination tests are carried out on Z-pinned unidirectional (UD) and woven laminates. Both UD and woven laminates exhibit enhanced delamination resistance and crack propagation stability through Z-pinning. The effects of various structural and Z-pin parameters on the mode I and mode II delamination behaviour are separately assessed.

The 4ENF testing configuration is deemed as the appropriate mode II configuration for the testing of Z-pinned laminates. A new basic friction rig is used to measure the friction coefficient between crack faces in woven laminates. An additional friction effect attributed to fibre architecture is identified. A specially designed delamination specimen is used to overcome the difficulty of accurately measuring crack propagation in Z-pinned woven fabric materials and aid data reduction using the available analytical methods.

The failure mechanisms involved in the mode II delamination of Z-pinned laminates have been investigated with the implementation of a new test. Z-pins fail under shear loading through a combination of resin crushing, laminate fibre breakage, pin shear, pin bending and pin pullout. The balance of the failure mechanisms is shown to be a function of the crack opening constraint, material type, stacking sequence, Z-pin angle and insertion depth to Z-pin diameter ratio.

Z-pin and material parameters influencing Z-pinning quality are identified, categorised and quantified. The importance of controlling Z-pin insertion depth is underlined and updated manufacturing procedures are proposed. Partial pinning appears as an advantageous alternative.

A reduction in in-plane stiffness and in-plane strength in UD and woven fabric composites is measured, whilst no significant change of in-plane shear stiffness of UD materials is observed. A reduction in the fibre volume fraction is the single most important parameter affecting the in-plane stiffness.

The performance of a Z-pinned sub-structural component is investigated. Enhanced loading carrying capacity and damage tolerance is achieved through Z-pinning.

Μι- Re+ Do+ Re+
Μόνος, οδηγάω μόνος, ατέλειωτος ο δρόμος, ατέλειωτες στροφές
La- Re+ Sol+ Re+
……

Μι- Re+ Do+ Re+
Φιλίες, οι παιδικές φιλίες, χαμένες παραλίες, χαμένη διαδρομή
La- Re+ Sol+ Re+

Μι- Re+ Do+ Re+
Στάση, κορίτσια πού'χω χάσει, πληγές πού'χω ξεχάσει, ανοίγουνε ξανά
La- Re+ Sol+ Re+

Μι- Re+ Do+ Re+
Βράδυα, τα εφηβικά μας βράδυα, τα πιο πικρά μας χάδια, πατρίδα μας γλυκειά
La- Re+ Sol+ Re+

……

Sol+ Re+ Mi- Re+ Do+
Μην ψάχνεις πια αλλού,
Fa+ Sol+ Re+
αφού το ξέρεις ήδη,
Sol+ Re+ Mi- Re+ Do+
μην ψάχνεις πια αλλού,
Fa+ Sol+ Re+
εδώ είναι το ταξίδι,
Mi- Re+ Do+
εδώ είναι το ταξίδι

……

«ΤΑΞΙΔΙ» - Ν.ΠΟΡΤΟΚΑΛΟΓΛΟΥ

Sol+ Do+
Μέσα σε σχολεία, σε πανεπιστήμια
Mi- Re+ Resus4/+/sus2
μέσα σε ωδεία, σε στρατούς και γυμναστήρια
Do+ Re+
πέρασαν χρόνια, άλλος μπήκα κι άλλος βγήκα,
Sol+ Do+ Re+
κι έχω την μόρφωση για όπλο και για προίκα
La-
κι ένσημο για το ΙΚΑ

……

Sol+ Mi-
Φεύγει η ζωή τελειώνει,
Sol+ Do+/Do+7
σα σεντόνι φανερώνει,
La- Re+
ό,τι αγαπούσα και το άφησα,
Sol+ Mi-
ό,τι μισούσα και το κράτησα,
Sol+ Mi-
Φεύγει η ζωή τελειώνει,
Sol+ Do+/Do+7
σα σεντόνι ξεδπλώνει,
La- Re+
τον εαυτό μου που τον ξέχασα,
Sol+ Do+
τον μέσα κόσμο μου που έχασα,
La-
με τέτοια πού'χω ψυχολογία,
La-
πώς θα βγώ στην συναυλία;

……

«ΑΔΙΕΞΟΔΟ» - Α.ΙΩΑΝΝΙΔΗΣ

To my parents,
for winning the hardest battle of all

Acknowledgements

I sincerely wish that all students can have the level of support and motivation from their supervisors that I have enjoyed. I would mostly like to thank my supervisor for guiding the focus of my research and for surrounding me with an international choice of expert and dedicated people to interact with and learn from. I can only say, I am proud to have been one of the children of Dr Ivana Partridge and I am deeply grateful to her for having being treated like one.

I am indebted to Denis Cartié for his continuous coaching on composite manufacture and science and for his honest friendship, as well as sharing his wide engineering knowledge and personal workshop (!). I want to express my gratitude to Prof. Antony Pickett for his willingness to offer advice and for inspiring research on a pivotal part of this thesis.

Thanks to Stephane Ferrari and Luca Barattoni for their important contribution to the experimental work. I would also like to thank all the members of technical staff and especially Tony Parker, Tony Scott, Andrew Dyer; not least of all, my friend Jim Hurley.

I am very thankful to Alex for constantly encouraging me to abuse his time and wisdom, and to Mihalis, without whom this thesis would not look any better than if it was written on the back of a cigarette pack. I am deeply grateful to all my friends for their support of all kinds. Last, thanks to the office team: Axel, Matt and Andrea.

Table of contents

List of figures

List of tables

Nomenclature

a	*Crack length*
a_0	*Initial crack length*
A	*Specimen cross section*
A_0	*Cross section prior to Z-pin insertion*
$A_{0.28}$, $A_{0.5}$	*Cross section of a 0.28mm and a 0.5mm diameter Z-pin respectively*
A_{PINS}	*Cross section after Z-pin insertion*
b	*Mode I or mode II specimen width*
B	*SENB specimen thickness*
c	*Thickness increase factor*
C	*Compliance*
C_0	*Initial compliance*
C_{CORR}	*Compliance correction*
d	*Areal Z-pin density*
$d_{0.28}$,$d_{0.5}$	*Areal density for 0.28mm and 0.5mm diameter Z-pins respectively*
D	*Z-pin diameter*
$D_{0.28}$,$D_{0.5}$	*Z-pin diameters, 0.28mm and 0.5mm respectively*
E	*Tensile modulus*
E_0	*Initial tensile modulus*
E_{11}	*Longitutinal modulus (relative to the loading axis)*
E_{22}	*Transverse modulus (relative to the loading axis)*
E_f	*Flexural modulus*
E_{MIS}	*Tensile modulus changed due to misalignment*
E_{PINS}	*Tensile modulus of Z-pinned laminate*
E_{THICK}	*Tensile modulus changed due to thickness increase*
f	*Calibration factor*
F	*Mode I correction factor*
G_{12}	*Shear modulus*
G_C	*Critical strain energy release rate for plastics*
G_{IC}	*Critical strain energy release rate (or delamination toughness) in mode I for fibre reinforces plastics*
G_{IIC}	*Critical strain energy release rate (or delamination toughness) in*

	mode II for fibre reinforces plastics respectively
h	*Mode I or mode II half laminate thickness*
H_1, H_2	*Dimensions of reinforced (Z-pinned) area*
j	*Exponential factor*
J	*Constant*
K_{TOTAL}	*Equivalent spring stiffness*
K_1, K_2	*Spring stiffness for two different springs (spring 1 and spring 2)*
l_1, l_2	*Mode I loading tab dimensions*
L	*Lower half-span of the 4ENF configuration*
L_P	*Embedded Z-pin length (or depth)*
m	*Mode II compliance calibration slope*
m	*Misalignment factor*
n	*Exponential factor*
N	*Mode I correction factor*
P	*Load*
s	*Z-pin spacing*
$s_{0.28}$,$s_{0.5}$	*Spacing between 0.28mm and 0.5mm diameter Z-pins respectively*
W	*SENB specimen width*
x	*Corrected (or corresponding to artificial slope) displacement*
S_L ,S_R	*Characteristic 4ENF configuration dimensions*
V_f	*Fibre volume fraction*
$V_{f,PINS}$	*Fibre volume fraction for Z-pinned laminates*
α	*Slope*
α'	*Artificial slope*
|Δ|	*Crack length correction*
Δ_I ,Δ_{II}	*Compliance correction for the DCB and ELS tests respectively*
δ	*Displacement*
ε_{xy}	*Shear strain*
ε_{45} ,ε_{-45}	*Strain measured by strain gauges at 45° and -45° angles relative to the loading direction*
θ_x	*In-plane misalignment angle*
θ_t	*Through-thickness misalignment angle*
μ	*Coefficient of friction in the crack wake*
μ	*Coefficient of friction measured using the friction rig*

μ'	*Coefficient of friction between specimen and fixture*
ρ	*Cross section Z-pin density*
σ_{xy}	*Shear stress*
τ_F	*Friction stress*
φ	*Energy calibration factor*

Abbreviations

ACK limit	*Aveston, Cooper and Kelly limit*
BVID	*Barely Visible Impact Damage*
CAI	*Compression After Impact*
CCM	*Compliance Calibration Method*
CFRP	*Carbon Fibre Reinforced Plastics*
DCB	*Double Cantilever Beam*
ENF	*End Notched Flexure (3pt bending)*
4ENF	*4point End Notched Flexure (4pt bending)*
SENF	*Stabilised End Notched Flexure (3pt bending)*
ELS	*End Loaded Split*
EPFM	*Elasto-Plastic Fracture Mechanics*
LEFM	*Linear Elastic Fracture Mechanics*
LVDT	*Linear Variable Displacement Transducer*
NCF	*Non-Crimp Fabric*
NL point	*Non-Linear point*
OHT	*Open-Hole Tension*
SEM	*Scanning Electron Microscopy*
SENB	*Single Edge Notch Bend*
SERR	*Strain Energy Release Rate*
TTR	*Through-(the-)Thickness Reinforcement*
UD	*Uni-Directional*
UTS	*Ultimate Tensile Strength*
ZPC	*Z-Pinned Control specimens*

1 Introduction

The use of fibre reinforced polymer composites is encountered in numerous applications. Carbon fibre reinforced polymer composites (CFRP) are popular with the most demanding of them, due to their high in-plane stiffness to weight ratio (aircraft, aerospace, racecars, marine), high strength (F1 tubs, sailing masts), high energy absorption capacity (vehicle crash structures), chemical resistance (chemical industry, surgical implants), thermal and low wear properties (aerospace, brakes, bearings), dimensional stability (aerospace), excellent fatigue characteristics (rotating shafts) and their complex forming potential [1-5]. Despite the wide range of manufacturing techniques now available for composites, for most of the applications of carbon fibre laminates high grade prepreg lay-up is used, in order to achieve the highest possible fibre volume content. Most composite material applications are sized by terms of stiffness and strength, both directly related to the fibre volume content [6,7]. An inherent drawback of laminated composites is the relatively low mechanical strength in the through-the-thickness direction, determined by the strength of the polymer matrix and/or of the fibre–matrix interface. Thus, their application in damage critical lightweight structures or components supporting out-of-plane loads is restricted. A common form of damage in these materials is delamination cracking, which can degrade the in-plane mechanical properties, especially compressive strength, as well as fatigue performance. There has been significant effort in constructing composites with a three-dimensional fibre architecture, such as 3D interlocked weaves. However, part designers still prefer laminated construction, especially in an integrally-stiffened co-cured form, because of the lower fabrication and assembly complexity and costs.

1.1 Mechanical response of composites

Composite materials and in particular CFRP are highly orthotropic. Their in-plane shear strength and especially their out-of-plane shear strength are only a fraction of their in-

plane principal strengths. The low out-of-plane strength is due to the lack of fibre reinforcement in the thickness direction. The properties of the matrix dominate the response of the composite in the case of out-of-plane loading, as well as in some in-plane loading cases. The importance and role of the matrix in composite materials is well-documented [8,9]. In particular, delamination toughness (or critical strain energy release rate G) is a matrix dominated property, which in turn governs the response to out-of-plane loading. Most probable locations for the presence of out-of-plane loading can be laminate free edges, hole edges, ply-drops, voids, resin poor regions, bonded or bolted joints and most significantly impact sites [3,9-13].

Impact, depending on the speed of the projectile and the peak load generated, can result in either penetration of the laminate or in delaminations. Penetration occurs at high speed impact and is related to matrix density and modulus [12]. A typical projectile speed for penetration is 20m/s. Lower speed impact produces delaminations which are hidden inside the laminate. This kind of damage is usually referred to as barely visible impact damage (BVID). The delaminated area is a function of the impact energy and laminate stiffness, therefore of the laminate thickness and fibre properties. The location for delamination initiation is typically where the shear stress is maximum, namely at the centre of the laminate in the thickness direction. There is a relation of impact force to the delamination resistance of the composite in shear, providing an estimate to the initiation of delamination [12,13].

Delaminations due to impact can reduce compression after impact strength (CAI) up to 70% for a thermoset matrix composite [12,13]. Delaminations in a laminate subjected to compression loading allow local buckling of the separated sub-laminates to occur and turn compression from a fibre dominated property to one governed by delamination resistance in the crack opening mode [9,10]. Therefore, CAI strength, along with in-plane shear strength, is affected by the properties of the matrix.

Carbon fibre composites containing no damage exhibit excellent fatigue performance under in-plane loading. For laminates containing delamination damage, fatigue crack

growth has been shown to be related to ΔG, the strain energy release rate range [3,9]. The Paris equation expresses the relation between the crack growth rate and ΔG:

$$\frac{da}{dN} = J \cdot (\Delta G)^j \tag{1-1}$$

The exponent j is large (about 5-10 [3,9]), which renders fatigue growth fast. The mechanisms of fatigue degradation are well documented, but there has been little research work in determining the criteria for fatigue crack growth thresholds, especially from impact damage, which is the important parameter [3,9]. Delamination crack growth is the major damage growth mechanism in practice. Subsequently, the susceptibility of laminated composites to delamination affects the design envelope of structural components.

1.2 Crack management in composite structures

The wide use of composite materials in structural applications has led to the creation or amendment of design regulations to accommodate these new materials. Examples of such regulations are the safety regulations of Formula 1 grand prix racing, or the ones for the certification of commercial aeroplanes. The latter are indicative of the level of confidence displayed in the design of structures with composite materials and the level up to which composite materials are exploited.

Assembly design of a structural component of a commercial aircraft such as a stabiliser or an empennage requires the presence of bonded and, more significantly, bolted joints [5,14]. Necessary changes of thickness translate into ply-drops. Frequent servicing, supplies and fuel as well as cargo loading result in frequent low energy impact loading of the airplane panels. Moving vehicles as well as tools dropping from a height of 3-4 meters involve impact speeds certainly less than 20m/s, resulting in low impact loading with delamination damage as a consequence. Airframe structures are therefore subjected to all kinds of out-of-plane loads during service and are very likely to be damaged.

More significantly, most impact damage is induced to upper parts of structures, being subjected to aerodynamic compressive loads, while most bolt holes reside in the lower part of such structures, being subjected to aerodynamic tension loads. All parts are inspected frequently, but at such a frequency as to keep the inspection from becoming uneconomical. Most inspection is visual inspection. The visible impact indentation threshold is considered to be 1.25mm [15] large enough to allow considerable amount of BVID to remain undetected. With the high rate of fatigue degradation and the large CAI strength reduction of delaminated composites, aircraft components are required to go through a strict certification procedure [14-17]. Since the presence of delamination is very likely, a no growth approach is adopted. The result of this is that the allowed design strain is set to 0.4%, significantly lower than the undamaged laminate strain potential.

1.3 Current practices

Improving the delamination resistance of CFRP is of high importance, in order to exploit fully the remaining advantageous material properties of CFRP. A probable solution is the use of a toughened resin system, as in the case of the Boeing 777 [14].

The use of textiles is also attractive. Use of quasi-laminar textiles as a starting point, such as a 2D woven fibre architecture fabric, is mostly considered as only minor changes need to be made to the manufacturing procedure. Use of unidirectional tape laminate material remains widespread, since woven architectures usually posses fractionally inferior stiffness and strength properties [9,18]. On the other hand, damage or impact tolerance is superior, as well as strain to failure and work of fracture [9,18]. Handling and manufacturing is usually also easier and there is more potential for integrating joints in the design or the use of robotic manufacture. Depending on the level up to which each textile technology has been developed, relative cost can be attractive or not.

Among 2D fibre architectures incorporating equal properties in the two directions, 2 by 2 twill woven fabric composites seem to present the best compromise in terms of delamination resistance, shear strength and stiffness [18].

The most popular new way to address the problem of delamination has become the adoption of through the thickness reinforcing (TTR) techniques. The preferred layered manufacture remains, along with the availability of fibres taking up through thickness stresses. One such TTR technique, on which this study focuses, is Z-Fiber® pinning, or simply Z-pinning. The improvement of TTR techniques on delamination resistance is substantial.

All current TTR solutions are described in section *2.3*. It will be portrayed that there is an additional effect of the implementation of these techniques on the in-plane properties. Since in-plane properties seem to be currently the primary aspect of material choice, investigation of this effect is important.

1.4 Objectives of this study

Previous studies on Z-pinning have investigated the beneficial effects of the technique on the delamination toughness of unidirectional materials. An assessment of impact performance and CAI strength has also been attempted [19,20]. Significant analytical modelling work is currently under way by international collaborators, also presented in section *2.6*.

This study presents an extension of current knowledge on the delamination performance in opening and shear modes and the mechanics of Z-pining on woven materials, as well as addressing the issue of in-plane property degradation. A better understanding of all factors and mechanisms involved in mode II delamination is being sought. Additionally, Z-pinning quality assessment will be addressed, as well as the application of the attained knowledge to the performance of simple Z-pinned structures.

1.5 Thesis structure

Chapter 1 reviews the problems associated with delamination and the load cases under which delamination occurs in structures. Enhanced delamination control can raise the design strain allowables.

Chapter 2 presents a review of delamination control techniques found in literature; both effects on delamination resistance and corresponding failure mechanisms are described. The influence of these techniques on the in-plane properties and failure mechanisms is also portrayed.

Chapter 3 describes the materials and the manufacturing procedures used in this study. A further assessment of the influence of parameters related to Z-pinning on the quality of the manufactured laminates is carried out and updated or alternative procedures and techniques are suggested. The effects of Z-pin density, Z-pin diameter, Z-pin angle and insertion depth are quantified and their effects on the meso-structure of the laminates are described.

Chapter 4 includes the testing procedure and results regarding mode I delamination. The testing standard and the Z-pinned specimen layout are described. The delamination toughness and microstructure of the M21 and M36 resin systems are quantified and examined. The effects of structural and Z-pinning parameters on the delamination toughness are individually assessed. The increase in delamination toughness as well as in the stability of crack propagation imposed by Z-pinning to UD laminates is also identified in woven fabric composites.

Chapter 5 investigates the effect of Z-pinning on delamination behaviour under mode II loading. The suitability of the available mode II testing configurations to Z-pinned laminates is evaluated. Critical issues concerning the measurement of mode II delamination toughness are examined; namely, the effect of friction between crack faces and the effect of crack length measurement on the application of data reduction methods on Z-pinned woven fabric laminates. A specimen specifically designed to aid the data

reduction method and the subsequent correction procedure is presented. The failure mechanisms and energy absorption potential of Z-pins under shear loading in UD and woven fabric materials are investigated using a new Z-pin shear test. The effects of structural and Z-pinning parameters on the delamination toughness are individually assessed.

The effect of Z-pinning on the tensile and in-plane shear moduli, as well as tensile strength is investigated in Chapter 6. The performance of Z-pinned UD and woven fabric laminates is compared. The source of the measured degradation is sought in the alteration of the meso-structure of the laminates imposed by Z-pin insertion

Chapter 7 investigates the potential of transferring the beneficial attributes of Z-pinning from coupon level to sub-structural level by testing a sub-structural component. Effects of Z-pin location and Z-pin parameters on the load carrying capacity, damage tolerance and failure mode of the component are examined.

Chapter 8 summarises the areas studied and further discusses selected issues. Chapter 9 states the important conclusions drawn and suggests issues on which work needs to continue.

2 Literature review on delamination control

The high risk of delamination cracking in composites either compromises the exploitation level of their use in engineering applications, or limits their application envelope to non primary structural components. The importance of improving the delamination resistance of CFRPs, as well as understanding the mechanisms behind delamination cracking, has been highlighted in chapter 1.

Delamination resistance can be partitioned into two main categories: (a) resistance to initiation, which represents the critical value of the interlaminar fracture toughness of a composite material to resist the onset of growth of a defect, and (b) resistance to propagation, which involves the capability of the material to arrest an existing crack. The role and importance of the matrix in the delamination resistance capacity of composites has been underlined. Firstly, the matrix based methods of improving delamination resistance will be presented. An overview of through-the-thickness reinforcement (TTR) methods follows, accompanied by a description of the mechanisms of fracture. Material effects as well as the effects of in-plane properties are dealt with next. Analytical and numerical modelling work is presented last. However, some very basic considerations of fracture mechanics need to be described initially.

2.1 Linear elastic fracture mechanics

Fracture mechanics is a macro theory that defines parameters which characterise failure over regimes of known size [21], following the assumption that all bodies contain flaws or cracks. Fracture mechanics studies the response of a material containing such a flaw or crack of a known length α. According to the response of the material, a fundamental division of fracture mechanics into linear elastic (LEFM) and elastic-plastic (EPFM) is made. EPFM is used when the material exhibits a high degree of plasticity at the crack tip zone, invalidating description by linear elastic fracture mechanics. The more general

J-integral method is then applied to characterise fracture. If the behaviour of the material is linear, elastic and homogeneous, even when large deflections produce a non-linear load-deflection curve [21], then LEFM can be applied. A good measure of the applicability of LEFM is a simple criterion described in the testing protocols [22,23]; after acquiring the load-deflection curve of the material, a new curve can be created by increasing the initial compliance of the material by 5% (Figure 2-1). If the ratio $P_{Max}/P_{5\%}$ is lower than 1.1, then LEFM can be applied. Fibre reinforced composite materials comply with LEFM conditions, being brittle in character, with small crack tip damage zones in comparison with other specimen dimensions.

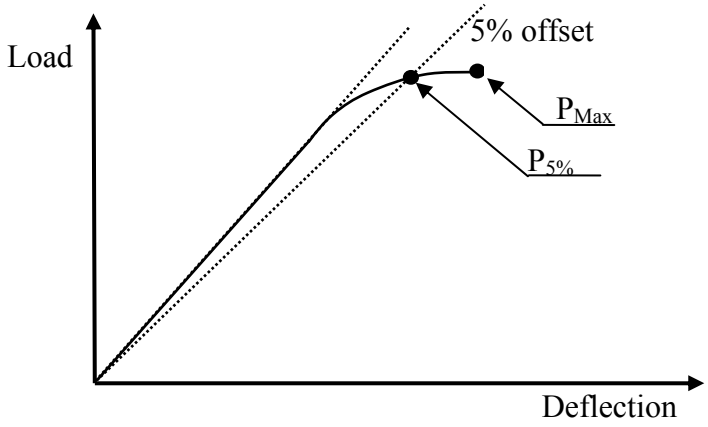

Figure 2-1: *Schematic representation of the construction of the 5% offset compliance curve based on the initial load-deflection curve, according to ISO 15024 [22].*

There are two LEFM approaches. The first is the elastic stress intensity field approach originally developed by Irwin, which uses the stress intensity factor K to describe fracture. Developed initially for isotropic materials, the solution of stress-field problems in anisotropic media, involves the use of complex analytic function theory, and can be very difficult [21]. The second is the global energy balance approach based on work by Griffith, which uses the strain energy release rate (SERR) G to describe fracture, assuming that crack growth can be characterised in terms of energy per unit area necessary to create a new surface area. This approach results in surprisingly simple solutions and can be a very useful tool for design purposes [21]. Delamination growth occurs when the SERR exceeds a certain critical value, G_C, usually referred to as delamination toughness of the material. G_C can be related to K_C, the critical value of the

stress intensity factor for delamination growth, depending on the assumed stress conditions [21,24].

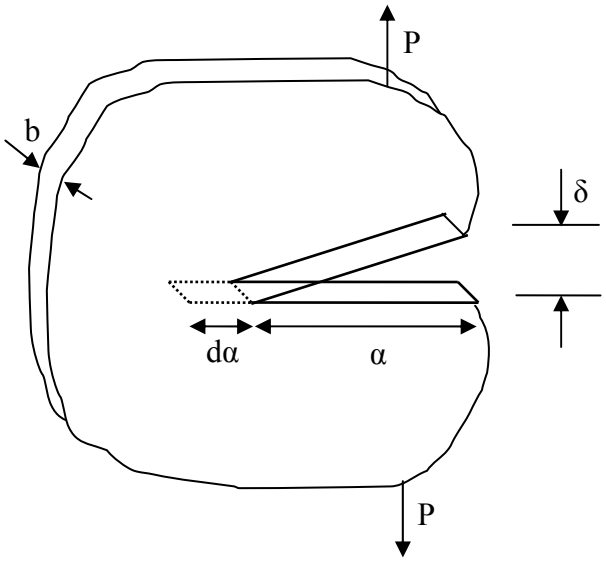

Figure 2-2: *General loading on a cracked body, as in [21]*

Considering the material of Figure 2-2, with a crack length α, a uniform thickness b, undergoing self-similar propagation with a crack speed of $\dot{\alpha}$, under an applied load P, the delamination toughness G_C is defined as the energy required for the creation of the fracture area $dA = b \cdot d\alpha$. By adopting the static LEFM assumptions (brittle fracture, small damage zones in comparison with other dimensions, all energy dissipation is embodied in G) and solving the energy balance equation, the fundamental expression for the strain energy release rate can be obtained:

$$G_C = \frac{P^2}{2b} \cdot \frac{dC}{d\alpha} \tag{2-1}$$

,where C is the compliance, defined as:

$$C = \frac{\delta}{P} \tag{2-2}$$

G_C is considered to be a material property, independent of specimen geometry. The specimen geometry proposed in test protocols is optimised to ensure consistency with LEFM conditions. Specimen dimensions ensure reduced deflections and edge effects, while the initial defect, simulating the crack, is well defined to produce reproducible and conservative data [20,23]. Delamination toughness G_C depends only on the mode

of fracture, which in turn is defined by the type of loading the crack tip is subjected to. Figure 2-3 depicts the three fundamental modes of fracture. Mode I is the crack opening mode, where a tensile stress is applied in the direction normal to the plane of crack propagation. Mode II is the crack shear mode, where a shear stress is applied in the plane of crack propagation, but normal to the crack tip. Mode III is the tearing mode, where a shear stress is applied parallel to the crack tip. There are, subsequently, three critical SERRs: G_{IC}, G_{IIC}, G_{IIIC}.

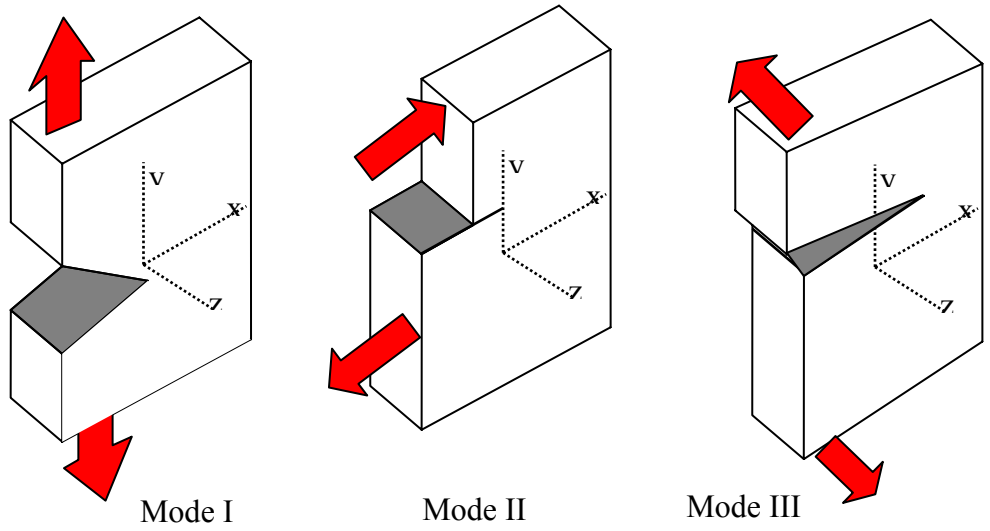

Figure 2-3: *The three fundamental modes of fracture*

Fracture in structures occurs under a triaxial state of stress, and the mode of fracture is seldom a pure one. However, it can be decomposed into the three fundamental modes, and the behaviour under the actual stress state can be characterised by the combination of the performance in the three modes.

Delamination testing protocols describe methods with which each mode of fracture can be isolated and the delamination toughness can be measured. Further details on delamination testing will be presented in sections *4.1* and *5.1*.

2.2 Matrix based techniques

The characteristic delamination toughness for a material in each fracture mode is defined by the resin toughness, interfacial strength between fibre and resin and the fibre properties. The first two are most essential in determining interlaminar fracture toughness. Matrix based techniques enhance resistance to crack initiation. Moreover, the use of a matrix based technique does not prohibit the additional application of a TTR technique for further delamination toughness enhancement.

2.2.1 Toughened resins

Due to the importance of matrix toughness in interlaminar failure of composites, the initial approach to tougher composites was to use toughened resin matrices. The amount of effort put into that approach and the findings are reviewed in [8,23,25] in detail. Popular ways to toughen resins are to modify the resin with a rubber or a thermoplastic or to use a thermoplastic matrix. The fibre/matrix interface can be in turn improved by coating the fibres with rubber or ductile plastic.

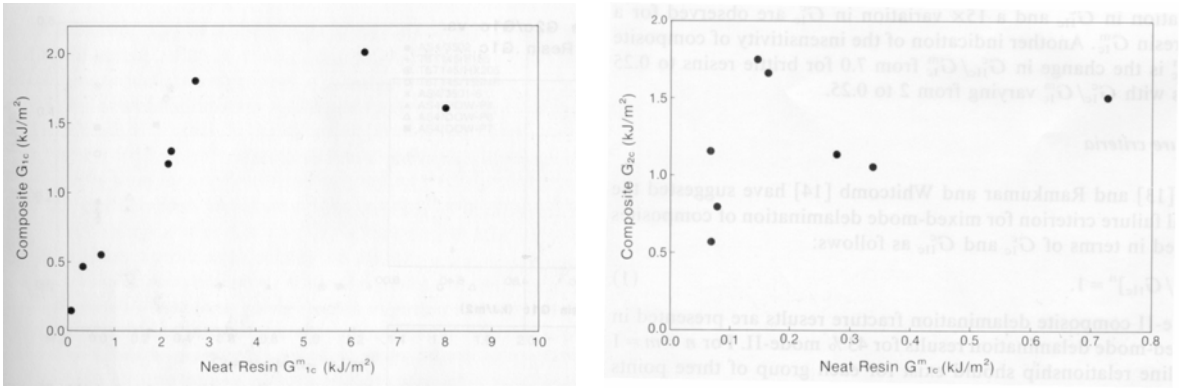

(a) *(b)*

Figure 2-4: *Mode I (G_{IC}) (a) and mode II (G_{IIC}) (b) delamination fracture toughness for a variety of composites, presented as a function of the respective neat resin toughness (GIm), after [8].*

Figure 2-4 depicts the trends of delamination toughness of composites with toughened resin systems for both fracture modes, G_{IC} and G_{IIC}, relative to the mode I delamination

toughness of the neat resin system, G_{Im}. The influence of resin toughness is different for mode I and II fracture of composites. It seems to be particular significant for mode I when the neat resin toughness is in the range of 0.1 to 0.4 kJ/m^2, moderately significant for G_{IC} in the range of 0.4 to 2 kJ/m^2, and fairly insensitive to neat resin toughness greater than 2 kJ/m^2. The resistance to mode II delamination is generally less sensitive; a 100 change in neat resin toughness would result in a 4 variation in G_{IIC} and a 15 variation in G_{IC}. Another indication of insensitivity of G_{IIC} to G_{Im} is the change in the ratio G_{IIC}/G_{Im} from 7 for brittle resins to 0.25 for very ductile resins with G_{IIC}/G_{Im} ranging from 2 to 0.25 [8].

The mechanisms of transferring resin system toughness into composite material toughness are complicated. The parameters affecting this transfer are many. The thermal history of composite and neat resin is different as the presence of fibres affect thermal conductivity. There are also residual stresses after cure. Moreover, the dispersion of any toughening thermoplastic particles with sizes comparable to fibre size can be different in the composite. A third phase in a region of 0.1μm to 3μm [23,26] around the fibres exists, with morphological and chemical features different to both the bulk resin and fibres. The extent of this interphase may be more pronounced for multiphase matrix composites [23].

Under any given loading, the stress field around the crack tip differs significantly between composite and neat resin. Crack tip strain to failure is much greater in the composite than one would infer from a neat resin tensile test. The stress field for mode I in a composite with orthotropic reinforcement decays more slowly ahead of the crack tip, while reducing peak stresses at the crack tip, compared to isotropic reinforcement. The strain field is long and narrow for both mode I and mode II and different to the field of the neat resin, depicted in Figure 2-5 [8].

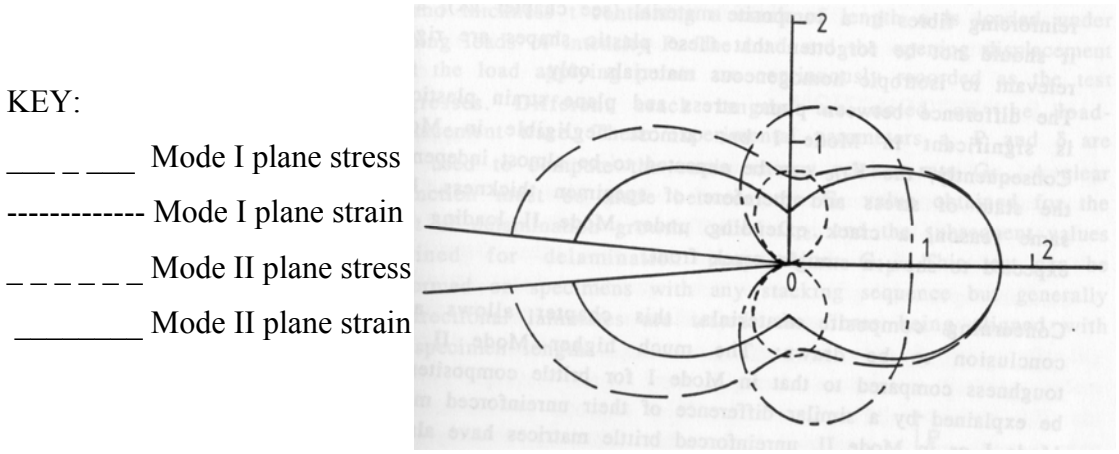

Figure 2-5: *Extents of plastic zones at the crack tip in a homogeneous and isotropic material (neat resin), after [25]*

For brittle resin systems the mode I plastic zone volume in the composite is close to 3.5 times larger than in the neat resin. Fibre induced stress concentration in this cases increases the amount of yielding of the resin [27]. The corrugated roof morphology of the fracture surface gives an actual fracture surface area 57% greater to the flat surface area of the neat resin. Furthermore, interfacial failures produce some fibre bridging behind the crack tip which reduce crack tip stresses and enhance toughness in propagation (Figure 2-6). All this explains how G_{IC} tends to be higher than G_{Im} for values up to 0.2 kJ/m^2 for the latter [8].

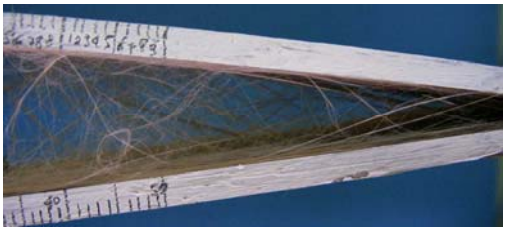

Figure 2-6: *Extensive fibre bridging in a failed glass-fibre/epoxy specimen under mode I loading.*

For ductile resin systems, the constraint imposed by fibre spacing on the size of the damage zone is most important. A large plastic zone will result in redistribution of the stresses away from the crack tip, while sufficient crack tip deformation would allow its blunting with beneficial effects. An increase of G_{IC} has been found with reducing the fibre volume fraction in ductile resin systems [8].

Mode II interlaminar fracture is associated with significant resin microcracking ahead of the crack tip. The decay of the stress field is much more gradual, and the sigmoidal shaped microcracking that develops ahead of the crack tip results in local softening and load redistribution of stresses, analogous to the effect of large plastic deformation. It is not surprising then that, even for brittle resin systems, G_{IIC} is large.

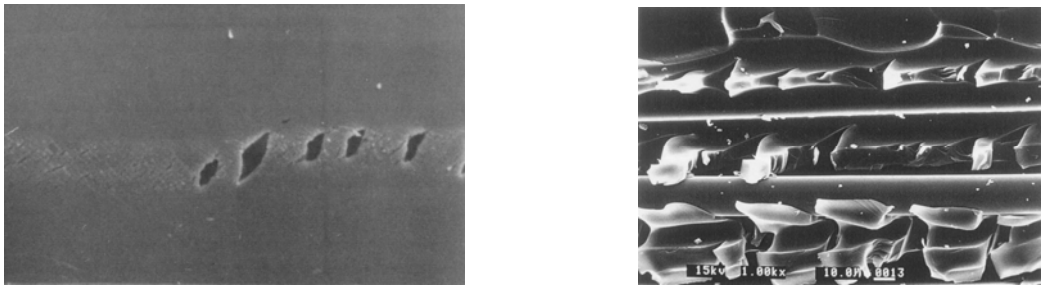

Figure 2-7: *Formation of microcracks in mode II [25], and typical example of corresponding fracture surface [23].*

The formation mechanism of microcracks, also called hackles or cusps, has been modelled with success by Turmel [23]. The model predicts quite accurately the difference in delamination toughness between mode I and mode II, due to the different cracking geometry.

Using the experimentally measured mode I delamination toughness and the value of the parameters from observations of a mode II surface, the delamination toughness in any mixed I/II mode ratio up to pure mode II can be predicted, in good agreement with experimental data. An easier way is to use the experimentally measured delamination toughness for both mode I and mode II and fit the values of these parameters to the data. The estimated values of these parameters turn out to be in qualitative agreement with fracture surface observations. In any case, the effect of the fracture surface discrepancy between mode I and mode II is modelled accurately. The model applies to thermoset based matrices and predicts initiation only, since no fibre bridging is assumed [23].

2.2.2 Interleaving

Having identified the constraining effect of the fibres on the development of large plastic deformation zones in toughened resin systems, hindering the full exploitation of the matrix toughness, interleaving is the logical development as a technique to improve delamination toughness. With rubber toughened resin systems suffering from compromised hot-wet performance and tough thermoplastics enduring lower operational temperatures and requiring different production technologies, interleaving is a sensible alternative [24,28,29].

Interleaving is the insertion of a tough layer of material in between prepreg plies in the lay up stage. The material can be an adhesive film or the self-same matrix resin. A varying chemistry of the interleaf has been investigated, as well as nylon particle interleaving, with particles attributing to the toughness mainly by acting as spacers between plies to create the required resin rich regions [24]. The thickness of the inserted material is determined by the potential height of the plastic zone of the interleaf material. The optimal thickness is considered to be equal to the minimum thickness required to allow the full development of this plastic zone (Figure 2-5). Any additional increase in thickness does not offer any benefits in delamination resistance; on the contrary, a reduction has been observed [28].

The benefits in delamination resistance can be up to a 10-fold increase in G_{IC} and a 7-fold increase in G_{IIC} [28]. With the appropriate thickness, estimated by application of a modified von Mises yield criterion or Irwin's plastic zone model [24,30,31], the toughness of the resin can be transferred fully to the composite. Although such a prediction matches the thickness where maximum toughness is observed experimentally, the actual maximum plastic zone heights in the composite material occur at greater thicknesses than predicted. That indicates that the height of the plastic zone alone does not govern fracture resistance [31].

Crack propagation can both be cohesive or interfacial, depending mainly on the loading mode [24,29,31]. Mode II or mixed mode delamination seldom is self-similar. As

propagation takes place in a thick isotropic layer, cracks tend to re-orient themselves to local mode I fracture, irrespective of the type of loading. Thermoplastic interleaves usually exhibit interfacial debonding in mode II and some fibre bridging in mode I. Thermoset interleaves exhibit microcracking ahead of the crack tip and elongated plastic zones in mode II. Delamination under mixed mode is most common. The understanding of mixed mode I/II fracture in interleaved composites is important and suitable criteria have been investigated for predicting delamination behaviour [24]. The elastic decomposition of the total fracture energy into mode I and mode II components can be misleading for interleaved composites [24].

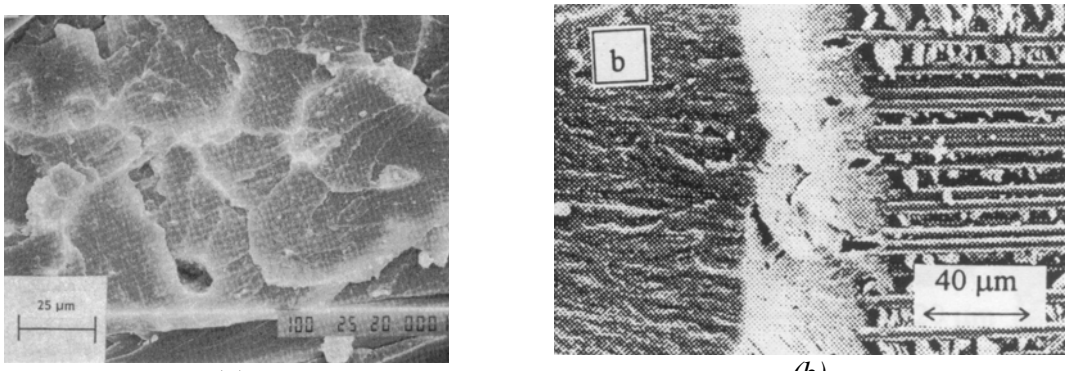

(a) *(b)*

Figure 2-8: *Crack planes of failed specimens. (a) Cohesive crack propagation in mode I [28] and (b) interfacial crack propagation in mode II starting from precrack [24].*

The thickness of interleaves required to toughen composites subjected to high mode II ratios is greater [28,30,31]. Small increases in interleaf thickness result in rapid improvements in delamination resistance. However, optimum thicknesses for mode II delamination range between 0.1mm and 0.7mm [28,30], quite large compared to those for mode I, ranging from 50µm to 150µm [24,28,31,32].

Finally, interleaving does not affect crack growth stability; the behaviour of crack growth is the same as that of the original matrix resin with the original thickness before interleaf insertion.

2.3 TTR techniques

In search of methods to arrest an existing crack in laminated composites, TTR techniques have been developed. The importance of resistance to crack initiation lies with the fact that composites tend to fail catastrophically thereafter, particularly under fatigue loading conditions. However, the newer concept of designing components under the presumption of pre-existing cracks or flaws and the difficulty of arresting a existing crack renders resistance to propagation more significant compared to resistance to initiation.

Through-the-thickness reinforcement (TTR) consists of the insertion of some kind of fibre reinforcement in the thickness direction of the laminated composite. Stitching (as well as Tufting) and Z-Pinning are the current existing methods. TTR bridges delaminations and shields their crack tips from the applied load so reducing the crack driving force. Crack growth can be rendered stable, which is a critical feature in damage tolerant design, ultimate strength can be increased and notch and impact sensitivity reduced [33-35]. TTR techniques can contain damage by completely arresting a propagating crack. TTR is currently the most promising method of confronting the problem of delamination in laminated composites.

2.3.1 Stitching

Stitching involves the insertion of a dry fibre (carbon, kevlar or glass) into the laminate and the formation of a loop or an interlocking pattern with another thread (Figure 2-9). This requires a two-sided access and therefore special tooling. The manufacturing advance most beneficial to stitching has been the introduction of resin transfer processes, which allow dry stitched preforms to be infused with resin. This enhances process speed and allows stitching through thicker material. It also reduces damage to the laminate fibres, considering the fact that a large diameter needle (2mm) is continuously driven through the laminate with considerable force [18,20,36]. The use of

stitching with prepreg materials is limited, as the viscous resin will foul up the needle making further insertions difficult.

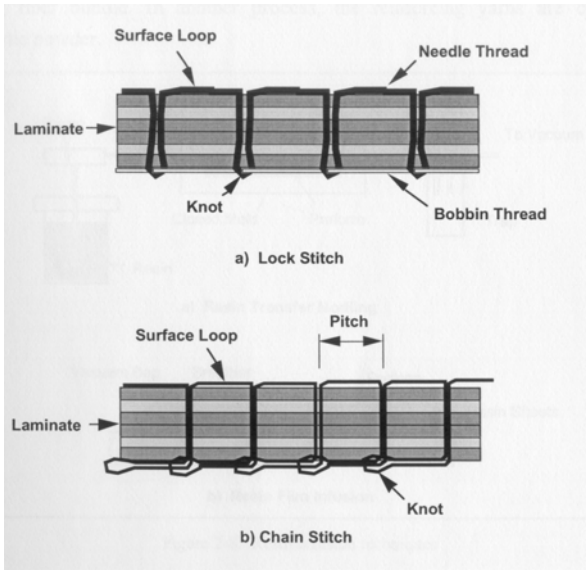

Figure 2-9: *Types of stitching used for through-the-thickness reinforcement, after [18].*

Stitching is also used to aid fabrication, by joining dry fibre preforms, allowing them to be handled with ease and without damage prior to liquid moulding. Therefore, like the use of textiles, it holds potential for process automation. Additionally, it compacts fibre preforms closer to the final desired thickness, ensuring high fibre volume fraction. Stitching holds considerable promise as a low-cost joining technique and as a mechanical fastener replacement. Stitching that attributes satisfactory damage tolerance, usually contributes in average around 2% of the total areal weight of the completed fabric [18].

Tufting uses a similar insertion technique to stitching, but it is a one-side access process. It still requires special tooling. A needle is used to push the yarn (the reinforcing fibre) through the laminate as well as through a form tool described as an ‘elastic foam’. The frictional forces, generated in the laminate and the foam, keep the yarn in the laminate, while the needle is allowed to withdraw.

Stitching is characterised mainly by the stitch density and type. Other parameters can be the linear density of the reinforcing fibre (yarn), the pitch and the row spacing. Yarn

thickness is specified either by dernier or yarn number. *Dernier* is the mass in grams of 9000 meters of yarn. *Yarn number* is the length in yards of 1 lb of yarn. *Pitch* is the spacing between insertion points. The stitching pattern is summarised by: (number of stitches per inch) (spacing between rows). For example, 8 1/4 means a density of 32 stitches per square inch (spsi), with a pitch of 1/8 of an inch and row spacing of ¼ of an inch. Most commonly used types are the lock stitch, the modified lock stitch and the chain stitch (Figure 2-9). One last parameter is the stitch direction relative to load direction.

Stitching improves interlaminar fracture toughness and impact damage tolerance dramatically [37-40]. The effects of stitching in composites are extensively reviewed in [36,38]. Increase of the crack-opening (mode I) strain energy for initiation and crack growth up to 80 times and 15.7 times respectively, have been reported for CFRP laminates [38,42]. The shear (mode II) critical strain energy release rate can improve by up to a factor of 15 [38]. The translaminar Young's modulus is also positively affected [38]. Significant improvements are reported in post-impact mechanical properties, at a wide range of impact speeds, particularly in compression-after-impact (CAI) strength [38,43].

It is worth noting that stitching of Glass or Kevlar fibre reinforced plastics (GFRP, KFRP) does not provide similar improvements in either mode II loading or in damage resistance and tolerance. On the contrary, degradation has been observed in some cases. It seems that at high stitch densities degradation in post-impact mechanical properties is more likely to occur [38].

2.3.2 Z-Fiber® pinning

Z-Pinning is the insertion of short rods (pins) orthogonally to the plane of the composite plies during the manufacturing process, before the resin matrix is cured, effectively pinning the individual layers together. The Z-pins are driven through the uncured prepreg in a two stage process, which involves the use of a specialised ultrasonic

insertion gun and a sequential removal of the collapsible foam (the 'preform'), in which they are held (Figure 2-10). The foam consists of two different densities, with the high density bottom part providing lateral support to the pins during insertion and preventing them from buckling, while the lower density upper part collapses under the pressure of the gun. Subsequently, the thickness of the lower density foam in the preform is required to be slightly bigger than the thickness of the laminate under process.

The most commonly used fibres are pultruded from bismaleimide resin impregnated carbon tows (T300/BMI), although a choice of materials is available (glass, quartz, boron, silicon carbide, steel, titanium and aluminium). Common Z-pin diameters are 0.28mm, manufactured by 1k tows (1000 tex, or 1kg per km of fibre bundles) and 0.5mm made from 3k tows, but diameters from 0.15mm to 1mm are possible. They are chamfered to an angle of about 45º at both ends to aid insertion and offer excellent adhesion to thermoset resins. After insertion, any excess length of the Z-pins is removed easily by shear cutting. The 'preforms' are characterised further by the areal density of the contained reinforcement, which ranges from 0.5% to 7% [19,44].

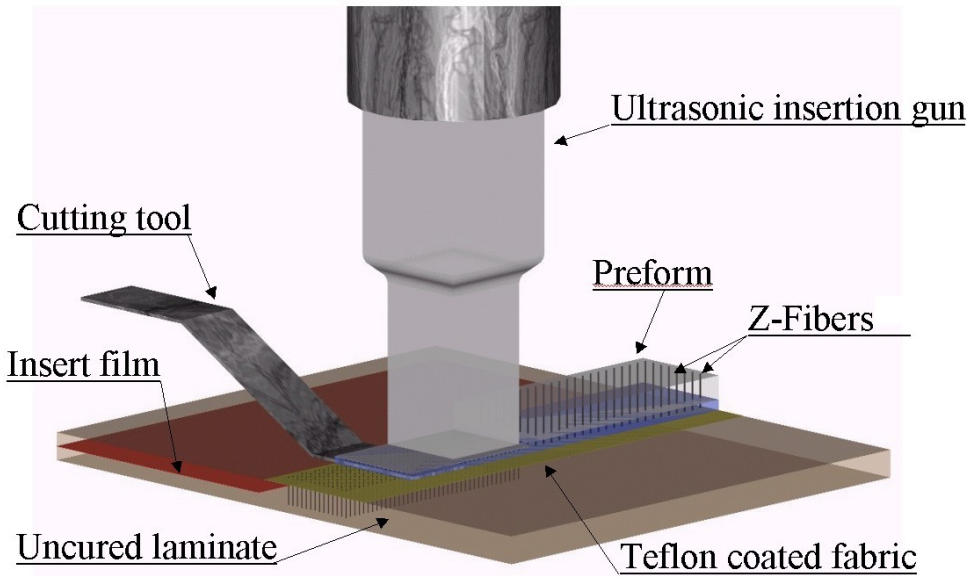

Figure 2-10: *Schematic of the Z-pinning process*

Z-pinning was originally intended as a mechanical fastener replacement, attributing at the same time improved damage tolerance properties. It currently does so successfully for the F/A 18 E/F US Navy aircraft, joining the duct and aft structure to the main

fuselage, since June 2000, with excellent weight and cost savings as a consequence. This property depicts the capability of Z-pinning to be used locally and selectively where an increase in the delamination resistance is required. There is further potential in extending the use of Z-pinning to help the integration of more structural components, while lowering manufacturing timescales and cost by selectively reinforcing structures.

Previous work shows that the interlaminar fracture toughness is improved by at least an order of magnitude, for the crack-opening mode (mode I) [19,20,45], and significantly for the shear loading mode (mode II) [19,20,45]. Resistance to impact loading is also similarly improved due to a reduction in crack formation (up to 30% decrease of damage area), as well as compression after impact (up to 50% increase of compression strength) [20,45,46].

2.3.3 Textile technology

Figure 2-11 illustrates the different forms of textile composites currently available. Straightforward quasi-laminar architectures to highly complex 3D configurations are possible. The latter contain fibres in the through-thickness direction; they possess through thickness properties that TTR techniques attempt to emulate, without adopting their complexity.

Apart from their complexity, the main drawback of 3D textiles is the low fibre volume fraction and the inconsistency in the mechanical properties, due to in-plane waviness, yarn twist and ‘pinching’. Their in-plane stiffness is therefore further compromised for sheet applications by 5% to 50% in 3D interlock weaves [56,57]. Tow strength is also degraded by about 30%. Only 2D braided and 2D woven fabrics regularly achieve a high degree of consistency in maintaining accurate in-plane tow positioning and corresponding mechanical properties. The compromised tailoring of the fibre orientation, local or global, is also a concern. Finally, despite the improved drapability and ease of handling or storage experienced with all textiles, 3D textiles tend to suffer

from increased inconsistencies in their mechanical properties when used in complex geometries [18].

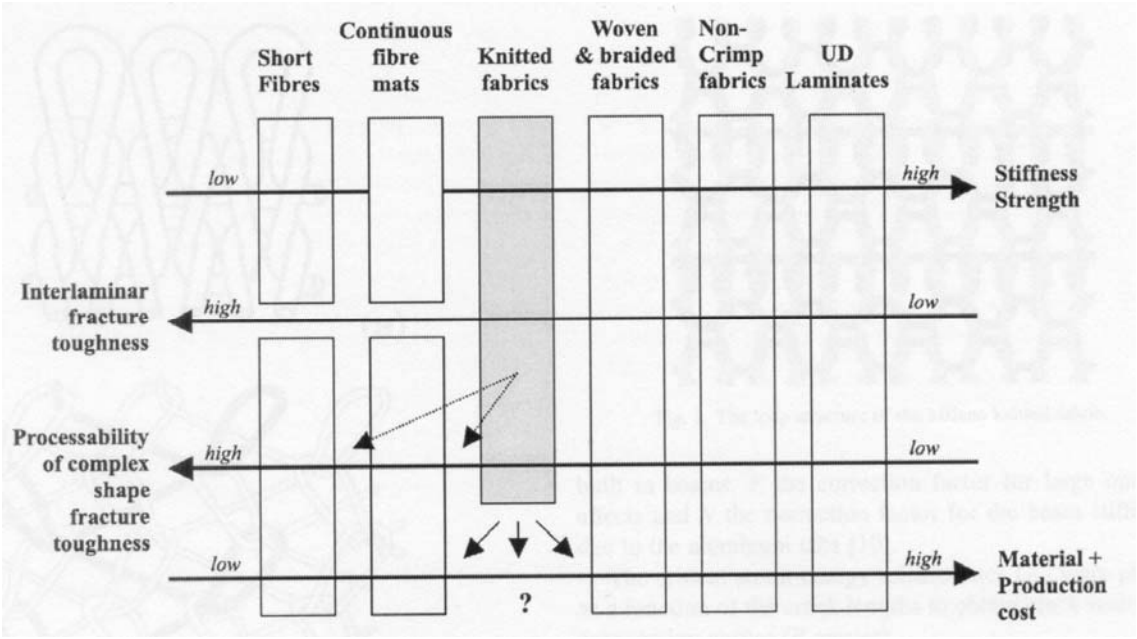

Figure 2-11: *Comparison between the main reinforcement fabrics used for composite materials, as in [59]*

Not all in-plane properties are compromised as compression strength is improved with the presence of a certain amount of through-thickness fibres, along with CAI strength [57]. An additional advantage is that the manufacture of joints or changes in geometry can be integrated in material forming, eliminating the initiation of delamination. Resistance to delamination is a major advantage of 3D textiles as the delamination toughness is increased by at least an order of magnitude when sufficient through-thickness fibres are used [58,59]. Moreover, strain to failure and shear strength are significantly increased. Finally, they exhibit excellent damage and impact tolerance as well as exceptional notch insensitivity, for notch lengths up to 100mm [18,57].

2.3.4 Failure mechanisms of composite laminates with TTR

A combination of failure mechanisms are associated with the delamination of stitched laminates under mode I loading conditions. The closed loops formed by the stitching yarns harnessing the laminate enable the reinforcement to work efficiently after initial debonding from the laminate. Debonding dissipates only a small amount of energy. The main failure mechanisms consist of tensile breaking of the yarns [34], which absorbs a significant amount of energy as well as friction between the failed yarn and the laminate, absorbing additional energy. The major contribution to the improvement of the delamination toughness transpires from the elastic stretching of the loops [39,42]. Tensile breaking takes place at the thread intersection at the outer surface of the composite. A 50% reduction in delamination toughness has been observed by machining off the loops [39]. The importance of the elastic stretching of the loops is also significant in mode II, where high pre-tension of the reinforcement (and therefore smaller margin for elastic stretching) results in lower delamination toughness plateau values [60]. An alternative energy absorbing mechanism in mode II loading, where the reinforcing yarns do not always fail in tension, is 'ploughing' [41]; the crack propagates around the reinforcing yarns and the yarns crush the surrounding resin dissipating energy. The flexible nature of the reinforcement allows tensile loading of the yarns to take place in both mode I and mode II loading modes.

Debonding and frictional pullout are also associated with the failure of Z-pinned laminates under mode I loading conditions. A significant alteration of the failure behaviour noted is the 'stick-slip' crack growth of both stitched and Z-pinned laminates, where the crack seems to grow rapidly (slip) between each row of reinforcing ligaments, before it temporarily rests (stick) and the load is increased enough to generate additional energy for the next sudden jump. This locally unstable type of growth renders propagation very stable macroscopically inside the reinforced area [20,39,40,47,48,61].

The density of the reinforcement and the length of the reinforced area also affect delamination behaviour. High density reinforcement can result in the complete arrest of

a propagating crack and introduce excessive bending under both mode I and mode II loading conditions. This results in bending failure (the outer plies fail in compression) [37]. Additional reinforcing layers of material need to be bonded to encourage crack propagation; however this affects the length of the bridging zone [39,63]. If the crack can propagate through the reinforced area and the length of the reinforced area is sufficient, steady state crack propagation can be reached. The bridging zone is fully developed and the shape of the R-curve becomes flat; the number of ligaments bridging the propagating crack stays constant [39,60].

2.4 Fibre architecture effect

Fibres have a significant effect on delamination: they regulate the direction of crack propagation. After the initiation of a crack due to an out of plane load, as described in the introduction, the crack will tend to propagate in the direction that requires the least amount of energy which is the direction of the adjacent fibres. Impacted panels, in which delamination has occurred, are a clear example. Evidently, the weakest interface would then be a '0 /0 ' interface, i.e. when the fibres of the plies that contain the delamination are aligned in the same direction. This occurrence in laminate lay-ups is quite common and therefore is the most interesting situation to study. Delamination protocols instruct the manufacture of specimens with fibres in the same direction (unidirectional, or UD for short), which is also the direction of crack propagation. Crack propagation in such a specimen is self-similar.

Crack propagation in angle-ply laminates has also been studied [20,49-51]. There are two different angles that need to be defined in such a laminate. One is the angle of crack propagation direction relative to the fibre angle of the midplane of the specimen, where the starter defect exists, and the second is the angle between the fibres above and below the crack plane. Delamination resistance is increased with the increase of either angle. More importantly, fibre angles greater than 22.5 in CFRP laminates result in intraply cracking and deviation of the crack plane from the initial interface [49].

Laminates fabricated by UD material or non-crimp fabrics (NCF), depending on the liquid moulding technique, can have flat ‘0 /0 ’ interfaces. On the other hand, laminates made from woven material have a much more complex interface. The most common arrangement of fibres in one ply of a woven material is 0 /90 , and there is also a certain amount of undulations, or simply waviness in the fibres, depending on the periodicity of the weave. This creates interfaces that include all four combinations of the two directions of the fibres, in a random ratio to each other (Figure 2-12 a & b). If the weave is balanced (equal amount of 0 and 90 fibres), the frequency of appearance of these combinations would tend to equalize between them, but the capacity to arrest an existing crack will depend on the local geometry. The varying interface and the subsequently varying delamination toughness are therefore quite important. Due to the waviness of the fibres, resin rich regions develop, with varying sizes, because of the random relative positioning of the plies to each other, but with the regularity of the weave pattern.

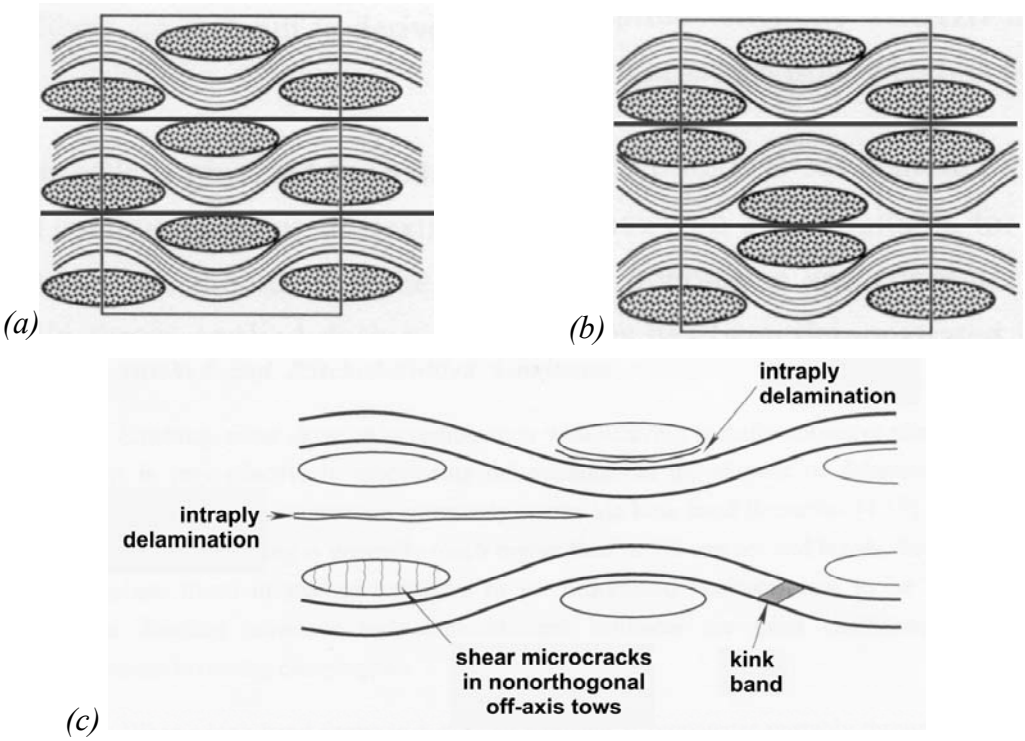

Figure 2-12: *Different interfaces between plies of a plain weave material, depending on stacking sequence(a-b) and crack propagation mechanisms in woven composites under mode II loading conditions (c), after [18].*

The regularity and self-similarity of the crack propagation is questionable. The crack propagation of a cross-ply laminate manufactured from UD material is very similar qualitatively to that of the woven material, introducing both crack plane variation or multiple plane cracking and intralaminar failure (Figure 2-12 c).

This kind of failure of mixed interlaminar and intralaminar cracking in non-UD materials is unavoidable. Additional energy is dissipated occasionally by fibre kinking and breakage and the development of secondary cracks. This occurrence is more pronounced in mode II, making crack propagation measurement with visual methods challenging, but most importantly, introducing great variations of measured delamination toughness in both modes of fracture [18,52,53].

2.5 In-plane effects

Techniques related to enhancing delamination toughness have an effect on in-plane properties. Most of the applications using laminated composites are sized by in-plane properties. The demands of load bearing can also be contradictory, like high stiffness combined with increased damage tolerance (aircraft structures), or increased capability of energy absorption (automotive applications). Apparently, providing that degradation of the properties due to delamination cracking can be restrained, the effect of these techniques themselves on in-plane properties has to be considered.

2.5.1 Effect on mechanical properties

In-plane properties seem to be compromised more, the more the toughening technique deviates from the original lamination process of laminated composites. ***Toughened resin systems*** have a minimal effect on in-plane properties. ***Interleaving*** has a bigger effect, namely lowering the fibre volume fraction, or equivalently adding weight. The increase in weight can be notable for interleaf thicknesses of 0.1mm to 0.7mm, the

range of optimal thicknesses mentioned previously. A representative drop in flexural modulus for such an optimised example, where interleaf thickness is 0.2mm, is 10% [24].

Stitching imposes fibre breakage, fibre misalignment, in-plane as well as in the thickness direction, and the creation of resin-rich regions, where porosity and microcracking of the matrix occurs, due in part to differences in the coefficients of thermal expansion between the reinforcing thread and the composite. All forms of damage have contradictory effects on in-plane properties, depending on many variables. These can either be the stitching variables, such as stitch geometry, type, direction, size and tension, the diameter and shape of the needle, or the type of composite and the lay-up orientation as well as the processing technique.

Distortions caused by stitching to the physical properties of the laminate are depicted in Figure 2-13. *Fibre breakage* is more pronounced in stitched prepregs, due to the increased difficulty of pushing the fibres aside during insertion, although the frictional stresses between the reinforcing yarn and the laminate fibres during insertion can also contribute to breakage, mostly in fabric preforms. Fibre damage can be from 0.5% to 5% [38,54]; however, average values are close or equal to 0.5% [36]. *Fibre misalignment* increases with increasing yarn tension during insertion, due to the increased friction stresses involved. It is weakly affected by the stitch diameter and is decreased when in-plane fibres are compacted densely before stitching. Fibre misalignment is more pronounced on the outer surfaces of the laminate, where fibres crimp in the thickness direction, due to the stitch loop. Fibre misalignment can range from 2.5 to 20 , with the average value being 10 [36]. Apart from its role in increasing the volume fraction, y*arn tension* is necessary during insertion to avoid crimping of the stitching yarns, after further compaction of the fabric preform during the liquid moulding process. The locations of *resin-rich regions* are also depicted on Figure 2-13. From the *material aspect*, better mechanical properties have resulted from using stitched preform followed by the liquid moulding processes than the autoclave cure of stitched prepregs [37]. There is also a relation between fibre architecture with the degree of fibre misalignment. Misalignment is constrained in smaller areas in woven preforms

(1mm [36]) compared to non-crimp fabrics, as the fibres in woven preforms are not allowed to spread as easily. Unidirectional fabrics can have large areas of misalignment, but can also contain misalignment in a smaller degree, as the fibres are allowed to spread enough for the resin pockets to extend from one stitch to the next [36].

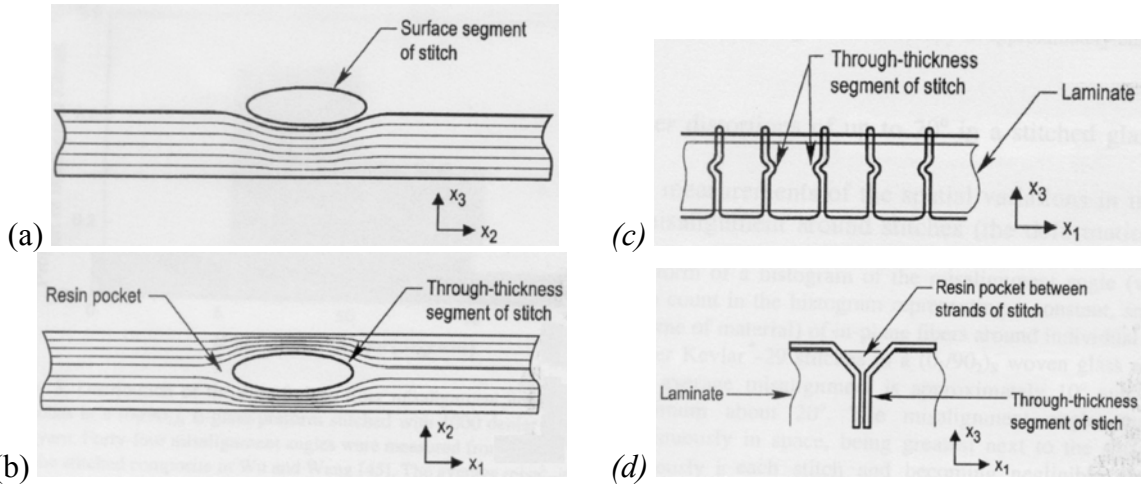

X_1 : in-plane direction along stitch rows, X_2 : other in-plane direction and X_3 : out-of-plane (through-thickness) direction

Figure 2-13: *Schematic of distortions caused by stitching, after [36]. a) Out-of-plane fibre misalignment at laminate surface, b) in-plane fibre misalignment around stitch, c)through-.thickness crimping and d) resin pocket formation between stitch strands.*

Important information on stitching can be found in detailed reviews in [38, 36]. These reports show that *tensile stiffness* is degraded by 15% in average [36]. Rarely does it exceed 20%, but a decrease of 30% has been measured, as well as a relative improvement [38]. Observed improvements reflect an increase in volume fraction compared to the initial laminate, due to the compaction of laminate fibres by stitching. The degradation can be attributed either to decreased volume fraction, fibre breakage or fibre misalignment, which is the dominant parameter. A crude estimate, using equations (2-3) to (2-5), as described in reference [36], gives good agreement with experimental data for the claimed average fibre misalignment value of 10 . E(φ) is the modulus in the loading direction, with fibres misaligned by an angle φ, E_1 is the tensile modulus, E_2 is the transverse modulus, G_{12} is the shear modulus (assumed to be unaffected by stitching) and v_{12} is the axial Poisson's ratio. The misaligned fibre volume of the laminate around the stitches is V_0, with f being the misaligned fibre volume fraction, η_s

being the areal stitch density and *h* the laminate half-thickness. Equation (2-4) gives the knockdown factor, where E_S is the modulus of the stitched laminate.

$$E(\varphi) = \left\{ \frac{\cos^4 \varphi}{E_1} + \frac{\sin^4 \varphi}{E_2} + \frac{1}{4}\left(G_{12} - \frac{2\nu_{12}}{E_1} \right) \cdot \sin^2 \varphi \right\}^{-1}, \tag{2-3}$$

$$\frac{E_S}{E_1(0)} = 1 + f \cdot \left[\frac{E(\varphi)}{E(0)} - 1 \right], \tag{2-4}$$

$$Where\ f = \frac{\nu_S V_0}{h} \tag{2-5}$$

The *tensile modulus* can be degraded up to 45%, but the average reduction is 15-20%. Observed improvements are again a result of increased volume fraction. Limited experiments show that *notched tensile strength* (open-hole tension) is also degraded [36].

Compression strength can be slightly increased, when the stitching rows are aligned parallel to the loading, or by biaxially stitching in both directions [38]. However, in most cases compression strength is significantly degraded, from 5% to 55% [38], with an average reduction of 15% [36].

On the other hand, *notched compressive strength* (open-hole compression) is clearly improved, in average by 30% [36]. The effect of stitching to the *compressive modulus* is unclear, since both slight improvements, as well as great reductions (up to 70%) have been observed. Equally unclear is the effect on strain to failure [38].

Flexural strength seems to be improved by a factor between 1.2 and 1.75 [36]. Reductions are also observed, rarely exceeding 20%, similarly to tension and compression strengths. Flexural behaviour of stitched laminates depends on the competition between suppressed delamination and therefore improved behaviour on the compressive side and inflicted fibre breakage on the tension side. Strain to failure in CFRP laminates is increased [38].

Creep properties are not affected in general and can be improved in cases. *Fatigue* life in *compression-compression* loading is degraded, mainly because of the initial knockdown on compressive strength. Fatigue life of GFRP is also decreased, mostly because the stitches detach early from the composite [55].

Effects of stitching on the in-plane shear modulus and strength have not been investigated, in contrast with interlaminar shear strength (not an in-plane property).

The effects of ***Z-pinning*** on the in-plane properties of composite materials have barely been investigated. Initial reports suggest a severe drop up to 40% in the compressive strength of unnotched UD material, while in more balanced stacking sequences (quasi-isotropic) or with the presence of a notch (Open-Hole) z-pinning has negligible effects (5% drop to 2% rise) [64]. A recent study has further examined the effect on compressive strength [65]. A degradation of approximately 33% was found, complementing the finite element analysis performed in the same study.

2.5.2 Mechanisms of in-plane failure

The dominant reason for the reduction in *tensile strength* in ***stitched*** laminates is fibre breakage. Despite the small total amount of broken fibres, these flaws are contained in clusters around the stitches and have a significant effect [36]. The principal tensile failure mode has changed from delamination cracking and fibre fracture to tensile failure along the stitchline [36].

Similarly to tension, *compressive failure* is not determined by some collective action of the stitches, but a local distortion. This is indicated by the insensitivity to stitch density [36] or to the type of yarn [54]. The dominant parameter, in this case however, is fibre misalignment. Unreinforced laminates fail by delamination cracking between plies, initiating by Euler buckling. Stitching changes the failure mechanism to kink band formation, initiating at the surface, where the out-of-plane misalignment is most pronounced (Figure 2-13). Fibre collapse, a third compressive failure mechanism,

requires minimal fibre misalignment (0.8 -2.3 [36]) and is not encountered in stitched composites. Analytical models exist, predicting the minimum stitch density required to suppress delamination initiating by buckling under compression loading. The critical fibre kinking stress in relation to the degree of fibre misalignment can also be estimated, subjected to a correction regarding the local ellipsoidal geometry around the stitches, with approximate agreement to experimental data [36]. A failure map for stitched laminates under compressive loads can subsequently be drawn (Figure 2-14). The importance of the out-of-pane fibre misalignment at the surface is demonstrated in [54]. An increase of 7% to 35% in strength compares to the original stitched laminates has been observed, by machining away the surfaces and therefore removing the stitching loops. The performance of the 'machined' laminates simulates the performance of a tufted laminate, having a 'discontinuous' arrangement of reinforcing fibres. The surface loop has no positive influence on CAI strength and no influence on damage containment [54].

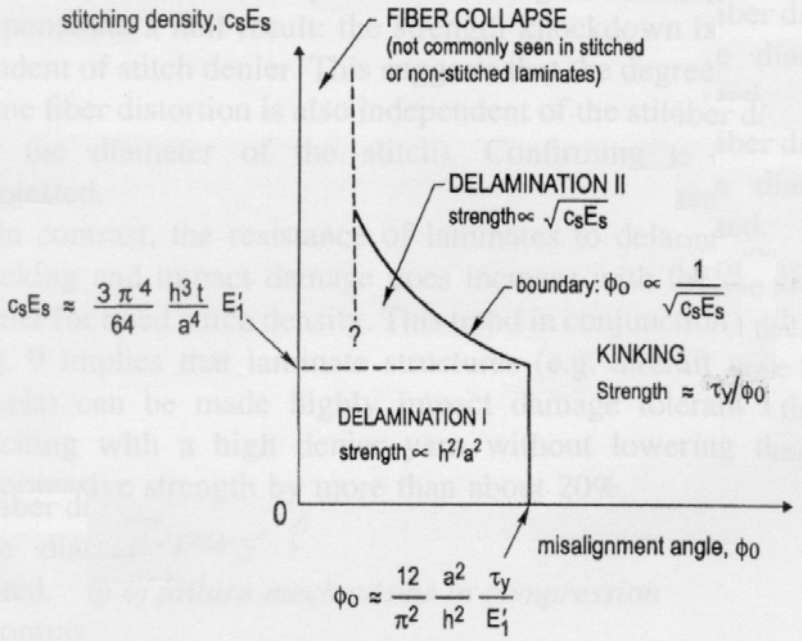

Figure 2-14: *A failure map for stitched laminates under compressive loading, after [36]*

Kink band formation remains the dominant mechanism responsible for the degradation of *notched compressive strength*, but in the presence of a hole, this kind of failure exhibits stable damage propagation, since the stress concentration falls with distance

from the hole. In unstitched laminates, kink initiation is followed by delamination, pre-empting stable damage growth of a kink band across the specimen, which would occur at a higher stress than delamination growth. Furthermore, the effect of stitching on the elastic constants, creates a softening effect at the notch, decreasing the stress concentration factor K [36].

The most noticeable failure mode change occurs in *flexure*, where delamination growth is arrested and tensile failure occurs instead [38]. On the other hand, no change in failure mode occurs in *fatigue in compression-compression*, as the mechanism of progressive fibre kinking is not affected by stitching; the slope of the S-N curves remain essentially unchanged. Fatigue strength in compression-compression loading is unlikely to be knocked down more than 20% and is probably independent of stitch density [36]. Limited data on f*atigue in tension* indicates a degraded fatigue life, probably due to a change in the failure mechanism to failure at the stitches. Additionally, fibre misalignment can produce axial shear stresses, causing resin damage, leading to fibre failure, due to wear against resin fragments [36].

Kink band formation is also the dominant mechanism responsible for the degradation of *compressive strength* in ***Z-pinned*** laminates. The in-plane misalignment responsible for the knockdown was evaluated at 9 , however the insertion of Z-pins in a different material, namely T300/914 carbon/epoxy prepreg, similar to this study, has resulted in smaller misalignment angles [65].

2.6 Modelling Work

A considerable amount of work has been carried out on both the numerical and analytical modelling of delamination failure with TTR. Since this is not the first time existing methods have been reviewed [20,66,67], a brief account will be given and the reader is encouraged to look in the references for the detailed derivation of the models mentioned.

2.6.1 Analytical modelling

Analytical micromechanical models for calculating the interlaminar fracture toughness as well as the crack growth resistance curves for stitched laminates loaded in both mode I and mode II loading conditions have been developed [39,40]. The mode I model best describing experimental observations [67] is the combination of two separate models [39]; the one referred to as the "discontinuous stitching model" assumes no interdependence between stitches and frictional pullout as the energy absorption mechanism, while the second, referred to as the "continuous stitching model", includes elastic stretching of the stitches and rupture at the delamination plane [62]. As rupture usually occurs at the outer surface of the composite, the combination of the two models contains the contribution of all mechanisms. The mode II model assumes elastic stretching of the stitches and rupture at the crack plane [60]. Good agreement with experimental data is found for both modes of failure. Detailed knowledge about the physical and interlaminar fracture properties of the unstitched laminate, the stitching conditions and the mechanical properties of the stitch material is required [67]. A separate simple analytical model simulates the load-deflection curves of stitched DCB beams [42] and is verified by FE simulations. The linear elastic model used to describe the stitch yarn is the source of disagreement with experimental data incorporating Kevlar stitches. Application of the model is simple and accurate for other stitch materials.

The behaviour of curved structures with TTR has also been modelled [68,61]. Both stitching and short rod reinforcement (effectively Z-pinning) are considered. Conservative design rules are derived and the appropriate density of the reinforcement can be calculated. The model uses concepts for bridged mode II delamination cracks extensively discussed in [69,70]. These models consider that crack growth can be described by two separate mechanisms; the intrinsic toughness of the material and the bridging tractions provided by the reinforcement. The bridging law, describing the bridging traction of the reinforcement, can be derived from the load and sliding displacements measured during an ENF test of a reinforced specimen, using the inverse formulation of the model. The forward formulation calculates the delamination fracture

toughness for a given bridging law. Two limiting cases are defined; a steady-state configuration indicative of non-catastrophic failure, where a crack is bridged by intact ligaments and a small scale bridging configuration indicative of catastrophic failure. Two corresponding length scales are determined; the ACK limit, where the critical shear stress for crack propagation has reached a constant value, independent of crack length and the small scale bridging limit, where the length of the bridging zone has reached a constant value [70]. Despite the fact that these models successfully overcome the inadequacy of LEFM to describe delamination in the presence of absorbing mechanisms other than crack growth, the application to a single delamination test to obtain either the bridging law or the delamination resistance requires considerable calculation effort.

Analytical modelling of mixed mode delamination of laminates with TTR has been examined in [71] and has been applied to sub-structural components [72]. Modelling of mode I delamination of a reinforced DCB beam under pure bending loading is investigated in [73]. A different approach consists of generating a representative bridging traction law by modelling a single discrete bridging entity (tow, stitch or Z-pin) under mixed mode loading [34]. The model includes mechanisms such as pullout, axial and shear loading of the ligament as well as lateral deflection of the ligament through the resin (‘ploughing’) through the resin. Despite the considerable calculation effort involved, the bridging law acquisition aims in optimising design of composites with TTR. An extension of the same study includes ‘snubbing’ effects introduced during the pullout of the ligament under mixed mode loading; the ploughing of the ligament introduces enhanced friction forces and their effect on the pullout behaviour is accounted for [74].

2.6.2 Numerical modelling

FE modelling provides a different approach in overcoming the existing deficiencies of existing data reduction methods for the evaluation of the effects of TTR on composite laminates. Initial models [75,76] have investigated the micromechanics of a Z-pin in a composite plate. The model described in [20,77] presents a numerical tool for parametric studies of Z-pinning in the delamination of composites under mode I loading. Experimental data are implemented in order to construct appropriate bridging laws for a single Z-pin. The effects of Z-pin density, Z-pin angle, Z-pin insertion depth as well as pinning quality deficiencies can be studied and the delamination toughness can be predicted. A different study investigates the effects of various bridging laws as well as the effects of Z-pin properties on delamination behaviour under mode I loading [78,79]. An ongoing numerical investigation examines the effect of Z-pinning on delamination behaviour in detail, using 3D finite element modelling [80].

2.7 Summary

The techniques required to enhance delamination resistance significantly, involve the introduction of some kind of fibres to carry the out-of-plane loads that drive delamination in laminated composites. The effectiveness of these techniques increases proportional to their complexity. Arguably, 3D fibre architectures provide the greatest delamination resistance. The significance of high grade and consistent in-plane properties, however, does not favour complex fibre geometries. TTR techniques offer the best compromise and facilitate the use of typical and well developed manufacturing processes, as they introduce few changes in the manufacturing procedure. They also enable the containment of existing cracks, in contrast to matrix based techniques.

Inevitably, the in-plane properties are affected depending on the amount of the reinforcement used. A wealth of information exists concerning the effect of stitching parameters on the in-plane properties of laminated composites. In contrast, little

information is available to the effect of Z-pinning on in-plane properties. The two techniques are complementary, as they are best suited to different types of materials; in particular, Z-pinning is best suited for use with prepregs, while stitching is best suited for use in dry fibre preforms. Considering the impact of stitching on in-plane properties and the similarity of the two techniques in principle, there is scope for research on the effects of Z-pinning under both static and dynamic loading.

Z-pinning is still a relatively new technique and the manufacturing procedure is not optimised relative to the requirements of different materials regarding laminate quality. The influence of the parameters of stitching on laminate quality and subsequent properties has been reported in the current chapter; little or no information is available on the effects of Z-pinning on laminate quality.

The identification of the failure mechanisms involved in the delamination of stitched laminates has facilitated analytical as well as numerical modelling of delamination failure. Mechanisms related to mode II delamination failure are more complex than in mode I and the applicability of analytical models in the mode II case requires the use of estimated laminate properties (such as the resistance of the resin against crushing) or the simplification of the failure type (such as the assumption of rupture of the stitches at the fracture plane). The type of failure of the Z-pins under mode II loading conditions, as well as the influence of material type on the type of failure has not been yet addressed.

3 Description of materials and manufacturing procedure

The procedure of manufacturing with Z-pins has recently become better known through publications [19], and has been described in section *2.3.2*. This chapter includes additional suggestions and techniques regarding the insertion procedure and new information concerning the use of Z-pins in woven carbon prepregs. Factors associated with Z-pining are categorised into insertion parameters and Z-pin parameters. A further understanding of the effect of these parameters on the quality of Z-pinned laminates is attempted, using both measurements and observations.

3.1 Materials

3.1.1 Prepregs

The materials used in this study can be categorised into two main categories: unidirectional (UD) prepregs and woven prepregs. All materials were supplied by Hexcel Composites Ltd, Duxford, UK. The names of the different materials, as well as the category they fall into, are presented in Table 3.1.

Material	Prepreg type	Fibre type	Nominal cured ply thickness (µm)
E-glass/914	UD	Glass	125
T300/914	UD	Carbon	125
IMS/924	UD	Carbon	125
IM7/M21	UD	Carbon	125
G986/M21	Woven	Carbon	275
G986/M36	Woven	Carbon	275

Table 3-1: *Materials used: Type and nominal cured thickness per ply*

The two woven materials in Table 3.1 were of the exact same fibre architecture, a 2 2 twill weave of 6K tows. Only the impregnated resin differs between them. Information about the properties and the microstructure of these two resins (M21 and M36) are presented in paragraph *4.2*. The nominal cured thickness of the woven materials differs from that of the UD materials and is also presented in Table 3.1. The UD glass fibre prepreg in Table 3.1 was used as tabbing material. The choice of materials was either determined by the research programme under which the current study was funded (MERCURYM), or to enable comparison of measurements with older data.

All prepregs were received in the form of rolls and were kept sealed in a deep freeze. The materials were allowed to defrost for a period of at least 8 hours in their sealed bags before use, in order to avoid moisture pick up. Then they were cut and laid up by hand. UD prepregs were debulked every four plies at 60 C under vacuum for 30 min. Woven prepregs were compacted using a hot press. This compaction procedure and the reasons for its application are further described in section *3.4.1*. The woven material used for the T-joint coupons described in chapter 8, was not consolidated using this technique, as coupon geometry excluded the use of the hot press. The typical debulking procedure was therefore used instead. The Z-pinning process follows afterwards. For the manufacture of testing coupons containing Z-pins in only part of their thickness, the required number of plies was then laid up on the outside of the already Z-pinned laminate. These "partially" Z-pinned laminates will be dealt with in detail in paragraph *3.4.1*. The nominal thickness of the laminates produced ranges from 1.5mm or 12 plies of UD material to 6.6mm or 24 plies of woven material.

Material	Pressure (bar)	Temperature (C)	Duration (min)	Rate (C/min)	Post – cure (hours)
E-glass/914	7	180	120	2	4
T300/914	7	180	120	2	4
IMS/924	7	180	120	2	2
IM7/M21	7	180	120	2	---
G986/M21	7	180	120	2	---
G986/M36	7	180	120	2	---

Table 3-2: *Cure cycles of materials used in this study*

After Z-pinning, the laminates were cured according to the manufacturer's recommendations. The curing cycles are described in Table 3.2. All cured laminates were inspected using C-Scan. The additional usefulness of the C-Scan procedure when inspecting Z-pinned laminates is portrayed in paragraph *3.4.1*.

3.1.2 Z-Fibre

The Z-pins used were pultruded T300/BMI carbon rods of two diameters, namely 0.28mm and 0.5mm, supplied in preforms with an areal density ranging between 0.5%, 1%, 2% and 4%. The areal density is defined by the percentage of the total preform or resulting laminate area covered by Z-pins. The length of the Z-pins used was enough to pin the required thickness each time. All Z-pin preforms were supplied by Aztex Inc [44].

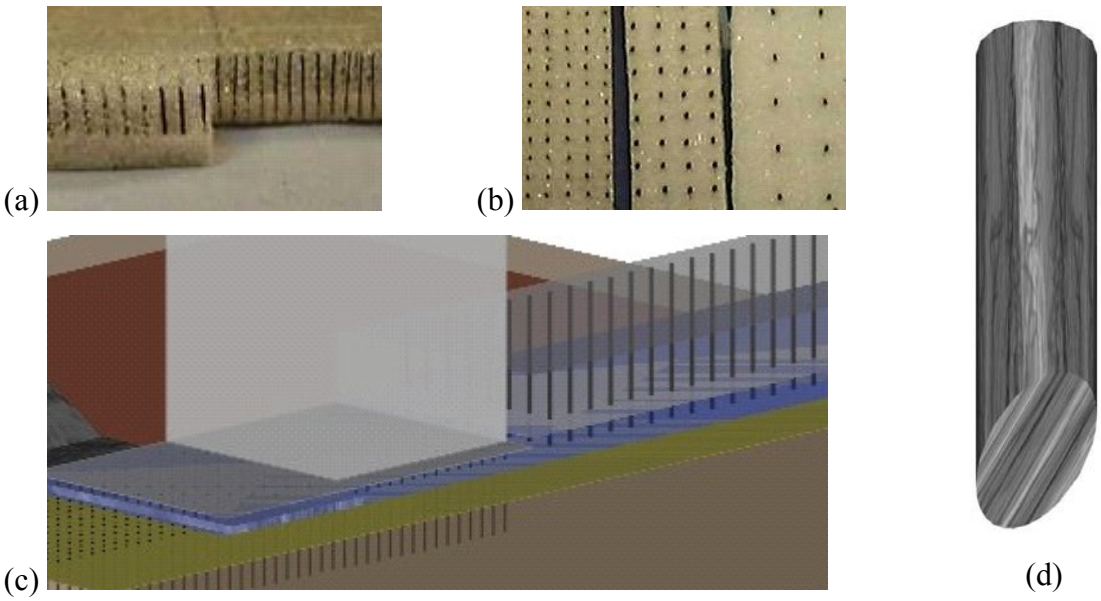

Figure 3-1: *(a) Z-pin preform consisting of foam of two different densities, (b)Z-pin preforms of various areal Z-pin densities, consisting of medium and low density foam, (c) low density foam crushing during insertion, (d) Z-pin 45 edge chamfer*

The preforms used consist of Rohacell foam of two different densities (Figure 3-1(a)). The collapsible low density foam located at the top, the medium density foam at the

bottom and the 45 chamfered edge of the Z-pins, as described in section *2.3.2*, are depicted in Figure 3-1(a-d).

3.2 Z-pinning procedure

The different parameters associated with the Z-pinning procedure can be classified into two main categories. First, there are the parameters related to the Z-pin insertion in the laminate, which will be referred to as ***"insertion parameters"***. These are the *pressure*, the *speed* and the *depth*. An additional parameter is also the angle of insertion; however in this study the angle of insertion was always orthogonal. Any angle of the Z-pins appearing in the finished laminate is a result of the existing parameters and will be dealt with in detail in sections *3.2.2* and *3.4.1*. Secondly, parameters related to the Z-pin preform used will be referred to as ***"Z-pin parameters"***. These are the Z-pin areal *density*, the Z-pin *diameter*, and the post insertion Z-pin *angle*.

3.2.1 Insertion apparatus

The Ultrasonically Assisted Z-Fibre insertion method (UAZ), as developed by Aztex Inc., was used throughout this study. It essentially consists of an ultrasonic gun that "hammers" the Z-pins into the laminate with a 20kHz frequency and a maximum amplitude of 20μm at full output. The ultrasonic gun assembly can be either accommodated in a hand-held unit (Figure 3-2), or in a bigger fixture called 'gantry' (Figure

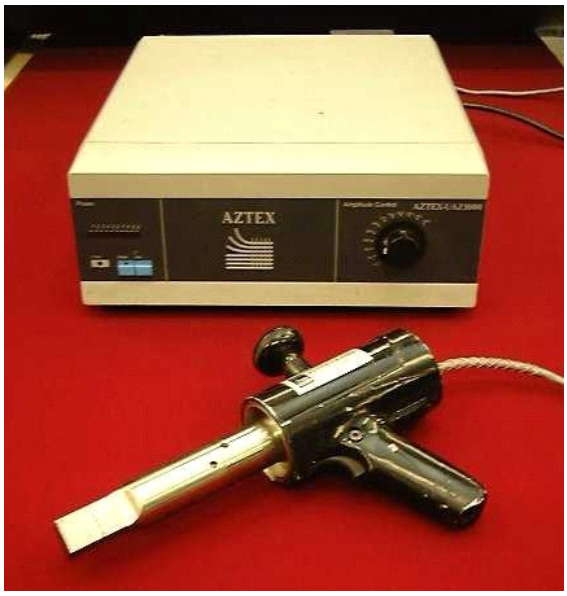

Figure 3-2: *Hand-held UAZ gun and generator*

3-3). The insertion parameters are affected by human intervention in the case of the hand-held unit, while, in the case of the gantry, they can be set and controlled mechanically. The gantry is also better suited to ensure the orthogonal insertion of the Z-pins, as well as increase the rate of manufacture. The advantages of using the hand-held unit lie in the ability to access and pin highly curved structures. A good example is the roll-over hoop of a Jaguar F1 car, as published in Racecar Engineering ([81], Figure 3-4). With access enabled from the outside by removing the outer part of the mould, the insertion was straightforward. Narrow strips of Z-pin preform were cut and placed on the outside curvature of the part. The preforms were slightly offset to each other, in order to avoid the intersection of the insertion paths of the Z-pins due to the curvature.

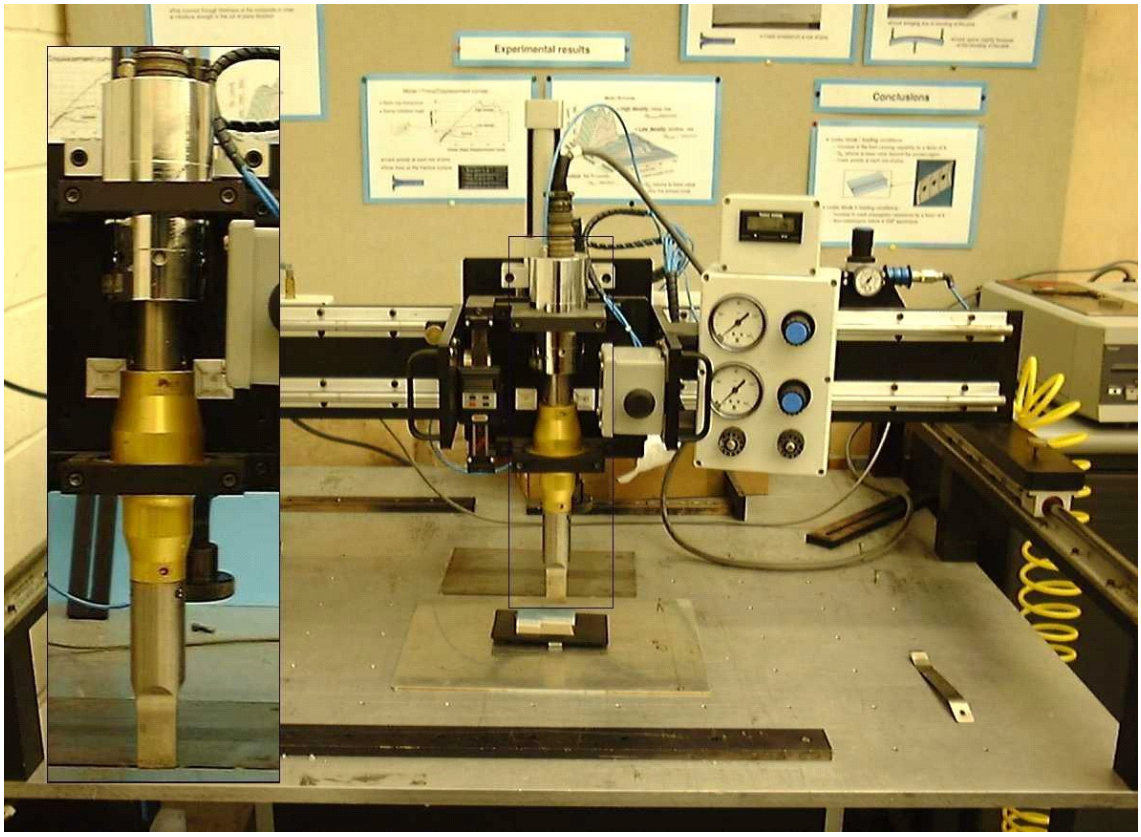

Figure 3-3: *Gantry UAZ unit used in this study*

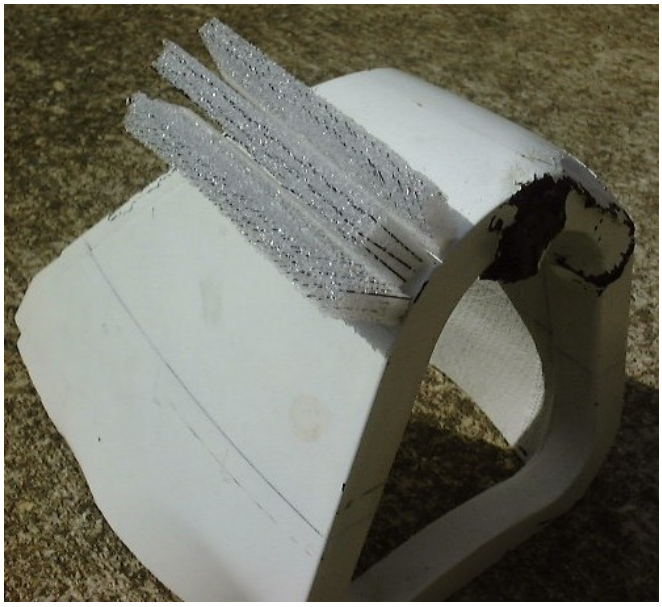

Figure 3-4: *Z-pinned roll hoop of a Jaguar F1 car. Component carries test damage; Z-pin preform placed to demonstrate the arrangement used to insert Z-pins before cure.*

3.2.2 Manufacturing issues

Throughout this study the gantry was used to pin most laminates. The manufacture of the T-joint coupons was the only case where the hand-held unit was used instead, due to the height of the T-joint mould, which excluded the use of the gantry. A very significant improvement when using the gantry instead of the hand-held unit is the accurate and reproducible depth of insertion. The criterion for the end of insertion when using the hand-held unit is either the appearance of Z-pin marks on the back surface of the laminate or when the edges of the Z-pins are crushed against the back plate. This method encourages the insertion of a Z-pin length that is greater than the thickness of the laminate, especially if the Z-pin density is high. When inserting a certain percentage of Z-pin material into the laminate material, the resulting laminate has to occupy more volume. Insertion tends to make the laminate "swell" in the thickness direction. This is more pronounced in a laminate with tightly packed fibres like a UD laminate, where little space for additional material is available in the first place. Since the laminate thickness after insertion is greater than the laminate thickness before insertion, and the inserted Z-pin is visible on the back face of the laminate, the inserted Z-pin length will be greater than the laminate thickness before insertion. In order to insert the appropriate

length of Z-pins into the laminate, the insertion depth can be adjusted when using the gantry not to surpass a required value. The depth (which is effectively equal to the length of the inserted Z-pins) can be measured accurately (±0.01mm) with a gauge mounted on the travelling part of the head of the gantry.

Before insertion, a film of Teflon coated glass fabric is placed between the laminate and the Z-pin preform. This film prevents the Z-pins from moving and protects the laminate from any damage, during the cutting phase. This means that the inserted Z-pin length is as much as the laminate thickness as well as the thickness of the Teflon film (0.15mm). If the backing paper is left on the back face of the laminate to assist noticing the ends of the Z-pins, when using the hand-held unit (since both the Z-pin and the laminate are black) then the inserted Z-pin length will be additionally longer, as much as the thickness of the backing paper. Thus, the possibility of inserting a Z-pin of greater length than needed is high; however, this can be controlled when using the gantry. The problems associated with the insertion of an excessive Z-pin length are dealt with in paragraph *3.4.1*

The laminate and the preform have to be held firmly during insertion. Any movement during insertion will cause misalignment of the Z-pins. When Z-pinning a woven material, the emerging angle will remain constant throughout insertion, due to the restraining effect of the laminate fibres. In a UD material there is a greater possibility that this angle will appear in a plane perpendicular to the laminate fibres. If this happens, the angle will increase as insertion progresses.

Insertion using the gantry begins by setting the speed and pressure of insertion. This is preferably done with an insertion test at a sacrificial edge of the laminate and a small piece of Z-pin preform. Although an experienced operator can avoid this step, one would still decide on setting the insertion parameters using a trial and error method. The next set of suggestions can help maintain a high quality Z-pinning procedure. High insertion speed can buckle the Z-pins. Low insertion speed allows long times of insertion and thus too much heat generation, which can make the foam lose its integrity and lead to Z-pin buckling. Not enough pressure will not insert the Z-pins. Too much

pressure will crush and split the edge of the Z-pins and terminate insertion. The time spent inserting every block of Z-pins should not exceed 4 or 5 seconds, otherwise the excessive heat generated can lead to foam melting and Z-pin buckling, Z-pin crushing, or the initiation of local cure of the laminate. The latter would make the laminate harder and would dramatically increase the friction between the laminate and the Z-pin, terminating insertion. On the other hand, if no set of parameters seems to lead into effortless insertion, moderate local heating of the laminate is recommended, up to a temperature that will not initiate the curing of the laminate when maintained for the duration of insertion. For the high temperature materials used in this study, a temperature of 60 C was the maximum required. The use of a thick metal plate underneath can delay heat dissipation and prolong the effective insertion time. However, a layer of an electrically insulating material should always be placed between the laminate and any metallic components, to prolong the life time of the ultrasonic generator. If contact is made between the Z-pin and any metallic part during insertion, when using close to full amplitude (which is advisable for effortless insertion), there is a danger of burning the power supply of the generator.

The second phase of insertion consists of determining the depth. The thickness of the laminate as well as the preform height (equal to the length of the Z-pins in the perform) are measured. The subtraction of the two values gives the lowest point the ultrasonic gun should reach. The gun is then set to this maximum depth with the use of a set of callipers. The depth gauge of the gantry is set to zero at this point. Insertion will be complete every time the gauge reaches zero again. For any change of preform height (perform height is custom and depends on the batch of material requested) or laminate thickness, the procedure of setting the maximum depth should be repeated. If the insertion depth required is less than the laminate thickness, this should be considered in the depth setup.

The thickness of the laminate can prove to be a limiting factor relative to what diameter Z-pins can be used. With an increasing laminate thickness a longer Z-pin preform is necessary, as well as a greater amount of pressure. This means that the possibility for buckling of the Z-pins increases. For 0.5mm diameter Z-pins, thicknesses up to 18mm

of woven prepreg and 25mm of UD prepreg have been Z-pinned. For 0.28mm diameter Z-pins a thickness of 6mm for a UD prepreg and 7mm for a woven prepreg have been Z-pinned. Experience indicates that a carbon Z-pin with a diameter of 0.28mm could prove inapplicable for laminates with a thickness of more than 10-12mm.

The Z-pin preforms used in this study were not all of the same height for different combinations of density and Z-pin diameter. The positioning of the same amount of Z-pins every time under the head of the ultrasonic gun was not always possible. A different number of materials was used and laminates of a variety of thicknesses were manufactured. The area of the coupons that were covered with Z-pins was quite small for most of them, so the amount of Z-pinning that has taken place is limited. Taking all that into account, it was not possible to produce a database of ideal set of parameters, namely pressure and speed, for each combination of material, preform and thickness. Z-pinning currently remains a procedure based on operator experience. However, the required experience is easily gained when following the aforementioned instructions and achieving satisfactory Z-pinning quality is a matter of a few hours. The use of a robotic insertion head, using preforms of fixed dimensions, as developed by Aztex Inc., would be a step to the direction of developing such a database.

Cutting the excessive Z-pin length afterwards is best done after freezing the laminate for 5 to 10 minutes. A sharp cutting tool and the application of pressure on the Teflon film over the laminate, to avoid relative movement of the Z-pins to the laminate, prevents any appearance of an angle. This is important for a UD laminate, particularly a thin one. The Z-pins can still move in the plane of the laminate fibre direction, when forced by a blunt cutting tool.

3.3 Tabbing

Tensile testing of composite laminates requires the incorporation of tabs. For the manufacture of tabs, glass/epoxy (E-glass/914) UD material, as described in tables 3.1

and 3.2, was used. All tabs were “square-ended”, since they give better results [82]. The lay-up of the glass tabs was symmetric, ±45 , to diffuse the gripping loads. The tabs were abraded with sandpaper, as well as the specimens, and wiped with a solvent; Redux 420 adhesive was used for bonding to the coupons. Bonding requires a temperature of 120 for 1 hour and the application of pressure. This helps to keep the adhesive layer to a minimum and prevent air entrapment. In order to retain the positioning of the tabs on the coupons throughout the duration of the procedure, coupons were placed in-between metallic plates in “pockets” of adhesive strips of cork (Figure 3-5). Release film between the coupons and their surroundings was used to keep the adhesive from spreading. A pressure of at least 5 bars was applied with the aid of a hot press, with heated top and bottom plates.

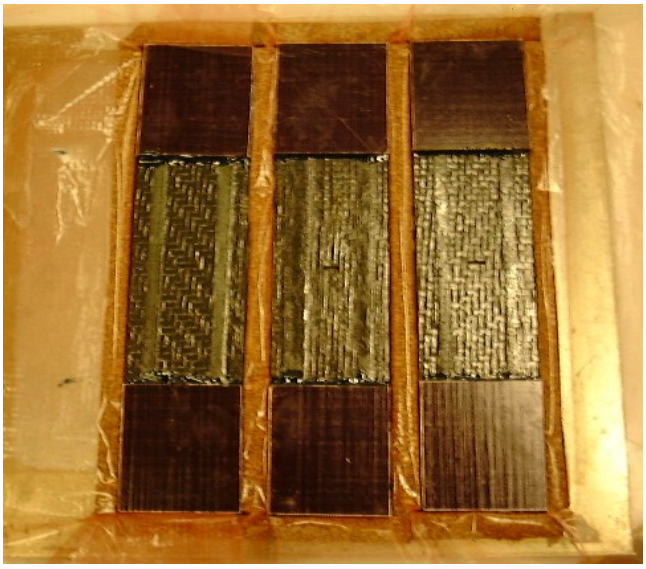

Figure 3-5: *Bonding tabs on tensile coupons; adhesive cork confines tabs into place*

3.4 Quality inspection

3.4.1 Effect of insertion depth

The importance of the insertion depth becomes apparent after cure. During cure the thickness of the laminate will decrease. This will be minimal for a tightly packed, thoroughly debulked laminate, but significant otherwise. Figure 3-6 illustrates how an excessive Z-pin insertion depth can lead into the appearance of a Z-pin angle after cure. Since the length of the Z-pins cannot decrease, the Z-pins tilt into an angle. The angle depends on the amount the laminate thickness decreases. In a woven laminate, Z-pins cannot tilt freely, since they are constrained by the laminate fibres. This leads to the final cured thickness being locally higher than the thickness of laminate without any excessive Z-pin length inserted. Any laminate after Z-pin insertion will have in turn greater thickness than the nominal, as defined by the manufacturer. Subsequently, the final cured thickness of a laminate Z-pinned with an excessive depth will be much greater than nominal, if the laminate has a fibre architecture constraining for the Z-pins. In a UD laminate Z-pins can tilt easier, so the resulting angles will be greater for a similarly excessive insertion depth.

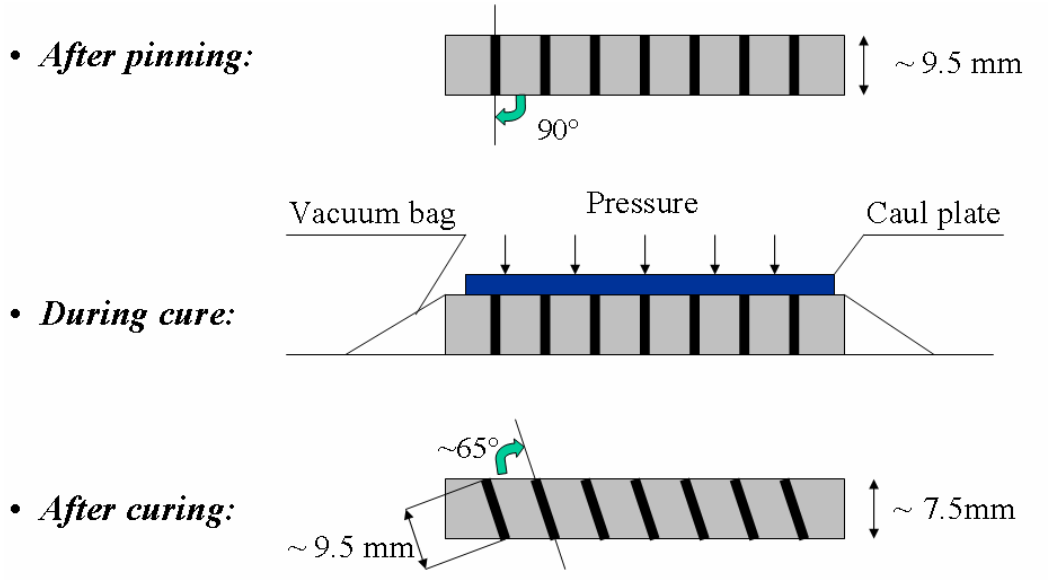

Figure 3-6: *Implications of dimensional changes during cure upon the final insertion angle of a Z-pin of length greater than required (nominal laminate cured thickness: 6.6mm*

Z-pins do not move along the thickness of a laminate during cure; autoclave insertion methods are only effective for low density performs [20,44]. This makes the initial positioning of the Z-pins along the thickness important. In order to produce, therefore, a laminate with Z-pins throughout its thickness at an orthogonal angle, controlling the initial thickness of the uncured laminate before Z-pinning is essential. The uncured thickness of both woven materials used was significantly greater than their nominal cured thickness. After applying the usual debulking procedure and stacking all plies, the uncured thickness of the G986/M21 was about 40% greater (9.5mm instead of 6.6mm - Figure 3-6). In collaboration with Hexcel Composites, Duxford, an alternative method was developed and adopted [83]. Every 4 plies, woven laminates were compacted using a hot press at a temperature of 70 C under a pressure of 10 bars initially for 5 minutes after reaching the required temperature, and 15 bars subsequently for another 5 minutes (Figure 3-6 (a)). This allows the resin to flow and fully impregnate the central part of each ply, as it is initially dry in the particular prepreg. Both upper and lower surfaces are heated. A thick metal plate, covering the laminate fully, is used to apply uniform pressure. The laminate is confined between strips of adhesive cork to prevent any deformation from the original rectangular shape, as well as resin bleed. The thickness of the adhesive cork strips is less than the thickness of the plate and the expected thickness of the laminate after cure together, and greater than the laminate before compaction. Release film is used between the laminate and its surroundings. No other property of the resin is affected apart from its viscosity, as it takes a long time and higher temperatures for gelation to commence (Figure 3-6(b)). The consolidation of the laminate using hot press compaction is improved significantly (Table 3-3). The measurements are taken after an allowed relaxation period of 20 minutes, after which no actual relaxation has been observed.

Consolidation method	**Additional thickness relative to nominal cured thickness before Z-pinning (%)**	***Standard deviation (%)***
De-bulking	(Approx.) 40	
Compaction	*10.4*	*2.7*

Table 3-3: *Comparison of consolidation methods*

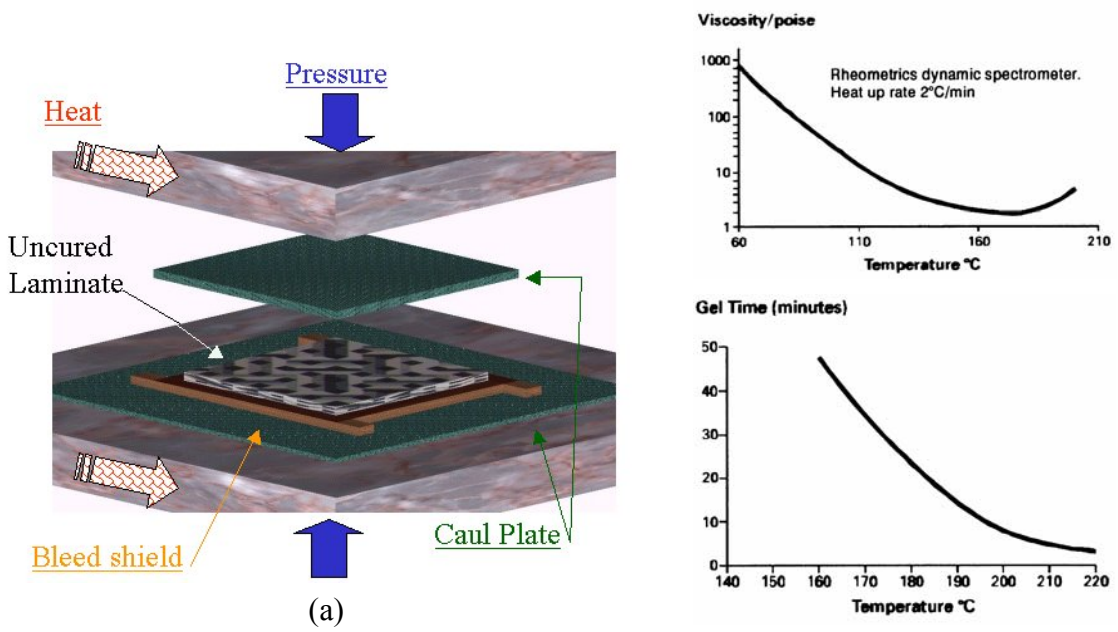

Figure 3-7: *(a) Compaction prior to Z-pinning, (b) viscosity and gel time of the M21 resin in dynamic and isothermal cure respectively; there are at least 50 min in a low viscosity liquid phase for M21 before gelation, at temperatures up to 160 C.*

The effect that the improved consolidation method has on the angle of the Z-pins after cure is presented in Figure 3-8. This is also illustrated by the C-scan in Figure 3-9. The black dots in the images are the imprints of the Z-pins. The difference in their shape and array demonstrates the improvement in Z-pin angle. The texture of the weave is also visible in the image.

(a) *Z-pins inclined from the original insertion angle (0.5 mm diameter pins)*

(b) *Z-pins maintaining the original insertion angle (0.5 mm diameter pins)*

Figure 3-8: *De-bulked (a) vs. compacted (b) laminate; effect on Z-pin angle*

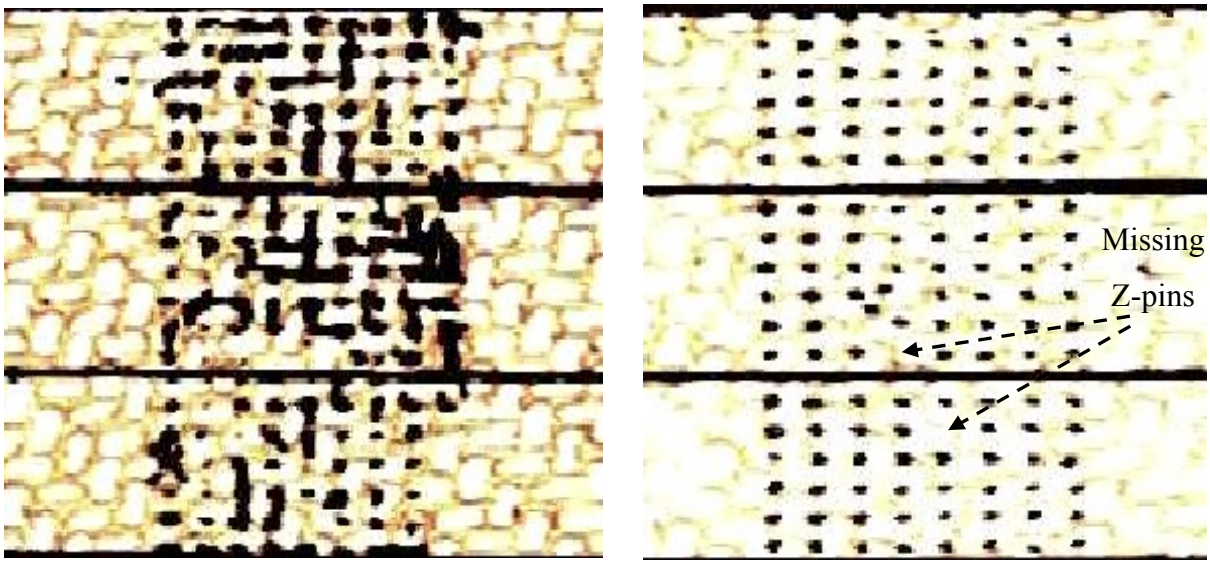

(a) *C-Scan corresponding to a specimen quality of* Figure 3-8*a*

(b) *C-Scan corresponding to a specimen quality of Figure 3-8b*

Figure 3-9: *De-bulked (a) vs. compacted (b) laminate; effect on Z-pin angle and array through C-Scan image*

Dark imprints that are not circular indicate an angle, with a magnitude proportional to the size of the dark area. C-scan can also help locate missing Z-pins, as illustrated in Figure 3-8b; missing pins can be detected at the top middle of the bottom coupon as well as the bottom middle of the middle coupon. The spacing and array can also be appreciated. Improvements of Z-pin array due to the improved consolidation method are also visible on the back face of the cured laminates.

(a) *De-bulked cured laminate; irregular array of z-pins (0.5 mm diameter pins)*

(b) *Compacted cured laminate Regular array of z-pins (0.5 mm diameter pins)*

Figure 3-10: *De-bulked (a) vs. compacted (b) laminate; effect on Z-pin array*

Another technique used to avoid the misalignment of Z-pins after cure is the "partial" pinning of a laminate. A partially pinned laminate is illustrated in Figure 3-11. Only part of the thickness of the laminate contains Z-pins. Such a laminate is manufactured by laying up the extra layers of material after the Z-pinning procedure. Any excess Z-pin length penetrates part of the new layers of the added material. The manufacture of a partially pinned laminate is the only way to completely avoid the appearance of any Z-pin angle, since it is the only way that the excessive Z-pin length due to the Teflon film thickness can be neutralised. The most time efficient way to fully evaluate the Z-pinning quality of such a laminate is the C-Scan method. Partial Z-pinning also allows the same good surface finish as the unpinned laminate.

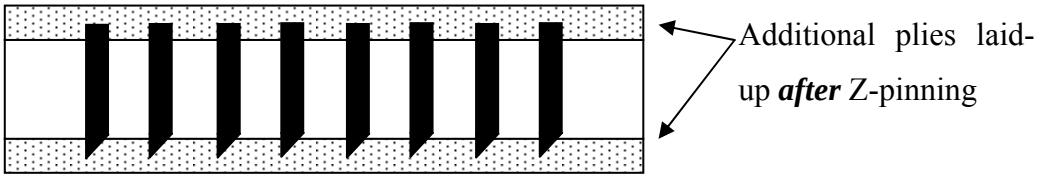

Figure 3-11: *Partially Z-pinned laminate; excess Z-pin length accommodated in additional laminate layers*

3.4.2 Resin pocket geometry

When inserting a Z-pin in a UD material the bulk of the laminate fibres are pushed away by the Z-pin and a resin rich area forms around the Z-pin, as illustrated in Figure 3-12. The shape of this resin "pocket", as it is called, will depend on the Z-pin diameter and the adhesion between laminate fibres through the uncured resin. The Z-pin density can also affect the formation of the pocket, as illustrated in Figure 3-13. If the spacing between the Z-pins, which is inversely proportional to the density, is too small, then two resin pockets may join into a continuous one. Even if such high density is not used, still variations of Z-pin spacing can occur.

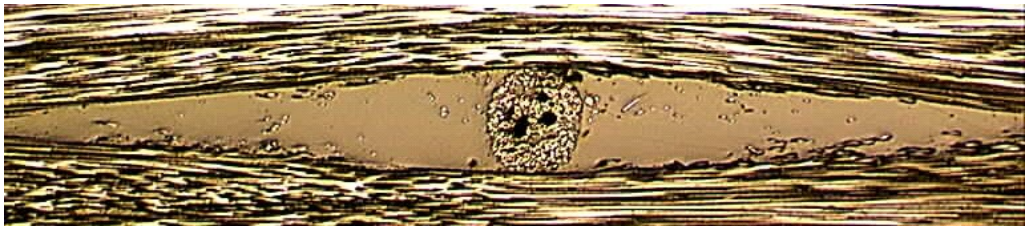

Figure 3-12: *Typical resin pocket in a UD, IMS/924 laminate (0.28mm Z-pin diameter)*

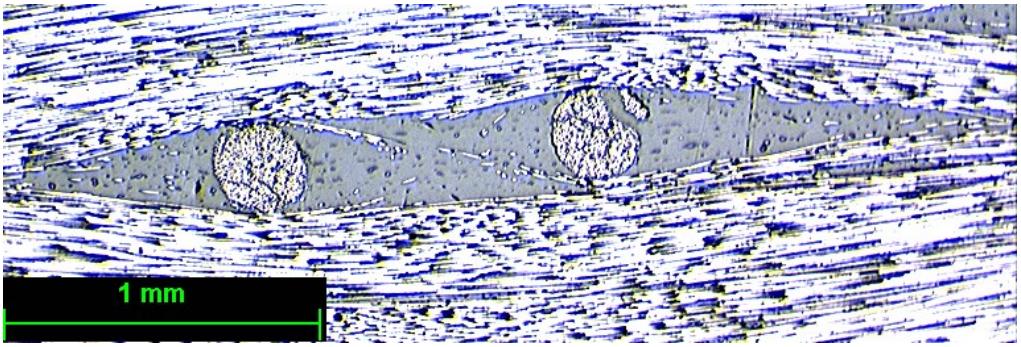

Figure 3-13: *Resin pockets "merging" together (0.28mm Z-pin diameter).*

From observations of the manufactured Z-pinned laminates, three types of resin pockets were identified and are depicted in Figure 3-14. On acquired images of such resin pockets, measurements were performed on certain dimensional characteristics, all depicted in Figure 3-14. L is defined as the resin pocket half length, l is the minimum opening of a merging resin pocket, and D represents the maximum opening of the resin pocket. This dimension is not equal to the diameter of the Z-pin, as it is the projection of the Z-pin onto the plane of a ply of the laminate. The value for D should coincide with the diameter of the Z-pin when then Z-pin is inserted orthogonally. The value of D increases proportionally to the cosine of the Z-pin angle.

Figure 3-15 presents the average value of D for each type of resin pocket for one material (IMS/924) and Z-pins of 0.28mm diameter and 2% density. There is clear indication that a larger value of D is related to the merging type of resin pocket. The Z-pin angle therefore increases fibre misalignment (as D increases), as well as the percentage and distribution of the resin rich areas. This indicates that the *Z-pin angle can have an effect on the in-plane properties* of a laminate made of UD material. This effect is apparent in all UD materials in this study and both Z-pin diameters. Such an example for the 0.5mm diameter Z-pin is illustrated in Figure 3-16.

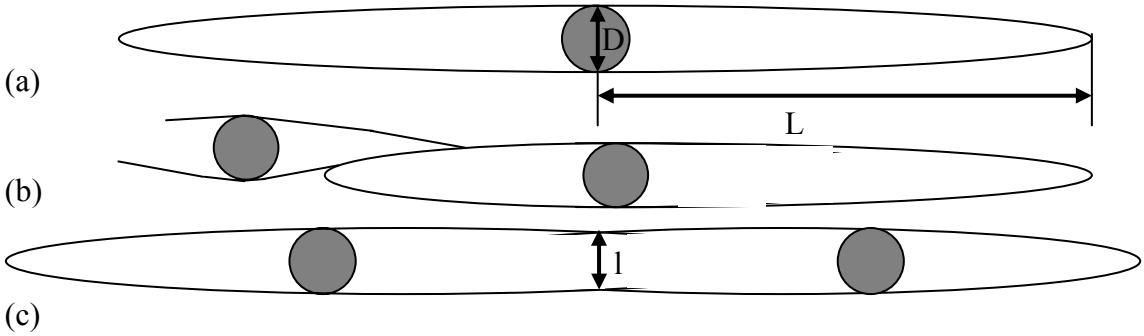

Figure 3-14: *Distinct types of resin pockets in a UD laminate. (a) Standard, (b) Weaving, and (c) Merging. Characteristic resin pocket dimensions also depicted.*

If the stacking sequence of the laminate is multi-directional, the length (2 times L - Figure 3-14) of the resin pockets will be smaller, as the frictional forces between plies with fibres of different orientation will restrain fibre movement during insertion. The magnitude the Z-pin angle effect will therefore be proportionally smaller; still the nature of the effect of Z-pin angle is expected to be the same. Figure 3-17 displays the tighter curvature of laminate fibres around a Z-pin in the ply boundary of a cross ply laminate.

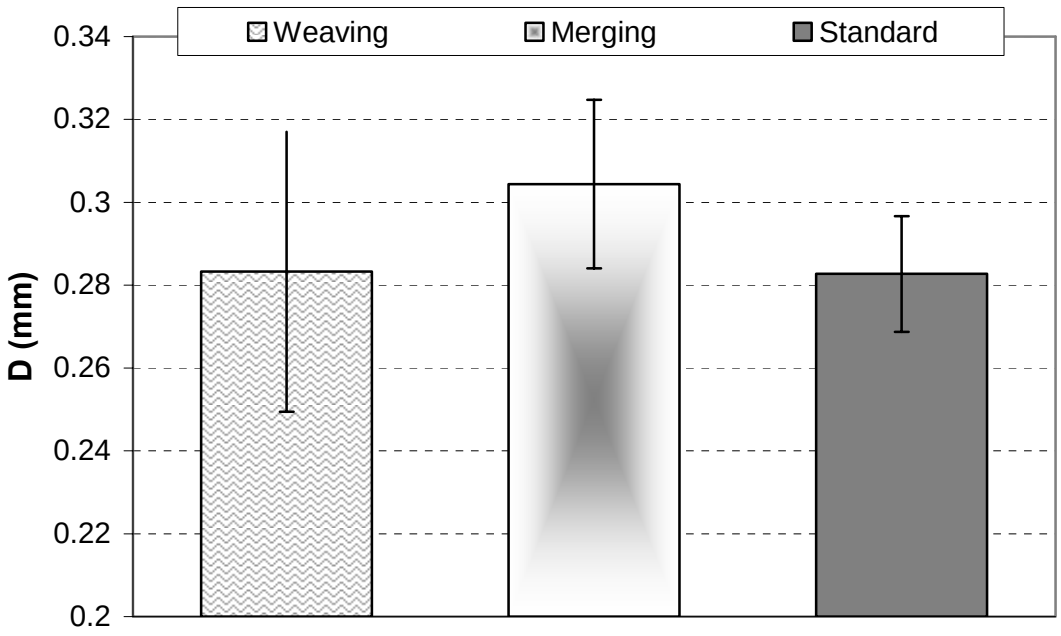

Figure 3-15: *Average values of dimension D for each type of resin pocket, in a UD, IMS/924 laminate (2% density, 0.28mm Z-pin diameter).*

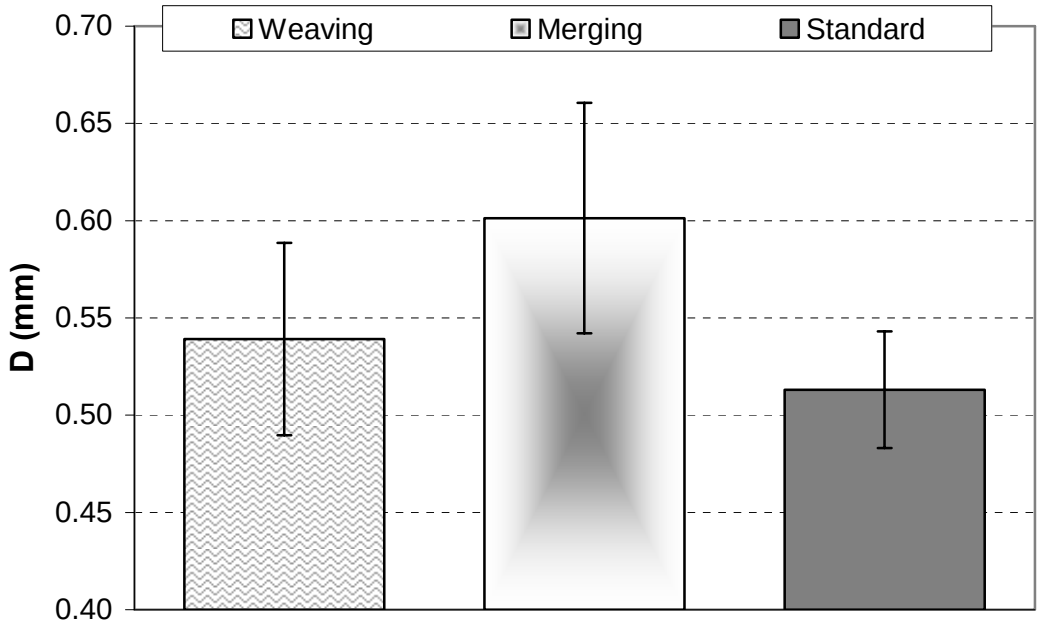

Figure 3-16: *Average values of dimension D for each type of resin pocket, in a UD, IM7/877-2 laminate (2% density, 0.5mm Z-pin diameter).*

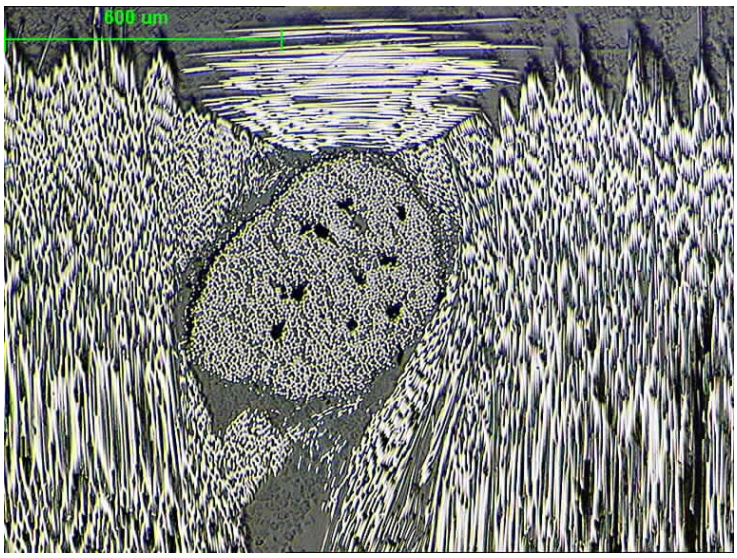

Figure 3-17: *Section of IM7/M21 cross ply laminate, made of UD prepreg, at a ply boundary, illustrating the tight curvature of laminate fibres around a Z-pin of 0.5mm diameter.*

The insertion of Z-pins in a prepreg with woven architecture has a minimal effect on the orientation of the bulk of the laminate fibres. The in-plane alignment of laminate fibres

is not visibly affected close to the Z-pin (Figure 3-18a). The visible resin rich areas in the woven laminates are an inherent property of this kind of material and are not created by Z-pin presence (Figure 3-18b).

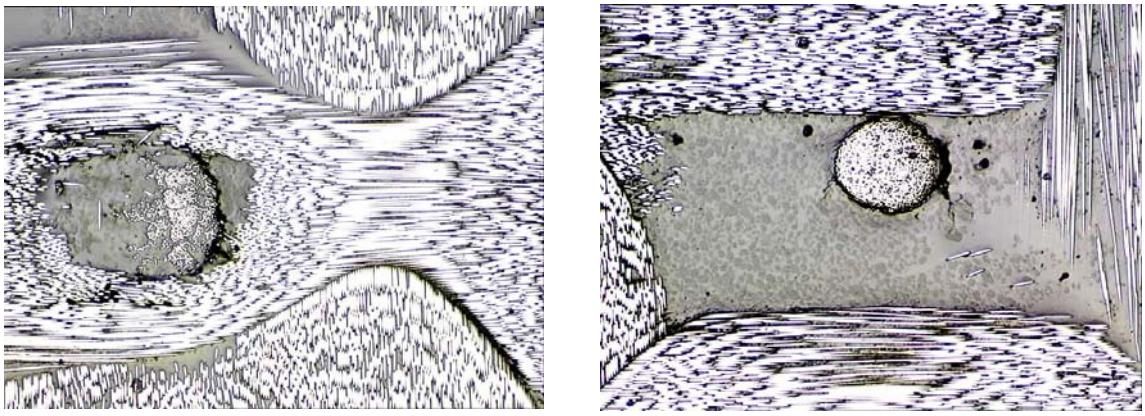

(a) *(b)*

Figure 3-18: *(a) 0.5mm Z-pin in a woven laminate (G986/M21) and (b) 0.28mm Z-pin in a resin rich area of the same material.*

3.4.3 Through-thickness geometry

The insertion of a Z-pin into a laminate has additional effects on the out-of-plane, or through-thickness plane geometry of the laminate. Laminate fibres fracture and tilt into the through-thickness direction. An extreme example is illustrated in Figure 3-19a, where the resin pocket of a 0.5mm Z-pin in a T300/914 laminate is full of sectioned laminate fibres. These fibres have been pulled along the insertion path of the Z-pin or have been fractured during insertion. This is not uncommon with 0.5mm diameter Z-pins and UD laminates. Damage observed for smaller diameter Z-pins (0.28mm) is more uncommon. Similar effects of fibre damage and through-thickness misalignment, due to the Z-pins, is also observed in woven laminates. Figure 3-19b portrays a Z-pin in the fracture plane of a G986/M21 woven delamination coupon after testing. The laminate fibres on its base have been fractured during insertion.

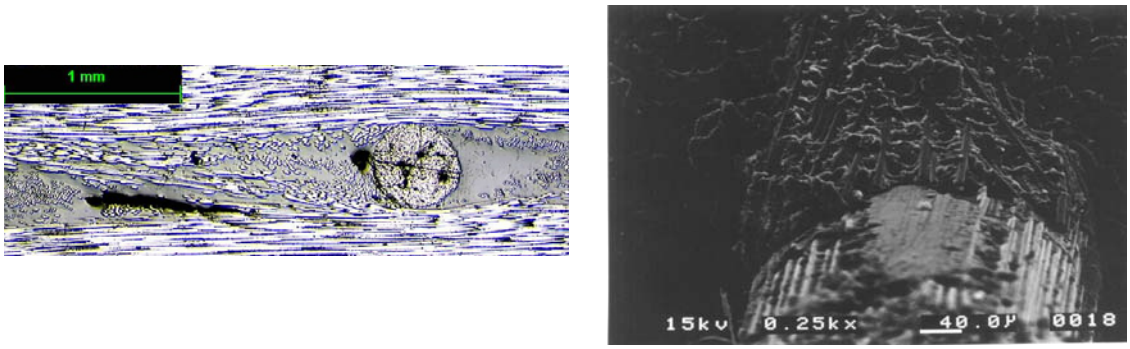

(a) *(b)*

Figure 3-19: *(a) Resin pocket in a T300/914 laminate (0.5mm diameter Z-pin), displaying laminate fibre fracture and (b) fractured laminate fibres along a pulled-out Z-pin*

Through-thickness misalignment is increased significantly when an excessive insertion Z-pin length is present, due to the aforementioned tendency of the Z-pins to tilt during cure (Figure 3-20).

Figure 3-20: *Increased laminate fibre waviness, after Z-pin tilting, due to excessive Z-pin depth*

The phenomenon intensifies along the insertion path of the Z-pin. The first layers of laminate fibres can move more freely to accommodate the Z-pin compared to the fibres in the centre of the thickness of the laminate. Any through-thickness laminate fibre misalignment imposed in the centre seems to carry itself along the rest of the thickness of the laminate (Figure 3-21).

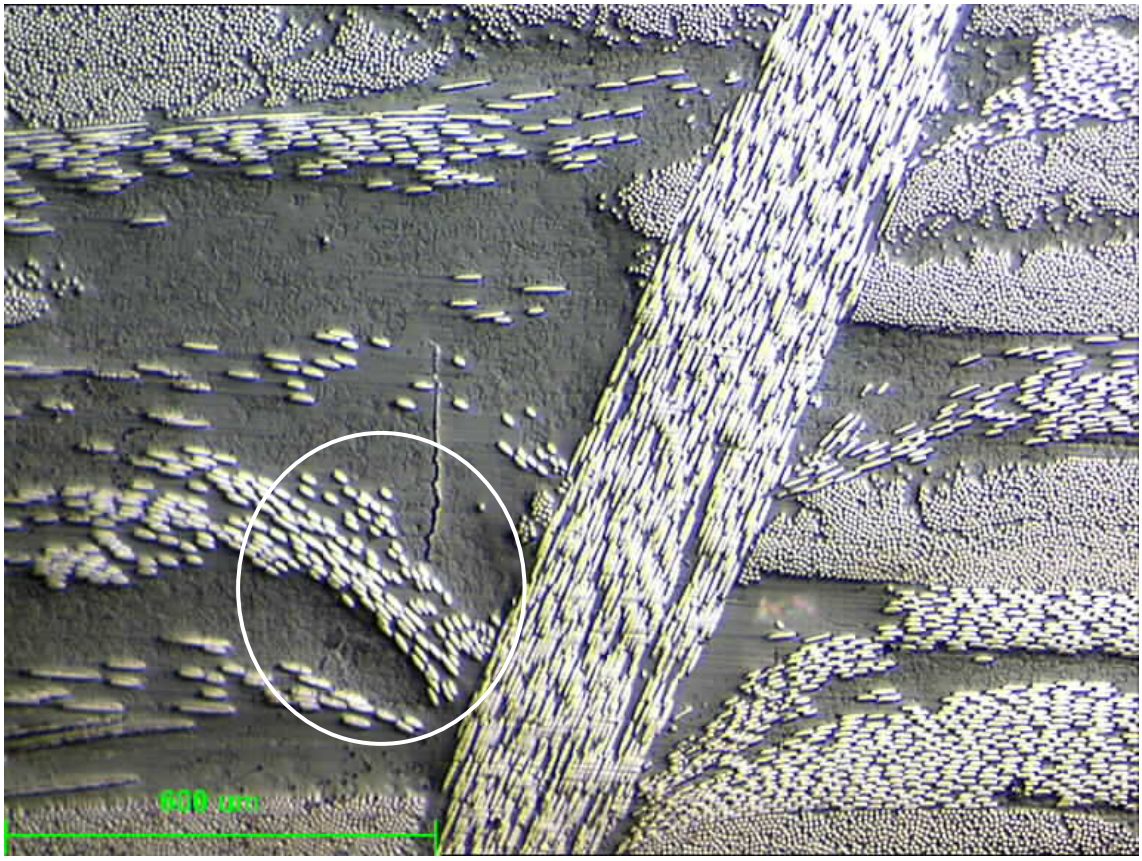

Figure 3-21: *Microscopy image of a side section of an angled Z-pin (0.28mm), showing through-thickness misalignment of laminate fibres (G986/M21).*

Alternatively, the laminate fibres can prove stronger than the Z-pin and cause the Z-pin to split during insertion (Figure 3-22). This is more likely to occur in UD laminates than in multi-directional ones. Similarly to laminate fibre misalignment, it is more pronounced for larger diameter Z-pins (0.5mm).

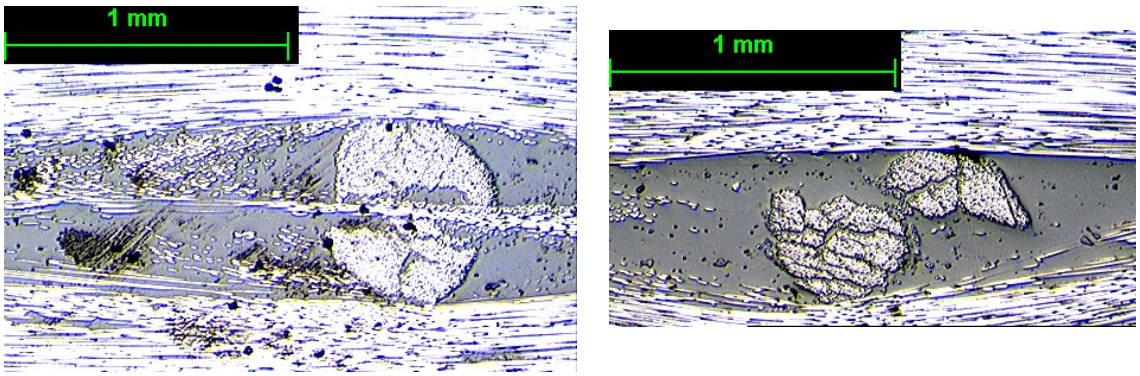

(a) *(b)*

Figure 3-22: *Z-pins split during insertion (UD, IMS/924)*

3.4.4 Specimen thickness variation

Despite the optimised compaction procedure before Z-pinning, the final cured thickness of a Z-pinned laminate is greater than the thickness of an unpinned laminate. The area of the manufactured laminates that was covered with Z-pins was a fraction of the total laminate area. This ratio is maintained in most testing coupons. The thickness of the Z-pinned area was measured and contrasted to the nominal thickness of the same material (without Z-pins) in all coupons. The average thickness increase for UD is presented in Figure 3-23 and for woven in Figure 3-24.

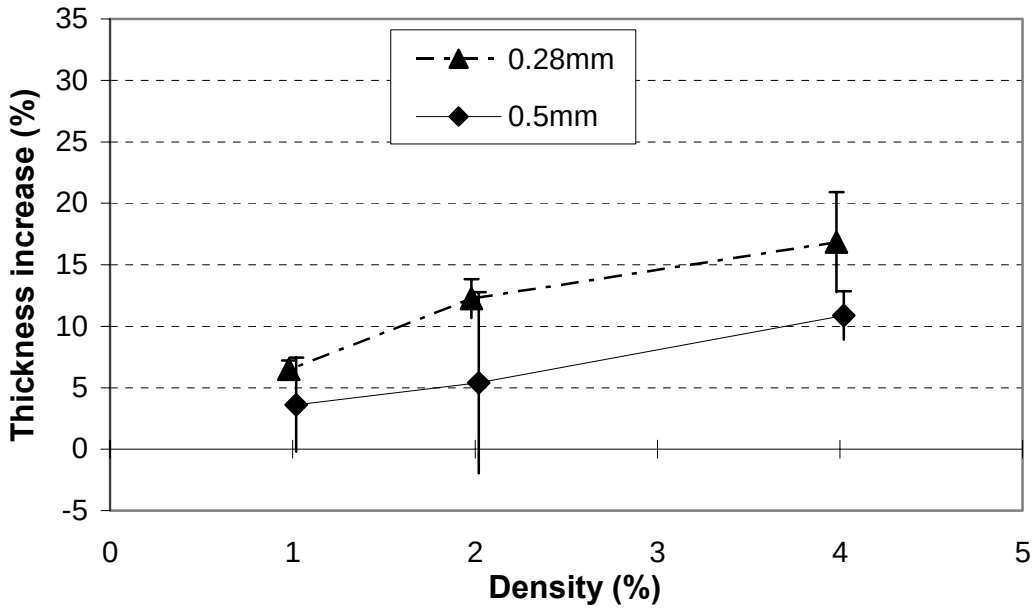

Figure 3-23: *Average thickness increase of a Z-pinned part of the laminate compared to the nominal (unpinned) thickness as a function of Z-pin density for all UD materials in this study and both Z-pin diameters*

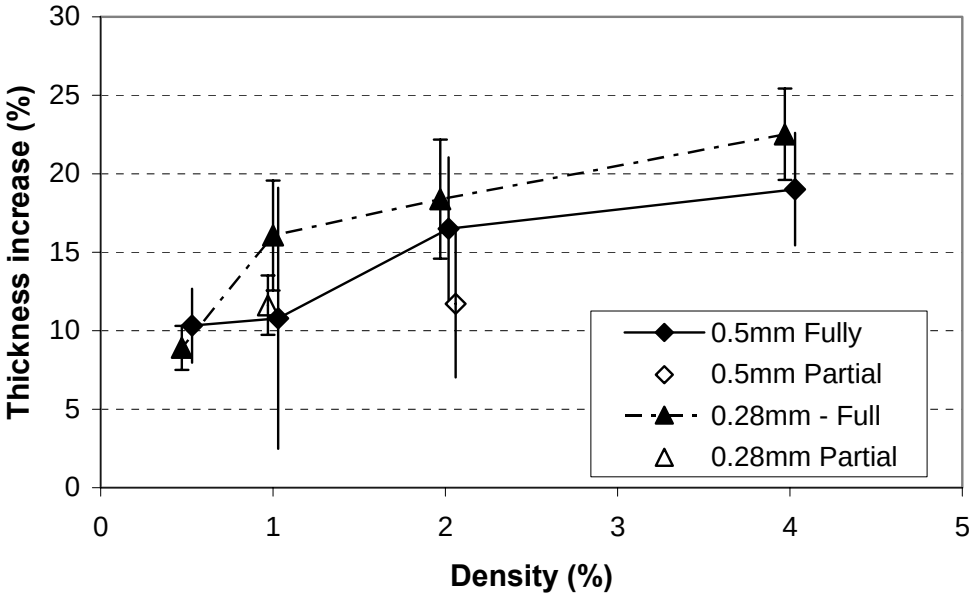

Figure 3-24: *Average thickness increase of a Z-pinned part of the laminate compared to the nominal (unpinned) thickness as a function of Z-pin density for all Woven materials in this study and both Z-pin diameters*

The error bars are equal to one standard deviation. The Z-pin densities are slightly offset on the horizontal axis for visual clarity. The graph for the woven material shows a relation between the increases in thickness and the increase in Z-pin density. Small diameter Z-pins (0.28mm) seem to have a greater effect than large ones (0.5mm). Partial pinning has a smaller effect on thickness; however it is not zero and the percentage increase is greater than the percentage value of Z-pin density, which equates to the volume fraction of the additional material inserted. The increase in thickness is close to the average value of the difference in thickness between the uncured compacted laminate and the nominal cured thickness (Table 3-3). The maximum increase is substantial and can reach up to 20%. Nonetheless, UD material exhibits a smaller sensitivity to increase of thickness than woven material.

When manufacturing a laminate with Z-pins in only a part of its total area, a variation of thickness throughout the laminate is expected. In order to attain a laminate with a thickness as uniform as possible, a thick (3.2mm) metallic plate was placed on top of the laminate during cure (Figure 3-6). Such a metallic plate would provide a uniform

compaction distribution on the laminate and is difficult to bend under autoclave pressure during cure. Despite that precaution, a variation in thickness within coupons is present. The variation is depicted in Figure 3-25 for UD and Figure 3-26 for woven material.

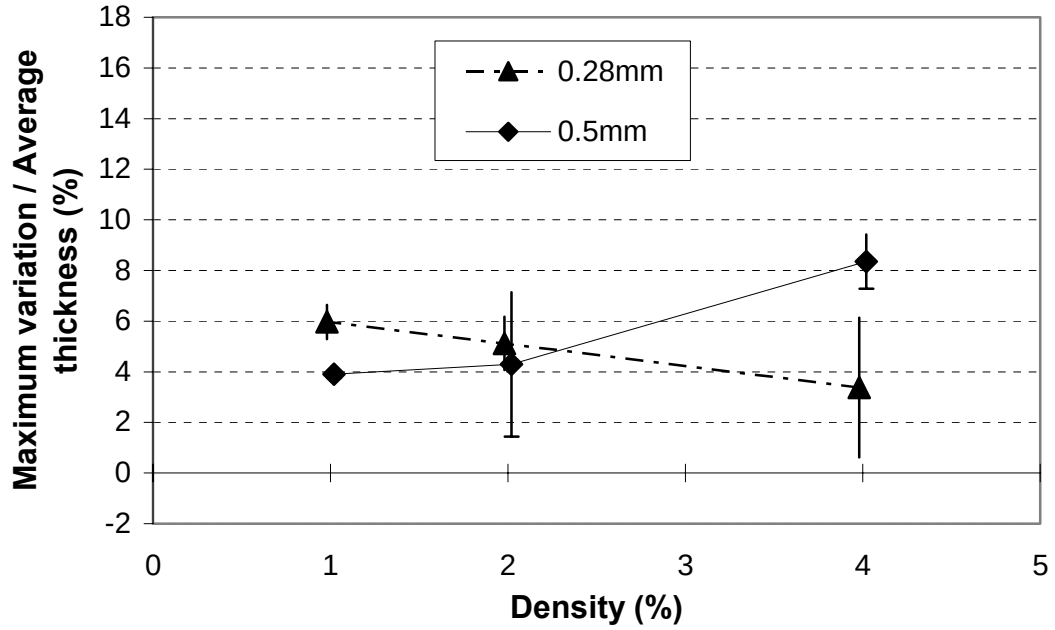

Figure 3-25: *Maximum variation in thickness of a UD laminate compared to the average laminate thickness as a function of Z-pin density, for both Z-pin diameters.*

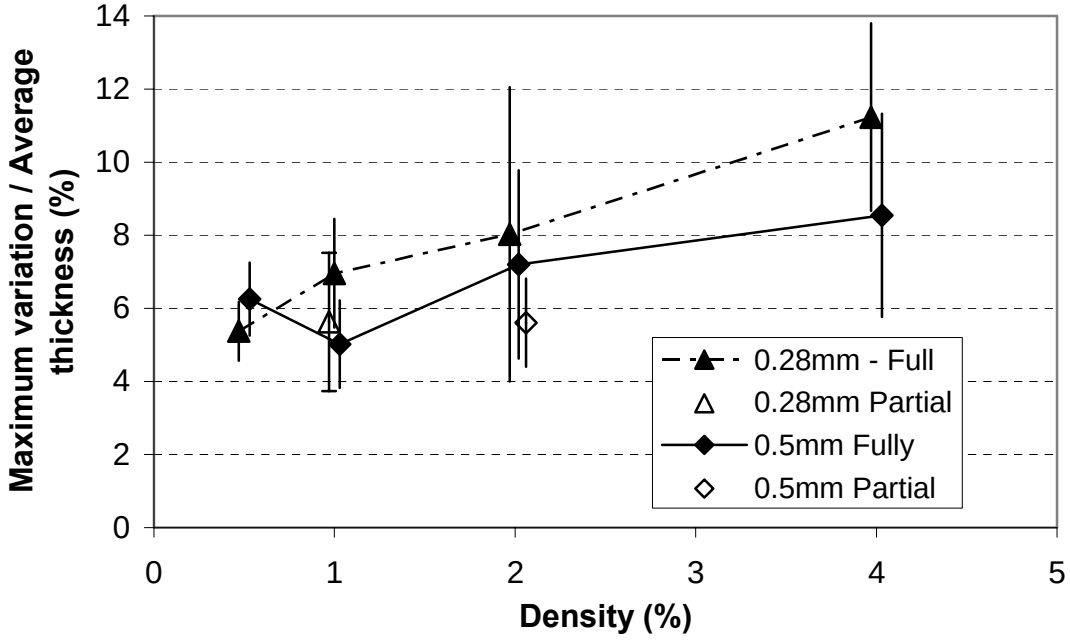

Figure 3-26: *Maximum variation in thickness of a woven laminate compared to the average laminate thickness as a function of Z-pin density, for both Z-pin diameters*

Both Z-pin diameters are considered. The y axis value is the maximum difference in thickness within a coupon over the average thickness of the coupon. This is plotted as a function of Z-pin density. Error bars are one time the standard deviation.

Trends are similar to those for the thickness increase to the nominal cured thickness. This variation in thickness within a coupon can have an effect on measurements. As will be explained in section *5.3.2*, values calculated from delamination tests are affected. This is also significant when designing a Z-pinned tension specimen, as will be explained in section 6*.3.2*.

3.5 Experimental apparatus

All thickness measurements were performed using a set of digital callipers (accuracy of ±0.01mm) or a micrometer (accuracy of ±0.01mm). A microscope with a digital gauge (accuracy of ±0.001mm) was used to measure the dimensions of the gauge length of the Iosipescu specimens.

All mode I delamination tests were performed using a Zwick screw driven testing machine with a load cell of 2.5kN. A screw driven INSTRON testing machine with a load cell of 5kN was used for mode II delamination tests, SENB tests and Iosipescu tests. The Z-shear test, the friction test, (both described in chapter 5) and the pull-off test (described in chapter 7) were also performed using the same machine.

Open-hole tensile tests were performed using a 100kN INSTRON testing machine with hydraulic grips and a 250kN INSTRON testing machine with bolt tightening grips.

Self-tightening grips were used for tensile specimens, incorporating alignment pins to ensure simultaneous sliding of the jaws and prevent the development of undesirable shear stresses. Specimens were placed with the tabs inside the jaws, as the jaws are manufactured with a minor chamfer at their ends to allow a degree of softening of the

load transition. This conforms to current practice [82]. A screw driven INSTRON testing machine with a load cell of 100kN was used.

Strain measurements were performed using a National Instruments (type SC-2345) strain gauge bridge and modules. The measurements were logged using LabView code.

3.6 Summary

Careful control of the insertion parameters is essential for high quality Z-pinning. The gantry provides significant improvement in procedure control and quality. The required operator experience is easily acquired.

An increase in thickness is noted after insertion. This is a function of Z-pin spacing and therefore combination of Z-pin density and diameter. It is also a function of initial laminate thickness and insertion depth. This can lead to the insertion of a Z-pin length greater than the nominal cured thickness of the laminate. Inclination of the Z-pins to the normal can emerge after cure to accommodate the excessive Z-pin length. Careful control of the insertion Z-pin length (or insertion depth) and sufficient consolidation of the laminate prior to pinning is therefore essential.

Inclination of the Z-pins to the normal can also emerge during cutting of Z-pins, but it can be avoided given the appropriate care during manufacturing. The resulting quality also depends on material type. There is indication of a potential connection of the effect of Z-pin angle to in-plane properties.

An additional technique to restrict or avoid Z-pin angle presence is partial pinning. Partially pinned laminates have minimal Z-pin angle, good surface finish and decreased thickness variation. A variation in thickness exists within a laminate, when Z-pins do not cover the whole of its surface. The C-Scan technique is best suited for quality inspection.

Three types of resin pockets have been identified. The geometry of resin pockets depends on the stacking sequence and material type.

Z-pinning inflicts minimal laminate fibre damage. Out-of-plane misalignment can be present. Contrary to a stitched laminate, this is more pronounced in the centre of the laminate and is usually carried to last part of the thickness to be pinned. The magnitude of misalignment varies along the laminate.

4 Response to Mode I Loading

4.1 Mode I delamination testing

Delamination tests under mode I loading conditions were carried out following the ISO 15024, implementing the Double Cantilever Beam (DCB) geometry. The standard dictates specimen dimensions, specimen preparation and testing conditions for UD laminates. Woven laminates were tested following the same standard, as no alternative protocol exists.

Specimens were cut to the suggested width (20mm) using a dry diamond coated saw. The edges were slightly polished and then coated with a correcting fluid to facilitate crack growth measurement. End blocks were bonded using high temperature adhesive (120 C), after abrading the appropriate faces of the specimens. Such a mode I delamination specimen is depicted in Figure 4-1.

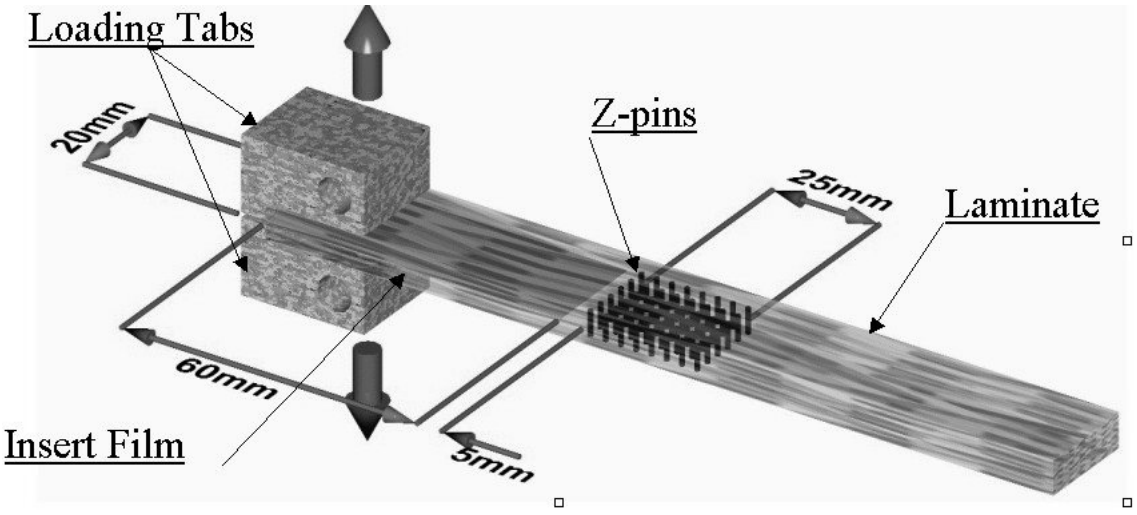

Figure 4-1: *Mode I delamination specimen; dimensions, insert film, pin position, end blocks and loading displayed*

The thickness suggested by the standard for UD carbon fibre specimens is 3mm. In this study the effect of laminate thickness was one of the parameters under investigation. The thickness of the specimens manufactured ranges from 3mm, to 4mm and to 6mm for UD specimens and from 3.3mm, to 4.4mm and to 6.6mm for woven specimens. Both unpinned and Z-pinned specimens were tested. The crack propagates in the middle plane of the specimen and initiates from a 12.5μm thick PTFE film, which is placed in the middle plane during the lay-up procedure. Using such a crack initiator, no pre-cracking is required [84-88]. Z-pins are positioned 5mm after the initial crack front (Figure 4-1), following the concept of evaluating the effectiveness of Z-pins to arrest an existing crack [20,47,48,89].

The loading is applied by increasing the opening displacement at a rate of 1mm/min. The load and the opening displacement were recorded electronically, while measurements of crack propagation were recorded manually, every millimetre if possible, by eye, with the help of a magnifying lens. For each measurement taken, an "event" is stored electronically in the software used. These "events" (a combination of load and displacement) were matched afterwards to the respective crack lengths for data reduction. When crack propagation displays "stick-slip" behaviour, where the crack arrests and re-initiates, as with testing Z-pinned laminates, the operator ideally needs to take measurements of the load, the displacement and the crack length exactly at every re-initiation point. With computer controlled testing machines working in real time, this is not always possible. Systematic recording of the crack propagation of a Z-pinned laminate is therefore important and a fine mesh of measurements can compensate for this inconvenience [20,22].

Data reduction is focused on calculating the critical strain energy release rate, G_{Ic}, or simply delamination toughness of the material. Three methods can be used for data reduction. First, the ***beam theory method*** evaluates the toughness using the following equation:

$$G_{IC} = \frac{3P\delta}{2ba} \tag{4-1}$$

Secondly, the ***corrected beam theory method*** incorporates the correction factors Δ, N and F. The toughness is finally expressed as:

$$G_{IC} = \frac{3P\delta}{2b(a+|\Delta|)}\frac{F}{N} \tag{4-2}$$

$$\text{With: } F = 1 - \frac{3}{10}\left(\frac{\delta}{a}\right)^2 - \frac{3}{2}\left(\frac{\delta l_1}{a}\right) \tag{4-3}$$

$$\text{and: } N = 1 - \left(\frac{l_2}{a}\right)^3 - \frac{9}{8}\left[1 - \left(\frac{l_2}{a}\right)^2\right]\left(\frac{\delta l_1}{a}\right) - \frac{9}{35}\left(\frac{\delta}{a}\right)^2 \tag{4-4}$$

Where:

$|\Delta|$: Crack length correction defined as the intercept of the plot of C1/3 versus crack length with the x-axis

F: displacement correction due to end block presence

N: stiffness correction due to end block presence

l_1 & l_2: characteristic end block lengths [iso]

Last, the ***experimental compliance method*** can be used. The compliance of the beam can be fitted with two parameters, *k* and *n*, determined experimentally by plotting C as a function of α. The aforementioned correction factors N and F can be included in the final expression of the toughness:

$$G_{IC} = \frac{nP\delta}{2ba}\frac{F}{N} \tag{4-5}$$

$$\text{With: } C = ka^n \tag{4-6}$$

The corrected beam theory method tends to produce the most conservative results [82]. In this study, data was reduced using the experimental compliance method, due to the unreasonable magnitude of correction factor Δ, according to [90], significantly fluctuating among similar types of specimens. A spreadsheet supplied by the ESIS committee was used to perform the data reduction [91].

4.2 Unreinforced resin testing

The SENB test configuration is used to characterise the toughness of plastics in terms of the critical stress intensity factor K_C and the energy per unit area of crack G_C, or simply toughness, at crack ***initiation*** [92]. Since the toughness G_C of the resin is a defining factor for the toughness of the composite, these data are valuable. The toughness of M21 and M36 epoxy based toughened resin systems had not been determined before this study. SENB tests were performed on samples from both resins.

The materials were supplied by Hexcel Composites Ltd., Duxford UK, in the form of fully cured plaques of uniform thickness. In the case of the M21 resin, two plaques were received; one consisting of the resin in its final form, which contains some toughening particles, and another consisting of the base resin without the toughening particles. Specimens were cut from the plaques; the dimensions are determined in the protocol in terms of ratios rather than actual values. If B is the thickness and W is the height of the specimen, a relation of 2B W 4B is suggested by the protocol (Figure 4-2). Since B is equal to the thickness of the plaques received and was therefore fixed, all dimensions of the specimens were determined by this value. The thickness of the plaques received and all specimen dimensions are presented in Table 4-1, for both materials. The actual span of the specimens was larger than the span required for the test to facilitate trouble-free positioning of the specimens. Increased specimen length also improves specimen alignment. The effective value of the span is the distance between the lower two rollers during the test (Figure 4-2).

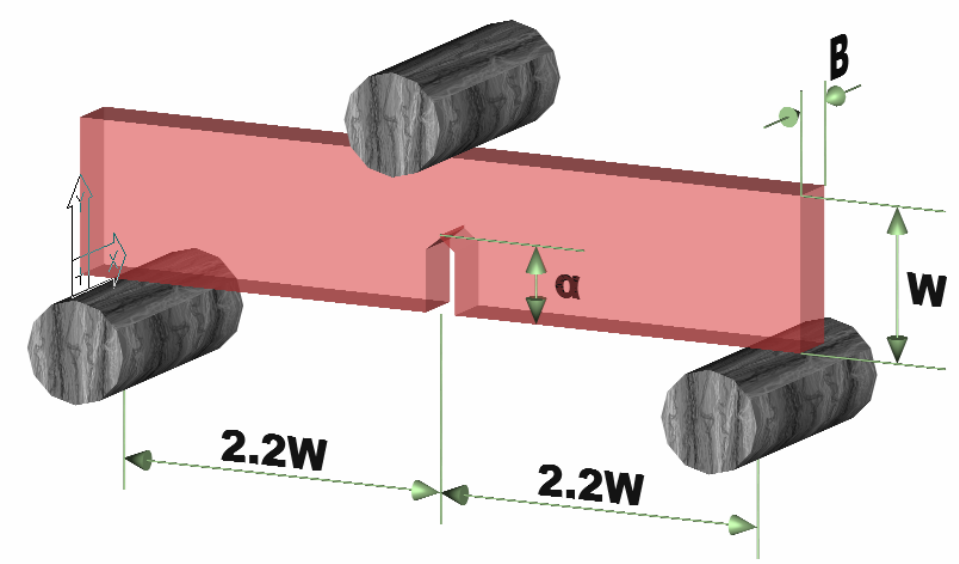

Figure 4-2: *Configuration of the SENB test*

Material	Plaque thickness B (mm)	W (mm)	/W
M21 (untoughened)	5-6	12	*0.5*
M21	4	9	*0.5*
M36	*7-8*	*20*	*0.5*

Table 4-1: *Specimen dimensions for the three types of resin systems under test*

After cutting the specimens to size, a notch is introduced in the middle of the span. The depth of this notch is half the specimen height. In order to obtain a valid measurement, the notch needs to be sharp, defined by a high ratio of crack length to crack tip radius. The notch is further sharpened using a razor as depicted in Figure 4-3a. The height from which the weight was dropped was the same for all specimens to obtain identical sharpening among specimens; this was confirmed after testing by measuring the razor sharp part of the notch. The height, determined by trial and error, was such as to obtain a long enough notch without further damaging the specimens in any way.

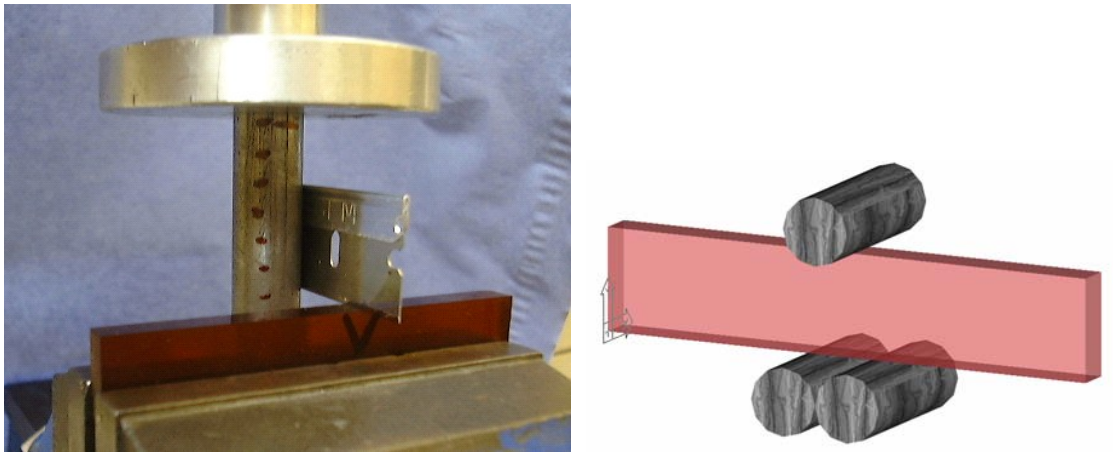

(a) (b)

Figure 4-3: *(a) Mock-up specimen preparation; notch sharpening, and (b) configuration for determining compliance correction of the SENB test*

Plastics are viscoelastic materials, thus the temperature and cross-head rate are specifically defined as 23 C and 10mm/min respectively. Furthermore, displacement data have to be corrected for total system compliance, loading pin penetration and sample compression. By using the arrangement of Figure 4-3b, at an unnotched part of the sample, the total compliance correction can be determined. This is subtracted from the compliance curve measured during the test.

Equations (4-7) and (4-8) give the required K_C and G_C values. The results for both resin systems are presented in Figure 4-4. Error bars demonstrate the accuracy of the measurement with 97.5% confidence level for a two sided normal distribution [93].

$$K_{IC} = \frac{f \cdot P_{\max}}{B \cdot W^{0.5}} \tag{4-7}$$

$$G_{IC} = \frac{1}{2} \frac{P_{\max}^2 \left(C - C_{CORR}\right)}{B \cdot W \cdot \varphi} \tag{4-8}$$

$$\text{With:} \quad f = 6a^{1/2} \frac{\left[1.99 - a(1-a)(2.15 - 3.93a + 2.7a^2\right]}{(1+2a)(1-a)^{3/2}} \tag{4-9}$$

$$\phi = \frac{A + 18.64}{dA/da} \tag{4-10}$$

$$A = \frac{16a^2\left[8.9 - 33.717a + 79.616a^2 - 112.952a^3 + 84.815a^4 - 25.672a^5\right]}{(1-a^2)} \qquad (4\text{-}11)$$

f: calibration factor

φ: energy calibration factor

Where: C: specimen compliance

C_{CORR}: compliance correction

P_{max}: Maximum load, as defined in the protocol

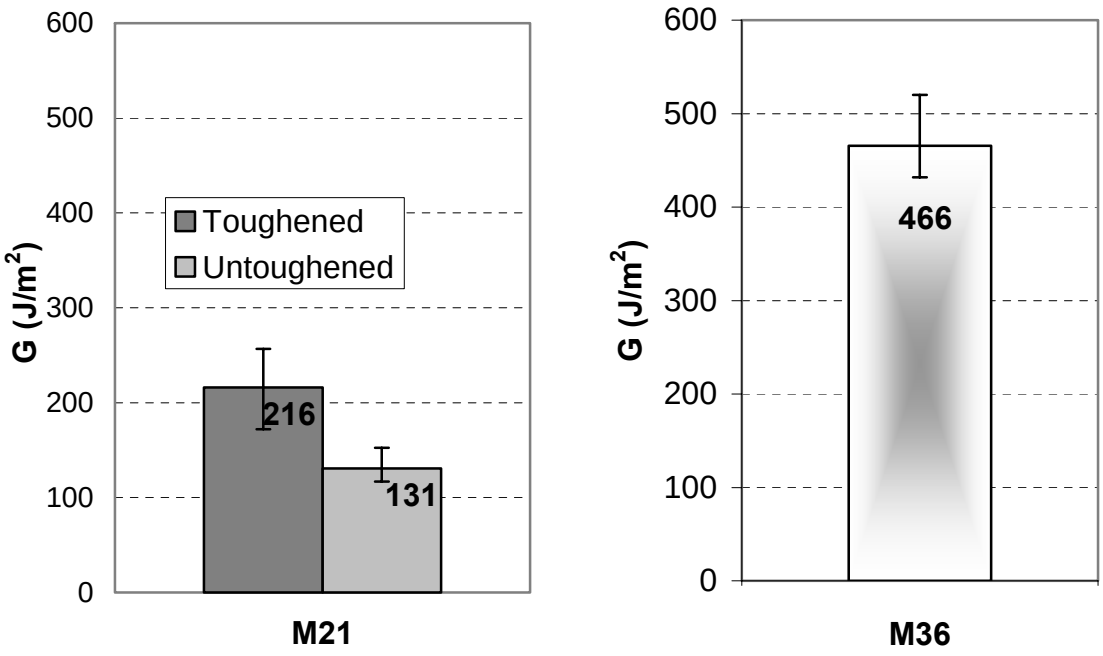

Figure 4-4: *Toughness of M21 and M36 resin systems*

Optical microscopy and SEM observations reveal the micro-structure of each resin system. The 'untoughened' M21 specimens do not display any distinguishing features. The toughened M21 resin contains a significant number of particles, with a size in the range of 30μm (Figure 4-5a). M36 consists of a larger number of toughening particles, of a smaller size, in the range of 15μm (Figure 4-5b). The toughening particles act as spacers between plies allowing the formation of a resin layer between individual plies, as well as instigate dispersion of the crack front into a tortuous path to enhance delamination resistance.

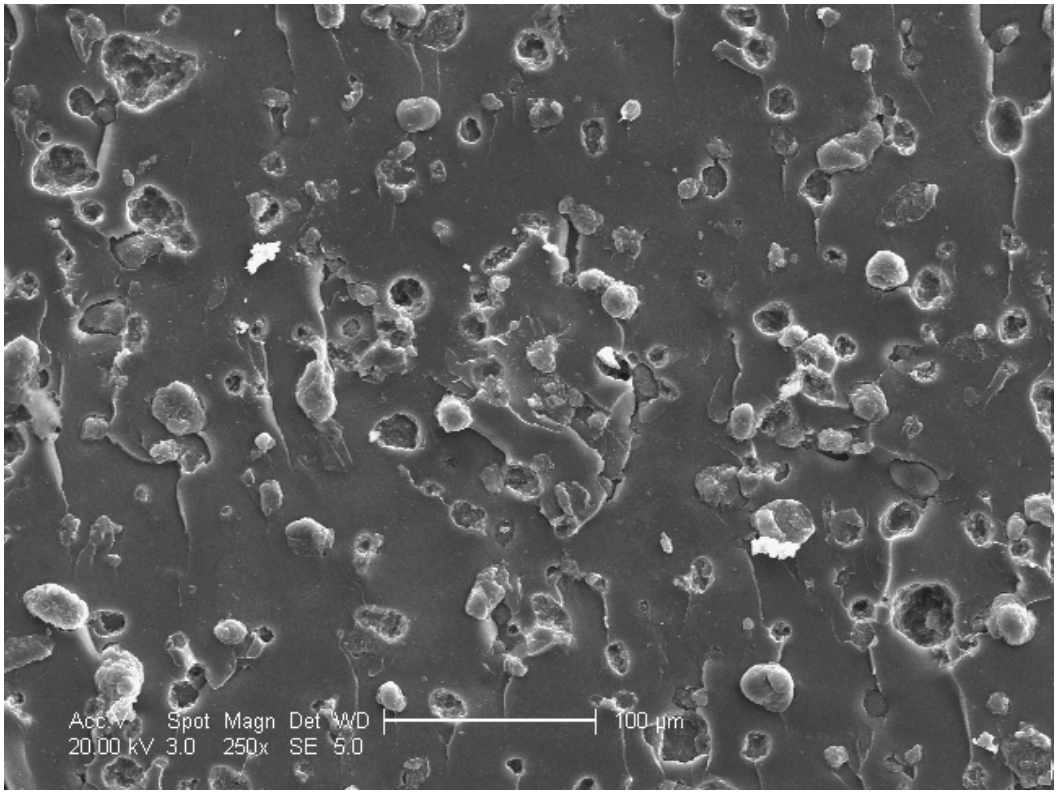

(a)

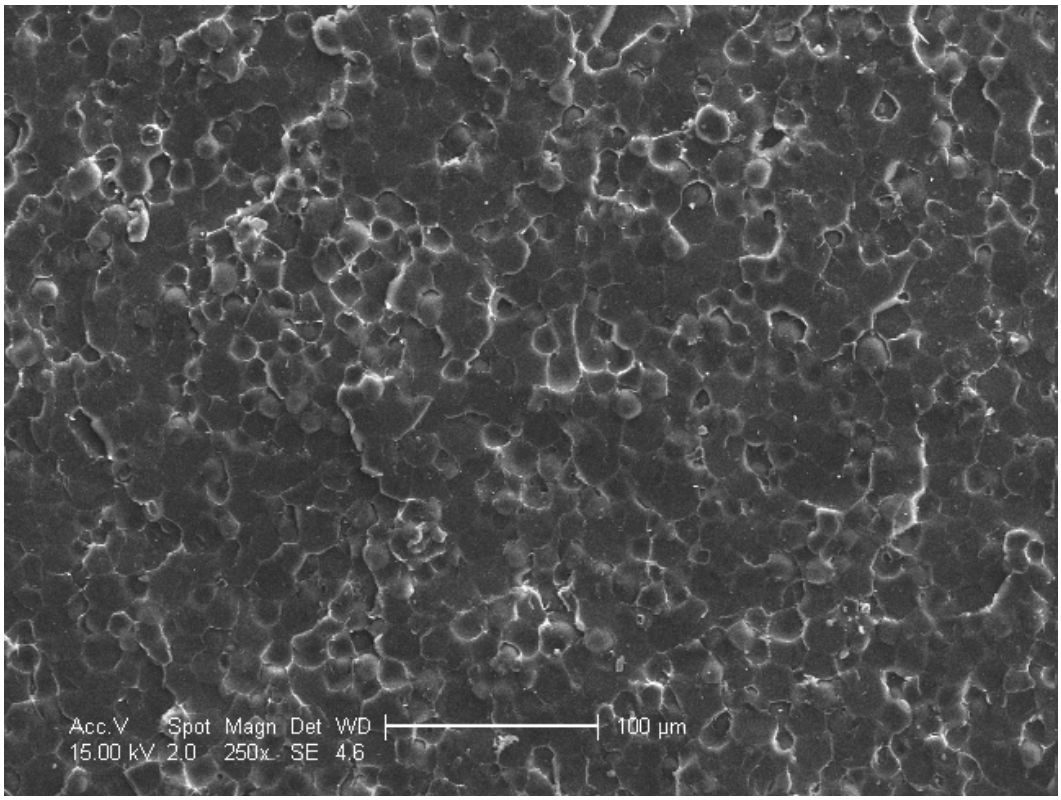

(b)

Figure 4-5: *(a) SEM image of M21 resin system, (b) SEM image of M36 resin system*

The corresponding impregnated woven materials used in this study (G986/M21 and G986/M36) contain the resin on the outside of the plies in uncured form; the central part of the prepreg is relatively dry. Full impregnation of the fibres takes place during cure. Toughening particles are infiltrated by the fibres, so base resin mostly occupies the central part of each ply after cure. Figure 4-6 illustrates the fracture surface of a delamination specimen; the location is a resin rich area at a junction of crossing fibres.

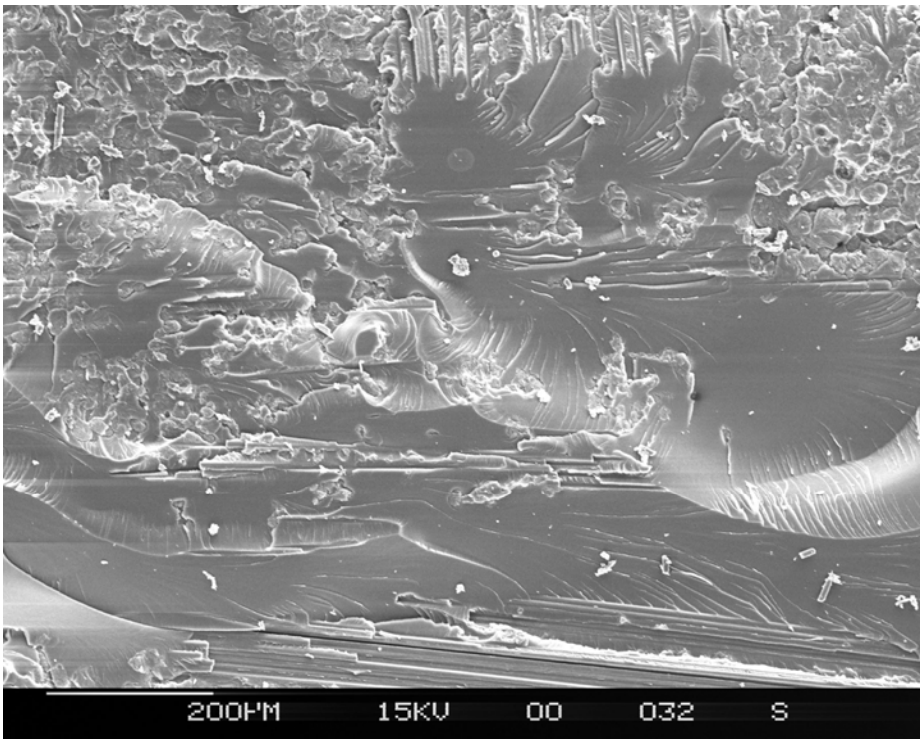

Figure 4-6: *Fracture surface at a junction of crossing fibres*

4.3 Mode I test cases

Table 4-2 lists all UD specimens used in this part of the study; Table 4-3 lists woven fabric specimens. The specimens are categorized according to their thickness, the Z-pin density, Z-pin diameter and the insertion depth. Specimens with any inconsistencies regarding their manufacturing quality and anomalous behaviour during testing were eliminated from the results. The specimens presented are the specimens that were finally chosen to construct the database.

Unpinned specimens were manufactured with every cure cycle that was carried out. Unpinned specimens help in evaluating the quality of the laminates and in ensuring that any variability caused solely by the curing procedure is accounted for.

The delamination tests of IMS/924 UD specimens are the work of Barattoni, and results are reproduced in this document from reference [94].

Material	Thickness (mm)	Density (%)	Diameter (mm)	Insertion depth (mm)	No. of samples
T300/914	6mm	---	---	---	*5*
T300/914	6mm	2	0.5	Full	*6*
T300/914	6mm	2	0.28	Full	*5*
T300/914	4mm	---	---	---	*2*
T300/914	4mm	2	0.5	Full	*6*
T300/914	4mm	2	0.28	Full	*5*
T300/914	3mm	---	---	---	*2*
T300/914	3mm	2	0.5	Full	*4*
T300/914	3mm	2	0.28	Full	*4*
IMS/924	6mm	---	---	---	*5*
IMS/924	6mm	2	0.5	Full	*5*
IMS/924	6mm	2	0.5	4	*4*
IMS/924	*6mm*	*2*	*0.5*	*3*	*5*

Table 4-2: *Mode I test cases of UD specimens*

Material	Thickness (mm)	Density (%)	Diameter (mm)	Insertion depth (mm)	No. of samples
G986/M36	6.6mm	---	---	---	*4*
G986/M21	6.6mm	---	---	---	*5*
G986/M21	6.6mm	4	0.5	Full	*5*
G986/M21	6.6mm	4	0.5	4.4	*5*
G986/M21	6.6mm	4	0.5	3.3	*5*
G986/M21	6.6mm	4	0.28	Full	*5*
G986/M21	6.6mm	2	0.5	Full	*5*
G986/M21	6.6mm	2	0.5	4.4	*5*
G986/M21	6.6mm	2	0.5	3.3	*5*
G986/M21	6.6mm	2	0.28	Full	*5*
G986/M21	6.6mm	2	0.28	4.4	*5*
G986/M21	6.6mm	2	0.28	3.3	*4*
G986/M21	4.4mm	---	---	---	*2*
G986/M21	4.4mm	2	0.5	Full	*5*
G986/M21	4.4mm	2	0.28	Full	*5*
G986/M21	3.3mm	---	---	---	*2*
G986/M21	*3.3mm*	*2*	*0.5*	*Full*	*1**

Table 4-3: *Mode I test cases of woven fabric specimens*

4.4 Failure mechanisms

Delamination of a Z-pinned laminate under mode I conditions results in gradual pull out of the Z-pins out of the laminate with increasing opening displacement (Figure 4-7a). Pull out is a two phase procedure. Initially, the Z-pin stretches elastically and gradually debonds from the laminate. After complete debonding, Z-pin pull out is controlled by friction. An experimental pull out curve of a single Z-pin is presented in Figure 4-7b. The maximum force generated during the debonding phase does not have to be the same as that in the frictional phase. Figure 4-8a illustrates such a case. However, the opening displacement related with the first phase is in the order of 10-20μm (point A), while the

total opening displacement is equal to embedded length of the Z-pin in the half laminate (point B); namely in the order of a few millimetres. The work associated with the debonding phase is therefore negligible in comparison with the total work [20,77-80]. In terms of energy, the pull out curve illustrated in Figure 4-8b is equivalent and can be used for numerical modelling [78-80].

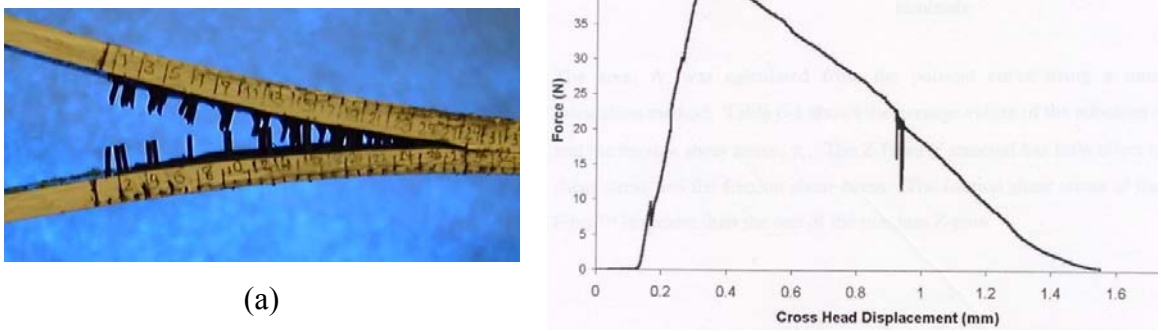

(a) (b)

Figure 4-7: *(a) Z-pin pull out during mode I delamination testing and (b) Experimental pull-out curve of a T300/BMI Z-pin from a UD laminate, after[20]*

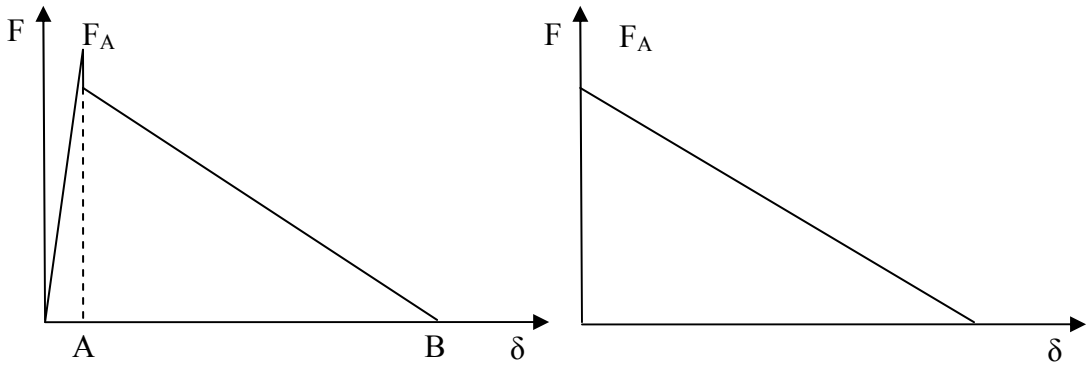

Figure 4-8: *Z-pin pull-out curves (a) complete and (b) energy equivalent simplification*

For a single Z-pin, where D is the diameter and L_P is the embedded length of the pin in the half laminate, under a friction stress τ_F, the force generated during the frictional part of the pull out is:

$$F = \pi \cdot D \cdot \tau_F \cdot L_P \qquad (4\text{-}12)$$

The arms of the mode I specimen undergo bending during the test. With the addition of Z-pins the load required to propagate the crack increases by the amount of load required to pull out the Z-pins. This increases the bending of the arms. Alternative modes of failure can appear if the bending forces exceed the strength of the material. Figure 4-9 illustrates such an occurrence, where bending failure has been initiated and crack propagation has stopped; bending failure follows.

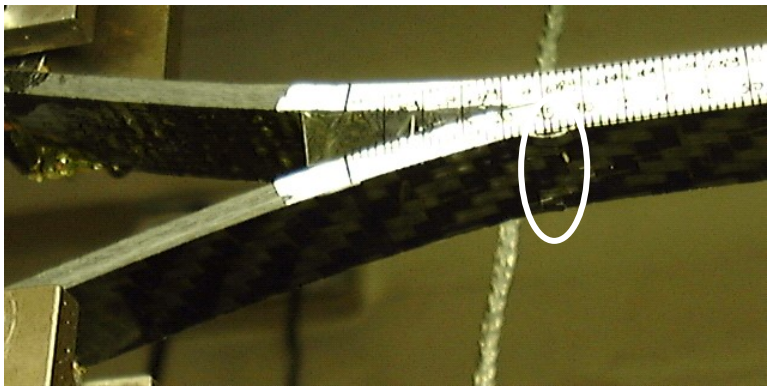

Figure 4-9: *Bending failure during a mode I delamination test of a Z-pinned specimen*

4.5 Stability of crack propagation

The delamination behaviour of all UD unpinned laminates under mode I loading conditions was as expected. In a mode I UD unpinned specimen the load rises linearly until the crack initiation point. The crack then propagates in a smooth manner under a load that decreases asymptotically to a plateau value. Such behaviour of an unpinned UD specimen is depicted Figure 4-10.

If an equivalent specimen contains a block of Z-pins, the crack propagation behaviour changes. The load reaches the same value at the initiation point and then the crack starts to propagate. The load decreases, until the crack advances a little further than the first row of Z-pins, located 5mm from the initial crack front. The Z-pins then begin to resist the opening movement of the arms of the beam and resist crack propagation. The load increases sufficiently to debond and pull out the Z-pins (see section *4.4*). Each row is in

turn debonded and pulled out during the test in small increments. During the time that the load is increasing without any pull out of the Z-pins the crack tip is completely shielded from any additional stress. With every incremental movement of the Z-pins some of the load is transferred to the crack tip. The load, as recorded in the test, is much higher in the Z-pinned specimen and is mostly carried by the Z-pins. This means that the stress transferred to the crack tip at each increment is too much for the crack tip to resist, leading to unstable crack propagation until the next row of Z-pins is introduced to the crack wake. This is described as 'stick-slip' behaviour, where the crack propagates from one discrete row of Z-pins to the next, arresting temporarily at each row Figure 4-10.

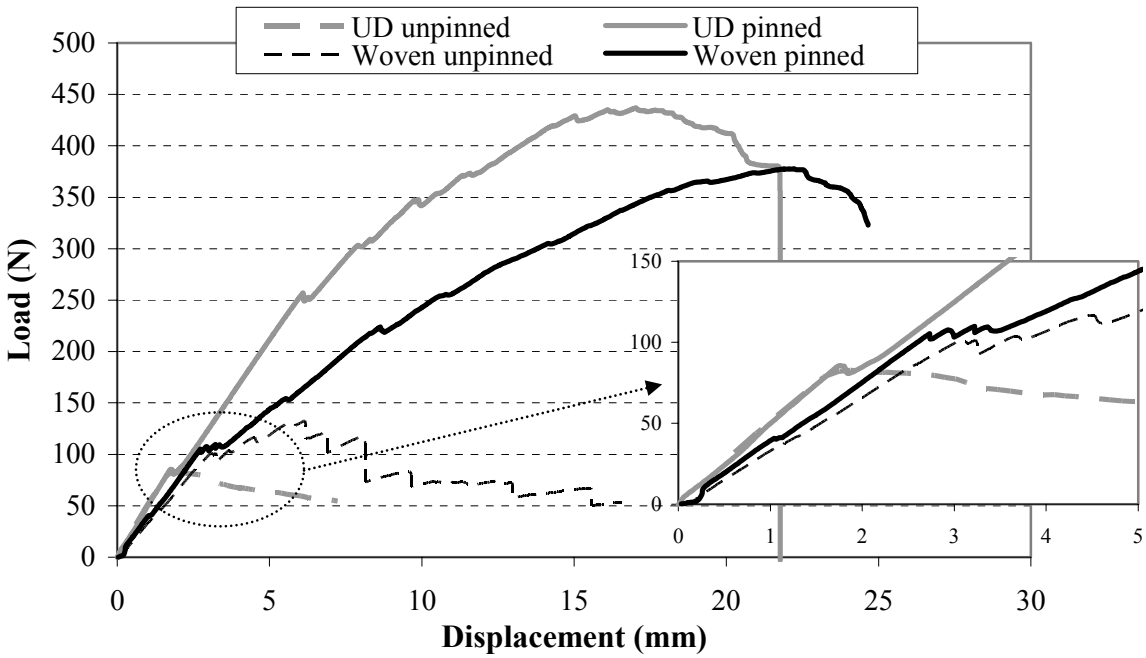

Figure 4-10: *Characteristic experimental curves (Load vs. Displacement) of unpinned and pinned specimens, for woven (G986/M21) and UD (T300/914) material.*

The spacing of the Z-pin rows (and therefore the Z-pin density) dominates the propagation behaviour and in particular the spacing of the load peaks on the experimental curve. The overall propagation behaviour cannot be characterised as unstable; firstly the load carried by the beam is increased by an order of magnitude; secondly, the load increases monotonically until it reaches a plateau. The reason why a plateau value is reached will be investigated in section *4.7*. The specimen fails

catastrophically when the crack propagates past the last row of Z-pins, since the original material, without Z-pins, cannot withstand the increased load.

A certain crack length beyond the Z-pins is required for the Z-pin to begin taking up load in order to inhibit crack propagation [34]. Before such a crack length is reached, the Z-pins are not subjected to any load and therefore do not shield the crack from stresses. Consequently, under mode I loading conditions, a Z-pinned laminate will not exhibit greater resistance to crack initiation. Any variations of the initiation values of a mode I specimen with Z-pins placed exactly at the crack tip, would only originate from the presence of resin rich areas (resin pockets) around the Z-pins. As long as the initial unpinned 5mm section is concerned, the toughness values are always similar to the values of a completely unpinned specimen. This provides a further opportunity to evaluate the manufacturing quality and the suitability or nor of any given data point to be included in the data base.

The response of woven unpinned specimens under mode I loading differs. The load increases up to the point of crack initiation, similarly to the behaviour of UD material. However, the propagation is unstable and the crack jumps considerable lengths. The load fluctuates above and below the value required for initiation. Ultimately, the load reaches a decreased plateau value and the fluctuations disappear (Figure 4-10). This is not unexpected, since it is characteristic of the loading configuration.

As with cross ply or angle ply laminates made from UD material, this fluctuation of load is caused by the constant changes and deviations of the crack path, already explained in section *2.4*. In contrast to UD laminates, the initiation value is not the same between different specimens made of woven material. The outline of the crack front at initiation is randomly determined by the local lay up of the laminate fibres. A different number of 0 /0 , 0 /90 and 90 /90 interfaces, as well as layers of resin of different thicknesses (due to the out of plane waviness) along the crack front, are responsible for the discrepancies in initiation values between specimens. Along a crack tip many times the length of the unit cell of the weave, discrepancies in toughness could fade; in the current configuration, the unit cell of the weave (9mm) is close to half the specimen

width (20mm). The toughness of a number of unpinned woven specimens is presented in Figure 4-11. This behaviour is one reason why average values of similar groups of specimens are used throughout this study.

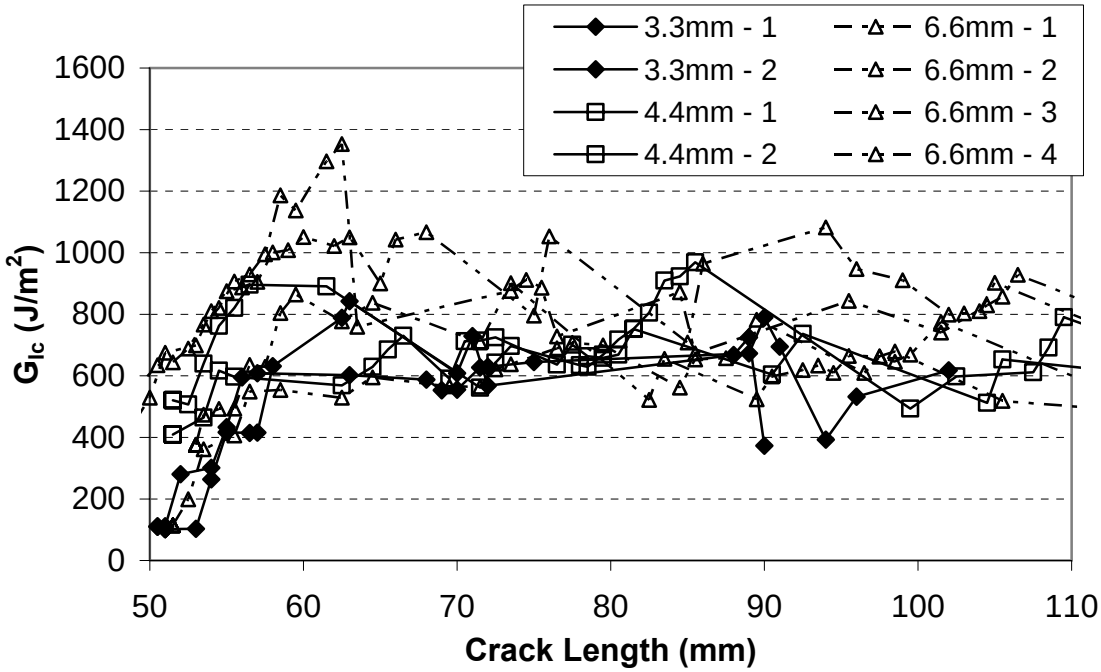

Figure 4-11: *Response of woven (G986/M21) unpinned specimens to mode I loading*

Inserting Z-pins into woven materials has an analogous effect. The load carried by the specimens begins to rise little after the first row of Z-pins and increases in average by an order of magnitude higher compared to unpinned specimens. The load reaches a plateau value and catastrophic failure follows, once the crack propagates past the Z-pinned portion of the beam. Examining the experimental curve (Figure 4-10) reveals that the inherent instability of crack propagation in the unpinned material has faded. The Z-pins again dominate the shape of the experimental curve, only in this case the curve is smooth, especially when using higher Z-pin densities.

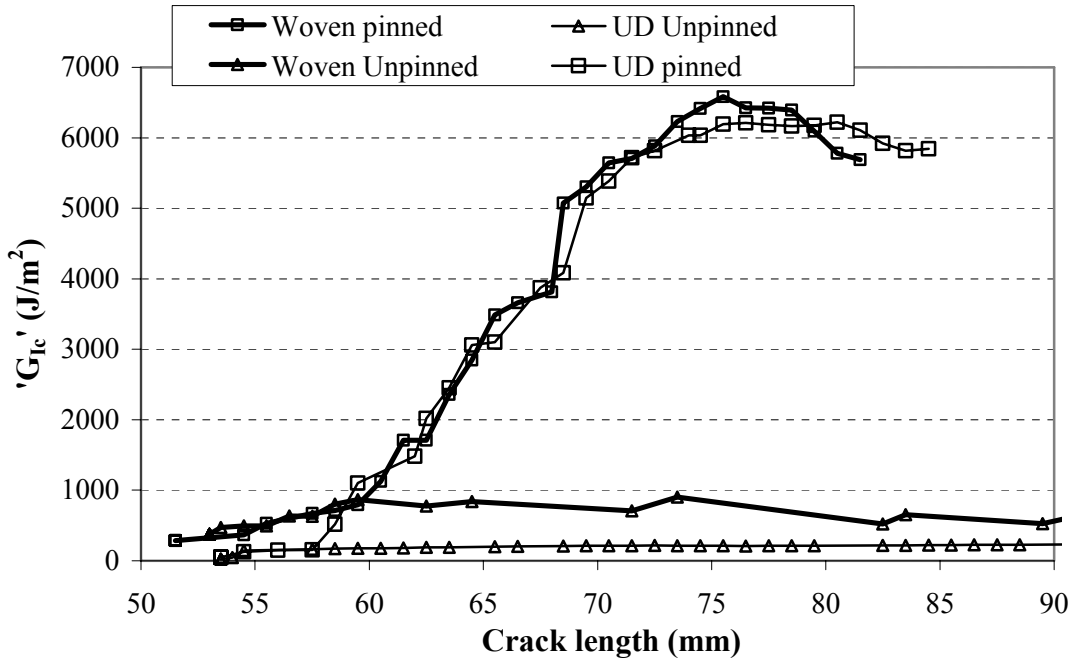

Figure 4-12: *Apparent toughness of unpinned and pinned specimens, for woven (G986/M21) and UD (T300/914) material.*

The instability of the woven material in mode I delamination is apparent in Figure 4-12. The number of measurements taken for the same crack length, shows how much slower and more stable the propagation in the Z-pinned specimen was. Measurements of crack length in the unpinned woven specimen are less dense and greater distances exist between sequential pairs. The stable propagation behaviour of an unpinned UD specimen is also depicted in the same figure.

Last, Figure 4-13 compares the mode I delamination toughness of the two types of woven material used in this study. As predicted, the relation of the toughness between the two - the resin system apart - identical materials, matches the relation of the toughness between the neat resin toughness of M21 and M36 resin systems. The delamination behaviour of both materials is identical and is dependent on the fibre architecture.

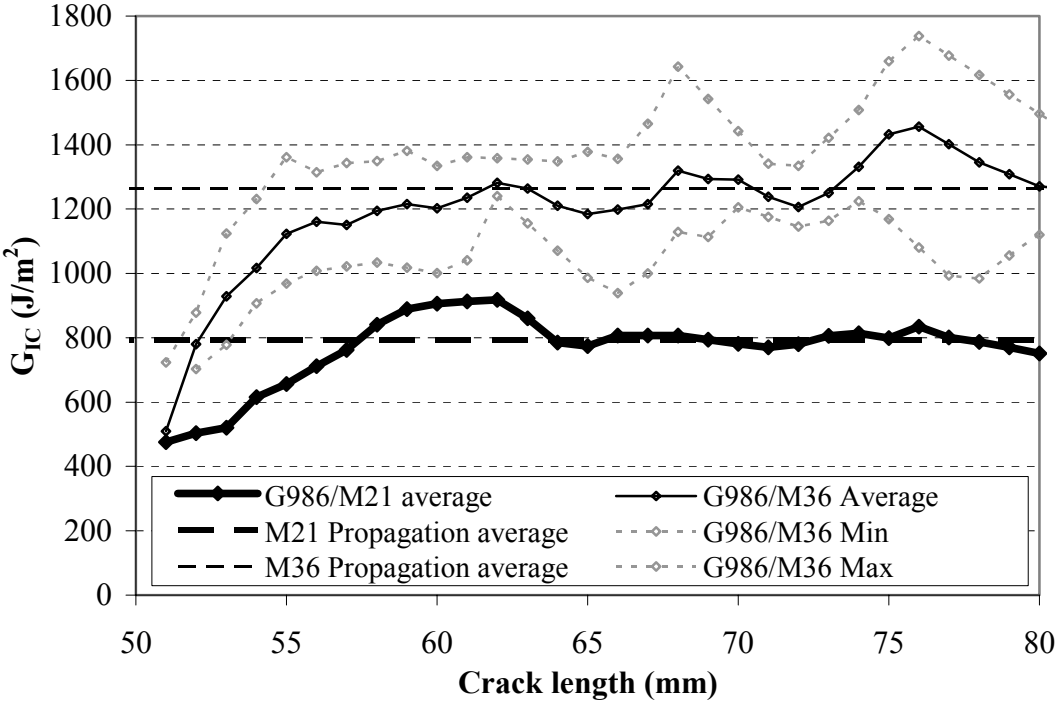

Figure 4-13: *Mode I delamination toughness of G986/M21 and G986/M36*

4.6 Effect of Thickness

Despite the fact that a specific thickness is suggested in the mode I standard, the same value for the toughness can be obtained when testing laminates of thicknesses comparable to suggested, as long as there is negligible laminate fibre bridging during the test. Thicknesses of up to 6.6mm do not invalidate any assumptions on which the data reduction procedure is based, even when testing a woven. In proof of this, Figure 4-14 illustrates the insensitivity of the measurement with respect to specimen thickness; the toughness of woven unpinned specimens with thickness varying between 3.3mm and 6.6mm does not change. In order to facilitate the comparison, average values are used to remove the aforementioned fluctuation. No fibre bridging was observed when testing either UD or woven type laminates under mode I loading conditions.

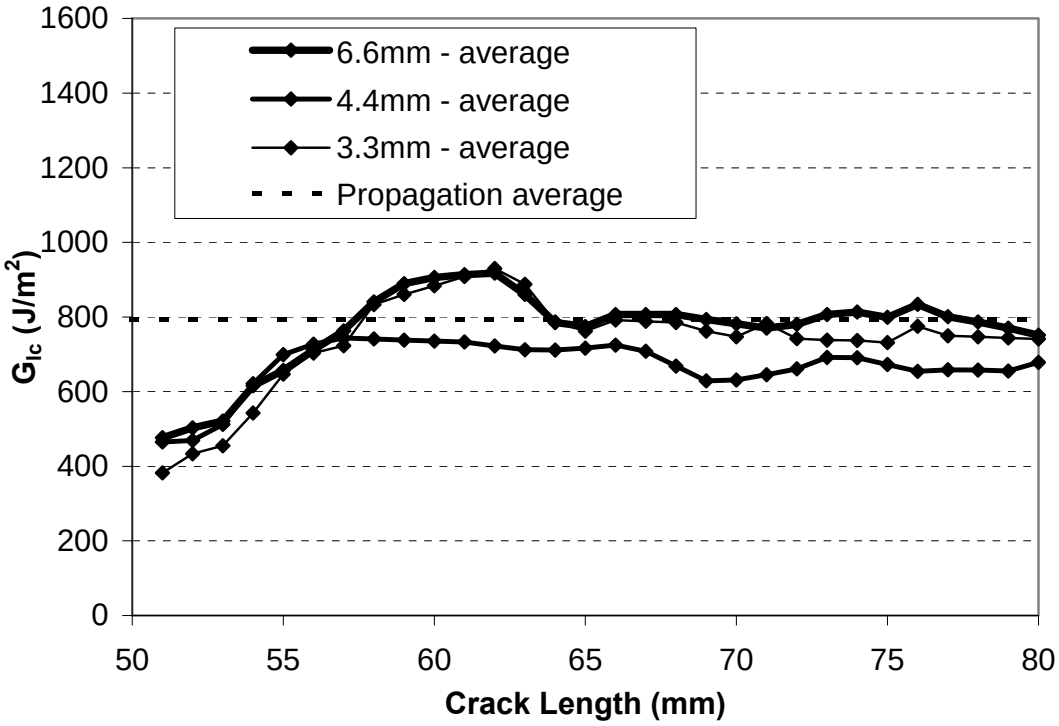

Figure 4-14: *Mode I delamination toughness of G986/M21 for varying laminate thicknesses.*

Toughness values from both UD and woven Z-pinned specimens display a dependence on specimen thickness. Figure 4-15 shows that, for both types of material, the toughness value measured increases as the thickness increases. Toughness values of Z-pinned laminates cannot be used as material properties. They are strictly specimen properties dependent on specimen geometry. The values measured will be therefore referred to as 'apparent toughness'. This is an important point, as it invalidates any use of such toughness values for design purposes using conventional calculation procedures. The significance of these measurements can only be appreciated in direct comparison to an unpinned laminate of the exact same geometry.

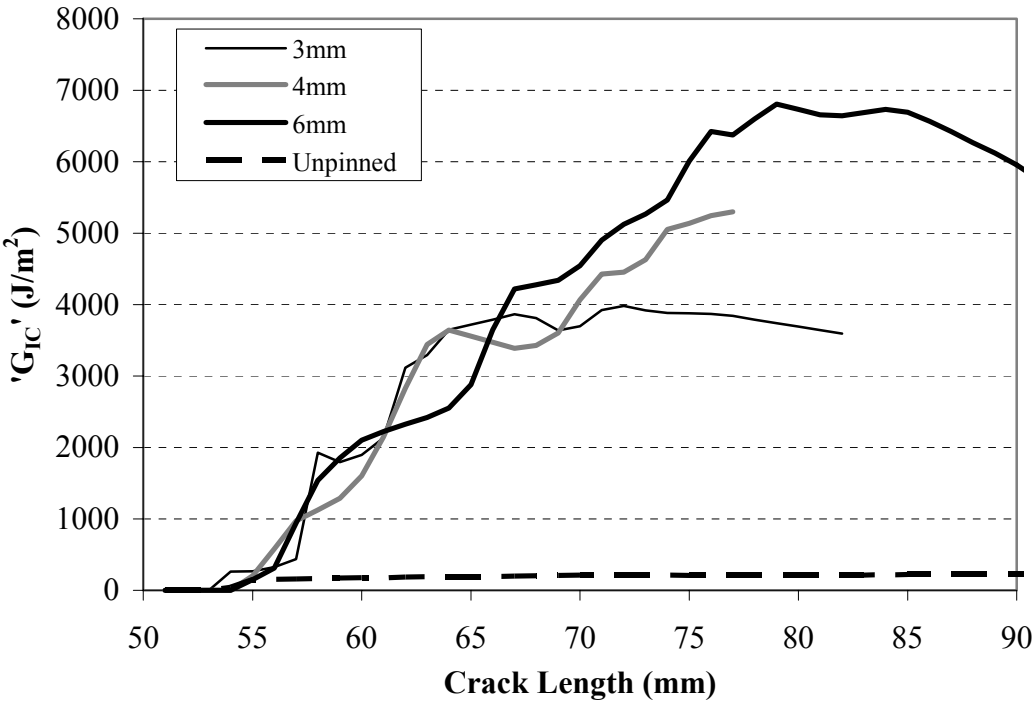

Figure 4-15: *Dependence of mode I interlaminar toughness on the thickness of Z-pinned laminates(UD T300/914, 2% Z-pin density, 0.5mm Z-pin diameter)*

In order to evaluate the effect of specimen thickness by specimen comparison, all remaining parameters need to be identical. This includes Z-pin diameter, Z-pin density and the insertion depth. Figure 4-16 shows the apparent toughness of two such types of specimens (in average values). The density is 2%, the diameter 0.5mm, and the insertion depth is 4.4mm. This was achieved by pinning the whole thickness of a 4.4mm thick laminate and partially pinning a 6.6mm laminate. After testing, the positioning of the Z-pins relative to the initial position of the crack is measured. The distance of the first row from the crack should always be 5mm, however this distance can vary slightly, due to mispositioning of the Z-pin preform on the uncured laminate by the ultrasonic gun operator during manufacturing. In the case depicted in Figure 4-16 this distance was between 7mm and 8mm for one of the types of samples. In order to facilitate comparison between the different types of specimens, the curves were plotted against the positioning of the first row of Z-pins in the specimens. The first row of Z-pins would therefore be placed at zero, while an X-axis value of -5mm would indicate the position of where the initial crack was intended to be. Figure 4-16 shows that the specimens with higher thickness reach higher apparent toughness values.

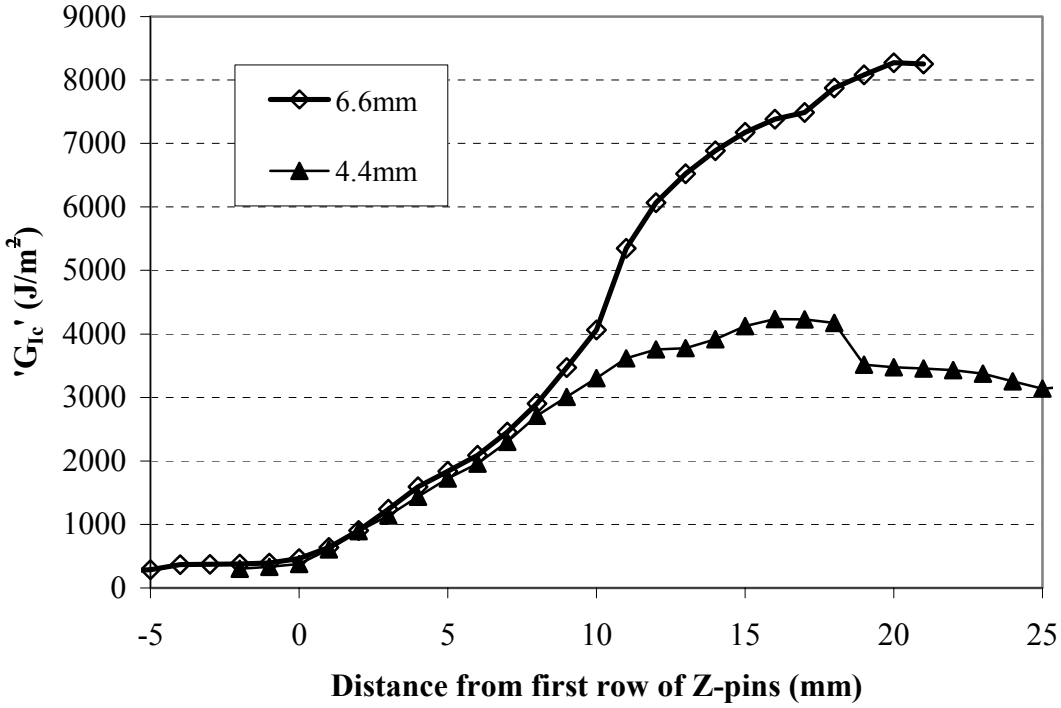

Figure 4-16: *Effect of laminate thickness on the apparent toughness; material G986/M21, density 2%, Z-pin diameter 0.5mm, insertion depth 4.4mm*

This is explained by the fact that the increased thickness provides a beam of higher stiffness, since the product of EI increases, with E being the modulus (same for the two beams) and I the second moment of inertia (proportional to the third power of thickness). The results in Figure 4-17 support further this conclusion. In this case, beams of similar thickness, but of different modulus are compared, with all other parameters remaining the same. The Z-pin insertion depth is 3.3mm. One curve is the average of woven specimens 6.6mm thick, with a 3.3mm insertion depth. The other is the curve from a woven specimen 3.3mm thick, with pins through the whole thickness. The 3.3mm specimen was reinforced externally by bonding 1.5mm thick, UD T300/914 carbon tabs. The total thickness was close to 6.5mm.

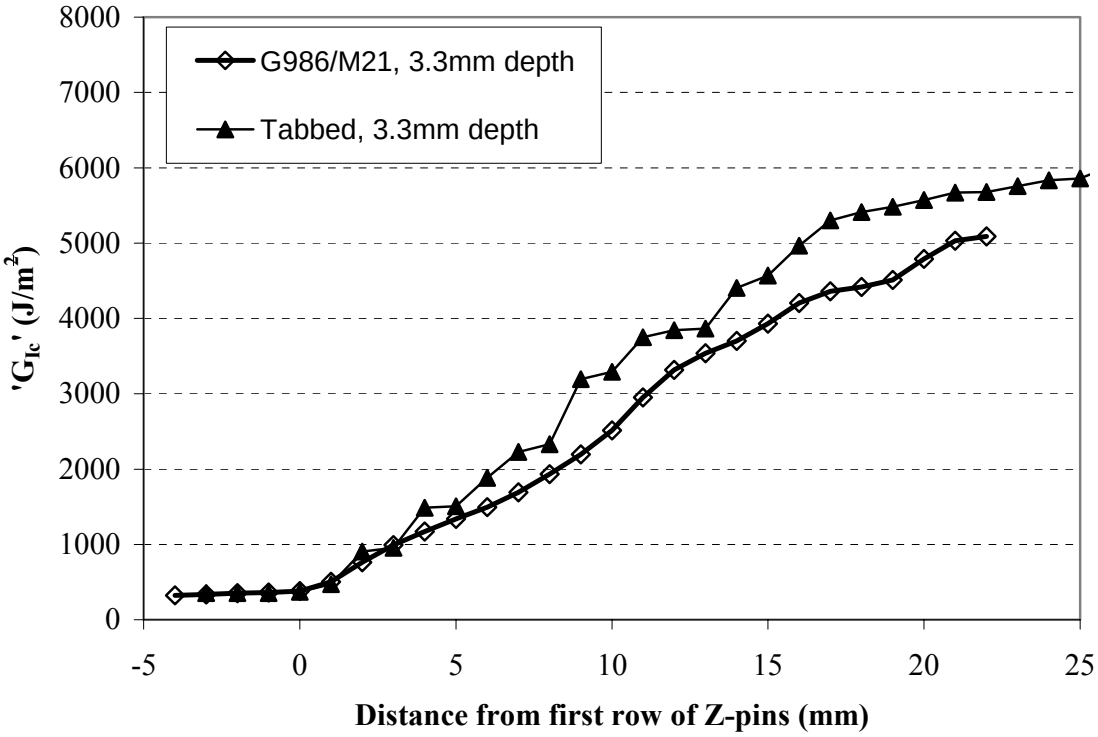

Figure 4-17: *Effect of beam stiffness on the apparent toughness; material G986/M21, density 4%, Z-pin diameter 0.5mm, insertion depth 3.3mm; tabbing material T300/914*

The increased beam stiffness restricts the bending of the arms of the beam, allowing a greater number of rows of Z-pins to resist crack propagation, before any row is completely pulled out. Figure 4-18 illustrates this effect. In the figure both beams appear to have an even distribution of bending along their length. The figure is deceptive in that respect. The bending of the beam is significantly reduced in the bridging zone. The figure illustrates even bending to attenuate the effect and facilitate the appreciation of the mechanism involved. Concluding, the thickness of a Z- pinned laminate affects the length of the bridging zone.

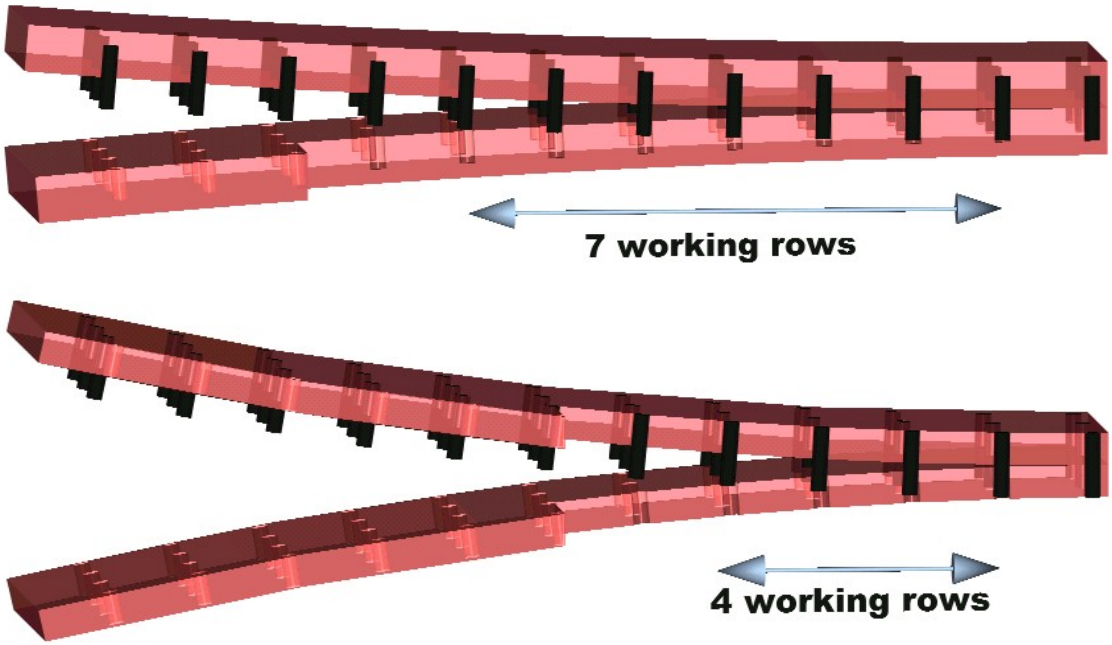

Figure 4-18: *Schematic of the effect of laminate thickness on the bridging zone length*

4.7 Effect of insertion Depth

The effect of Z-pin insertion depth was investigated using specimen comparison. Figure 4-19 shows the apparent toughness of woven Z-pinned specimens with a varying insertion depth. Specimen thickness is 6.6mm, density is 2% and Z-pin diameter is 0.28mm. Curves are plotted again against the positioning of the first row of Z-pins in the specimens. The first row of Z-pins is placed at zero, while an X-axis value of -5mm indicates the position of where the initial crack was intended to be. Figure 4-19 presents a similar arrangement of specimens for a different Z-pin diameter, namely 0.5mm. Propagation values for the fully pinned specimens in Figure 4-19 are obtained only for the first few millimetres; the specimen arms break, as described in section *4.4*.

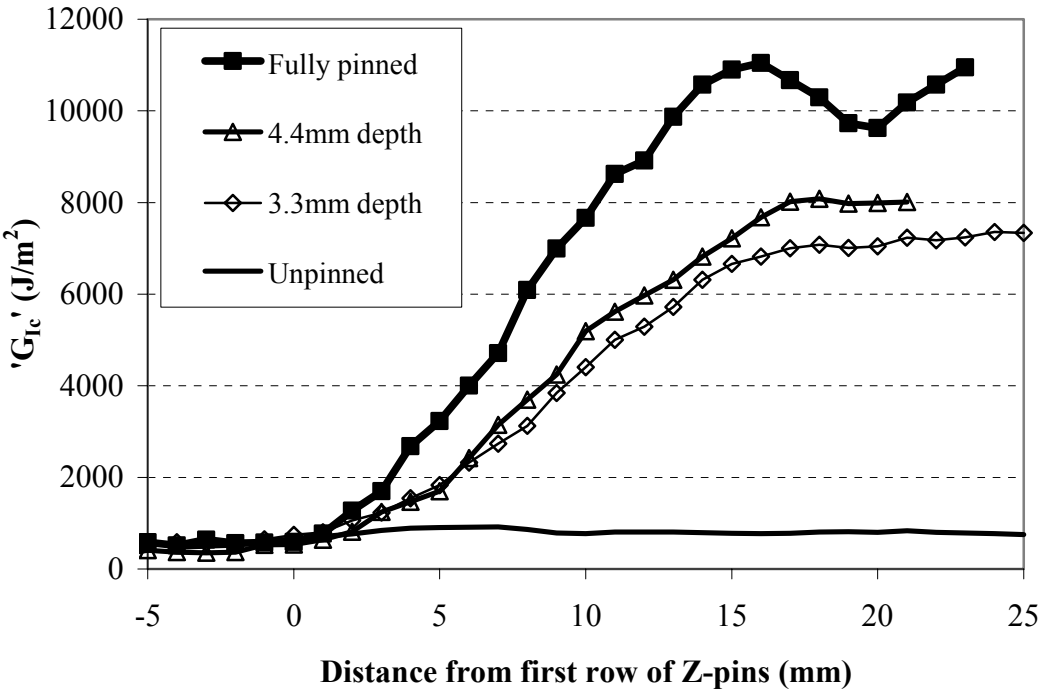

Figure 4-19: *Effect of insertion depth on the R-curve; material G986/M21, specimen thickness 6.6mm, density 2%, Z-pin diameter 0.28mm*

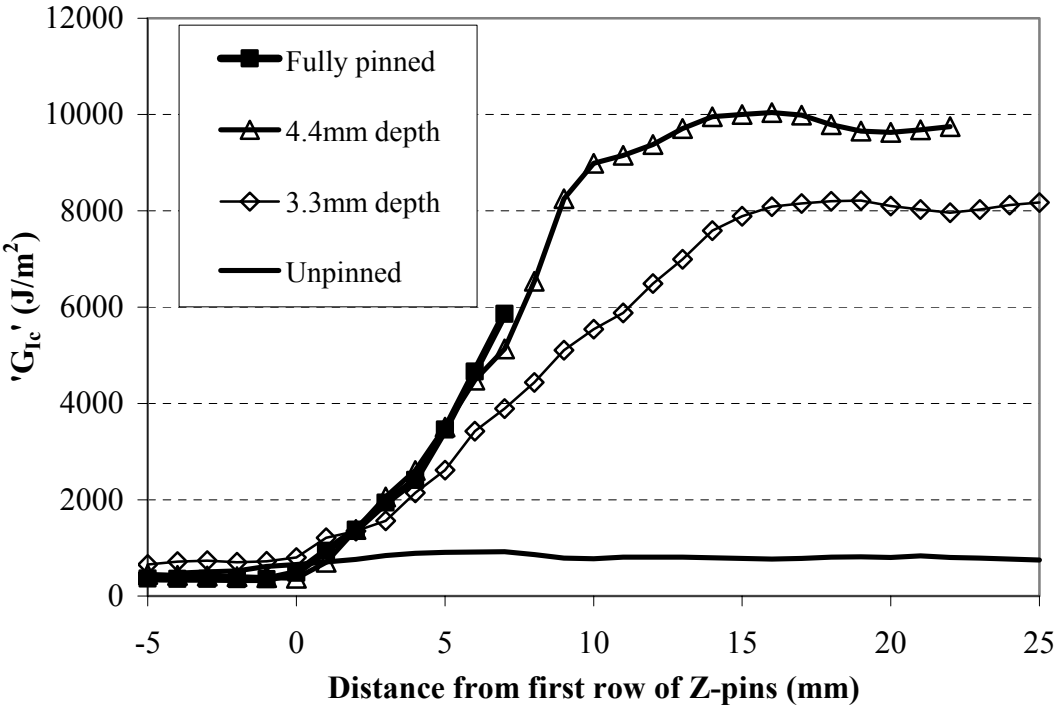

Figure 4-20: *Effect of insertion depth on the R-curve; material G986/M21, specimen thickness 6.6mm, density 4%, Z-pin diameter 0.5mm*

Observation of the figures reveals a dependence of the apparent toughness value on the insertion depth. The same is apparent in Figure 4-21, where a comparison between UD specimens is performed. Individual specimens are depicted. The plateau value of the apparent toughness increases with increasing insertion depth. Moreover, the slope of the R-curve becomes steeper as the insertion depth increases.

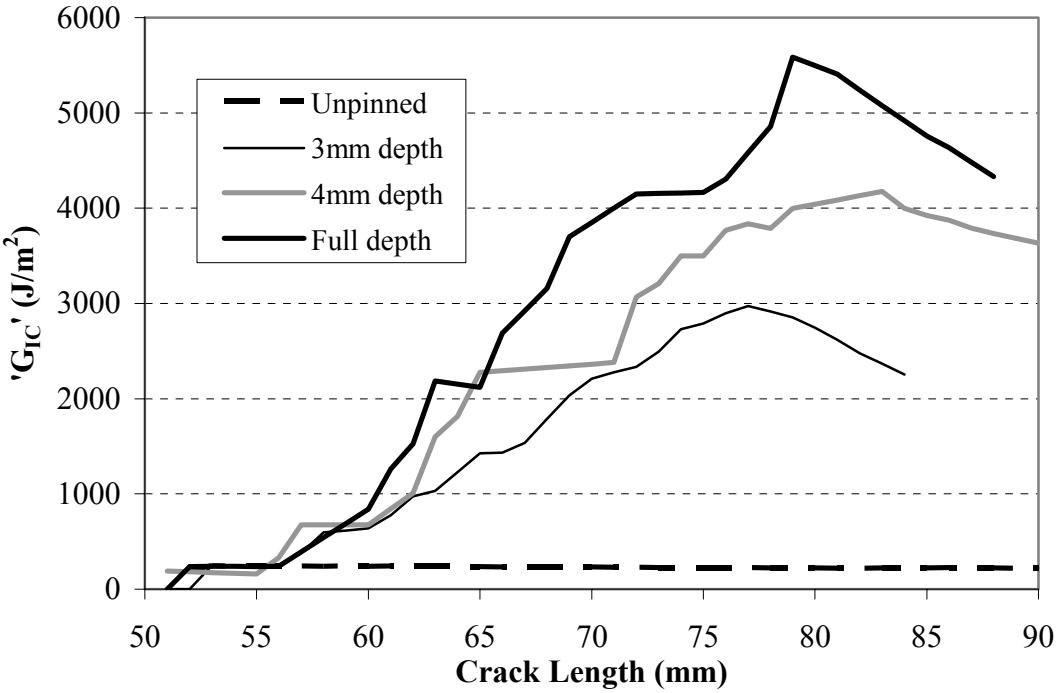

Figure 4-21: *Effect of insertion depth on the R-curve; material UD IMS/924, specimen thickness 6mm, density 2%, Z-pin diameter 0.5mm*

The first trend can be explained by investigating the effect of insertion depth on the length of the bridging zone. A Z-pin with small insertion depth requires proportionally small opening of the two beam arms to pull out completely. At the point where the first row of Z-pins has pulled out of this specimen, the first row of Z-pins in an otherwise equivalent specimen with a greater insertion depth has still not completely pulled out. This row is still resisting crack opening. In order for the first row in this second specimen to pull out, the crack is required to advance further. When the crack advances further, additional rows of Z-pins are introduced in the crack wake and the total number of "working" rows increases. The apparent toughness therefore increases. Figure 4-22 illustrates how a greater number of working rows is achieved with an increased insertion depth.

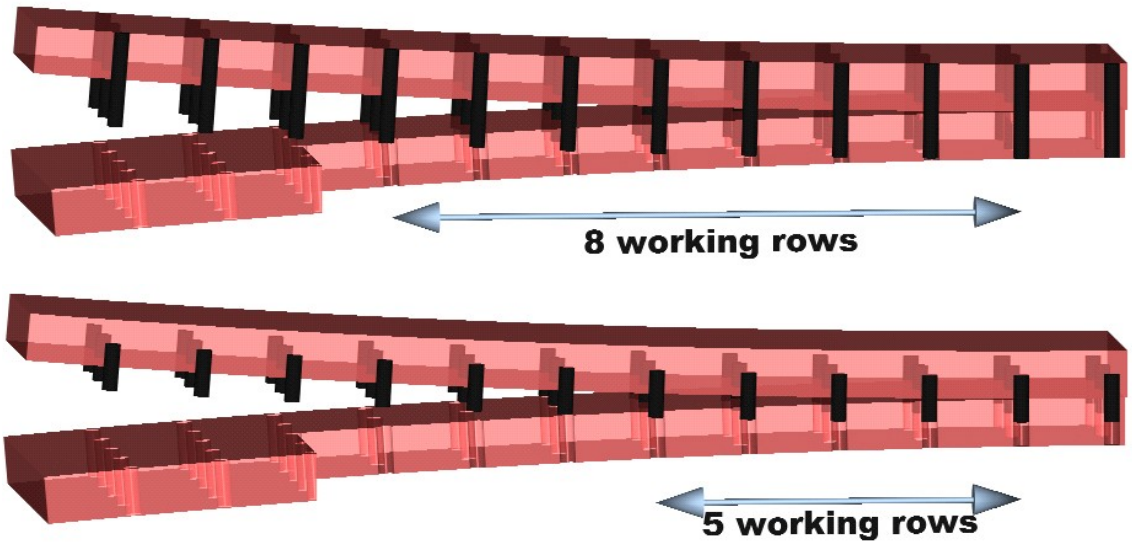

Figure 4-22: *Effect of insertion depth on the length of the bridging zone*

At the point where the first row pulls out completely, a steady state is reached. For every row pulling out, a new one is introduced in the crack wake and "replaces" the first one. This is why a plateau value is reached. This plateau value can be sustained until there is no additional row available to "replace" the row that is pulling out. The number of "working" rows is therefore smaller than that required to withstand the load and the specimen fails.

The second trend is a result of the pull out curve of the Z-pin. Looking at Figure 4-19 to Figure 4-21 it is apparent that a Z-pin with greater length can initially resist a higher load. The maximum pullout force, generated at the onset of pullout, is smaller for a shorter Z-pin.

The rate with which a new row is introduced to the crack wake depends on the Z-pin spacing and thus is fixed for a certain Z-pin diameter and density. The rate with which the sum of forces, generated by Z-pins, increase and shield the crack tip is therefore constantly lower for a specimen with a smaller insertion depth. This results in the decreasing slope of the R-curve with decreasing Z-pin insertion depth.

4.8 Effect of Density

The Z-pin density defines the amount of reinforcement inserted in a composite laminate. It is expected to exhibit a proportional relation to the apparent toughness. Figure 4-23 confirms the predicted trend; apparent toughness increases with increasing Z-pin density. This is true for any combination of the rest of the Z-pin parameters, for both types of materials investigated.

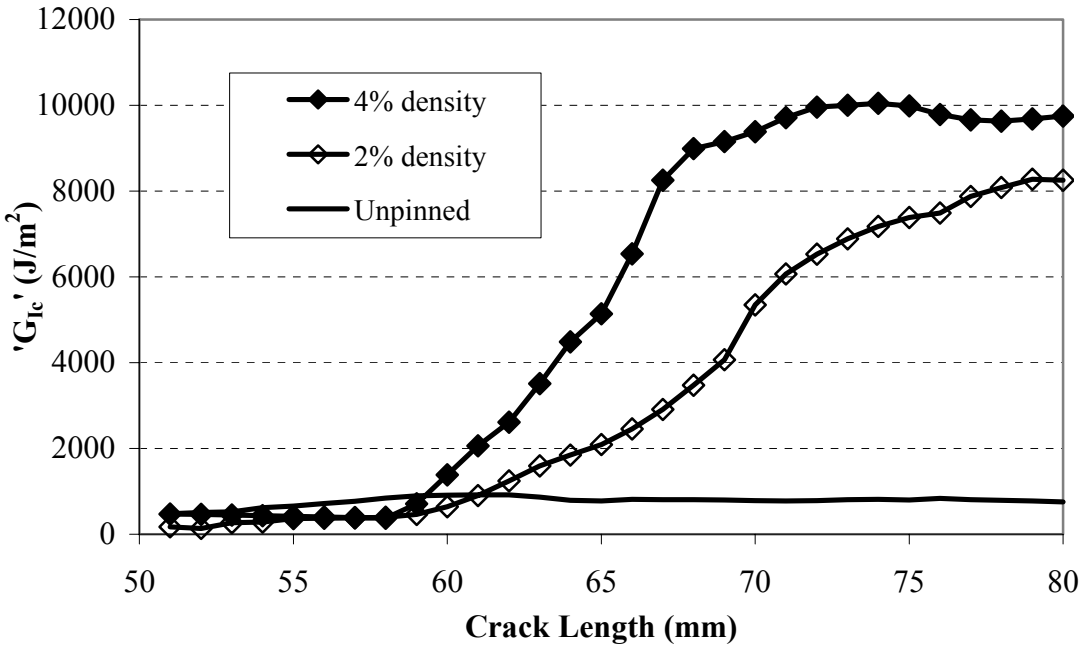

Figure 4-23: *Effect of Z-pin density on the apparent toughness*

A secondary effect can be observed in the same figure; the slope of the R-curve rises with increasing density. Increasing density equals decreasing Z-pin spacing and subsequently the rate with which new rows of Z-pins are introduced in the crack wake, as the crack propagates, is higher, explaining this occurrence.

4.9 *Effect of Diameter*

The mechanism that generates the Z-pin reaction force during pullout is friction. The amount of friction decreases with pullout and is, thus, proportional to the circumferential area of the Z-pin that is embedded in the laminate. For a fixed insertion depth, the circumferential area of a Z-pin is, in turn, a function of its diameter (equation (4-13)). In a bridging zone of a fixed length, the total force resisting crack opening is the sum of forces generated by Z-pins (Figure 4-22). For fixed Z-pin density, the number of Z-pins acting in the bridging zone is determined by equation (4-14).

Circumferential area of *each* Z-pin: $$A = \pi \cdot D \cdot L_P \tag{4-13}$$

Number of Z-pins: $$n = \frac{H_1 \cdot H_2}{s^2} \tag{4-14}$$

Definition of areal density: $$\rho = \frac{\frac{\pi \cdot D^2}{4}}{s^2} \tag{4-15}$$

Where :
- s: Z-pin spacing,
- L_P: Z-pin insertion depth (Z-pin cylinder height)
- H_1,H_2: reinforced area (or bridging zone) dimensions
- D: Z-pin diameter

The total frictional area of the reinforcement is then:

$$A = n \cdot \pi \cdot D \cdot L \tag{4-16}$$

According to (4-15), equal densities lead to the following formula:

$$D_{0.5} = D_{0.28} \Rightarrow \frac{s_{0.5}^2}{s_{0.28}^2} = \frac{D_{0.28}^2}{D_{0.5}^2} \tag{4-17}$$

By combining equations (4-13), (4-14), (4-16), (4-17), the ratio of frictional areas is:

$$\frac{A_{0.5}}{A_{0.28}} = \frac{D_{0.28}}{D_{0.5}} \tag{4-18}$$

The frictional areas are inversely proportional to the Z-pin diameter. The apparent toughness should retain a similar relation; however, apparent toughness will not be exactly inversely proportional to the Z-pin diameter. For fixed density, insertion depth and laminate thickness, at a certain crack length, the force required to continue crack propagation under mode I loading will be higher for Z-pins of smaller diameter. The higher forces generated by the smaller diameter Z-pins will alter the amount of bending of the arms of the beam. Thus the length of the bridging zone will be affected. The relation between the apparent toughness and Z-pin diameter will change; on the other hand, the trend of obtaining higher apparent toughness values for smaller diameter Z-pins should remain. This is confirmed for all laminate thicknesses, Z-pin densities, and insertion depths. An example is given in Figure 4-24.

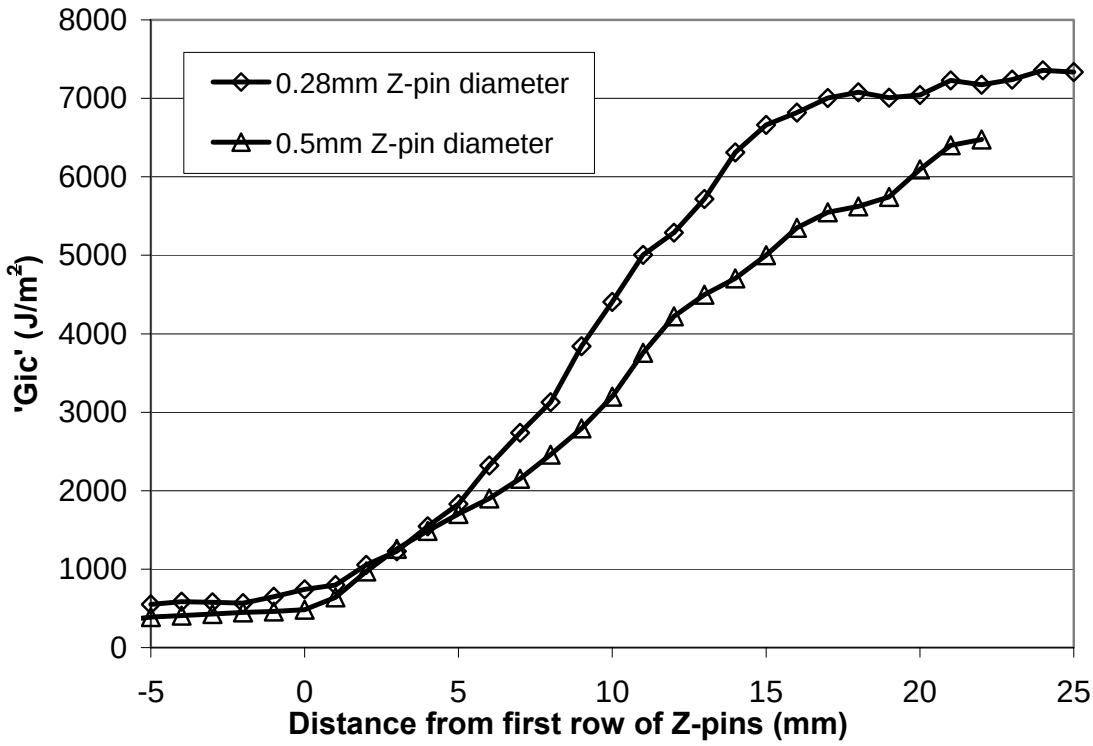

Figure 4-24: *Effect of Z-pin diameter on the apparent toughness; material G986/M21*

4.10 Summary

A fine mesh of measurements of the crack length is important for the accurate data reduction of delamination toughness. The difference in the microstructures of the M21 and M36 resin systems is responsible for the difference in the neat resin toughness. The instability and pattern of the mode I delamination behaviour of the unpinned woven laminates however is a result of the laminate fibre architecture.

Z-pins perform two tasks. Firstly, they increase the delamination toughness by an order of magnitude in both types of material. Secondly, the provide stability during propagation.

Failure mechanisms consist of Z-pin debonding and frictional pull out. Alternative modes of failure of the specimen can be introduced for highly increased fracture toughness.

Mode I delamination toughness of a Z-pinned laminate is a function of laminate thickness, insertion depth, Z-pin density and Z-pin diameter. An increase in density increases the traction forces in the crack wake accordingly; an increase in insertion depth enhances the potential energy absorption by the Z-pins; an increase in thickness results in a greater number of working Z-pins at any given time; an increase in Z-pin diameter reduces the total friction area resisting the crack opening and thus reduces the measured delamination toughness.

5 Response to Mode II Loading

There are four available test configurations to investigate the response of composite laminates under mode II loading. This chapter begins with a brief presentation of these configurations. The 4ENF configuration is selected as the most appropriate for testing Z-pinned laminates.

The measurement of delamination toughness under mode II loading is related to and obstructed by the presence of friction between crack faces. The investigation of its effect in woven laminates is attempted with the help of a purpose built **friction rig**. A further association of friction with crack propagation behaviour of woven laminates is established. This association is illustrated by the sensitivity of the delamination toughness of unpinned woven fabric laminates to laminate thickness.

The fracture mechanisms of Z-pinned laminates in shear loading are identified in relation to the material and the Z-pinning parameters; insertion depth to Z-pin diameter ratio, material type, laminate thickness and imposed constraints regarding the opening displacement, all play a role in determining the failure type of Z-pins. A specifically designed **shear test rig** is utilised to facilitate the investigation. An optimum insertion depth to Z-pin diameter ratio exists, where energy absorption is at maximum. Additional effects of Z-pin density and angle are identified. The introduction of an additional mode I loading component under shear loading conditions is attributed to Z-pin presence; fractography images support this concept.

The experimental compliance calibration method (CCM) is selected to reduce data from 4ENF delamination tests. The CCM method is time efficient and produces the most conservative values. The insertion of Z-pins in a mode II specimen, however, introduces a level of inaccuracy in the delamination toughness measurement; in particular in the correct determination of compliance. A compliance correction is applied to facilitate comparison between different Z-pinning configurations regarding their effect on mode

II delamination toughness, G_{IIC}. The correction is performed with a **purpose designed specimen** in order to nullify the manufacture introduced irregularities, as well as the effect of the complex fracture mechanisms that further impede the correct compliance determination, while retaining the effect of the Z-pins on the mechanical in-plane properties of the material.

The effects of Z-pin density, Z-pin diameter and insertion depth in 4ENF delamination testing are identified and measured for woven laminates. The understanding of Z-pin behaviour under shear loading, developed through the shear rig experiments, is used to explain test results under 4ENF mode II loading.

5.1 Mode II delamination testing

Delamination tests under mode II loading conditions were carried out using the 4ENF configuration (4 point End Notched Flexure) [88,95,96]. Specimen dimensions and specimen preparation are identical to those required to mode I delamination testing according to ISO 15024. Both UD and woven laminates are tested without any differences in the procedure.

Specimens are cut to the suggested width (20mm) using a dry diamond coated saw. The edges are slightly polished and then coated with correcting fluid to facilitate crack growth measurement. The thickness of the specimens manufactured ranges between 3mm, 4mm and 6mm for UD specimens and 3.3mm, 4.4mm and 6.6mm for woven specimens. Testing of UD specimens using the 4ENF configuration was performed by Alessandrini [97]; only three unpinned UD specimens are presented. The crack is propagated in the middle plane of the specimen and initiates from a 12.5μm thick PTFE film. Z-pins are positioned 5mm after the initial crack front (as in the mode I specimen, see Figure 4-1), following the concept of evaluating the effectiveness of Z-pins to arrest an existing crack [20,47,48,89].

Initiation values defined using the NL point [22,95] are higher from inserts or mode I pre-cracks when using the 4ENF configuration. Pre-cracking in mode I can also induce fibre bridging [98] and introduces a different mode to the crack tip [99]. Inserts usually yield the highest initiation values [87,98,100]. Pre-cracking in mode II is advisable [101,102,103], and this was done in the present study.

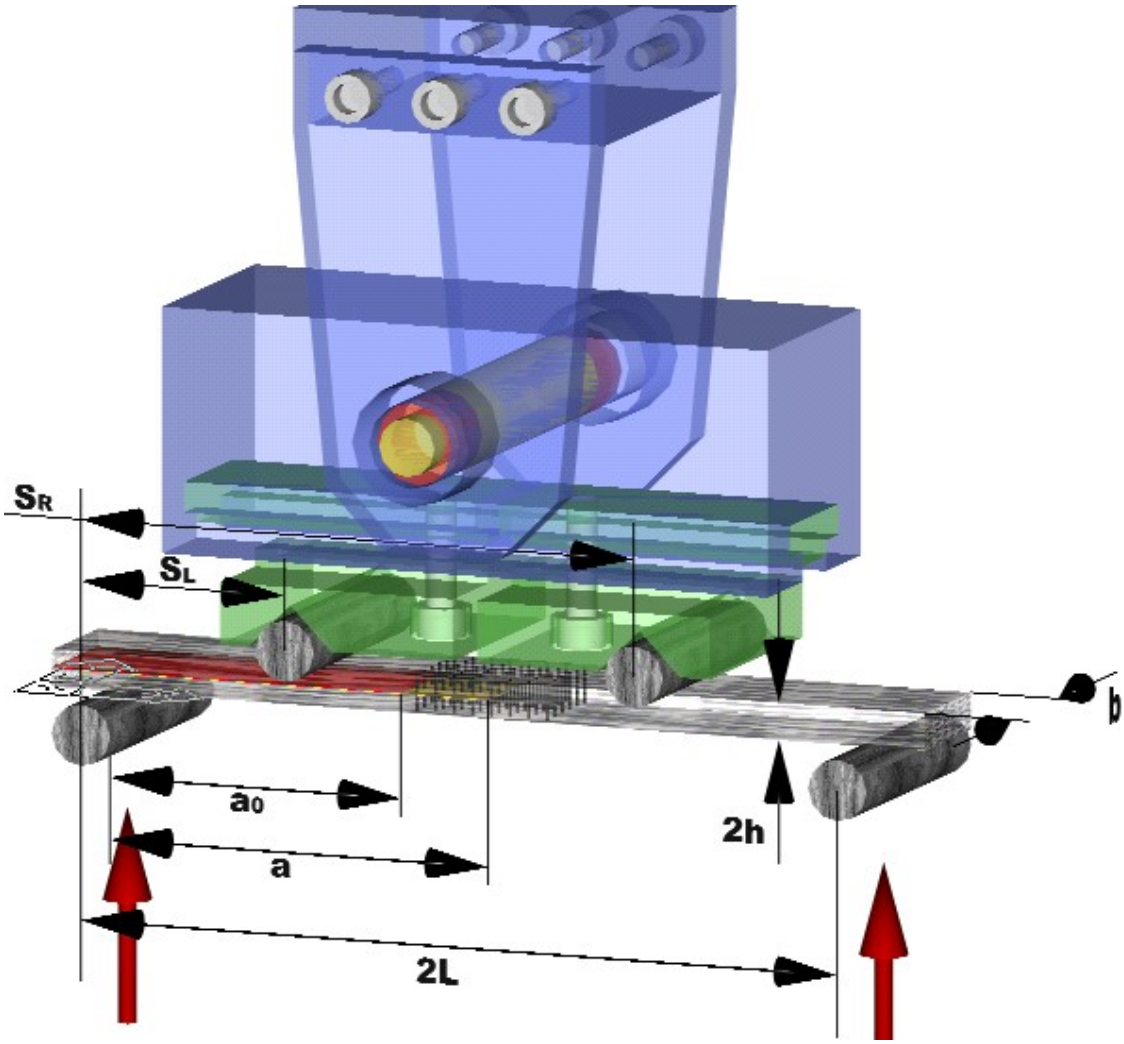

Figure 5-1: *II delamination specimen and 4ENF fixture; test dimensions, insert film, pin position, and loading displayed*

The loading is applied by increasing the crosshead displacement at a rate of 0.5mm/min. The load and the crosshead displacement are recorded electronically, while measurements of crack propagation are recorded for every millimetre, if possible, by eye, using a 3-axis travelling microscope.

Methods available for data reduction [82,96,102] include the ***beam theory method*** (equation *(5-1)*) and the ***experimental compliance method*** (equation *(5-2)*):

$$G_{IIC} = \frac{9P^2S_L^2}{16E_f b^2 h^3} \tag{5-1}$$

$$G_{IIC} = \frac{P^2}{2 \cdot b} \cdot m \tag{5-2}$$

$$\text{With: } C = C_0 + m \cdot a \tag{5-3}$$

Where:
E_f: the flexural modulus
C: specimen compliance
C_0: initial specimen compliance
Dimensions depicted in **Figure 5-1**

5.1.1 Comparison of test methods

Four basic test configurations are used for mode II fracture tests; the *ENF* configuration (End Notched Flexure), the *SENF* configuration (Stabilised End Notched Flexure), the *ELS* configuration (End Loaded Split), and the *4ENF* configuration (4 point End Notched Flexure).

The ***ENF*** configuration has been the most popular and it is a 3-point bend configuration of a beam containing an initial crack of 25mm [95]. Pre-cracking under mode I loading conditions is advised, as it provides conservative values; initiation from inserts exhibit instability [88,101,102]. Similarly to mode I, there are three data reduction methods [82, 101,102]. In order to use the experimental compliance calibration method, the slope of compliance change m has to be determined before the test. A small number of bending tests with each specimen, placed in different positions so as to achieve different crack lengths, is performed to obtain the calibration curve. Correction factors N, F and S are used to compensate for the effects of large displacements and transverse shear [82, 88,102]. The initial parameter dimensions are L=50mm and α_0=25mm.

The ENF test is in theory stable for a crack length of α=35mm [104]. However, the kinetic energy due to the initial instability leads the crack to propagate further than the loading point at α=50mm, rendering the propagation values invalid [20,88,102]. The ENF method is mostly used for obtaining initiation values, as it gives values on the lower bound.

The ***SENF*** method is an ENF configuration with a difference in the controlling parameter of the test. The shear displacement at the split end of the specimen is measured with a clip gauge, and a *constant shear displacement speed* is used instead of applying a constant crosshead speed. Both beam theory and an experimental compliance calibration method are used for the data reduction [102]. The complicated fixture that provides the constant shear displacement speed and the questionable stability of crack growth, when using this method, are its main drawbacks [88, 101,102].

The ***ELS*** configuration introduces mode II loading conditions by bending a split cantilever beam. Data reduction methods include both beam theory and experimental compliance calibration [95,102]. A significant advantage of using the experimental compliance calibration data reduction method is that compliance calibration can be performed during the test [102,88,101]. This provides a more accurate compliance calibration than when performing the calibration beforehand [96]. Otherwise, compliance correction Δ_{II} is determined through the corresponding compliance correction Δ_I for a mode I DCB test [82,105]. If the modulus E is unknown, a simple flexural test on the uncracked part of the beam can provide this value.

Examining the stability as before deduces that the ELS configuration offers stable crack growth for more than 35mm. It can therefore be used to obtain crack propagation values and is strongly preferred by many laboratories [102, 103].

The ***4ENF*** configuration is the most recently developed of the available tests and has been designed to reduce friction effects between the crack faces and propagate the crack in a stable manner [96]. It introduces mode II loading conditions by applying a constant moment between the inner loading points. Subsequently, the stability of the test is

independent of crack length, which means the test is *always* stable. The experimental compliance calibration method is preferred, as data reduction using the beam theory method overestimates the toughness by 20% [101]. The compliance calibration, as with ELS, is performed during the test. The proposed configuration of the test ($d=S_R-S_L$=60mm, 2L=125mm) provides at least 40mm of stable crack propagation. Initiation values deduced using this configuration are, however, the least conservative [101,102].

5.1.2 "Shear measurement or sheer myth?"

Mode II delamination toughness, as typically measured, is not universally accepted as an independent material property characteristic of the interlaminar shear fracture toughness of a composite material. The absence of a universally accepted test protocol to measure G_{IIC} is indicative of this fact. Significant issues, such as the measuring of the crack length with an acceptable degree of accuracy when microcracking occurs, have not yet been addressed in the existing protocols. An examination of the critical issues associated with the measurement of G_{IIC} has been presented by O'Brien [98]. Another relevant recent review examines the role of friction in the mode II loading response of composites [99].

Section *5.2* attempts to investigate the issues of friction between crack faces. The friction coefficient of different interfacial surfaces is measured and friction is correlated to the crack propagation behaviour. Section *5.4* will later deal with the issue of crack measurement.

5.2 Effect of friction

Substantial work has been published in the attempt to quantify the effects of friction in mode II testing, and is reviewed in [99]. Findings by different workers are not always in agreement among each other. Delamination toughness values are argued to be affected by 5% when the 4ENF configuration is used and 2% when using the 3pt ENF [107]. However, an overestimation of delamination toughness by 20% is possible due to friction when using the ENF configuration [108]. The effect of friction appears to increase with increasing specimen thickness [109], as well as with an increasing span ratio of *d/2L* in the 4ENF configuration [107]. According to the latter prediction, friction accounts for 5% to 9% of the delamination toughness for the span ratio used in the current study, considering the greatest thickness of specimens used (6.6mm).

An analytical expression regarding the effect of friction on the delamination toughness can be reached using beam theory [110]. Both friction between crack faces and at the loading and support points is accounted for:

$$G_{II} = \frac{9P^2 S_L^2}{16Eb^2 h^3}\left(1 - \frac{8\mu h}{3S_L}\right) \tag{5-4}$$

$$G_{II} = \frac{9P^2 S_L^2}{16Eb^2 h^3}\left(1 - \frac{8(\mu + 2\mu')h}{3S_L}\right) \tag{5-5}$$

An accurate measurement of the friction coefficient is required for the application of the above formulas.

5.2.1 Friction coefficient measurement

The coefficient of friction between two surfaces can be evaluated by measuring the load required to initiate and maintain the relative sliding displacement for a given normal load applied to the surfaces. Several subsidiary issues need to be addressed before

performing such a test. Appropriate contact between the whole specimen surfaces, a uniformly applied load and assurance of testing a representative pair of surfaces are the most important. Quite complicated fixtures have been used to ensure the accuracy of measurement [111,112]. In this study, specimens previously delaminated under mode II loading conditions were used. Woven fabric specimens (G986/M21 and G986/M36) were cut from 4ENF delamination specimens and UD specimens (T300/914) were cut from 3pt ENF delamination specimens. Additional specimens were cut from mode I delamination specimens for comparison. Cut-offs from the insert film area of delamination specimens were also tested. Each pair of surfaces tested belongs to the same delamination specimen and consists of "matching" surfaces, namely surfaces that were joined before delamination. The millimetre-accurate marking scale on the sides of the delamination specimens ensures that the relative positioning of the surface pairs matches their initial position before delamination.

The purpose built friction rig is depicted in Figure 5-2. The lower part of the friction specimen lies in a 20mm wide aligning channel. Specimen movement in the sliding direction is prevented by a protruding surface of the fixture (A in Figure 5-2). The upper half rests on top of the lower half and the sliding frame is placed around it. The sliding frame applies the sliding displacement. The frame lies in its own aligning channel and thus aligns the upper specimen half. A loading "saddle" is then placed on top of the upper specimen half (B in Figure 5-2). The saddle is in contact with the specimen only and does not obstruct in any way the movement of the frame; the entire normal load is therefore applied only on the specimen surface. A fixed weight is then placed on top of the saddle. Next, the frame is pulled horizontally and, pressed against the upper half of the specimen only, applies the sliding displacement to the upper half. The frame does not come in contact with the lower specimen half, as its own aligning channel restricts its downward movement. The frame is pulled via a brake wire. The wire is deflected against a free resting rod, restricted only against upward or downward movement. The other end of the wire is clamped in the machine jaws and the pulling load is measured in the load cell. All contacting metallic surfaces are finished with oil to minimise any additional frictional sources.

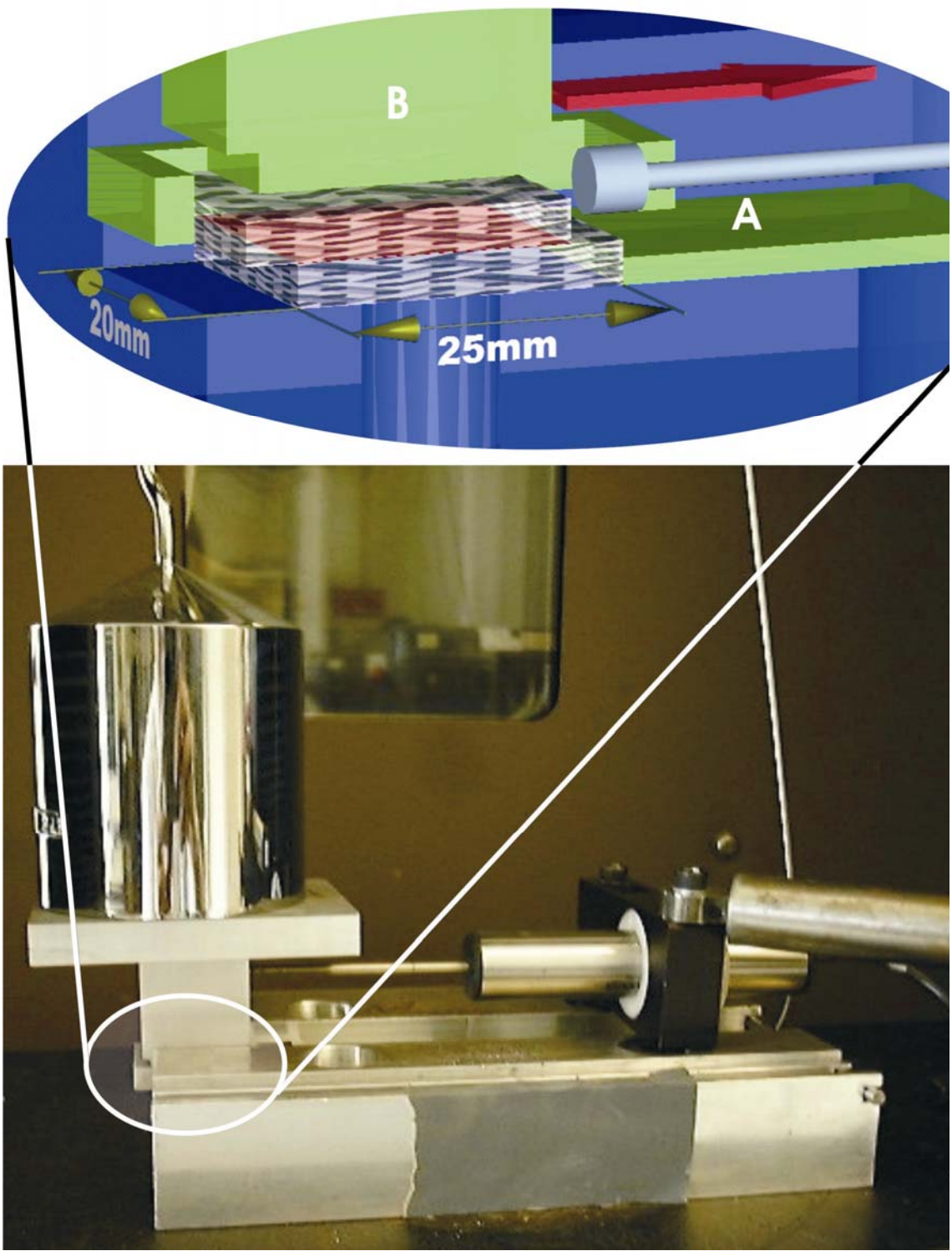

Figure 5-2: *Friction test rig illustrating the wire load application and the LVDT measurement; section of a detail of the rig revealing specimen positioning and dimensions. Red arrow indicates sliding displacement direction; red surface between specimen halves is under test.*

The sliding displacement is measured with an LVDT resting against the saddle, measuring therefore the actual displacement of the upper specimen half. The LVDT applies an additional load of approximately 1N on the saddle, opposed to the sliding direction. Measurements are corrected against all additional frictional sources, by subtracting the fixture generated friction. The fixture generated friction is measured by performing the test in an identical fashion using ball bearings between the saddle and the bottom surface. The only inaccuracy using such a correction procedure is that the amount of friction at the point where the loading wire is deflected is not measured accurately; friction depends on the applied load and the load reached during the measurement of the fixture generated friction is significantly lower.

Figure 5-3 displays the friction coefficient as a function of the sliding displacement. The friction of the fixture is also presented and has been subtracted from all curves. The average rig friction coefficient is 0.09; the curve however is not completely flat. The small undulations are caused by the contact of the wire at the deflection point. For higher loads, an additional inaccuracy is introduced due to the stretching of the wire. The correlation between the values of the friction coefficients measured and the level of friction between crack faces during the mode II delamination test is debatable. The elastic stretching of the wire for the maximum load during the friction test amounts to a strain of 0.1%. More importantly, the contact load between the surfaces using the friction rig is constant and the sufaces remain flat. In contrast, in the mode II delamination test, the changing compliance of the beam due to crack propagation change the distribution of contact forces and the surfaces follow the bending of the beam.

However, there are two arguments in favour of the validity of any trends or patterns observed in the results. Firstly, there is the sufficient detail and reproducibility in the measurement of the relatively low friction coefficient of the insert film specimens. Secondly, the diminishing of the undulations of re-tested specimens indicates the authenticity of the initially observed undulations. In the same figure, the curves of specimens denoted with “B” in their name, represent specimens being tested for a second time. The wear of the surfaces is the reason for the fading of the undulations.

Figure 5-3 reveals the effect of the difference in the resin system on the friction coefficient. Both types of woven material have identical fibre architecture. The ratio of friction coefficient between G986/M21 and G986/M36 is close to 3. Furthermore, the number and magnitude of peaks and dips are significant for G986/M21 and moderate for G986/M36. Another difference is the significant peak in load required to detach the initially matching surfaces, observed clearly in G986/M21. The differences in particle size and number, as discussed in section *4.2*, may alter the contact friction between surfaces. The amount of surface undulation may also depend partly on the resin micro-structure. It should be noted, that the consolidation of G986/M36 relative to the prepreg nominal thickness was better, compared to G986/M21; better consolidation implies smaller undulations between plies. In retrospect, testing cut-off surface pairs from the insert film region of G986/M36 delamination specimens and comparing with tests on the equivalent G986/M21 specimens would reveal the consistency of this claim.

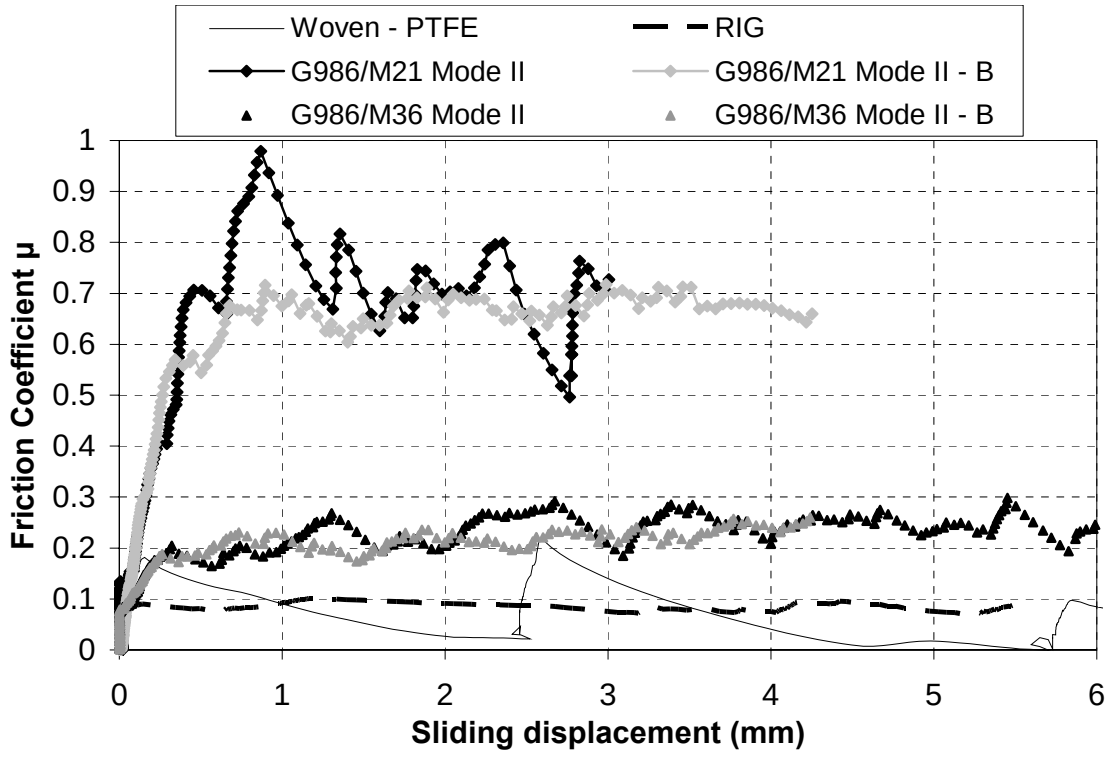

Figure 5-3: *Friction coefficient versus sliding displacement for different test cases*

The surface undulation and the varying relative fibre orientation between surfaces account for the shape of the curves. Insert film specimens have distinct behaviour. The load peaks with a periodicity of 2-3mm, which is similar to the width of the fibre bundle. The width and orientation of the fibre bundle determines the profile of the undulations. Sliding is arrested every 2-3mm until the load rises and then the surfaces are released again. This reflects observations during mode II delamination testing, where any occurrence of stick-slip behaviour would cause crack propagation for a length of 2-3mm or infrequently 5-6mm (twice as much). The size of the micro-cracking region was also between 2-3mm for G986/M21, while it was close to 5mm for G986/M36. The latter material does not exhibit significant load peaks when the initial surfaces are detached.

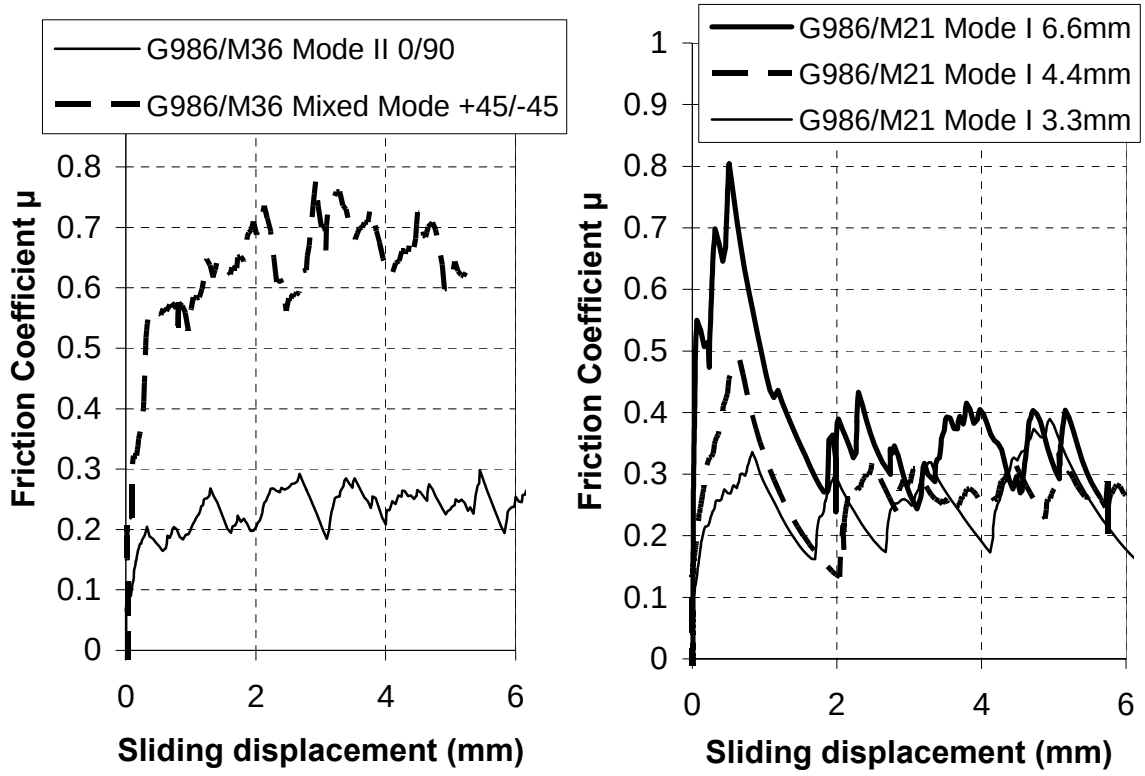

Figure 5-4: *Effect of relative fibre orientation (left) and laminate thickness on the friction coefficient.*

Fibre orientation influences the friction coefficient significantly [111]. The significance of the role of the fibres can be appreciated also in Figure 5-4. The ±45 mixed mode surface pair was generated from the delamination of a T-joint, subjected to a pull-off load. The significance of the surface undulations is portrayed in the same figure. The curves presented correspond to different specimen thicknesses. The friction coefficient appears to increase with increasing laminate thickness. This can be due to increasing surface undulation with increasing thickness; however the number of samples with smaller thickness is too low for definite conclusions to be reached.

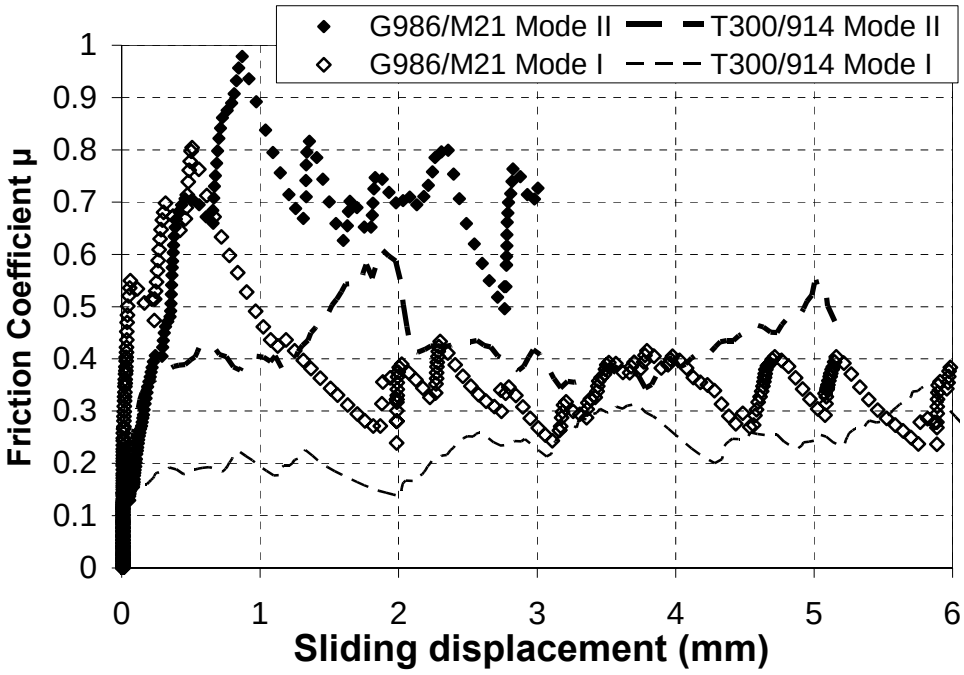

Figure 5-5: *Effect of fracture mode on the friction coefficient*

Figure 5-5 presents the effect of fracture type on the measured friction coefficient for both UD and woven materials. The difference between mode I and mode II fracture surfaces is illustrated in Figure 5-6. Mode II fracture in woven composites displays multiple cracking and a tortuous crack patch, frequently changing interfaces, as discussed in section *2.4*. This exposes laminate fibres, as depicted in Figure 5-6c, increasing significantly the contact friction between surfaces.

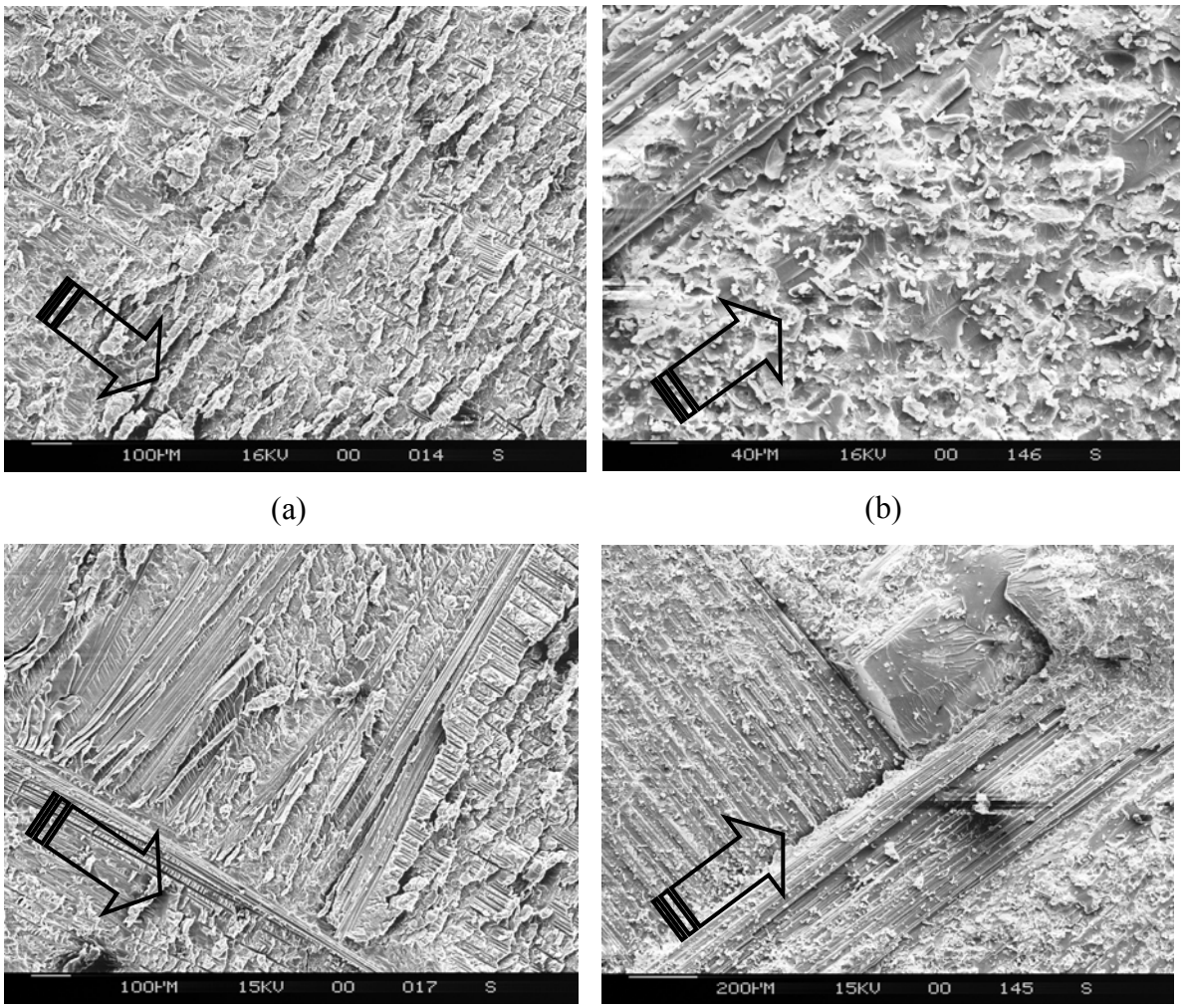

(a) (b)

(c) (d)

Figure 5-6: *(a-b) SEM of a typical resin rich G986/M21 mode II fracture surface and an equivalent mode I fracture surface, (c-d) SEM of a typical G986/M21 mode II fracture surface with fibre bundle damage and an equivalent mode I fracture surface. Arrow denotes crack advance direction*

5.3 Z-pin behaviour under shear loading

The test configuration described in this section aims at isolating and measuring the contribution of the Z-pins to the shear fracture toughness of a Z-pinned composite specimen. It imposes shear loading onto a block of Z-pins contained in a composite specimen while constraining the allowed opening displacement ("Z-shear"). The configuration is a development of the single pin shear rig by Cartié [20]. The objective behind using a block of Z-pins instead of a single pin is to eliminate the effect of manufacturing variability between specimens.

5.3.1 Description of Test & Test cases

The test configuration and the specimen dimensions are illustrated in Figure 5-7. The test cases examined are listed in Table 5-1. Both UD (IM7/M21) and woven (G986/M21) specimens were manufactured. Combinations of three separate Z-pin densities, both Z-pin diameters and five separate insertion depths were considered. Results include the work of Ferrari [113], and his contribution is denoted in the table. The number of Z-pins contained in each kind of specimen was dictated by the capacity of the load cell used; the maximum resistance force generated by the Z-pins should not exceed a force of 5kN. The upper part of the rig is fixed to the load cell and held in place by a steel loading pin. The downward motion of the lower part introduces the shearing load. Although the load cell is fixed to the machine, its protruding connection is only supported inside the load cell. Inspection during initial testing revealed that under increased loads (above 1.5kN), the protruding load cell connection could rotate and introduce an opening displacement. To prevent any unexpected load cell rotation, a rolling cylinder was added to the upper part of the rig. The cylinder was made of steel and was supported only by contact forces against a rigid extension of the machine frame. Experimentation, excluding specimen use, confirms that no additional friction forces were imposed on the load cell; alterations of the load cell reading, due to

deliberate sliding movement of the rolling cylinder by hand, were in the range of 10N to 30N for loads in the range of 2kN to 3kN.

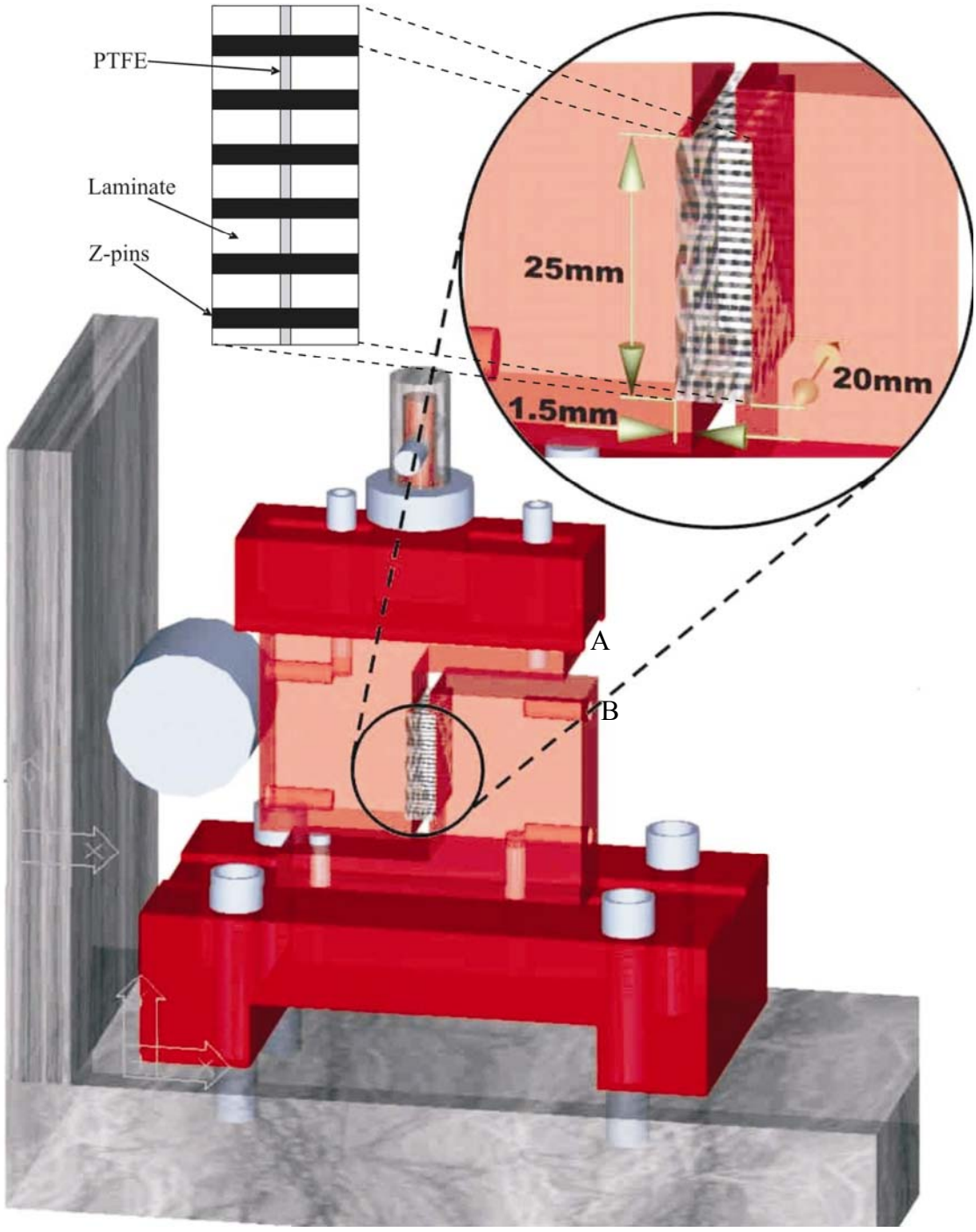

Figure 5-7: *"Z-Shear" test rig and specimen dimensions*

The upper connection of the rig to the load cell, as well as the bolts and the loading pin are made of steel. The central part and the base of the rig are made of aluminium. The

central pieces of the rig are positioned in aligning channels to ensure satisfactory enclosure of the specimen. The projecting lips have a height of 1.5mm, facilitate load application and secure the specimen in position during the test. Specimens have insert film in the middle plane and are held together ***only*** by Z-pins. Nominal specimen thickness was 6.6mm for G986/M21, and 6mm for IM7/M21. The angle of Z-pin insertion used was normal to the plane of the specimen. Any deviations in angle were a result of additional ply consolidation during cure (see section *3.4.1*).

Material	Density (%)	Diameter (mm)	Insertion depth (mm)	No. of Samples	Tested* by
G986/M21	0.5	0.5	Full	2	T
G986/M21	1	0.28	Full	2	T
G986/M21	1	0.28	3.6	2	T
G986/M21	1	0.5	Full	2	T
G986/M21	2	0.28	Full	2	T
G986/M21	2	0.5	Full	8	T & F
G986/M21	2	0.5	4.2	4	F
G986/M21	2	0.5	3.6	2	T
G986/M21	2	0.5	3.2	4	F
G986/M21	2	0.5	1.8	5	F
IM7/M21 (UD)	0.5	0.5	Full	1	T
IM7/M21 (UD)	1	0.28	Full	4	T
IM7/M21 (UD)	1	0.28	3	2	T
IM7/M21 (UD)	1	0.5	Full	2	T
IM7/M21 (UD)	2	0.28	Full	2	T
IM7/M21 (UD)	2	0.5	Full	4	T
IM7/M21 (UD)	*2*	*0.5*	*3*	*2*	T

Table 5-1: *"Z-Shear" test cases. (*T stands for Troulis, F for Ferrari)*

The sliding displacement is measured using both the crosshead extension and a clip gauge mounted at points A and B in Figure 5-7. The measurement obtained from crosshead displacement is used in the results, as no difference was observed compared to the clip gauge measurement (Figure 5-8). The latter displays irregularities, associated

with load changes, corresponding to stages of Z-pin failure, and is therefore not used in the presentation of results.

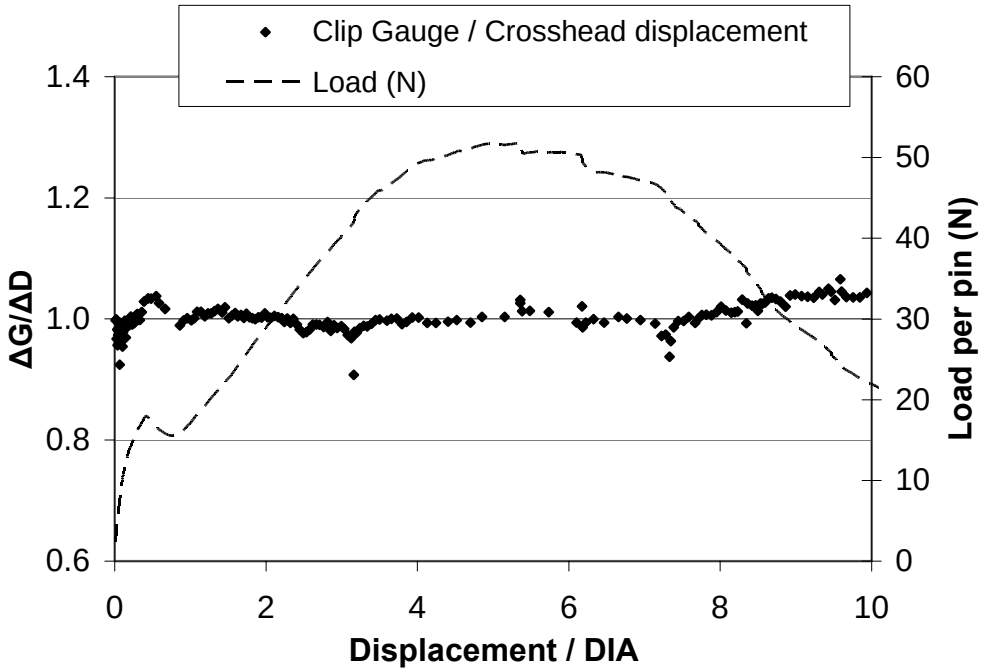

Figure 5-8: *Comparison of the clip gauge reading to the crosshead displacement ratio, and the load per Z-pin (UD IM7/M21, 1%, 0.5mm, fully pinned).*

5.3.2 Effect of Z-pin diameter

Figure 5-9 presents a typical load trace of the Z-shear test for a woven fabric specimen. Load is plotted against displacement normalised to the Z-pin diameter. Specimens with both diameter Z-pins are depicted, pinned through the whole thickness (7mm insertion depth). In specimens of 0.28mm Z-pin diameter failure occurs reproducibly when displacement reaches 1.8 times the Z-pin diameter. For 0.5mm Z-pins failure ranges from a normalised displacement of 1.8 to 2.5.

Figure 5-11 depicts the equivalent load trace for UD specimens with a full insertion depth. A completely different type of failure is evident, at a displacement many times the Z-pin diameter.

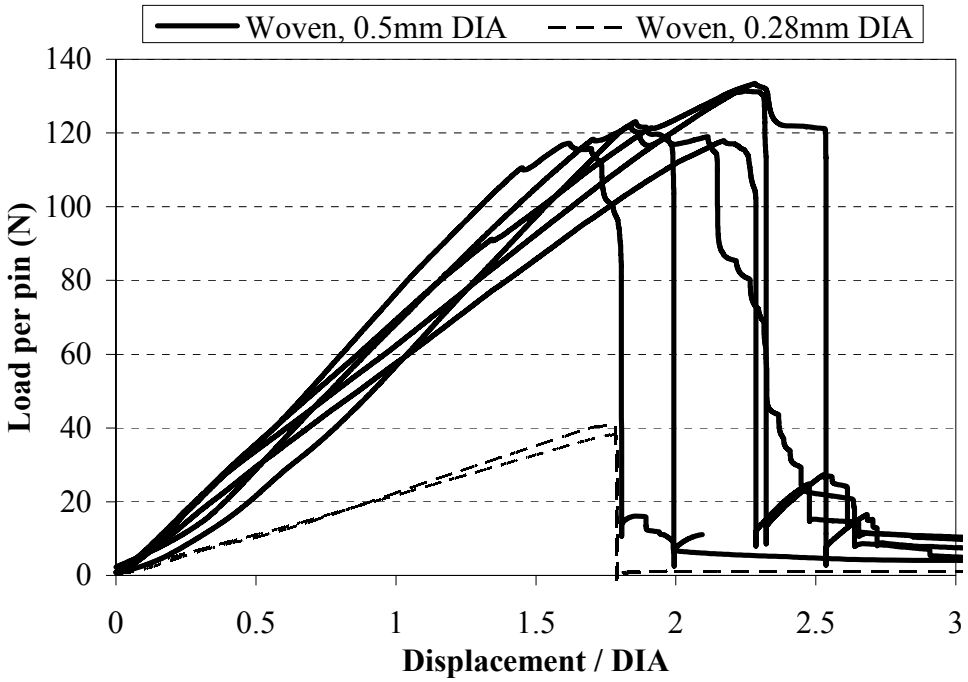

Figure 5-9: *Load as a function of normalised displacement for Z-pinned woven fabric G986/M21 under shear loading (full insertion depth).*

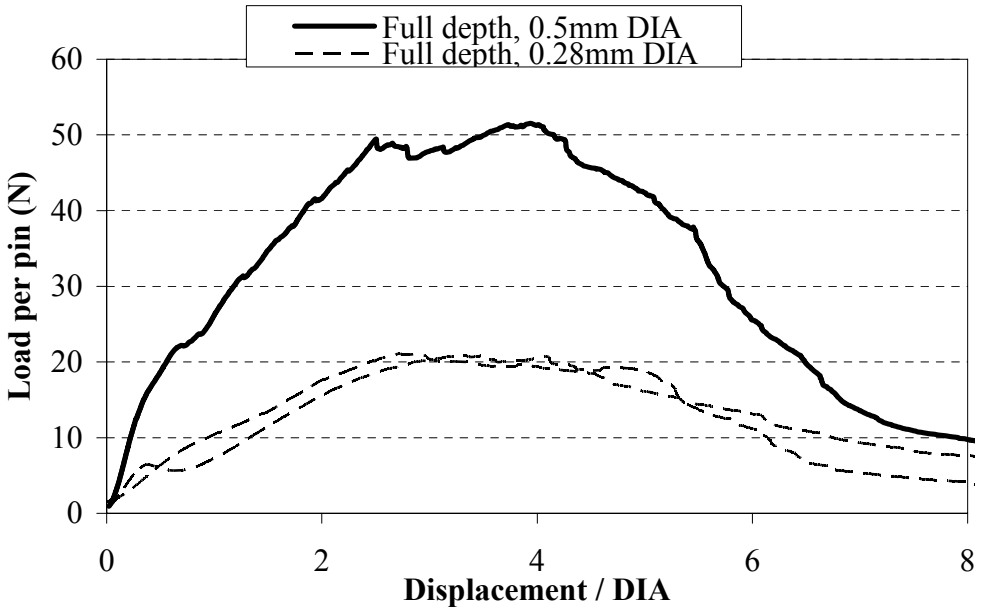

Figure 5-10: *Load as a function of normalised displacement for Z-pinned UD IM7/M21 under shear loading (full insertion depth)*

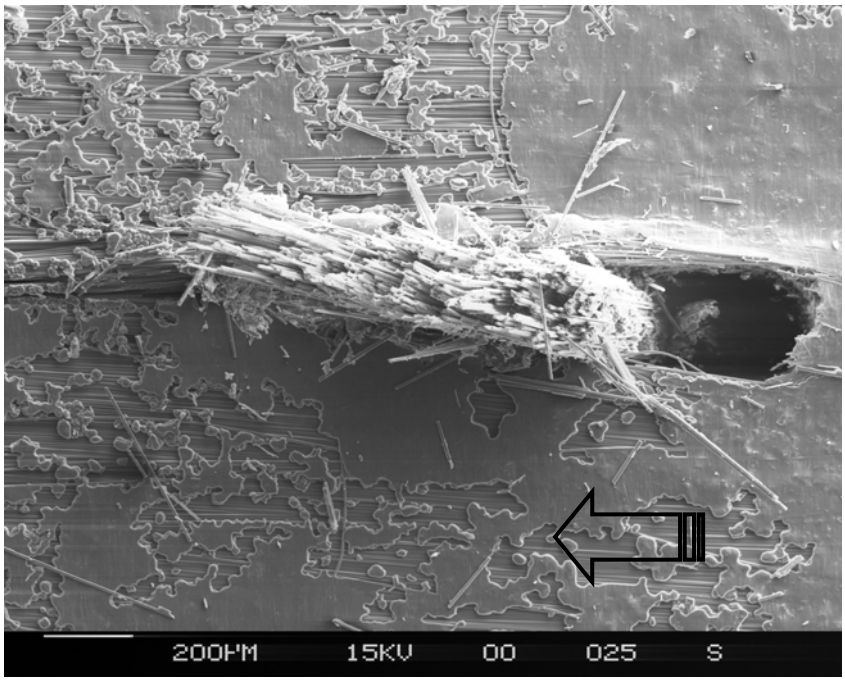

(a)

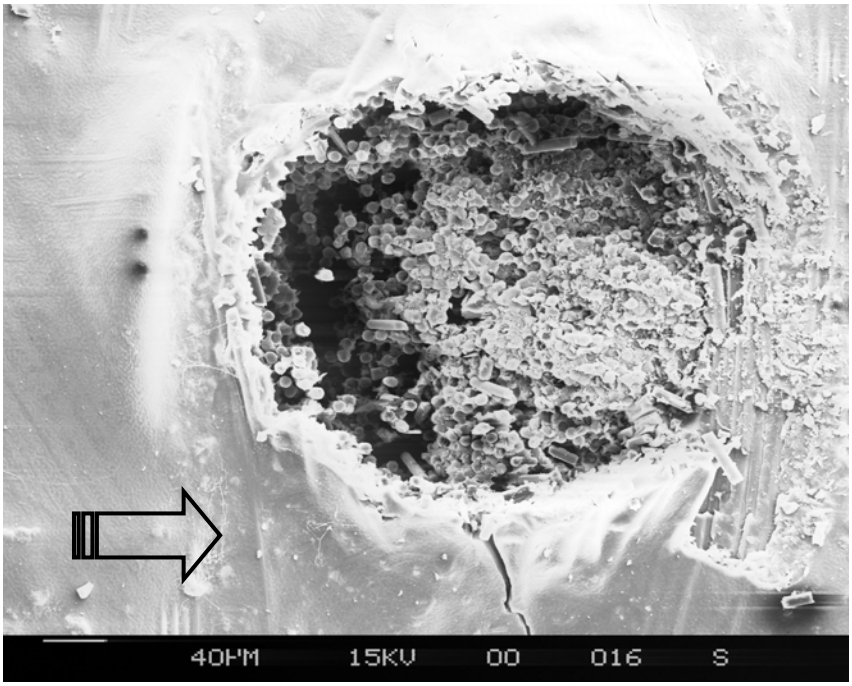

(b)

Figure 5-11: *SEM image of failure of a 0.28mm diameter Z-pin under shear loading; (a) in UD IM7/M21, (b) in woven fabric G986/M21. Arrow denotes test direction.*

Figure 5-11 displays images of failed 0.28mm diameter Z-pins for the UD and the woven case. The Z-pin is able to plough through the resin rich area within its own resin pocket in UD, while it is significantly constrained in woven fabric. Extensive splitting and pullout is evident in UD; a shear type of failure dominates in woven fabric.

Using images obtained during the Z-shear test and standard imaging software, the relative sliding and opening displacements were measured; the measurement was straightforward as no bending is present. The distance between the outer surfaces of the specimen was measured to determine the opening displacement, as it produces more accurate and reproducible results. Marks drawn on the side of the test specimens after preparation with a correction fluid, facilitates the sliding displacement measurement. Figure 5-12 displays a sequence of test images, from which such measurements can be taken. Lines drawn are 5mm apart and are used as the reference length.

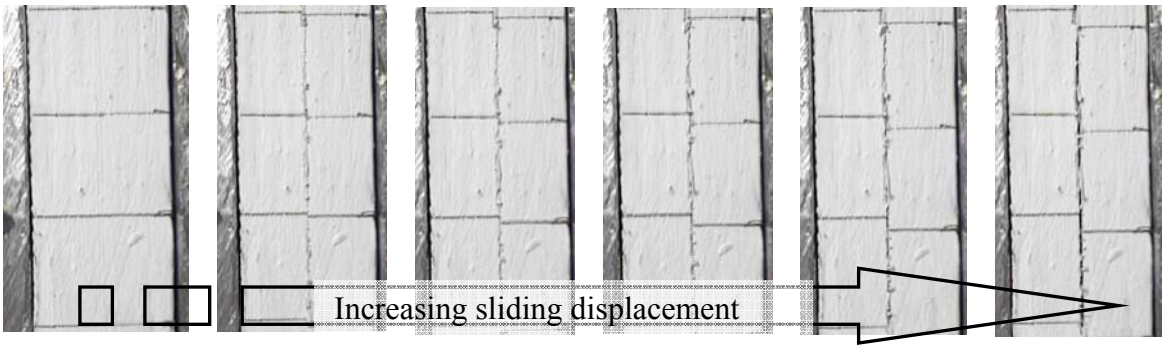

Figure 5-12: *Sequence of digital images of a specimen under test*

Opening displacement is constrained during the test, as the specimen is positioned between the aluminium loading blocks. The constraint is not complete, as the more compliant aluminium loading blocks can accommodate some opening displacement; the actual amount is a feature of the test rig. However, since the loads reached during the test are similar for all specimens, any difference in the measured opening displacement is a specimen characteristic. Comparison of the measured opening displacement between specimens is therefore valid.

In woven fabric Z-shear specimens a certain amount of opening displacement is necessary, since the sliding surfaces of the specimen are undulated. More lateral space

is required after they detach from their initial position. In order to establish whether the imposed opening displacement is a feature of the woven fabric laminate or the Z-pins, an additional specimen containing ***no*** Z-pins was tested. The two halves of the specimen are held together with the help of some 'tacky tape' before positioning in the test rig. Figure 5-13 displays the opening displacement of G986/M21 Z-shear specimens plotted against the sliding displacement for 0.28mm and 0.5mm diameter Z-pins, as well as the unpinned specimen. Both opening and sliding displacements are normalised by the Z-pin diameter. The measurements from the unpinned specimen are normalised to both Z-pin diameters for comparison; thus, two traces for the unpinned specimen are plotted.

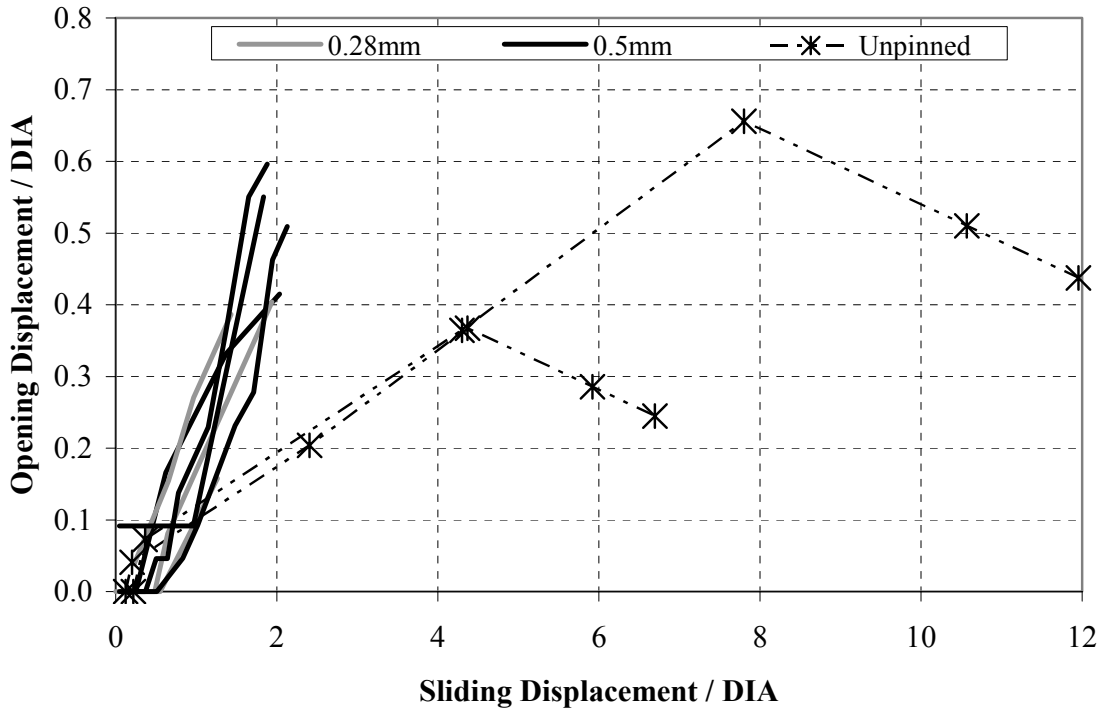

Figure 5-13: *Comparison of opening versus sliding displacement in woven fabric G986/M21 "Z-shear" specimens (full insertion depth only) with unpinned case.*

The opening displacement imposed in the Z-pinned woven fabric specimens occurs for very low sliding displacements compared to the unpinned sample. This indicates that the presence of the Z-pin introduces an opening displacement, independently of the laminate material. The ratio of normalised opening to normalised sliding displacement is similar for both Z-pin diameters; only the maximum values reached differ.

Figure 5-14 depicts the equivalent normalised opening to sliding displacement ratio for UD IM7/M21. The ratio is different for each Z-pin diameter and independent of the insertion depth. As expected from the load versus displacement traces, the sliding displacement required for a certain opening displacement to be reached is significantly higher than in woven fabric specimens.

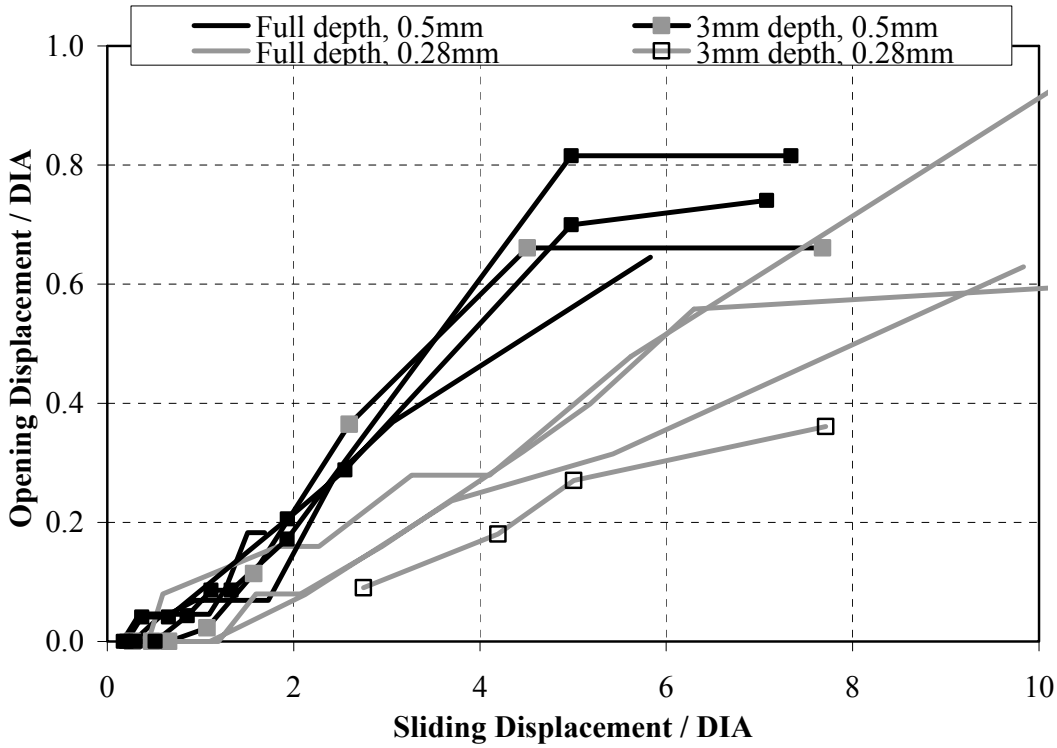

Figure 5-14: *Comparison of opening versus sliding displacement in UD IM7/M21 "Z-shear" specimens of different Z-pin diameters.*

5.3.3 Effect of Z-pin density

Figure 5-15 displays load versus normalised displacement traces of woven specimens with 0.5mm diameter Z-pins for different pinning densities. The load has been normalised by the number of Z-pins. The curves of the lower pinning density specimens exhibit a steeper slope. Moreover, the normalised displacement to failure is increasing with increasing pinning density. Low pinning density specimens with 0.5mm diameter

Z-pins exhibit normalised displacement to failure similar to specimens with 0.28mm diameter Z-pins.

No effect of pinning density was observed for 0.28mm Z-pin diameter woven fabric specimens or for any of the UD specimen cases, for the Z-pin densities used in this study.

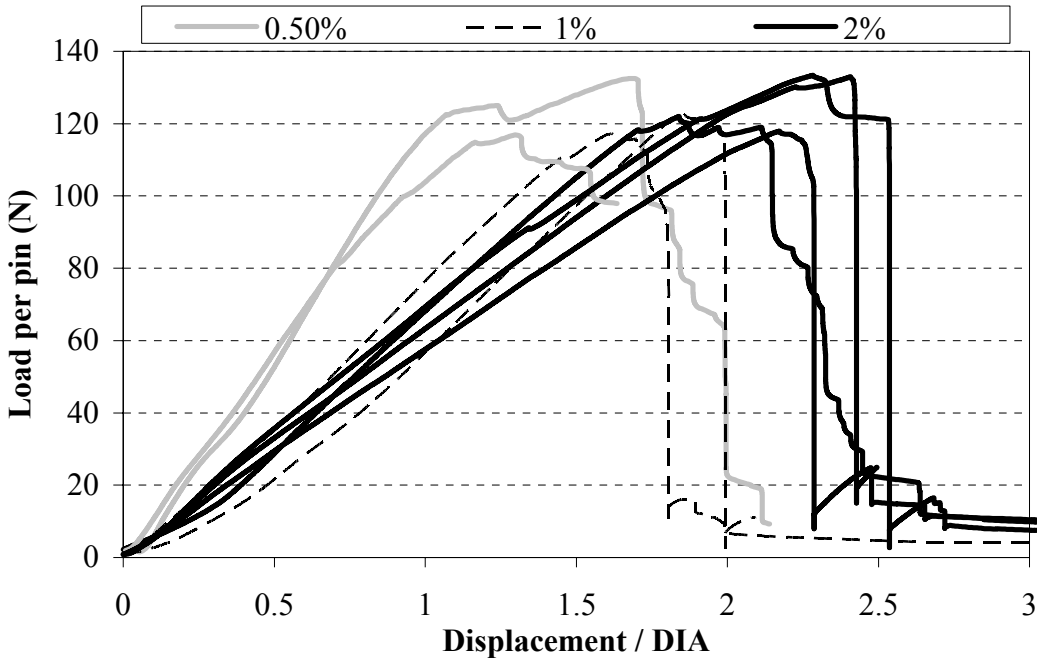

Figure 5-15: *Effect of pinning density on traces of load versus normalized displacement of 0.5mm diameter Z-pins in woven fabric G986/M21 under shear loading.*

5.3.4 Effect of angle

Cases where the Z-pin angle deviated from normality to the plane of the specimen were also tested. The angle was determined as the average of the angle of the Z-pins on a side of the specimen, where Z-pins were visible. If no visible row of Z-pins existed, the angle was measured after the test; the specimen side was polished down to the next row of pins to facilitate Z-pin angle measurement using a microscope. Z-pins with inclination towards the relative sliding direction are considered to have a positive angle; opposite inclination signifies a negative Z-pin angle.

Figure 5-16 presents the effect of angle on the load versus normalised displacement trace of UD specimens with 0.5mm diameter Z-pins. A positive angle aligns the Z-pin to the sliding direction. Pullout is assisted and a lower peak load is recorded. A high negative angle results into a higher peak load and premature failure relative to the zero angled Z-pin; the ratio of Z-pin splitting to pullout is increased. If a low negative angle is present, the Z-pin appears to re-align through ploughing. The curve presented for a Z-pin with an angle of -9 , is similar to that of the zero angled Z-pin, shifted to the right on the plot. Similar trends have been observed in a previous study on the effect of Z-pin angle UD laminates [20].

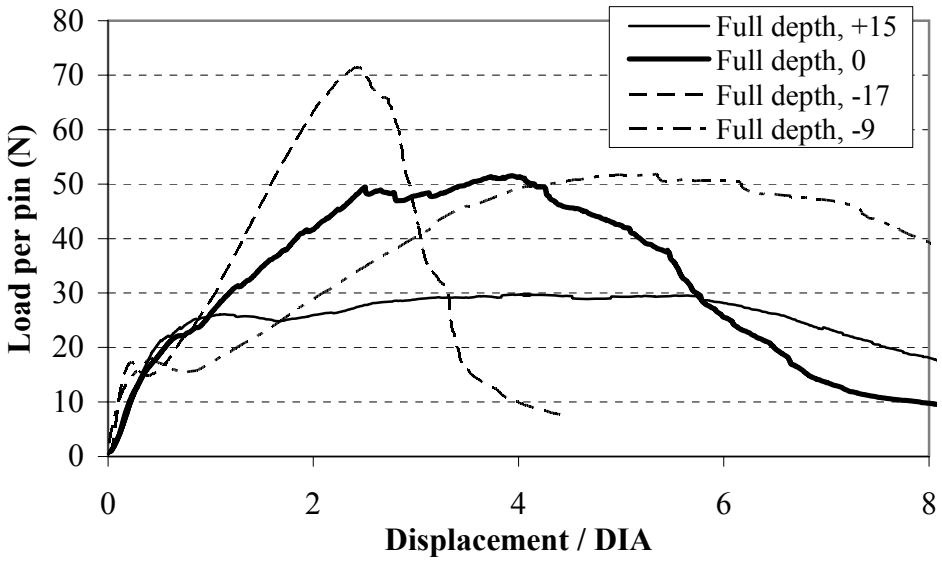

Figure 5-16: *Effect of Z-pin angle on load versus normalized displacement of 0.5mm diameter Z-pins in UD IM7/M21 under shear loading*

Observations in woven fabric specimens reveal similar trends. Figure 5-17 depicts the effect of Z-pin angle in G986/M21 with 0.28mm diameter Z-pins. Similarly to the UD case, a positive angle assists Z-pin pullout and a negative angle results in premature failure. However, the peak load is lowest with a negative Z-pin angle and highest when the Z-pin is normal to the specimen plane.

It has to be noted that the differences in trends can be an effect of material as well as an effect of the different Z-pin diameter. Results in this study do not fully characterize the difference of the effect of Z-pin angle between UD and woven fabrics.

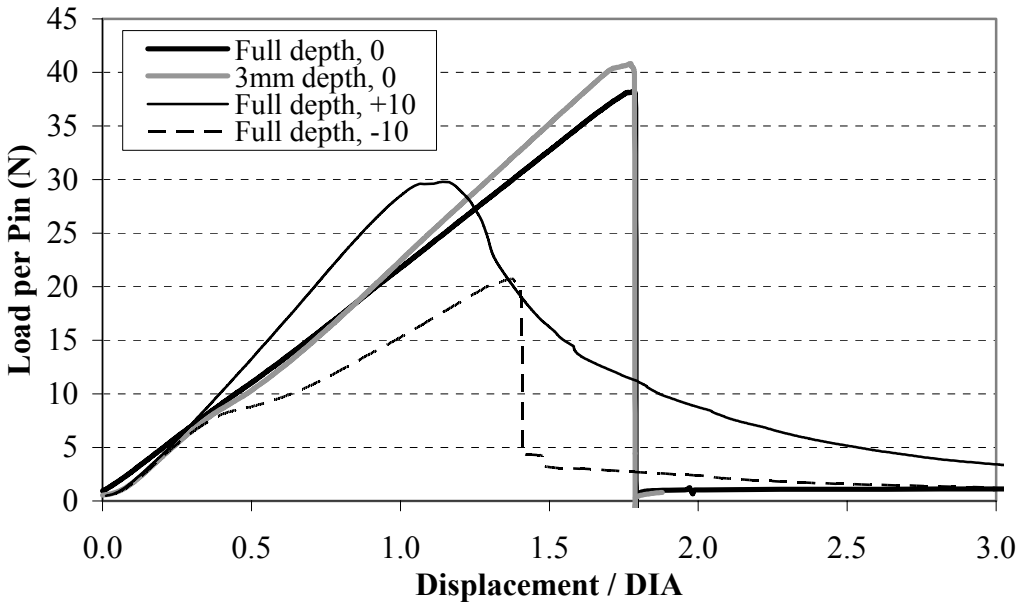

Figure 5-17: *Effect of Z-pin angle on load versus normalized displacement of 0.28mm diameter Z-pins in woven fabric G986/M21 under shear loading*

5.3.5 Effect of insertion depth

Figure 5-18 illustrates the effect of insertion depth on Z-pin failure in UD laminates under shear loading. Specimens with a positive angle exhibit Z-pin pullout; a decreased insertion depth leads into premature failure, as the shorter Z-pin pulls out at a lower displacement. In specimens with a negative angle, a change in the type of failure occurs; the Z-pin is allowed to partly re-align and pullout. The failure is again premature due to the decreased length of the Z-pin. Decreased insertion depth facilitates Z-pin pullout in both cases.

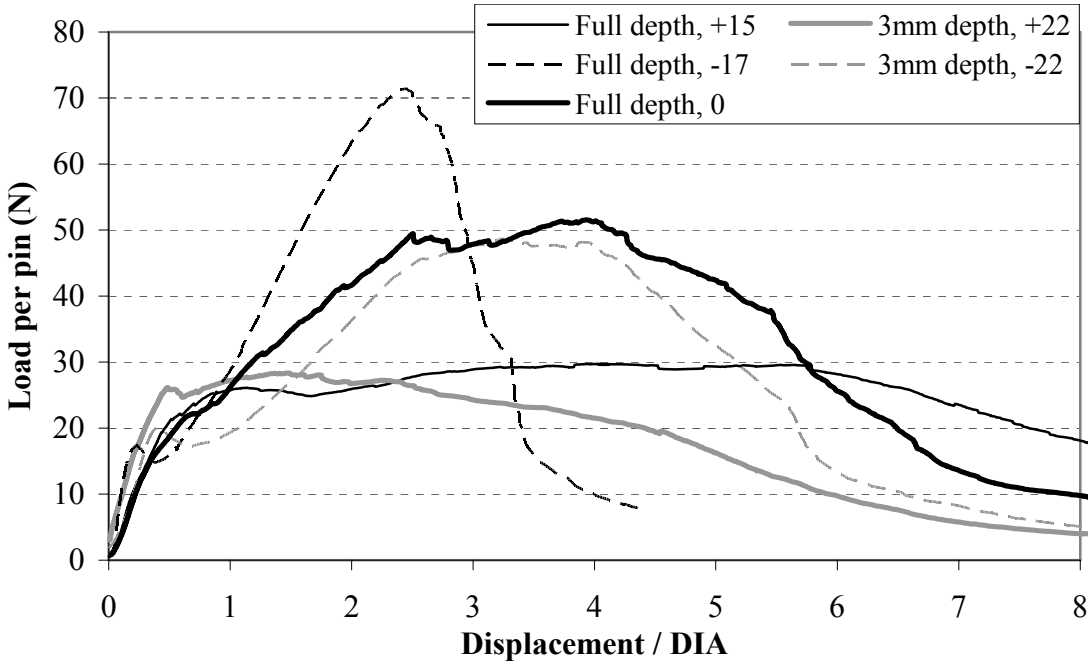

Figure 5-18: *Effect of insertion depth on load versus normalized displacement of 0.5mm diameter Z-pins in UD IM7/M21 under shear loading*

Figure 5-19 displays load versus displacement curves obtained in testing of woven fabric specimens with 0.5mm diameter Z-pins for five separate insertion depths. In specimens pinned throughout the whole thickness, failure initiates late and is catastrophic in manner. Complete failure occurs at a normalised displacement of 2.5. In specimens with a 4.2mm insertion depth failure initiates slightly earlier. Effective failure occurs at a similar normalised displacement, but it is not complete; a small portion of load can be sustained for a further 0.5 of normalised displacement. A further reduction in insertion depth (3.6mm case) does not exhibit differences in the failure initiation load. However, the failure is progressive and extends significantly after 2.5 of normalised displacement. Further reduction of the insertion depth reduces the both the failure initiation load as well as the required normalised displacement to failure.

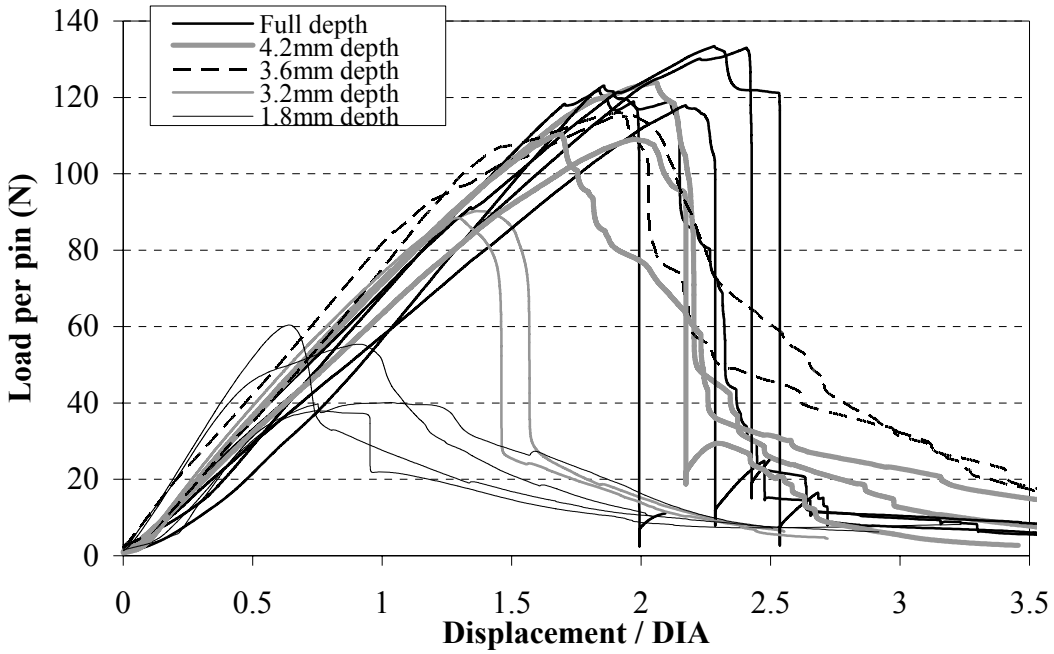

Figure 5-19: *Effect of insertion depth on load versus normalized displacement of 0.5mm diameter Z-pins in woven fabric G986/M21 under shear loading*

Figure 5-20 illustrates the differences in failure type, relative to the changing insertion depth. In the first image (a), the pins have pulled out completely from the side where the Z-pins are chamfered. The pullout length, the length of the pins protruding from the laminate, is 0.9mm, exactly half of the insertion depth. The progressive pullout is reflected in the continuous shape of the load versus displacement curve. In the second image (b), the pin has split and failed; the protruding length then pulled out of the laminate. This explains the two stage failure observed from the experimental curve.

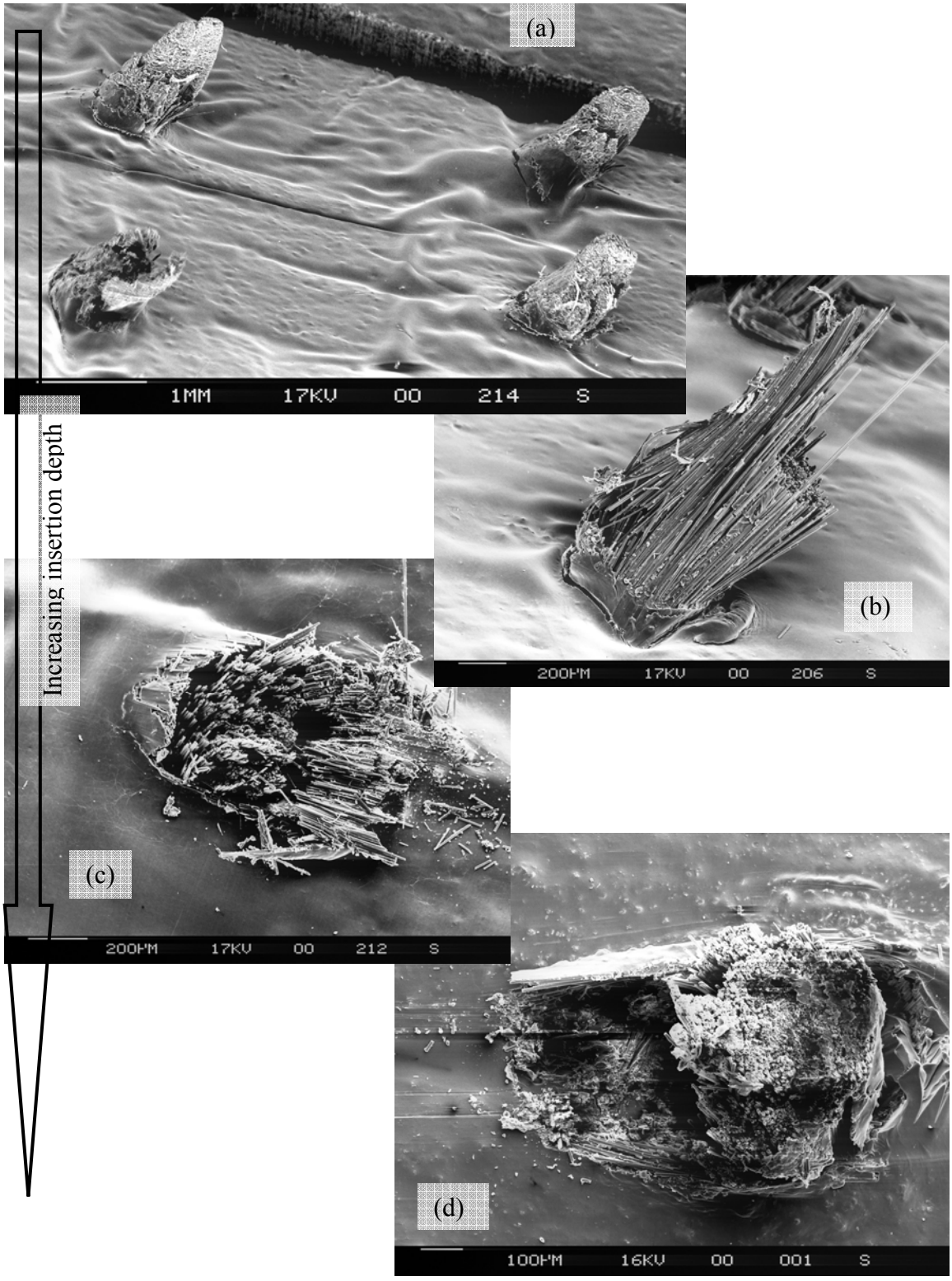

Figure 5-20: *SEM images of Z-pins in woven fabric G986/M21 under shear loading for different insertion depths, (a) 1.8mm (b) 3.2mm, (c) 4.2mm, and (d) full (7mm)*

The next image (c) indicates minor pullout of small fibre bundles of fibres from the Z-pin. The type of failure, however, is mainly splitting and extensive bending of the Z-pin fibres, as well as a certain amount of resin damage through minor ploughing. The last image exhibits a different type of failure. Significant resin crushing has allowed a small bundle of the Z-pin to pullout. The Z-pin has failed predominately in shear. It has to be noted that in all images the local laminate fibre direction is the same and is identical to the sliding displacement.

It can be argued, that the sustained load after main failure in the load versus normalised displacement curve for some cases (namely for 3.2mm and 4.2mm insertion depth) can be the result of friction. As few of the Z-pins pullout and wedge themselves between specimen halves, friction increases. The additional load measured due to friction can be identified at the end of the test; the load measured after failure will be caused by friction. While the specimen is still in the fixture, the displacement is operated manually in both directions and the maximum load is recorded. This procedure was applied for a small number of specimens, which were afterwards eliminated from post-mortem microscopy. The load measured was between 60N to 90N; compared to the full load for the whole specimen (ranging between 2kN to 3kN) a percentage of 5% at maximum is deduced. This is lower than the value of sustained load apparent in the figure. This implies that the difference in the shape of the curves is indicative of a difference in the failure mechanism.

Figure 5-21 displays the different amount of opening displacement imposed due to Z-pin presence for different insertion depths. The ratio of opening to sliding displacement is consistent for insertion depths of 3.6mm or higher. As the insertion depth increases further than 3.6mm, the opening increases.

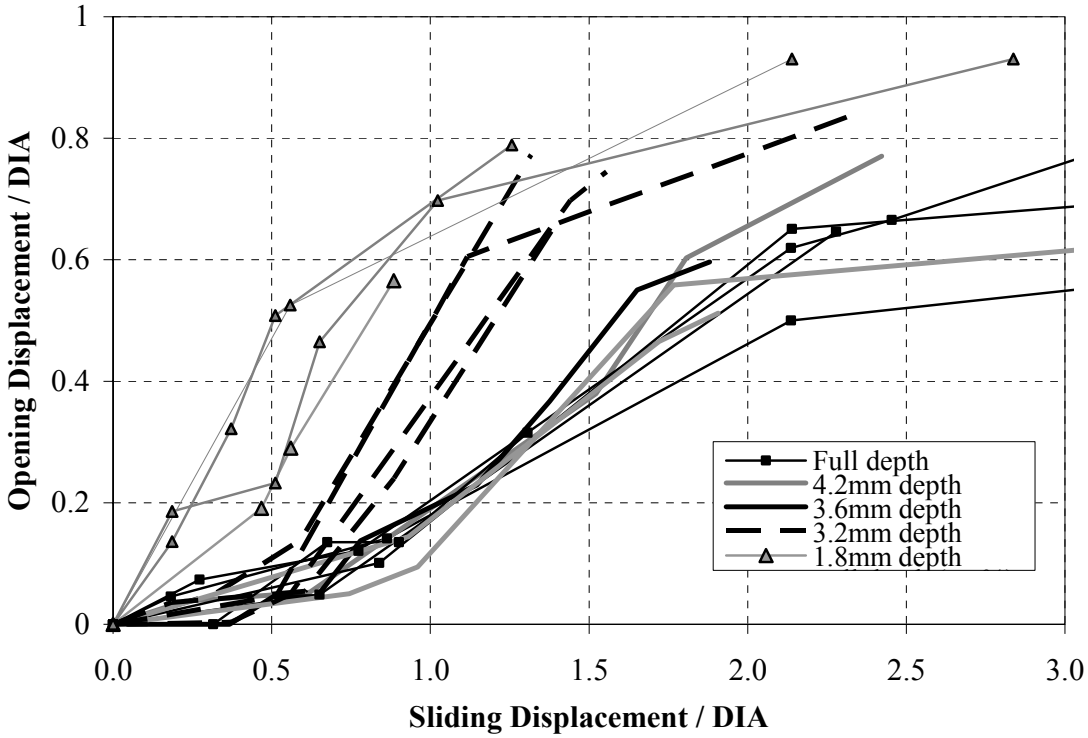

Figure 5-21: *Comparison of opening versus sliding displacement in woven fabric G986/M21 "Z-shear" specimens for different insertion depths*

5.3.6 Geometric considerations

With the opening constraint being a property of the testing fixture, two main additional influencing parameters have been identified, as long as the type of failure is concerned; the Z-pin insertion depth-to-diameter aspect ratio, and the laminate material type. With regard to the latter parameter, significant difference exists in the amount of Z-pin 'ploughing' between woven fabric and UD material. A further implication is the effect of the stacking sequence. This is apparent in the woven fabric, as the orientation of laminate fibres at the delamination plane varies between 0 /0 , 0 /90 and 90 /90 interfaces, with regards to the sliding direction. The effect of laminate fibre orientation, or, equivalently, of the stacking sequence is illustrated in Figure 5-22; the two extreme instances of partial pullout and laminate fibre damage are depicted. Although an additional effect of Z-pin angle on the obtained experimental curves has been observed, its effect on the failure type has not been fully investigated.

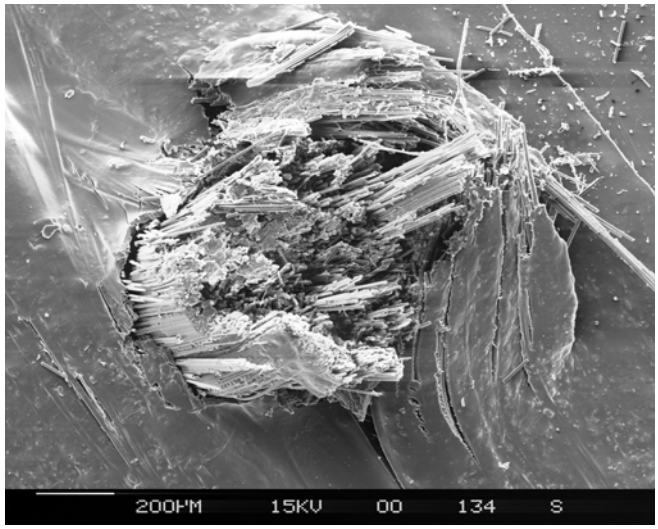

(a)

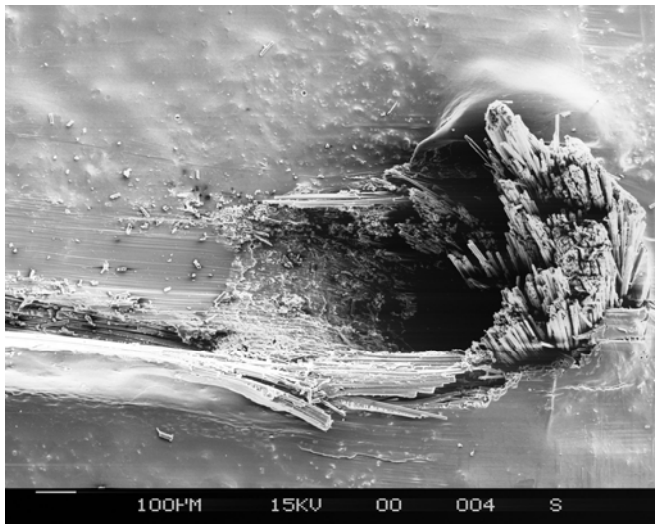

(b)

Figure 5-22: *Effect of laminate fibre orientation of the interface in the delamination plane on the failure type of Z-pins; (a) failure of a 0.5mm diameter Z-pin with full insertion depth at a 90 /90 interface, (b) failure of a 0.5mm diameter Z-pin with full insertion depth at a 0 /0 interface.*

5.3.7 Z-pin energy absorption in shear

The area under the load versus displacement traces contains the amount of energy dissipated through fracture. The dense mesh of measurements obtained during the tests allows the accurate integration of this energy using the trapezoid method. There are two approaches regarding the calculation; integrating up to a certain displacement or integrating until ultimate failure. Using the first approach, the superior performance of Z-pins with 0.5% density in woven fabric can be demonstrated; the increased area under the experimental curve in Figure 5-15 for small displacements is apparent.

For the evaluation of the effect of insertion depth, the second approach was adopted. The area under the load versus displacement curves was calculated until the point where the load decreases down to 5% of the maximum recorded. Any effect of friction is therefore partly eliminated. Figure 5-23 displays the energy absorbed by 0.5mm diameter Z-pins in woven fabric as a function of the insertion depth. The scatter is one time the standard deviation.

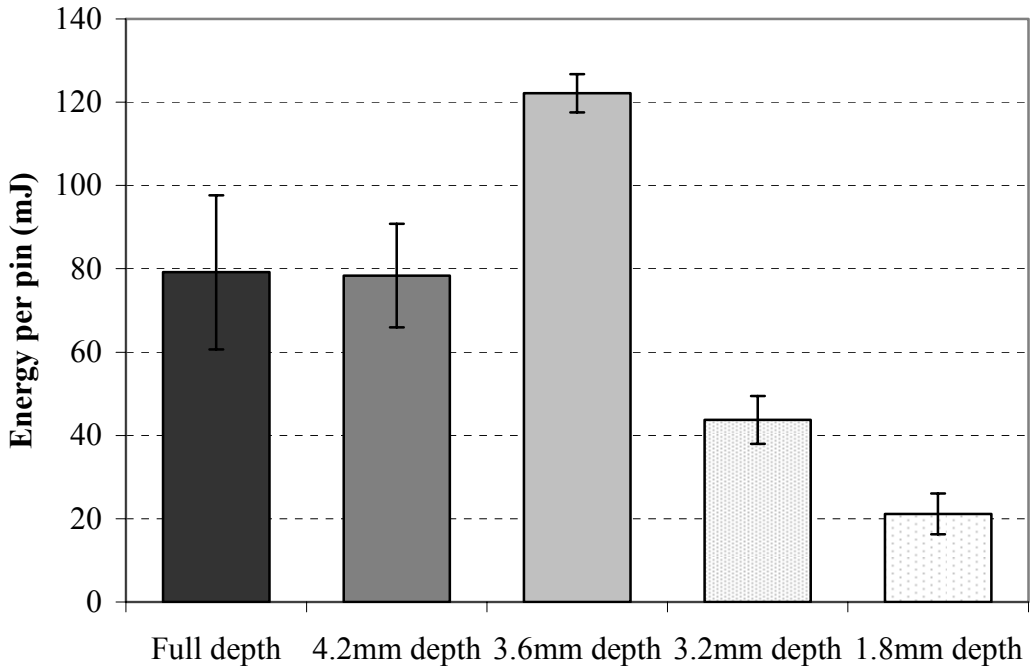

Figure 5-23: *Energy dissipated by a single 0.5mm diameter Z-pin under shear loading, using the 'Z-shear' configuration for woven fabric G986/M21*

In combination with the microscopy images, the shape of the load versus displacement curves and the change in opening to sliding ratio, this figure indicates a change in fracture mechanisms with insertion depth. Apparently, there is a certain insertion depth where the energy that can be potentially absorbed is highest.

Figure 5-22 presents the equivalent plot for Z-pins of both diameters in UD material. The dominance of pullout as a failure mechanism is indicated from the fact that the amount of energy dissipated is a close to linear function of insertion depth. For 0.28mm diameter Z-pins the energy is half for half the insertion depth. For 0.5mm diameter Z-pins, this is not the case. However, tests of UD specimens with full insertion depth were stopped before ultimate failure, due to the restricted available displacement of the clip gauge (5mm).

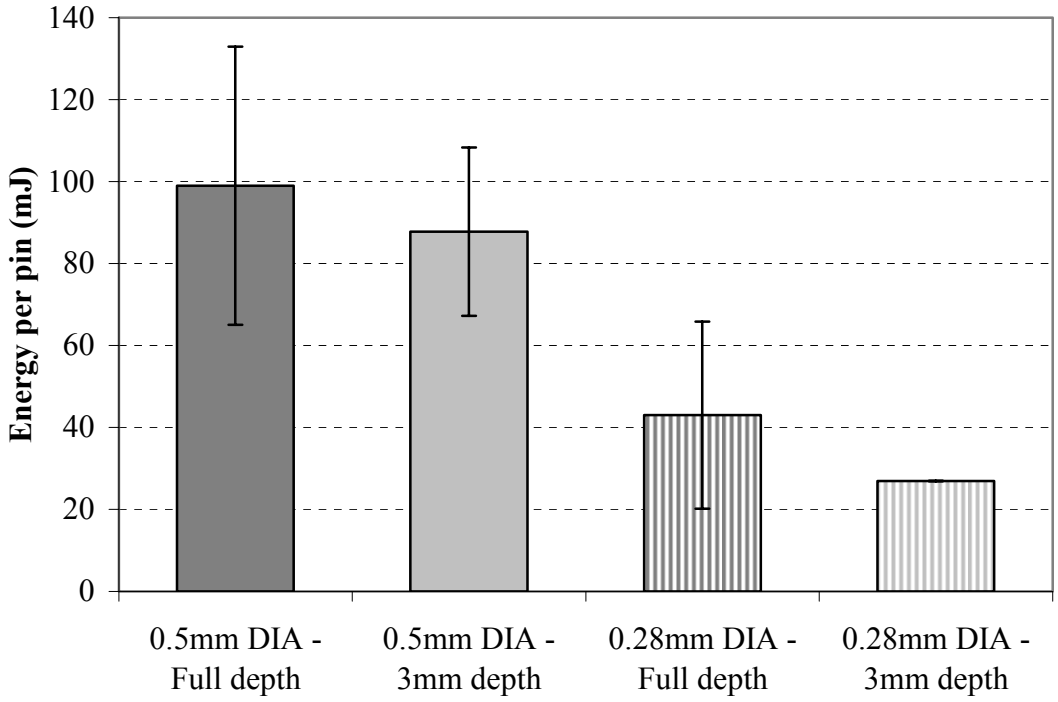

Figure 5-24: *Energy dissipated by a single Z-pin under shear loading, using the 'Z-shear' configuration for UD IM7/M21*

5.3.8 Z-pin failure mechanisms under shear loading

In mode II the failure mechanism is a function of the crack opening constraint, material type, stacking sequence and insertion depth to Z-pin diameter ratio. Figure 5-25 illustrates a single Z-pin under shearing loading conditions. Ideally, the pair of shearing forces lies on parallel axes marginally distanced from each other. As the distance between them increases, the ratio of bending to shear (of the Z-pin) increases. The distance between the applied forces depends on the ply geometry of the laminate. A resin rich area surrounds the Z-pin. The Z-pin can crush the resin and plough into the resin rich area under lateral loading. Laminate fibres at a 0 angle relative to the lateral displacement of the Z-pin provide little constraint, while fibres at a 90 angle provide the most. The amount of constraint will therefore vary with fibre orientation above and below the displacement (or delamination) plane. The distance between the equivalent pair of shearing forces varies with it. This distance is usually considerable compared to the Z-pin diameter, as the Z-pin tends to plough even under the maximum constraint; local fracture of 90-degree fibres due to Z-pin ploughing has been observed. This induces a local bending load on the Z-pin. In combination with resin crushing and the developing space, the Z-pin is allowed to incline locally according to the bending loading.

The highly orthotropic properties of the Z-pin tend to favour failure in longitudinal shear (splitting) under lateral loading. Splitting separates the Z-pin into numerous fibres. Since the diameter of each Z-pin constituent fibre is significantly smaller than the Z-pin diameter (7-10 m), the bending to shear loading ratio increases further. Z-pin fibres are loaded less in shear and more in tension, since they are allowed to align with the lateral displacement axis more easily after splitting occurs. For the latter to happen, at least a minor amount of stretching or pullout of the Z-pin is required. If the inserted depth of the Z-pin can resist the pullout due to the tension loading of the Z-pin fibres, while the constraint against ploughing is severe both above and below the displacement plane, the Z-pin will fail in shear. If a debonded Z-pin experiences initial pullout, the change in the frictional tractions on the Z-pin, as it is pressed against the constraining laminate due to ploughing (also called ‘snubbing’ effect [74]), can constrain further pullout;

delamination planes exhibit failed Z-pins protruding marginally from *both* fractured surfaces. If pullout commences, an opening displacement is introduced to accommodate the unbroken Z-pin fibres between the laminate plies, since the amount of possible lateral ploughing of the Z-pin is finite.

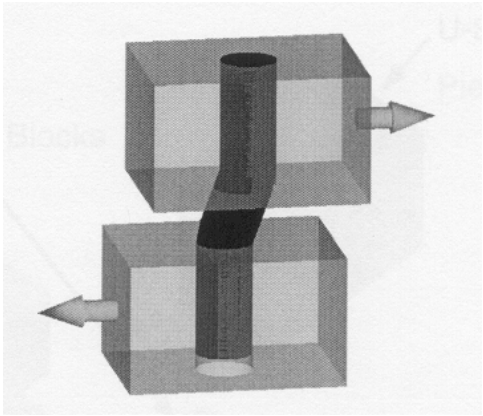

Figure 5-25: *Z-pin under shear loading*

The amount of opening displacement introduced depends on the initial loading mode ratio and the constraint against crack opening. A laminate constraint by other sub-components of a structure or a laminate of significant thickness allows smaller opening displacements to be introduced. The failure mode of the Z-pin, as the lateral displacement continues to increase, is a combination of pullout, fibre fracture and resin crushing. The amount of energy absorption depends on this balance.

5.4 Validity of the crack measurement in 4ENF delamination testing of Z-pinned laminates

The effects of friction and Z-pin presence are reflected in the mode II delamination testing of Z-pinned laminates. Before combining all this information together with toughness measurements from mode II delamination tests, it is important to ensure that the toughness measurement is meaningful. The applicability of typical data reduction techniques to Z-pinned laminates is examined in this section.

5.4.1 Coalescence of microcracks

Crack measurement is performed by eye during a delamination test. Following a crack during a mode I delamination test is straightforward. Unless the crack is moving between plies, as when testing a cross-ply specimen, the crack tip is easily distinguishable. Magnifying lenses and travelling microscopes enable accurate crack measurement. Still, a convention has to be adopted, as to what is considered to be a crack. The side of a delamination specimen is coated with correction fluid. As the crack propagates, two characteristic areas close to the crack tip can be identified. One, where a barely visible line appears on the correction fluid, but still no gap is visible. This line is typically 1mm long. The second area is where a gap is visible and the line is therefore black. Testing can be valid when the edge of one of these lines is *always* considered to be the crack tip in all specimens. This is one reason why there can be variations in the toughness measurement of the same material between different labs. The position of the actual crack tip may be offset compared to the indication on the side of the specimen, and has been observed to be so in glass fibre specimens with transparent matrix, where the crack is also visible from above, through the specimen [106]. This, however, cannot be verified in carbon fibre specimens during testing.

As for mode I tests, a similar convention is necessary for mode II. The difficulty with following a crack in mode II is that there is no visible gap close to the crack tip. The

crack is a much finer line than a mode I crack. High magnifications have to be used. Additionally, visible cracking takes place further than the continuous line of the main crack in the shape of crazes or hackles (microcracking). These increase in number and size and finally coalesce in one crack. This is typical for crack propagation under mode II loading. It is therefore important that one is consistent with the application of one's convention. Figure 5-26 illustrates how a crack propagates in mode II and where the crack tip is considered to be in each case. In this study a magnification of 21 was used. The length of the area covered with microcracks in woven fabric specimens tested (G986/M21 and G986/M36) was between 2mm and 5mm.

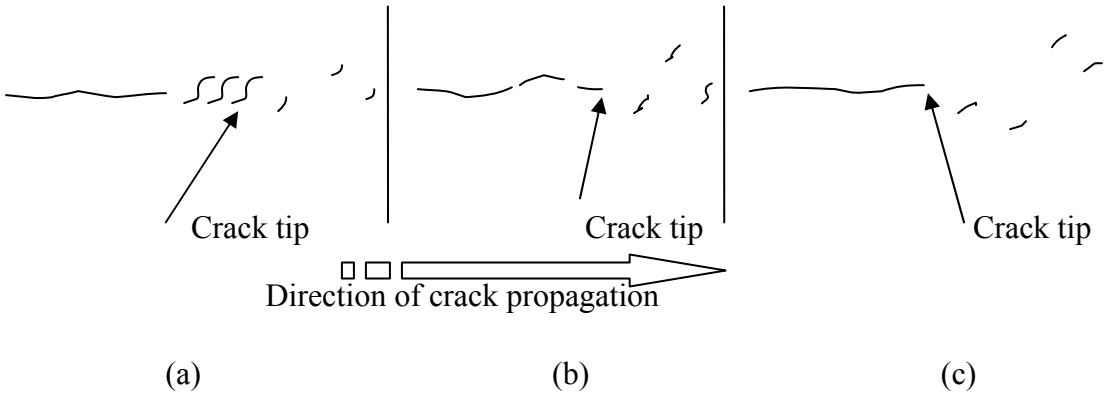

Figure 5-26: *Examples of visible crack paths and crack branching at the edge of the 4ENF specimen; point selected as crack tip displayed*

Inaccuracies in crack measurement can be enlarged when the difficulty to establish the exact location of the crack tip results in a reduction on the number of measurements. As explained in section *4.1*, a fine mesh of measurements is important to the data reduction.

Another aspect is the effect of the material on the crack path. In woven specimens the crack path is hardly self-similar, as explained in section *2.4*. Crazes up to 2 or 3 plies above and below the crack plane are not uncommon, further hindering the measurement. Figure 5-27 depicts C-scan images of unpinned woven mode II specimens with 4.4mm thickness, revealing the delamination front. In both specimens the delamination front appears perpendicular to the specimen length; however the beam is not fully cracked behind the crack front. The pattern of the crack path is dictated by the pattern of the weave.

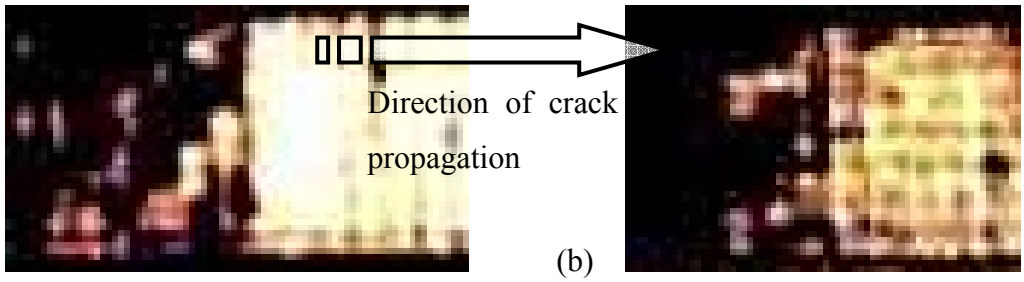

Figure 5-27: *C-scan images revealing the delamination front in unpinned woven specimens*

5.4.2 Accuracy of measurement – Regression coefficient

Compliance calibration data are obtained during the test. Compliance calibration data are fitted linearly after the test to determine the slope of compliance change, m, according to equation (5-3). The regression coefficient shows the accuracy of the fitting and subsequently the accuracy of the measurement. A regression coefficient above the value of 0.99 is considered acceptable. Despite all efforts to obtain a high regression coefficient, it remained under the suggested value. Figure 5-28 displays the regression coefficient of G986/M21 specimens of 6.6mm thickness and different sets of Z-pinning parameters. Specimens with regression coefficients lower than 0.94 were withdrawn from results, on the basis that an additional source for the low coefficient value was a poor crack length measurement during the test.

Figure 5-29 displays compliance calibration curves of two Z-pinned specimens. Specimen thickness is 6.6mm. The path of the data points descends for crack lengths between 55mm and 65mm. As the crack propagates further, the inclination of the data path increases again. This phenomenon is common among all Z-pinned specimens, at different magnitudes. The source is the thickness variation of the manufactured specimens. The thickness is at its maximum close to the centre of the 25mm long block of Z-pins inserted in the specimens, which is close to the point of change of inclination of the compliance curve. The effect on the accuracy of the crack measurement becomes apparent by observing the low regression coefficients of the specimens in the figure.

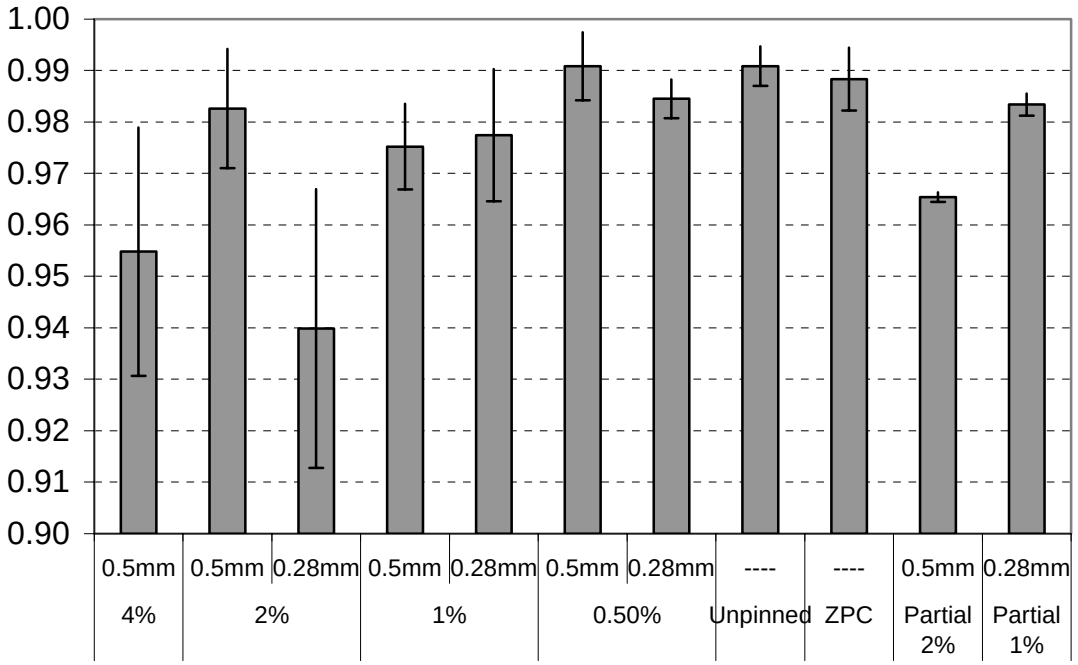

Figure 5-28: *Compliance calibration regression coefficients of 6.6mm thick G986/M21 specimens for different test cases; error bars show the standard deviation*

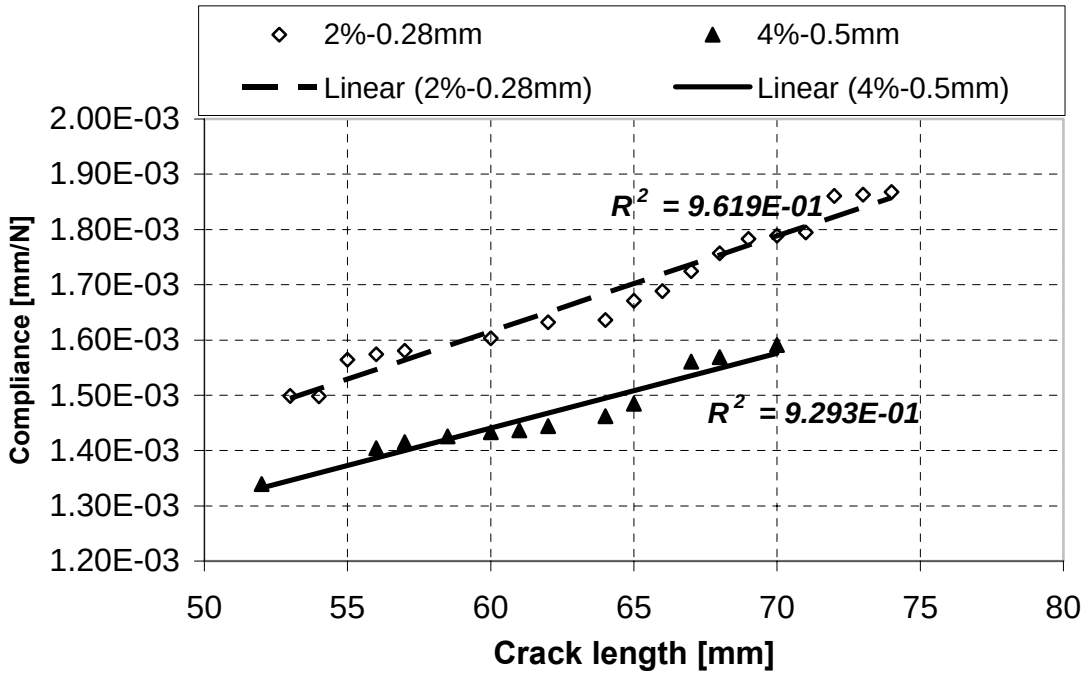

Figure 5-29: *Compliance calibration curves of two specimens with 6.6mm thickness*

5.4.3 Alternative data reduction methods

The use of beam theory for data reduction requires the use of material data for the determination of the fracture toughness. Moreover, the experimental compliance methods generally provide more conservative values [101,105]. In both the ELS and 4ENF test configurations, the modulus E required to match beam theory with experimental data is usually 10% to 20% higher than the independently measured modulus of the material [101,105]. The inclusion of the crack length in the final expression of the delamination toughness for the ELS test configuration allows the errors in crack length measurement to be evaluated. This is achieved by rearranging the corrected beam theory expression for the toughness with respect to the crack length and the incorporation of the measured compliance [105]. Such an evaluation is not possible when using the 4ENF test configuration, since the measured delamination toughness is independent of the crack length.

Furthermore, the sensitivity of the accuracy to determine the delamination toughness to the value of the modulus [102], is attenuated in Z-pinned specimens, as the modulus varies along the specimen length. The experimental compliance method is used in this study.

5.4.4 Introduction of a uniform compliance calibration slope m

The significance of the exact value of the slope of the experimental compliance calibration curve can be appreciated from equation (5-2). Any miscalculations of the slope m, due to deficient linear fitting of the compliance calibration curve, will be reflected in the calculation of the delamination toughness.

To reduce errors in determining the compliance, two techniques are recommended [107]. One is defining the compliance from the load versus displacement curve, which means tests are conducted in a load-unload-reload manner. The applicability of the technique with Z-pinned specimens is questionable, since unloading introduces

additional damage to the Z-pins, altering the delamination resistance they provide. The second technique involves performing the compliance calibration beforehand, as with the ENF test.

In order to appreciate the complete effect of Z-pinning on the flexural behaviour of a delaminating beam, a different type of specimen was manufactured. This delamination specimen contains Z-pins in the upper and lower half of its thickness only; no Z-pins protrude from one half into the other. Figure 5-30 illustrates the Z-pin layout. Manufacturing was achieved by partially Z-pinning each half of the laminate before stacking the two halves together. Two plies of material remained unpinned in each half of the specimen to prohibit any penetration of the middle plane by Z-pins during cure. This type of specimen will be referred to as "Z-Pinned Control" (ZPC). The dimension of the Z-pin block inserted is identical to all Z-pinned specimens (25mm long). Two 6.6mm and two 4.4mm thick specimens were manufactured. For each thickness, one specimen was Z-pinned with 2%, 0.5mm diameter pins and the second with 2%, 0.28mm pins. The crack interface remains identical to that of the unpinned specimens. Any discrepancies in delamination toughness originate from the altered flexural behaviour. Figure 5-31 contrasts the delamination toughness of ZPC specimens against unpinned ones.

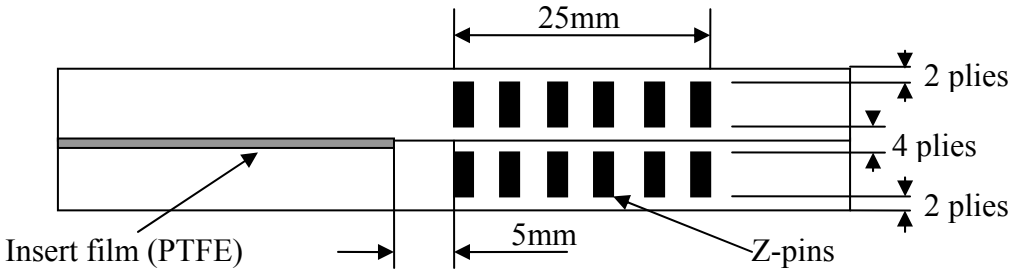

Figure 5-30: *Z-pin layout of a Z-Pinned Control (ZPC) specimen*

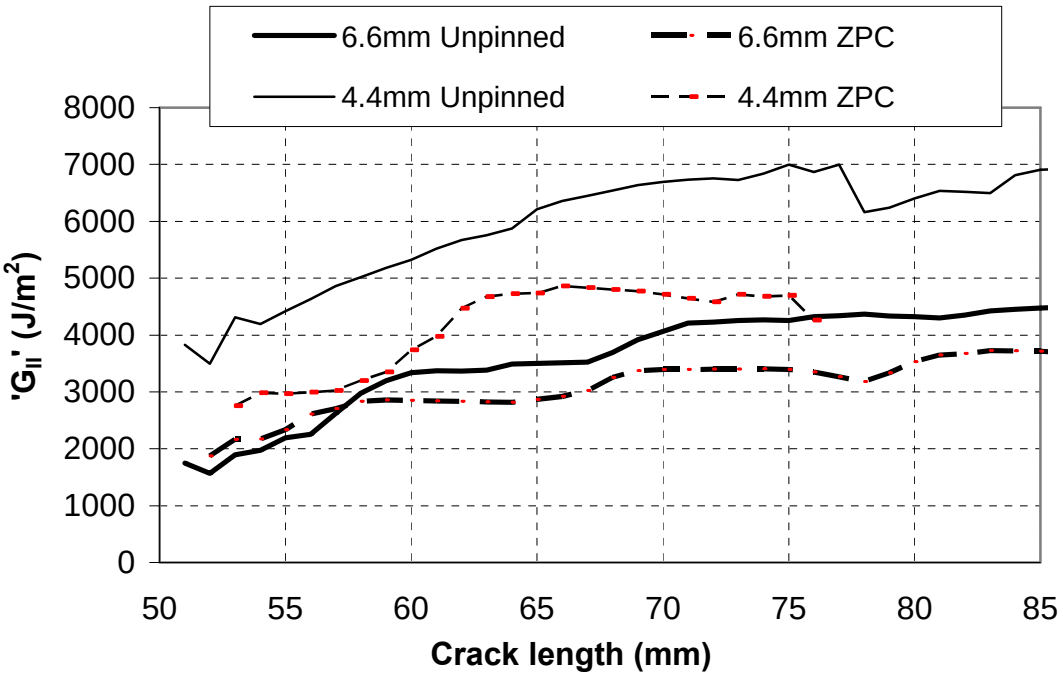

Figure 5-31: *Delamination toughness of unpinned and ZPC woven (G986/M21) specimens for 4.4mm and 6.6mm laminate thickness*

The regression coefficient of ZPC specimens is similar to that of the unpinned specimens and is close to the suggested value of 0.99. The slope m of the ZPC specimens was used in the calculation of the delamination toughness for all Z-pinned specimens instead of the slope deduced from each test. This would negate the emergence of errors in the delamination toughness calculations, caused by inaccurate compliance calibration slope values. An example of the variation of the slope m deduced from tests, and subsequently an indication of the potential error introduced in the delamination toughness calculation without the aforementioned correction, is illustrated in Figure 5-32.

In support of the application of the correction procedure, Figure 5-33 displays the mode II delamination toughness of high density Z-pinned specimens (4% density, 0.5mm Z-pin diameter) in contrast to unpinned specimens. Specimen thickness is 6.6mm. Figure 5-33a has been produced without correction, while Figure 5-33b includes the correction. Average values are displayed, as well as the upper and lower bounds of the measurements for Z-pinned specimens.

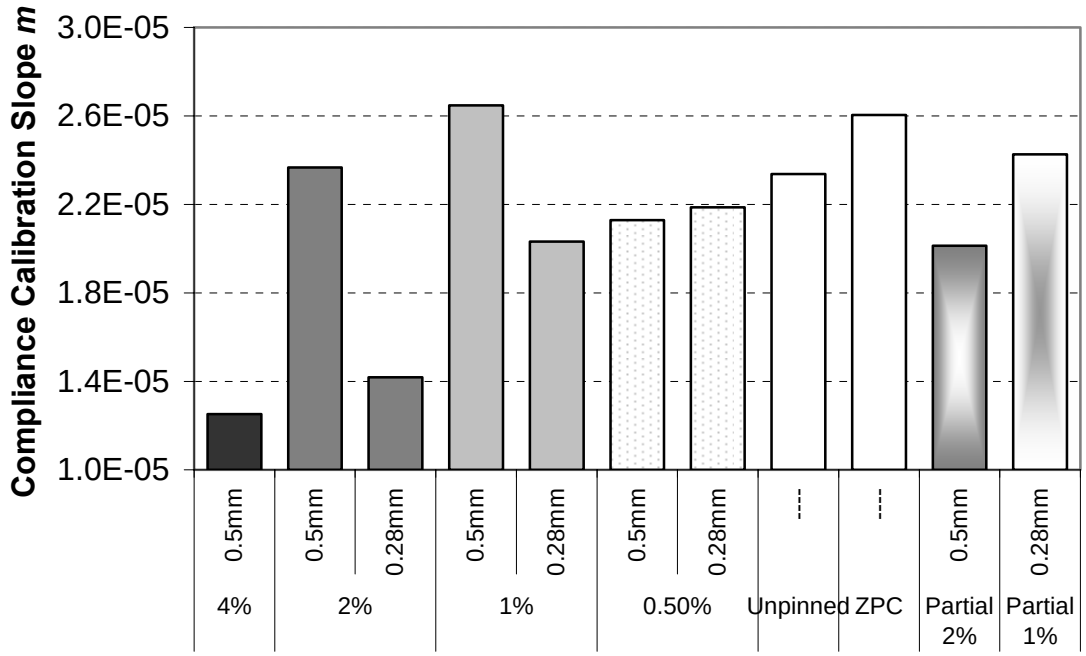

Figure 5-32: *Compliance calibration slope m of 6.6mm thick G986/M21 specimens for different test cases*

Before the correction, in Figure 5-33a, the delamination toughness of the Z-pinned specimens is initially lower than the toughness of the unpinned specimens, despite the fact that no difference exists between them in the first 5mm of crack length, *before* the crack propagates past the first row of Z-pins. The curve rises to a value similar to the unpinned case and propagation stops around 72mm of crack length. During the experiment, the crack was completely arrested and the Z-pinned specimens failed in bending. According to Figure 5-33a, propagation should have continued.

After applying the compliance calibration slope correction, in Figure 5-33b, the source of crack arrest is apparent. The delamination toughness at the point of arrest is twice the toughness of the unpinned specimens. A rise in the Z-pinned R-curve above the unpinned R-curve for a crack length of 55mm can also be observed, which corresponds to the position of the first row of Z-pins.

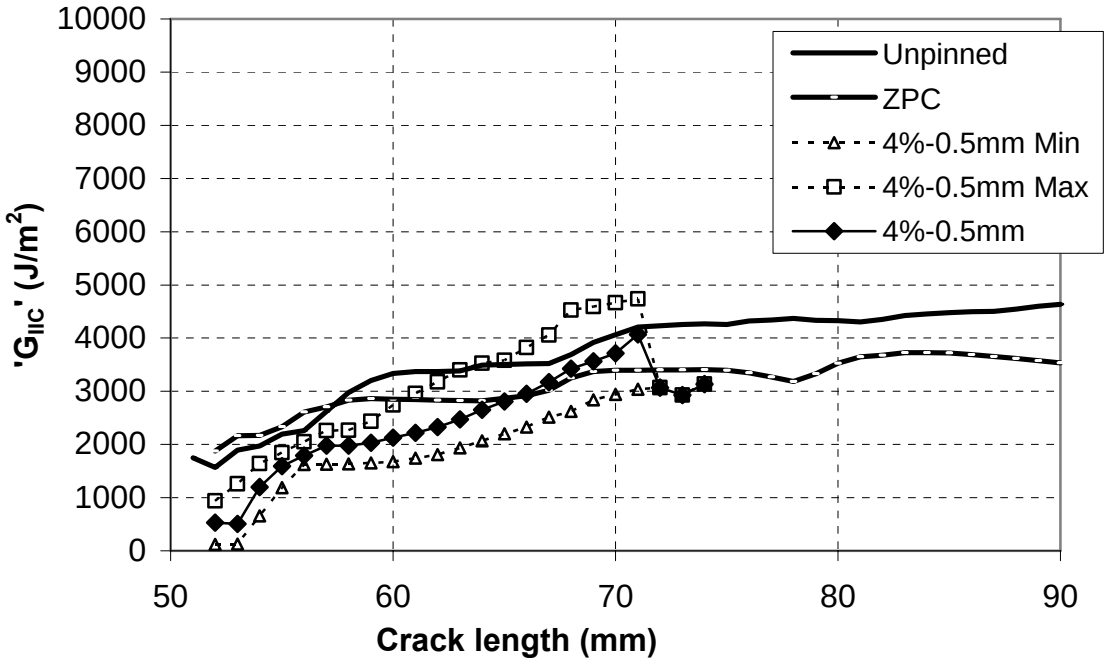

(a)

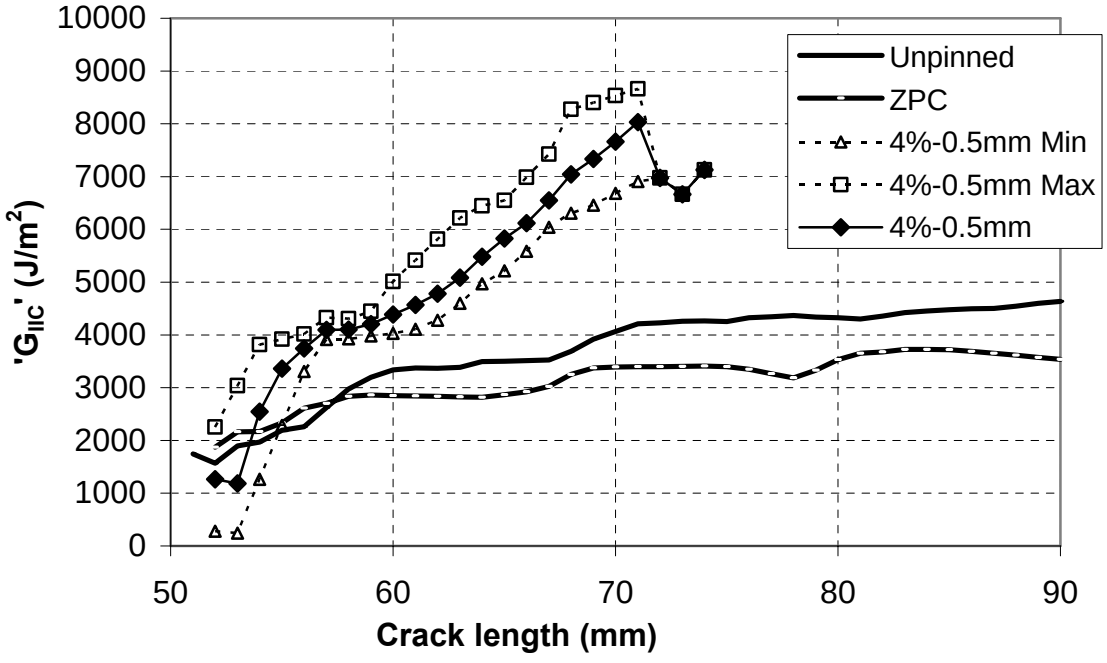

(b)

Figure 5-33: *Delamination toughness of woven Z-pinned specimens (G986/M21, 6.6mm thick, 4% density, 0.5mm Z-pin diameter) without (a) and including (b) compliance correction. Average values and upper and lower bounds displayed*

5.5 4ENF mode II test cases

Table 5-2 displays the test cases included in the presentation of results.

Material	Thickness (mm)	Density (%)	Diameter (mm)	Insertion depth (mm)	No. of samples
G986/M21	6.6mm	---	---	---	5
G986/M21	6.6mm	(ZPC)	(ZPC)	(ZPC)	2
G986/M21	6.6mm	0.5	0.5	Full	3
G986/M21	6.6mm	1	0.28	Full	3
G986/M21	6.6mm	1	0.28	3.6	2
G986/M21	6.6mm	1	0.5	Full	2
G986/M21	6.6mm	2	0.28	Full	4
G986/M21	6.6mm	2	0.5	Full	3
G986/M21	6.6mm	2	0.5	3.6	2
G986/M21	6.6mm	4	0.5	Full	4
G986/M21	4.4mm	---	---	---	6
G986/M21	4.4mm	(ZPC)	(ZPC)	(ZPC)	2
G986/M21	4.4mm	0.5	0.5	Full	2
G986/M21	4.4mm	1	0.5	Full	2
G986/M21	4.4mm	2	0.28	Full	1
G986/M21	4.4mm	2	0.5	Full	6
G986/M21	4.4mm	2	0.5	2.2mm	2
G986/M21	4.4mm	4	0.28	Full	1
G986/M21	4.4mm	4	0.5	Full	1
G986/M21	4.4mm	4	0.5	2.2mm	1
G986/M36	6.6mm	---	---	---	2
G986/M36	6.6mm	1	0.28	Full	2
G986/M36	6.6mm	1	0.28	3.6	2
G986/M36	6.6mm	2	0.5	Full	2
G986/M36	*6.6mm*	*2*	*0.5*	*3.6*	2

Table 5-2: *4ENF mode II test cases*

Details on ZPC type specimens have been presented in section *5.4.4*. The delamination toughness of all pinned specimens has been corrected to the experimental compliance calibration slope of the ZPC specimens, as discussed in section *5.4.4*.

5.6 Mode II results: identification of parameter effects

The following mode II delamination results illustrate that Z-pinning enhances mode II delamination toughness. However, it is more important to present the results in a way that aids the identification of any effects the Z-pinning and material parameters have on the delamination toughness.

5.6.1 Effect of laminate thickness

The suggested thickness for a 4ENF mode II test of a carbon fibre/epoxy laminate is 3mm. Similarly to mode I, the thickness should not affect the measurement of the delamination toughness, when no fibre bridging is present. Figure 5-34 presents the mode II delamination toughness of G986/M21 for beam thicknesses of 4.4mm and 6.6mm. The specimens presented are unpinned. Average propagation curves are presented, as well as the upper and lower bounds for each thickness. It is clear that thickness affects the measurement significantly. Apart from the fact that propagation values are significantly different, initiation values are also far apart.

Establishing initiation values for both woven materials G986/M21 and G986/M36 using the 4ENF configuration has proven difficult. Measuring the initiation toughness is made difficult by problems associated with obtaining an accurate determination of the crack length, as explained in section *5.4*. Alternative methods can be implemented, when determination of the initiation is not possible. One of them is by determining the point of initiation of non-linearity on the load displacement curve.

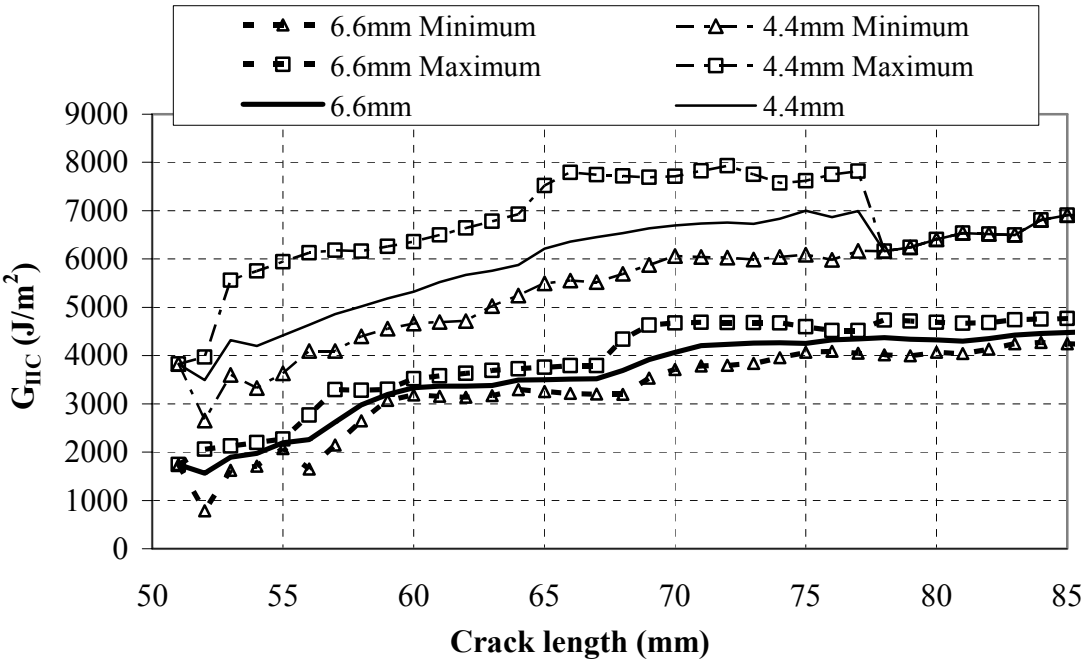

Figure 5-34: *Mode II delamination toughness of G986/M21 for different thicknesses; 4.4mm and 6.6mm*

Application of this method results into labelling points on the experimental curve as initiation points, up to which a crack of over 3mm or 4mm was already observed visually. The increased thickness of the specimens in conjunction with the high toughness resin system [100] decrease the efficiency of this method; non-linearity due to large displacements in this configuration is of a softening form and can be confused with the non-linearity associated with initiation [82,88]. The second method of taking the intersection point of the experimental curve with a line drawn from the origin and offset by a 5% compliance increase from the original specimen compliance, determined by the linear portion of the experimental curve, did not produce an intersection point.

Figure 5-35 depicts the delamination toughness of UD IM7/M21 for beam thicknesses of 3mm, 4mm and 6mm. The R-curves are predominately flat, and the toughness between different thicknesses is similar; only the 3mm thick specimen exhibits a lower toughness value. It has to be noted, that only one specimen from each thickness was tested. The difference with the woven fabric specimens is apparent.

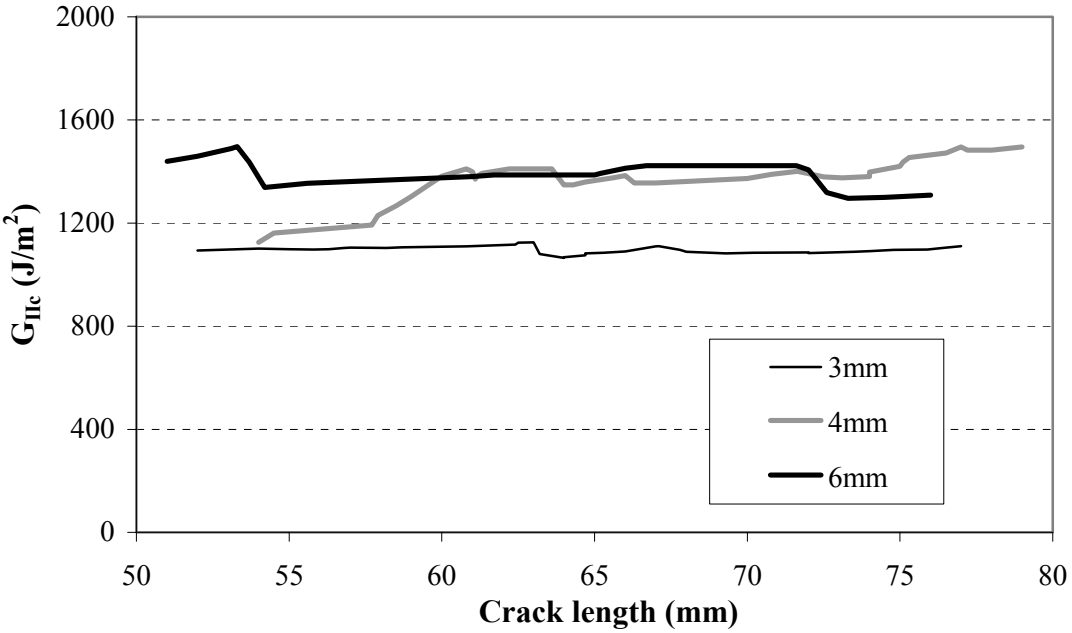

Figure 5-35: *Mode II delamination toughness of unpinned UD IM7/M21 for different thicknesses; 3mm, 4mm and 6mm*

When performing delamination tests, specimens are assumed to be deformed in the elastic domain only. This is a prerequisite for the validity of the data reduction method. After testing 4.4mm woven samples, permanent deformations were observed. These are believed to have been inflicted at crack lengths above 80mm. The data after that point cannot be trusted for 4.4mm laminates. No unloading curves were obtained.

The reason for the appearance of an effect of thickness in unpinned woven laminates may only be attributed to fibre architecture. Looking back at the friction tests in section *5.2.1*, there was an increase resistance during the initial detachment of the woven cracked surfaces, not observed with UD material. Specimens of different thicknesses fail under different loads and different crosshead displacements during mode II delamination testing. Thin specimens undergo an additional amount of bending compared to thick specimens; 4.4mm thick specimens reach crosshead displacements of 13.5mm, while 6.6mm thick specimens reach crosshead displacements of 8mm. Under significant bending loads the resistance of the surfaces to detach will increase. This explains the higher propagation values, as well as the higher initiation values of thin specimens.

A way of further evaluating the effect of friction between crack faces on the mode II delamination toughness is by testing specimens with and without the addition of insert film. The use of a film cushion (a polymer spacer between crack faces) during testing is a similar approach in altering the friction contribution during mode II delamination testing. Findings show that a reduction in the friction contribution, achieved by using a film cushion, causes an appreciable reduction in toughness values [101]. The approach adopted in this study introduces an increase in the friction between crack faces.

All specimens are fabricated using insert film, thus specimens emulating the absence of insert film were created by delamination testing. After initially delaminating a typical 4ENF specimen for a certain crack length, the specimen was unloaded and repositioned so that the crack length was 50mm, as in the first test (Figure 5-36). The specimen was then re-tested. Re-tested specimens are denoted with B, while original specimens are denoted with the specimen name type only in the figures. Specimens were long enough to facilitate frictional testing.

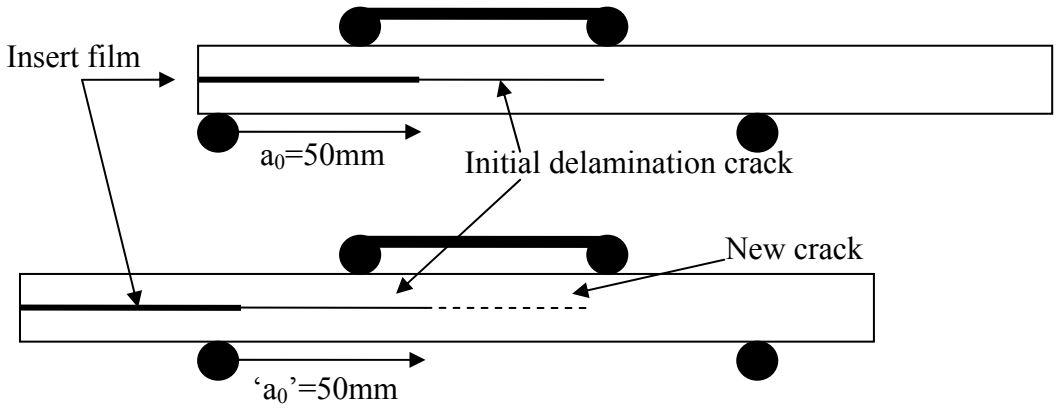

Figure 5-36: *Specimen re-positioning to emulate frictional testing*

Only unpinned and ZPC type specimens (see Figure 5-30) were re-tested. All curves represent averages for several identical type specimens. All specimens with a thickness of 6.6mm were moved by 40mm; 4.4mm specimens were moved by 20mm only. Figure 5-37 shows the effect of friction on the apparent mode II delamination toughness. The toughness of all normally tested specimens is rising, while the curves of the frictional

specimens are mostly horizontal. The delamination toughness, as measured using the 4ENF test configuration is independent of the crack length (see Equation (5-2)). This means that the frictional curves are effectively the extensions of the original ones. Indeed, in the unpinned and ZPC G986/M21 specimens, the toughness value at the beginning of frictional curve is equal to the value at the end of the original curve; however, that is not the case with G986/M36 specimens. The shape of the curves suggests an increasing influence of friction with delamination crack length, even inside the area of pure moment. The value of the apparent delamination toughness is rising with advancing crack length in a discrete, step-like fashion. These steps have a finite length similar to the value of the unit cell, which is 9mm, particularly at low crack lengths. The determination of a single value for the friction coefficient is therefore of no meaning for a woven delamination specimen.

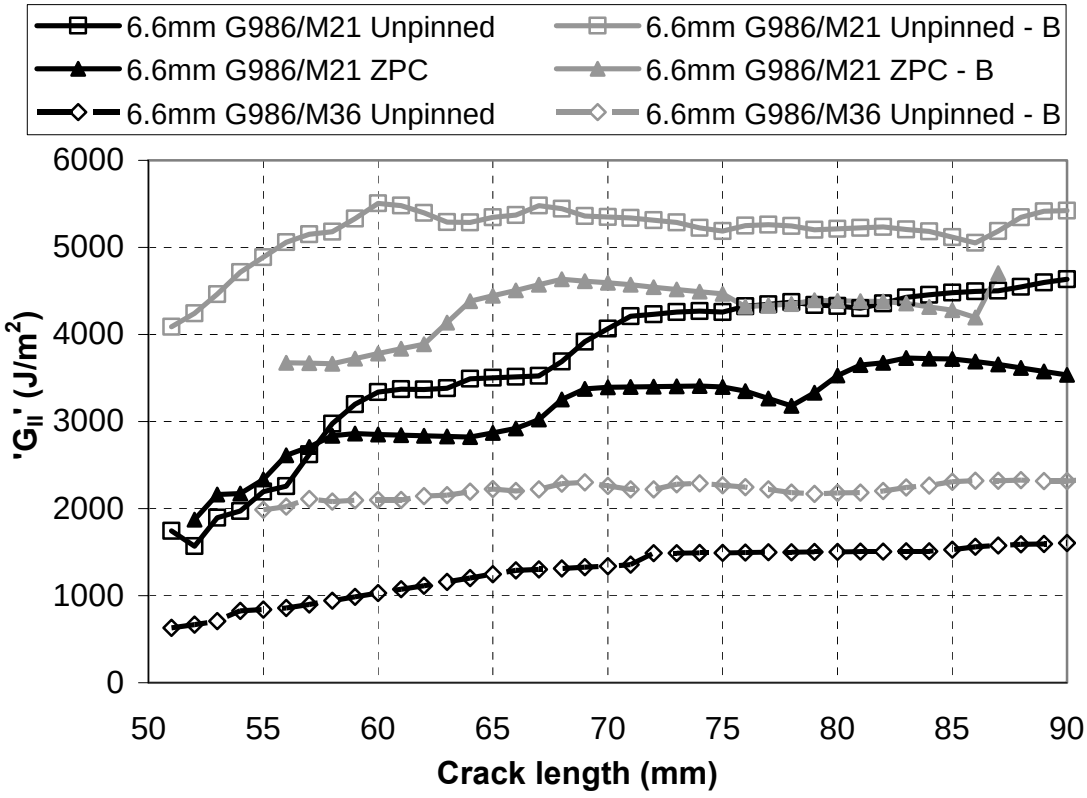

Figure 5-37: *Comparison of mode II delamination toughness of typical and re-tested specimens*

5.6.2 Effect of laminate material

Figure 5-38 presents the mode II delamination toughness of G986/M21 and G986/M36, as measured using the 4ENF configuration. The dotted lines present the average values in the first 15mm of crack propagation. The aforementioned crack length was selected, since it includes enough data points to eliminate the inaccuracy of initiation values and also as a means to partly eliminate the effect of the fibre architecture. The ratio of the average values is close to 3.

The relative performance of the two materials in mode II differs to their relative performance in mode I, as well as the relative performance of the pure resin systems. A summary of all toughness properties measured is presented in Table 5-3. The ratio of the mode II measured toughness is similar to the ratio of the friction coefficient of the two materials. The emerging suggestion, that the delamination toughness measured in woven fabric materials using the 4ENF configuration is an artifact of friction, is not correct, as the delamination toughness under mode II loading conditions would have to be zero. However, this presents an additional suggestion for the role of friction in mode II testing.

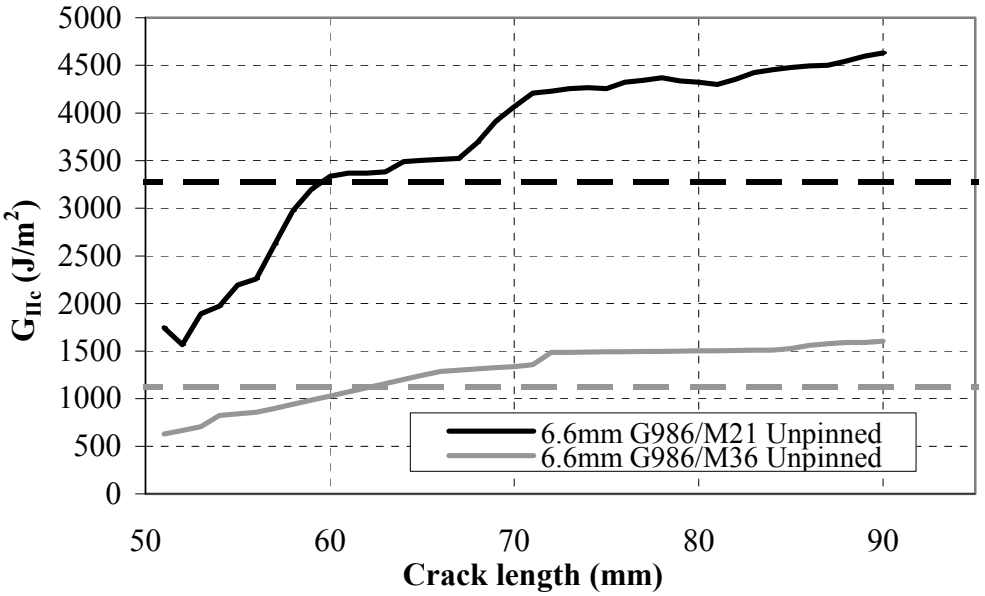

Figure 5-38: *Mode II delamination toughness of G986/M21 and G986/M36; dotted lines are the averages values in the first 15mm of crack propagation in each case.*

	G_C resin system (J/m^2)	G_{IC} initiation (J/m^2)	G_{IC} propagation average (J/m^2)	G_{IIC} *average of first 15mm of crack length (J/m^2)*
M36	*466*	---	---	---
M21	*216*	---	---	---
G986/M36	---	*510*	*1263*	1119
G986/M21	---	*476*	*792*	3275
Ratio	2.16	1.06	1.60	0.34

Table 5-3: *Summary of properties related to the M21 and M36 resin systems*

5.6.3 Effect of insertion depth

The effect of insertion depth with 0.28mm diameter Z-pins for both G986/M21 and G986/M36 is presented in Figure 5-39.

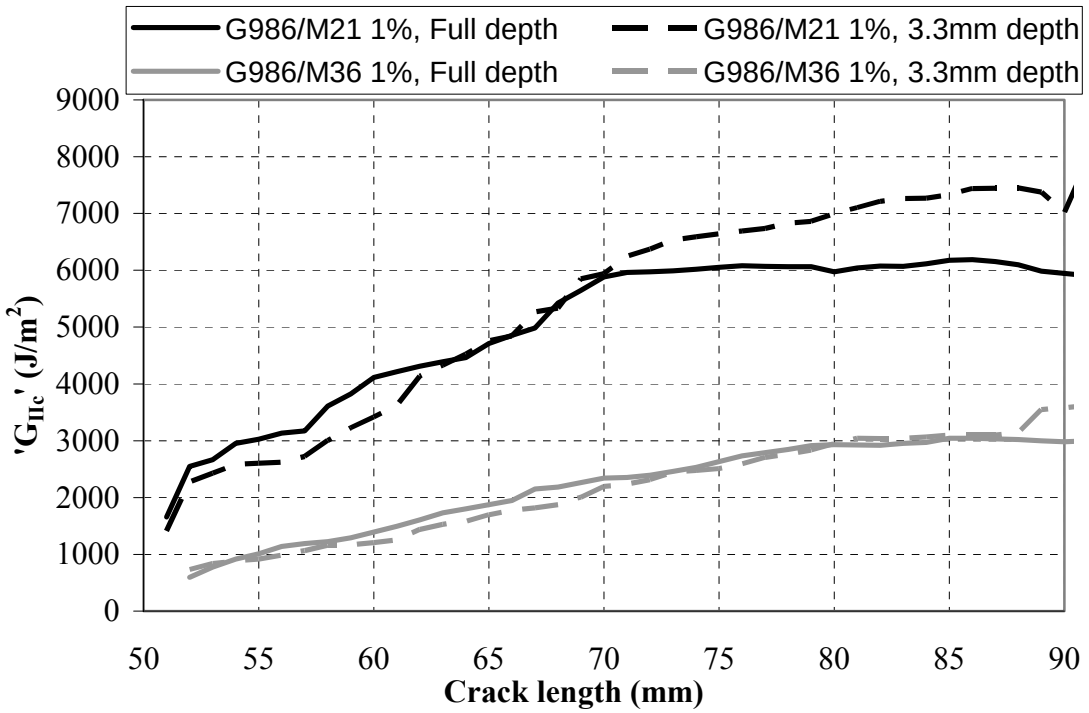

Figure 5-39: *Effect of insertion depth on the apparent delamination toughness in woven fabric specimens (6.6mm thick) with 0.28mm diameter Z-pins (G986/M21 & G986/M36)*

The curves of the partially pinned specimens appear to be below the curves of the fully pinned specimens for the first 20mm of crack propagation and above for the next 20mm; the effect is more pronounced in G986/M21. The values, however, are effectively similar between different insertion depths, reflecting the findings of the Z-shear test. Initiation values are also similar, as the presence of Z-pins at a distance 5mm from the original crack tip should not have an effect.

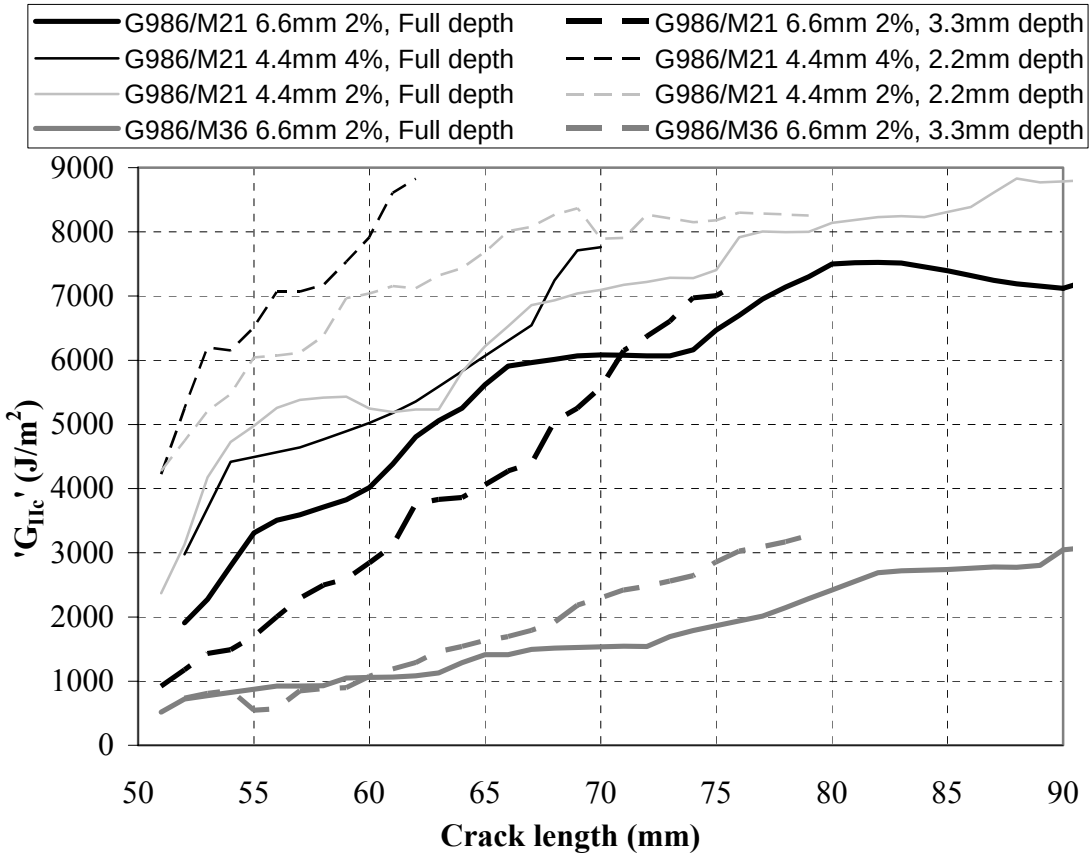

Figure 5-40: *Effect of insertion depth on the apparent delamination toughness in woven fabric with 0.5mm diameter Z-pins (G986/M21 & G986/M36)*

The behaviour differs with 0.5mm diameter Z-pins. Figure 5-40 depicts the effect of insertion depth on the apparent delamination toughness of different materials and different thicknesses. The findings of the Z-shear test are reflected in the performance of the 4.4mm specimens, as well as 6.6mm thick G986/M36 specimens, as partial pinning provides increased apparent toughness. This is not the case, with 6.6mm thick G986/M21 specimens. It has to be noted, however, that in this case, propagation is arrested in partially pinned specimens at a crack length of 75mm and bending failure

follows. The relative trend of the unpinned and pinned curves described for the specimens with 0.28mm diameter Z-pins is also apparent in 6.6mm thick specimens with 0.5mm diameter Z-pins.A prominent difference to the previous figure is the difference in initiation values between partially and fully pinned G986/M21 specimens. The range of insertion depths used implies a change in failure mechanism of the Z-pins, according to the Z-shear tests. The constraint against opening displacement is different between the Z-shear test and the 4ENF configuration; in the Z-shear tests it is a property of the test rig, while in the 4ENF configuration it is related to specimen thickness. This suggests that an insertion depth of 3.6mm might not necessarily be the critical insertion depth where the balance of failure mechanisms changes, as in the Z-shear test. However, the presence of a significant difference in apparent toughness values in the figure with a changing insertion depth indicates that a change in the balance of failure mechanisms is present.

5.6.4 Effect of Z-pin Density

No effect of density was observed in the performance of a single 0.28mm diameter Z-pin in the Z-shear test, as discussed in *5.3.3*. The contribution of pinning to the apparent toughness will be a function of the number of Z-pins bridging the crack. A higher density is therefore expected to yield a higher apparent toughness. Figure 5-41 depicts the effect of pinning density to the apparent delamination toughness with 0.28mm diameter Z-pins. For both thicknesses displayed, higher pinning density results in higher apparent toughness, verifying the initial assumption.

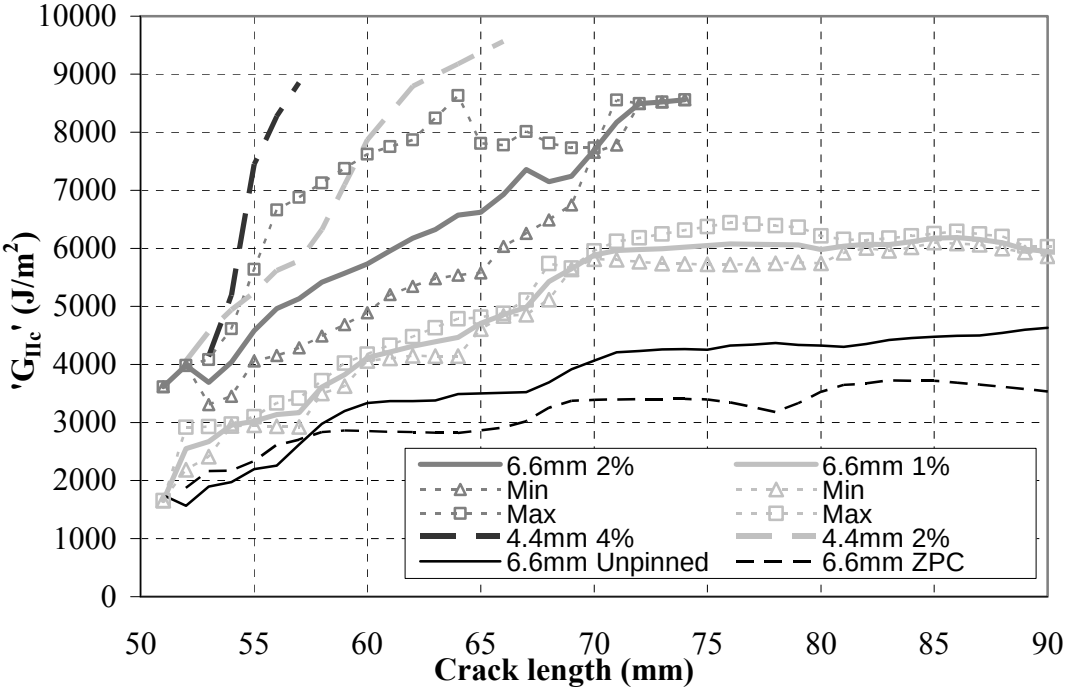

Figure 5-41: *Effect of pinning density on the apparent delamination toughness in woven fabric with 0.28mm diameter Z-pins (G986/M21). Unpinned and ZPC cases displayed for reference.*

A more complicated behaviour is observed with 0.5mm diameter Z-pins. The curve for 0.5% pinning density exhibits higher apparent toughness than the 1% case for small crack lengths and similar for large ones. The two curves intersect at a crack length of 82mm. A possible explanation can be given from the Z-shear test, where 0.5% density Z-pins dissipate more energy for small displacements, as discussed in section *5.3.7*. As the crack propagates further, the difference in the number of Z-pins that bridge the crack between the 0.5% and 1% density cases increases. The sliding displacement increases as well. At higher densities the influence of the significantly greater number of Z-pins dominates, and the curve of the 4% and 2% case lie above the curves of the other two densities in that sequence. Finally, the difference of the initiation values between the curves has to be noted.

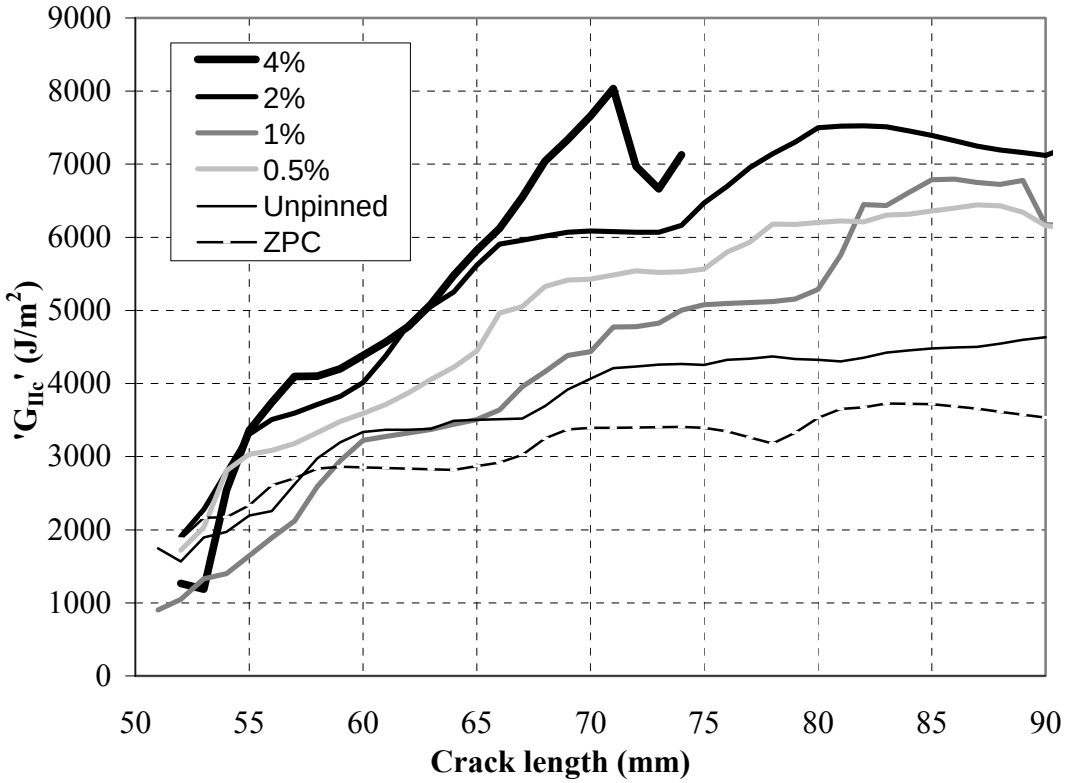

Figure 5-42: *Effect of pinning density on the apparent delamination toughness in 6.6mm thick woven fabric with 0.5mm diameter Z-pins (G986/M21). Unpinned and ZPC cases displayed for reference*

5.6.5 Effect of Z-pin Diameter

The next two figures present the effect of Z-pin diameter on the apparent delamination toughness. In all cases, 0.28mm diameter Z-pins outperform 0.5mm Z-pins of the same density. In order to use findings from the Z-shear test to investigate the performance difference, two assumptions are required; firstly, that the type of failure in the same for both diameter Z-pins. The minimum insertion depth used in the results presented here is the minimum laminate thickness, namely 4.4mm. The validity of the first assumption depends on how similar the opening constraint is between the two tests. Secondly, the ratio of the potential energy absorption per pin between the two different diameters is assumed to be close to 3, in favour of the 0.5mm diameter Z-pin. This is derived from

the slope of the Z-shear curves in Figure 5-9. The difference in potential energy under the curves for a similar sliding displacement is reflected by the difference in slope.

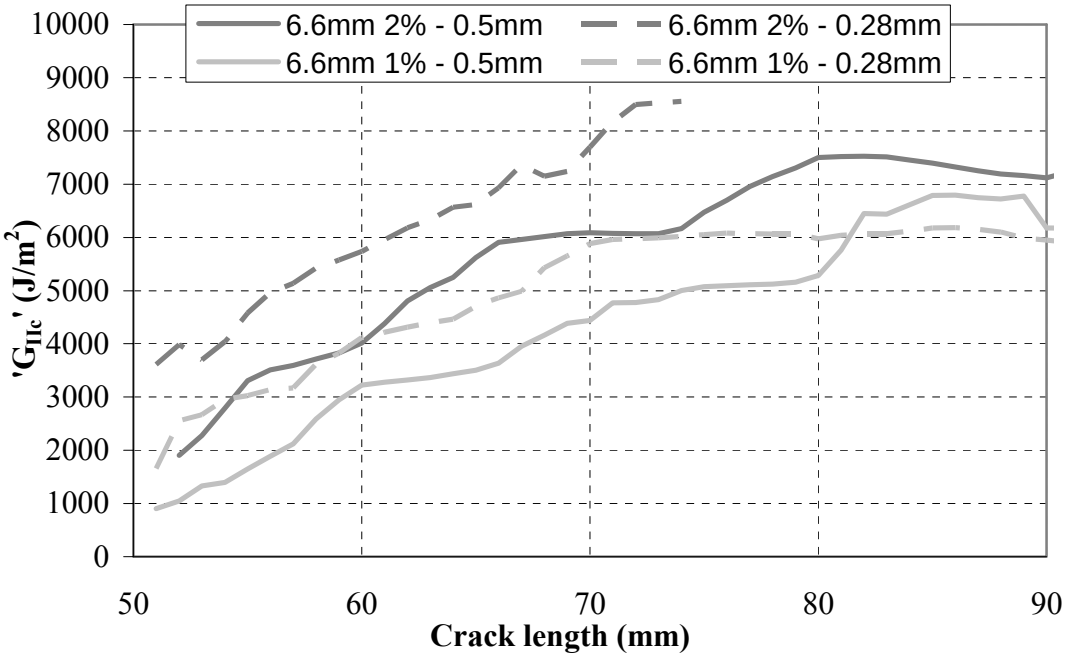

Figure 5-43: *Effect of Z-pin diameter on the apparent delamination toughness in 6.6mm thick woven fabric (G986/M21)*

The ratio of the number of Z-pins per unit area between the two diameters is also close to 3, in favour of the 0.28mm diameter Z-pin. This is derived by Table 5-4. Z-pin arrangements with the same pinning density should therefore have similar performance in a bridging zone of the same size.

The initiation values of curves with similar densities are different in Figure 5-43; however they are similar in Figure 5-44. Despite the emerging suggestion from the difference in initiation values, the Z-pin diameter effect is not an artifact of errors in measurement or the correction procedure, as for an apparent delamination toughness above 8000 J/m^2, the crack is arrested and specimens fail in bending; specimens with 0.28mm diameter Z-pins reach that point earlier. No sufficient explanation is currently provided for this effect.

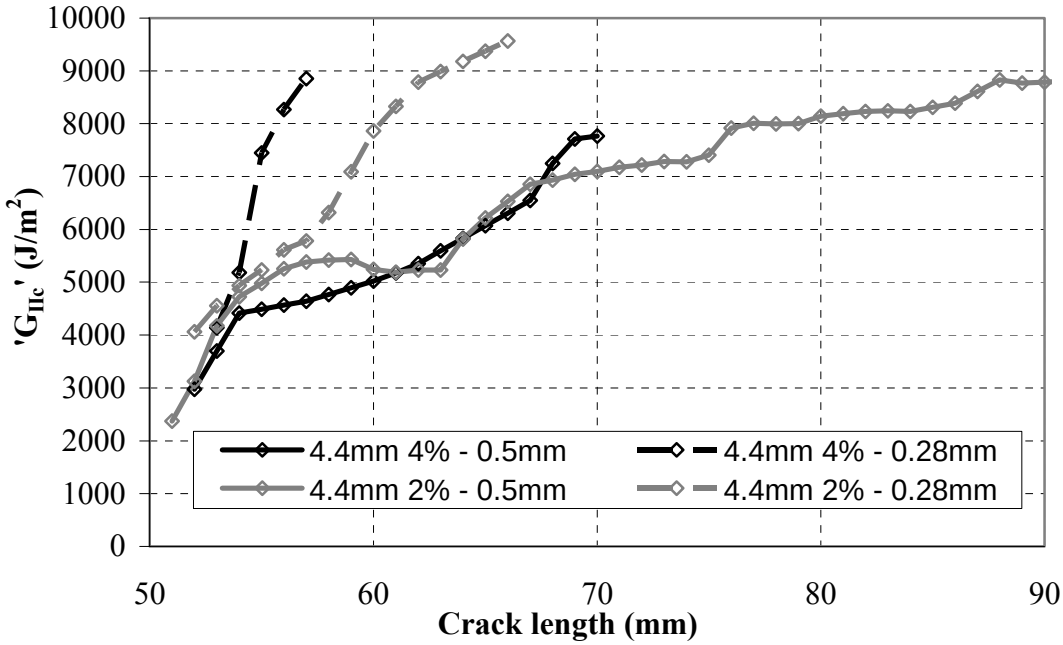

Figure 5-44: *Effect of Z-pin diameter on the apparent delamination toughness in 4.4mm thick woven fabric (G986/M21)*

Z-pin Diameter (mm) \ Z-pin Density (%)	**0.5**	**1**	**2**	**4**
0.28	*3.51*	*2.48*	*1.75*	1.24
0.5	6.27	4.43	3.13	2.22

Table 5-4: *Z-pin spacing in millimetres for all arrangements used in this study*

5.7 Summary

The 4ENF configuration has been selected as the most appropriate for testing Z-pinned laminates, mainly due to the significant available crack length within which stable crack propagation can be achieved. There are other advantages, such as the straightforward data reduction when using the CCM method and the ability to perform the compliance calibration simultaneously with the test.

The interference of the friction between crack faces with the toughness measurement is an inherent feature of mode II delamination configurations. Previous attempts have been made to quantify its effect on the measurement. Further investigation using the friction rig described in sections ***5.2.1*** and ***5.6.1***, revealed that friction is associated with the sensitivity of the delamination toughness of unpinned woven fabric laminates to laminate thickness. The differences in ply undulation and specimen bending under test conditions are responsible for the change of the amount of friction and the subsequent change in behaviour of woven laminates.

An additional issue concerning the compliance calibration of Z-pinned laminates during the mode II test has arisen. In order to facilitate the comparison of the effect of different Z-pinning configurations to mode II delamination toughness, the compliance calibration data was substituted with data from a purpose built specimen. This allowed manufacturing irregularities and the introduction of different fracture mechanisms to be nullified, while retaining the effect of the Z-pins on the mechanical in-plane properties of the material.

The change in fracture mechanisms of Z-pinned laminates in shear loading is attributes to a combination of material and Z-pinning parameters. Increased insertion depth to Z-pin diameter ratio, multidirectional fibre orientation increased laminate thickness and imposed constraints regarding the opening displacement, all impede Z-pin pullout. An optimum insertion depth to Z-pin diameter ratio exists, where energy absorption is at maximum, which is unique to laminate material and thickness. Z-pin density also plays a role in the change in fracture mechanisms with multidirectional fibre orientation, while small variations of Z-pin angle are unimportant to the delamination performance of UD laminates. The change in fracture mechanisms depends on how all the parameter changes affect – by intensifying or diluting - the introduction of the additional mode I loading component due to Z-pin presence.

6 In-plane properties of Z-pinned carbon fibre / epoxy composites

In chapter 3, the alteration of the meso-structure of a laminate due to Z-pin insertion was discussed. Fibre orientation and laminate thickness are affected, while resin rich regions are introduced. As with all composites with 3D architecture, stitching included, this is expected to compromise the in-plane stiffness and strength of a laminate. An investigation of the effect of Z-pinning on the tensile stiffness and strength, as well as on the in-plane shear stiffness, is presented in this chapter.

6.1 Tensile testing

Tensile testing of Z-pinned laminates was performed using two different testing configurations. The ***Tensile*** configuration, as described in the ASTM D3039/D3039M protocol, was used for acquiring predominantly stiffness values of Z-pinned laminates. Specimen edges were polished to the final dimensions and tabs were bonded, as described in section 3.3; tab thickness was 1.5mm. The aspect ratios of all specimens were sufficiently high to avoid Saint-Venant effects [82,114]. Two configurations were used for UD specimens (IM7/M21), one for testing along the fibre direction (0 , Figure 6-1a) and one for testing transversely to it (90 , Figure 6-1b). Woven specimens (G986/M21) required only one configuration (Figure 6-1c). Specimen width was limited by the width of the grips to 25mm; nevertheless, this is sufficient to accommodate 2.7 unit cells of the weaving pattern.

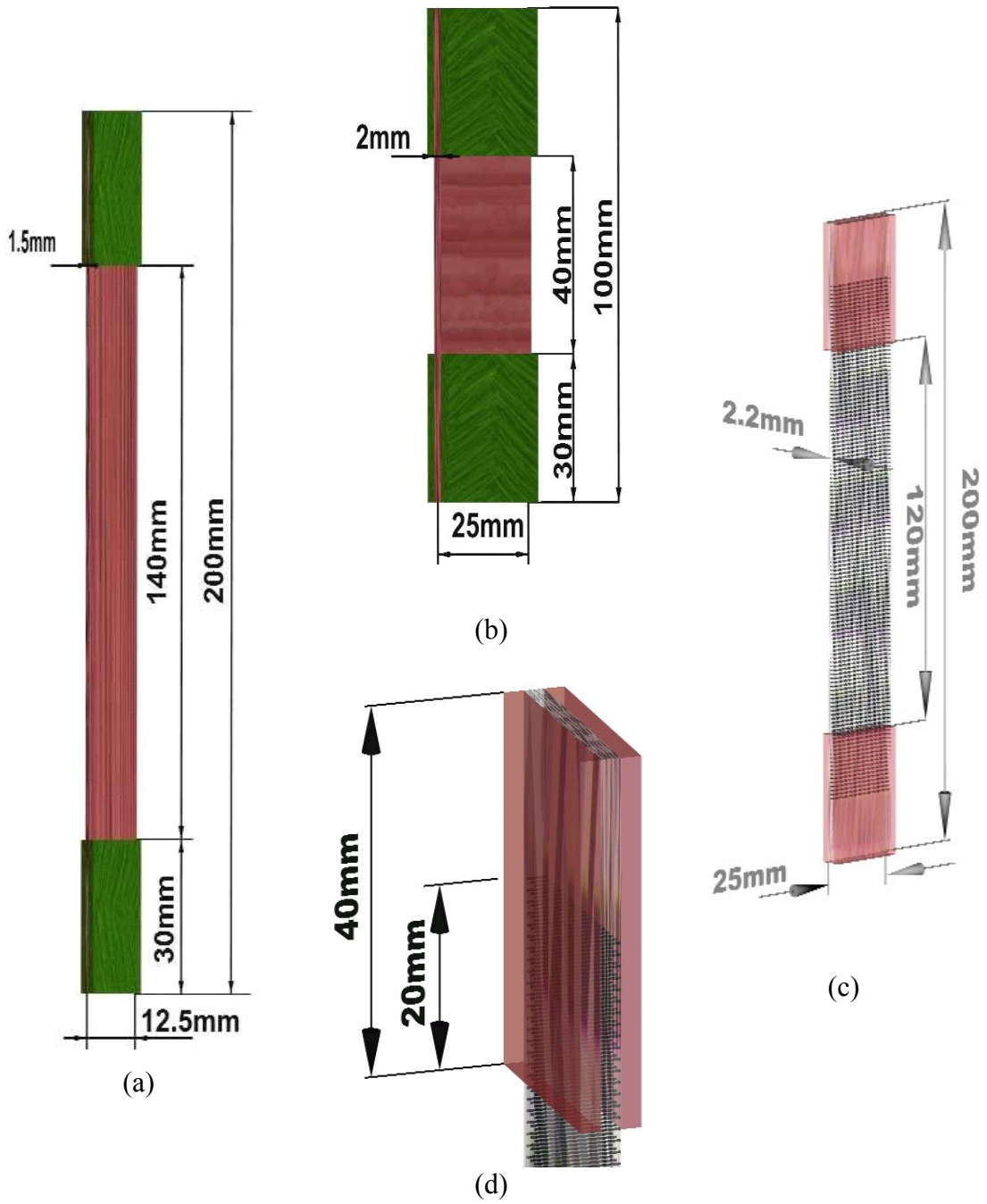

Figure 6-1: *Tensile test configurations: (a) 0 UD (IM7/M21) specimen, (b) 90 UD (IM7/M21) specimen and (c) woven (G986/M21) specimen, (d) detail in the tabbed area*

To facilitate accurate stiffness measurements and a desirable failure type of Z-pinned specimens, the length of the Z-pinned area was selected to be larger than the gauge length (Figure 6-1d); the tabs cover part of the pinned portion of the specimen. If the extents of the Z-pinned area were within the gauge length, failure would always occur at the edges of the Z-pinned area. That would invalidate any acquired strength values.

Acquired strength values are acceptable only when failure occurs in the gauge length of the specimen [82]. Despite the use of compliant tabs (±45) to diffuse the load transition, failure usually occurs close to the tabs in a Tensile test. In order to contain failure completely within the gauge length, the ***Open Hole Tensile*** test (OHT) configuration was used, abiding by the ASTM D576/D5766M protocol. The presence of the hole ensures that failure occurs at the midsection and renders tabs unnecessary. Furthermore, the size of the required Z-pinned area is significantly reduced. Specimens were drilled using a carbide tip drill supported against a sacrificial backing plate.

Utilising a cross-ply stacking sequence for UD prepreg allows a comparison to be made with woven material, in terms of the influence of Z-pinning on in-plane properties. Specimens manufactured from UD prepreg (IM7/M21) were therefore laid-up in a $[[0\ /90\ ]_8]_S$ sequence. Detailed specimens dimensions are portrayed in Figure 6-2.

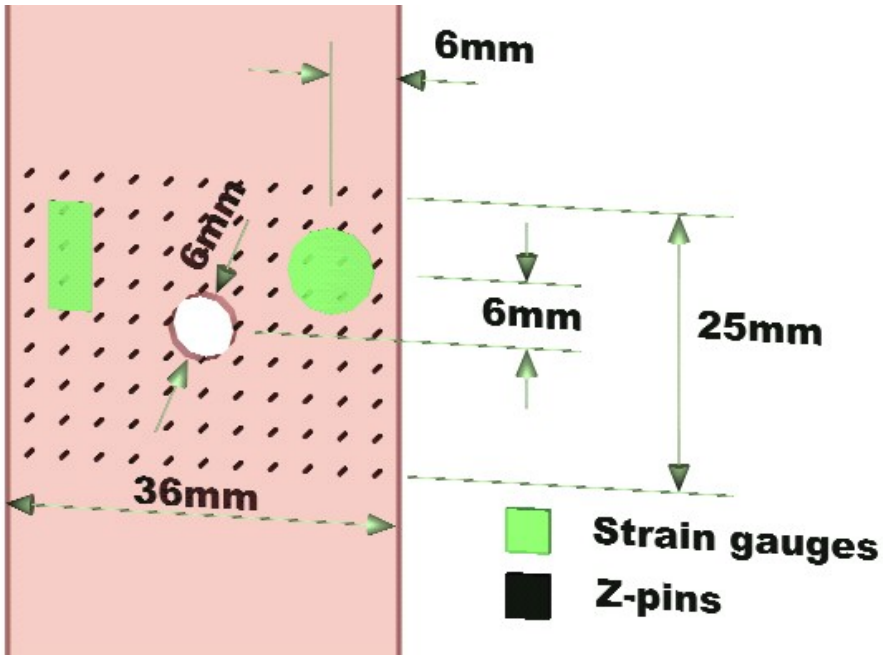

Figure 6-2: *Open Hole Tension (OHT) specimen and gauge positioning*

6.1.1 Instrumentation

Foil strain gauges with lead wires were used to measure strain. Strain gauges were supplied by Techni Measure. The required size of strain gauges differs for each material, since it is required to be greater then the unit cell of the material under test. The concept of a unit cell does not apply to UD or cross-ply specimens, while the unit cell size of the woven G986/M21 is 9mm. 3mm long gauges were used in 0 and 90 Tensile UD specimens, while 10mm long gauges were used on Tensile woven specimens. The strain gauge length must be large enough to remain unaffected by the relative position of the unit cell size. Initial tests were performed using both 10mm and 30mm long gauges, confirming by means of comparison that 10mm gauges were sufficiently long, relative to the unit cell of the material, to acquire accurate measurements.

A uniform strain distribution of a pure tensile stress state at a known cross section for a known applied load is required to obtain modulus values. The OHT configuration does not comply with these requirements. In order to extract stiffness data from OHT specimens, a comparison between Z-pinned and unpinned specimens was implemented. In Z-pinned specimens, strain gauges were positioned within the bounds of the Z-pinned area in a locally uniform strain area; the positioning was reproduced in unpinned specimens. The selected position is depicted in Figure 6-2. Positioning the gauges at the symmetry axis of the specimen was avoided and a minimum distance equal to the size of one hole diameter along the width of the specimen was maintained to ensure locally uniform strain [9,11]. A FE quarter model of an OHT specimen confirms local uniformity of the strain around the strain gauge. The model was built using LUSAS 13.4 software. Figure 6-3 displays a large uniform longitudinal strain area for both unpinned and Z-pinned specimens in the vicinity of the gauge position. The Z-pinned specimen in the figure is modelled using a reduced modulus within the Z-pinned area, according to the measurements. Since absolute values of the tensile modulus cannot be obtained from OHT specimens, the reduction in stiffness is only presented in percentage terms, after comparison of the Z-pinned and unpinned specimens.

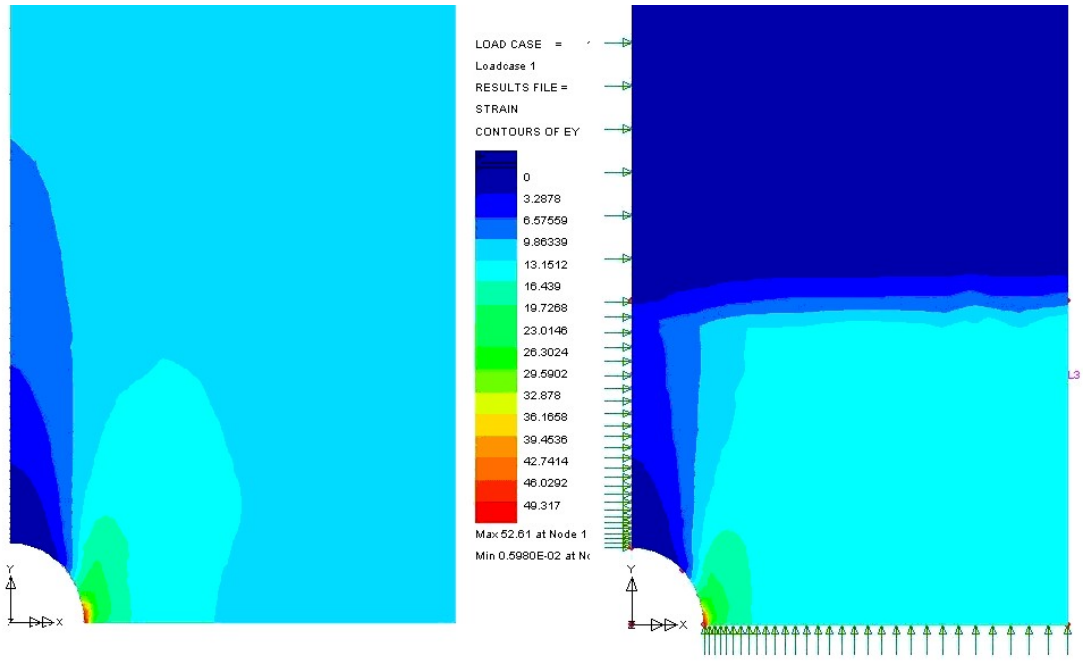

Figure 6-3: *Longitudinal strain map of quarter section of OHT specimen; unpinned (left) and Z-pinned (right) case.*

6.2 Tensile test cases

Table 6-1 presents all OHT specimens included in the results. Table 6-2 lists the Tensile specimens of this study. Specimens with anomalies in their stress-strain curves were disregarded from calculations deducing stiffness. Similarly, specimens with failure outside the gauge length area were withdrawn from calculations determining strength. Not all OHT specimens were equipped with strain gauges; a single asterisk in Table 6-1 indicates that only one specimen was instrumented; a double asterisk signals complete absence of strain gauges. Specimens tested without strain gauges are only used to provide strength data.

Material	Prepreg type	Lay-up	Density (%)	Z-pin diameter (mm)	No. of Specimens
G986/M21	woven	$[0/90]_8$	---	---	8
G986/M21	woven	$[0/90]_8$	4%	0.28	4
G986/M21	woven	$[0/90]_8$	4%	0.5	4
G986/M21	woven	$[0/90]_8$	2%	0.28	6*
G986/M21	woven	$[0/90]_8$	2%	0.5	6*
G986/M21	woven	$[0/90]_8$	1%	0.28	4
G986/M21	woven	$[0/90]_8$	1%	0.5	4
IM7/M21	UD	$[[0/90]_8]_S$	---	---	8
IM7/M21	UD	$[[0/90]_8]_S$	4%	0.28	4
IM7/M21	UD	$[[0/90]_8]_S$	4%	0.5	4
IM7/M21	UD	$[[0/90]_8]_S$	2%	0.28	6**
IM7/M21	UD	$[[0/90]_8]_S$	2%	0.5	6*
IM7/M21	UD	$[[0/90]_8]_S$	1%	0.28	4
IM7/M21	UD	$[[0/90]_8]_S$	1%	0.5	2

Table 6-1: *Open Hole Tension (OHT) test cases; one asterisk denotes only one instrumented specimen; double asterisk denotes absence of instrumentation.*

Material	Prepreg type	Lay-up	Density (%)	Z-pin diameter (mm)	No. of Specimens
G986/M21	woven	$[0/90]_8$	---	---	5
G986/M21	woven	$[0/90]_8$	4%	0.28	5
IM7/M21	UD	$[0]_{12}$	---	---	7
IM7/M21	UD	$[0]_{12}$	4%	0.28	8
IM7/M21	UD	$[90]_{16}$	---	---	10
IM7/M21	UD	$[90]_{16}$	4%	0.28	9

Table 6-2: *Tensile test cases*

6.3 Effect on Tensile Stiffness

6.3.1 Tensile stiffness results

Figure 6-4 and Figure 6-5 present the effect of Z-pinning on the tensile modulus for two different types of materials. Z-pins of 0.28mm diameter at a 4% density are used. The selected high density case should comprise an upper bound regarding the severity of the effect Z-pins can have on laminate stiffness. Error bars demonstrate the accuracy of the measurement with 97.5% confidence level for a two sided normal distribution [93].

A reduction in stiffness between the unpinned and 4%-0.28mm pinned cases can be observed for both materials. The significant scatter in the measurement of the transverse modulus for the UD material can in part be attributed to minor misalignment of the grips during tightening. The longitudinal and transverse moduli of the woven material are identical; the weave is completely balanced in the amount of fibres aligned in each direction.

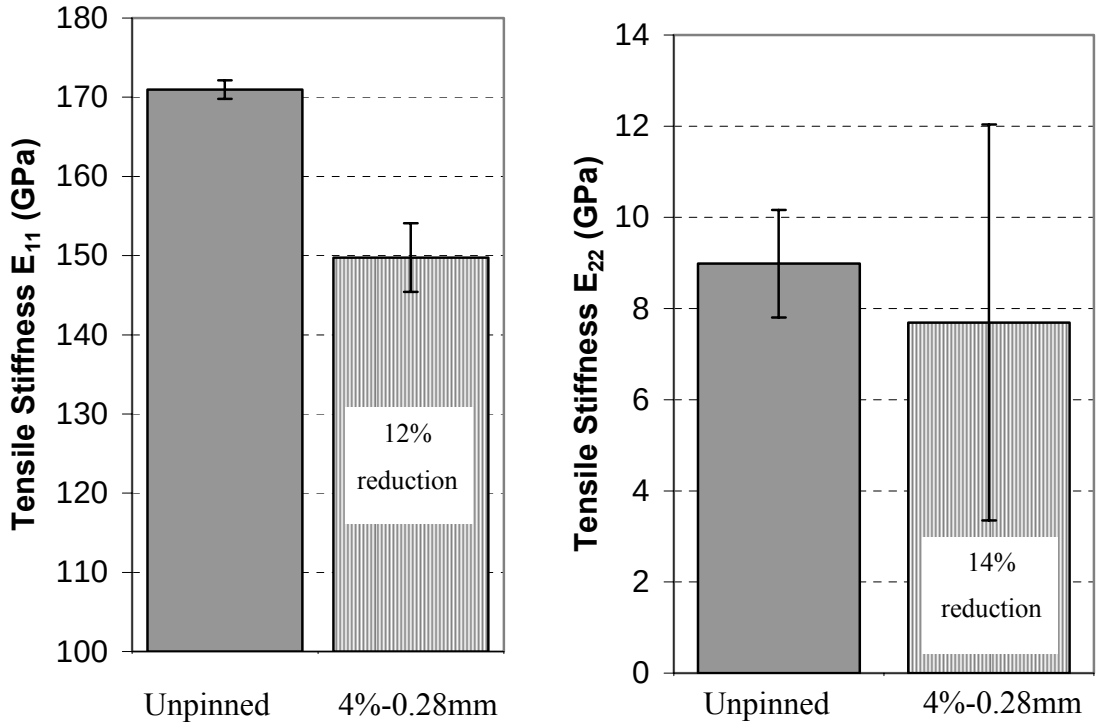

Figure 6-4: *Longitudinal and transverse tensile modulus of unpinned and Z-pinned UD IM7/M21laminate*

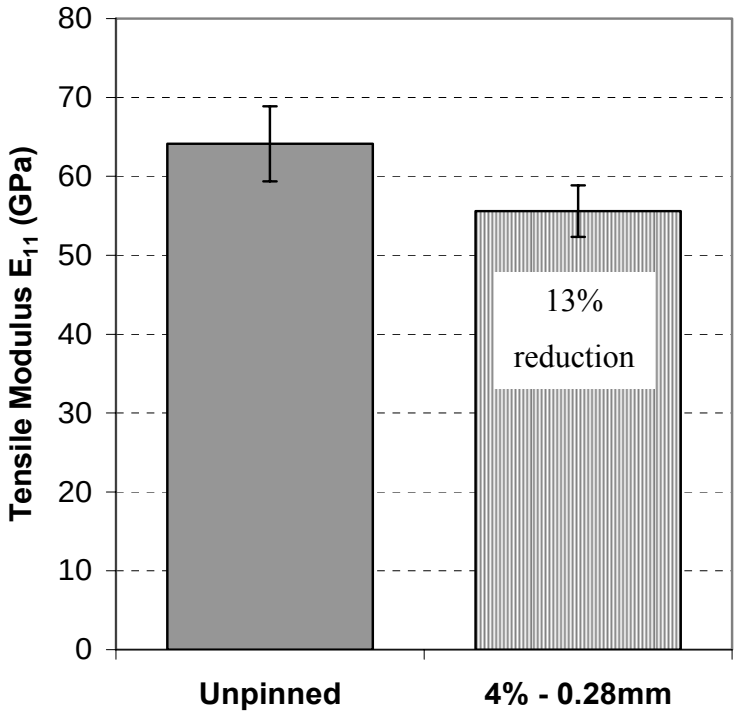

Figure 6-5: *Tensile modulus of unpinned and Z-pinned woven G986/M21laminate*

6.3.2 Geometric approximation

The geometric changes imposed on a laminate by the insertion of Z-pins are namely: (a) the increase in thickness, as described in section *3.4*, (b) the in-plane laminate fibre misalignment, (c) the out-of-plane laminate fibre misalignment and (d) laminate fibre damage. Items (a) and (b) have been measured accurately and are discussed in chapter 3; the in-plane misalignment angle can be calculated from the ratio L/D, the characteristic resin pocket aspect ratio, examined in section *3.4.2*.

Imposed laminate fibre damage is minimal and will currently be omitted from calculations. Laminate fibre misalignment will be also omitted from calculations in woven laminates, since it is negligible relative to the inherent undulations of the laminate fibres. Only factor (a) will therefore be considered for woven laminates, while factors (a), (b) and (c) will be considered for laminates made from UD prepreg. Initially, a complete expression will be constructed, deducing the altered modulus E_{PIN}, after Z-pin insertion, relative to the original laminate modulus E_0. For UD laminates the

expression will only correspond to the modulus along the fibre direction, since the calculation is based on the fact that the modulus is a fibre dominated property. Geometric approximations predicting the change in the transverse modulus have not been attempted.

A cross section at a row of Z-pins is considered, as being the most compliant and therefore determining laminate stiffness. As the stiffness of the cross section under investigation and a cross section containing no Z-pins are less than 20% different, this first assumption is not entirely accurate. The stiffness will be a combination of both, according to the model of two springs in line, described by equation (6-1). Working with volumes of fibres of the same alignment as in [36] or a streamline model as in [115] is more accurate.

$$K_{TOTAL} = \frac{K_1 \cdot K_2}{K_1 + K_2} \tag{6-1}$$

Where: K_{TOTAL}, K_1 and K_2: Equivalent and initial spring stiffnesses

The increase in thickness alters the size of the cross section of the laminate. The new load bearing cross section will be equal to the original one multiplied by a thickness increase factor, subtracting the cross-sectional area covered by Z-pins:

$$A_{PINS} = c \cdot (1 - \rho) \cdot A_0 \tag{6-2}$$

$$\rho = \frac{2}{\sqrt{\pi}} \cdot d \tag{6-3}$$

Where: A_0: Cross section prior to Z-pin insertion
A_{PINS}: Cross section after to Z-pin insertion
c: thickness increase factor
ρ: cross section Z-pin density
d: areal Z-pin density

The increase in thickness occurs without the introduction of additional laminate fibres; a localised increase in resin volume fraction accounts for the increase in thickness. The localised fibre volume fraction is therefore reduced. Bearing in mind that the ratio

between the modulus of the fibres and the resin is close to 100, the contribution of the resin can be ignored, as in [36]:

$$E = V_f \cdot E_f \Rightarrow \frac{E_{THICK}}{E_0} = \frac{V_{f,PINS}}{V_f} \tag{6-4}$$

$$\frac{A_0}{A_{PINS}} = \frac{V_{f,PINS}}{V_f} \tag{6-5}$$

Where: E_0: Modulus prior to Z-pin insertion

E_{THICK}: Changed modulus due to change in thickness

V_f: Fibre volume fraction

The change in fibre volume fraction is inversely proportional to the increase in thickness, and combining equations (6-4) and (6-5), the following expression is obtained:

$$E_{THICK} = \frac{E_0}{c \cdot (1 - \rho)} \tag{6-6}$$

The change in modulus due to misalignment can be written as:

$$E_{MIS} = E_0 \cdot \cos\theta \tag{6-7}$$

The total misalignment angle θ can be found from the following equation:

$$\tan^2\theta = \tan^2\theta_x + \tan^2\theta_t \tag{6-8}$$

With: $$\cos^2\theta = \frac{1}{1 + \tan^2\theta} \tag{6-9}$$

Where: θ_x: the in-plane misalignment angle

θ_t: the through-thickness misalignment angle

Not all laminate fibres are misaligned after Z-pin insertion. From observations under digital microscope, laminate fibres seem to be unaffected at a distance equal to the Z-pin diameter from the Z-pin. This means that a length equal to three Z-pin diameters at

the cross section contains misaligned laminate fibres. Half of the aforementioned cross section has already been subtracted by applying equation (6-2). The modulus change due to misalignment will therefore be:

$$E_{MIS} = \left[m \cdot \rho \cdot \cos\theta + \left(1 - m \cdot \rho\right)\right] \cdot E_0 \tag{6-10}$$

Where: m: misalignment factor, equal to 2

Combining equations (6-6) and (6-10), with respect to equation *(6-9*), the final expression for the change in modulus becomes:

$$E_{PINS} = \frac{1}{c \cdot \left(1 - \rho\right)} \cdot \left[m \cdot \rho \cdot \sqrt{\frac{1}{1 + \left(\tan^2 \theta_x + \tan^2 \theta_t\right)}} + \left(1 - m \cdot \rho\right) \right] \cdot E_0 \tag{6-11}$$

Where: m: misalignment factor, equal to 2

The formula is applied with parameter values that correspond to the pinning configuration used in the tensile tests in section *6.3.1*. The parameter values and the formula results are presented in Table 6-3. The thickness increase factor is taken from figures 3-23 and 3-24. The out-of-plane misalignment is minimal for 0.28mm diameter Z-pins and is considered zero in all materials. The table also presents the formula result assuming an out-of-plane misalignment angle equal to the in-plane one for UD material. The additional effect is small (0.6%). There is good agreement with experimental data, considering the scatter in the measured thickness of all specimens in this study, from which the thickness increase factor c was derived (e.g. Figure 3-23).

Results from the application of the model in [36], presented in section *2.5.1,* are also presented in the same table. As this model includes only the effect of misalignment, the measured misalignment angle was used in its application for both UD and woven materials. The material properties used in the model were the properties of the unpinned laminate for each material. Despite the disagreement between the two models on the significance of the effect of misalignment alone, the fact that the change in volume fraction is the dominant factor in the degradation of the modulus is apparent.

Material	Density (%) - diameter (mm)	Thickness increase factor *c*	θ_x	θ_t	*Reduction in modulus (%)*		
					model from [36]	Equation (6-11)	experimental
G986/M21	4% - 0.28	1.23	0	0		14.5	*13*
IM7/M21	4% - 0.28	1.17	6	0		11	*12*
IM7/M21	4% - 0.28	1.17	6	6		11.6	*12*
G986/M21	4% - 0.28	---	6	---	2.0		*13*
IM7/M21	4% - 0.28	---	6	---	5.3		12

Table 6-3: *Parameter values for the application of both the stiffness approximation formula and the model from [36], and comparison with experimental*

The agreement between formula and experiment indicates that the greater part of the reduction in stiffness is a consequence of the reduction in fibre volume fraction. Moreover, the assumption of absence of any additional misalignment due to Z-pin insertion for the woven material is validated. The omission of the through thickness fibre misalignment and the assumption of zero laminate fibre damage for the cross-ply material did not hinder the accurate prediction of the stiffness reduction, suggesting the validity of the assumptions. Current observations confirm previous findings on the negligible amount of through thickness misalignment induced by Z-pinning [65].

6.3.3 Open Hole Tension stiffness results

Considering the fact that the OHT configuration is unsuitable for providing accurate tensile modulus values, as explained is section *6.1.1*, all stiffness data from Z-pinned specimens are presented in terms of relative stiffness contrasted against the stiffness of the unpinned material, as measured in the OHT configuration.

The validity of the discussion in section *6.1.1* can be examined by comparing measurements between the two test configurations for identical Z-pinning cases. Figure 6-6 presents the effect of Z-pinning on the stiffness of woven laminates. Error bars are one time the standard deviation of the measurements. The 4%, 0.28mm diameter case is identical to the Tensile configuration case tested. The reduction in stiffness is 16%; the

agreement with the 13% reduction measured with the Tensile configuration is not completely satisfactory. However, it is interesting to investigate the differences of the effect of Z-pinning due to material architecture.

For both materials the severity of the reduction increases with increasing areal Z-pin density (Figure 6-6 and Figure 6-7). Smaller diameter Z-pins cause a greater reduction for similar densities in both materials. The maximum reduction is 16% for woven, with either 0.5mm or 0.28mm diameter Z-pins, and 12% for cross-ply with 0.28mm diameter Z-pins. The latter is equivalent to the reduction in the longitudinal and transverse modulus measured in UD; 12% and 14% respectively. However, the effects of Z-pin insertion differ slightly in the cross-ply stacking sequence, as discussed in section *3.4.2*, and the comparison is not pertinent.

Using equation (6-6), the data can be corrected to produce Figure 6-8 and Figure 6-9; The effect of the change in volume fraction – or equivalently, the thickness increase effect – can be excluded from the plots. The difference in relative stiffness due to fibre misalignment can now be observed. The new error bars include the deviation of the stiffness measurement and the deviation of the subtracted stiffness - in equation (6-6) – due to the thickness variation [93].

For the woven material (Figure 6-8), the value of the reference stiffness is always within the scatter. This again indicates the absence of additional laminate fibre misalignment due to Z-pin insertion, compared to the existing laminate fibre undulations. With the cross-ply, two out of four error bars range within values that are lower than the value of the reference stiffness. Fibre misalignment therefore has an influence on the stiffness of the cross-ply laminates, but to a lesser extent than in UD. Considering the geometric differences of the resin pockets between material types, as discussed in section *3.4.2*, and current results, it is safe to assume that increasing complexity of the stacking sequence may well diminish the amount and effect of laminate fibre misalignment on laminate stiffness.

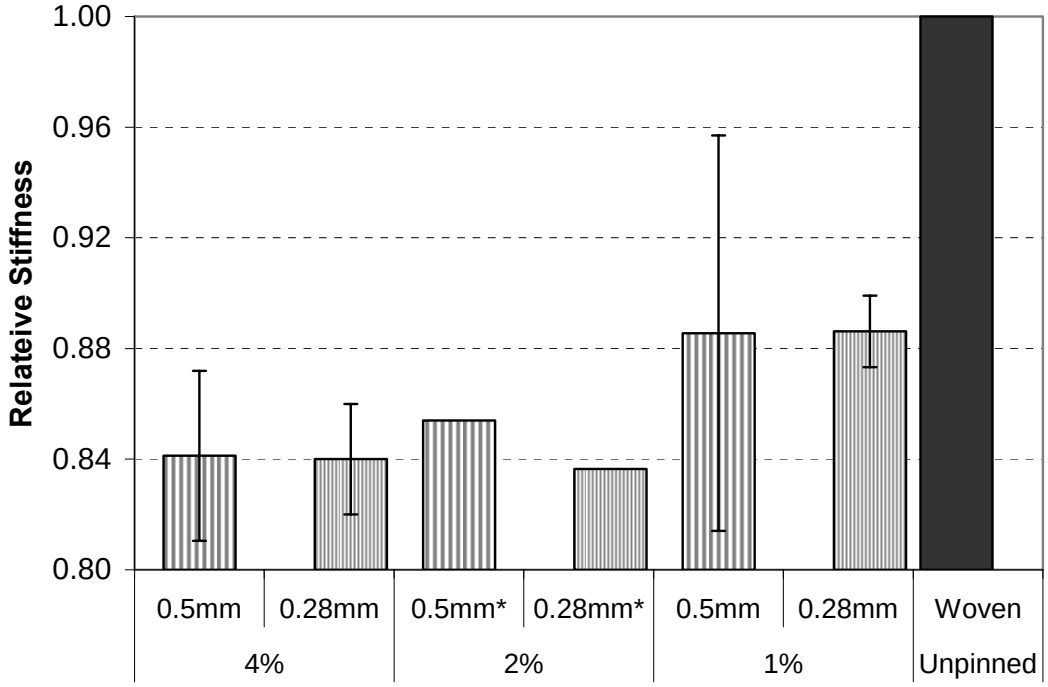

Figure 6-6: *Relative stiffness of Z-pinned woven G986/M21; asterisk indicates only one specimen tested.*

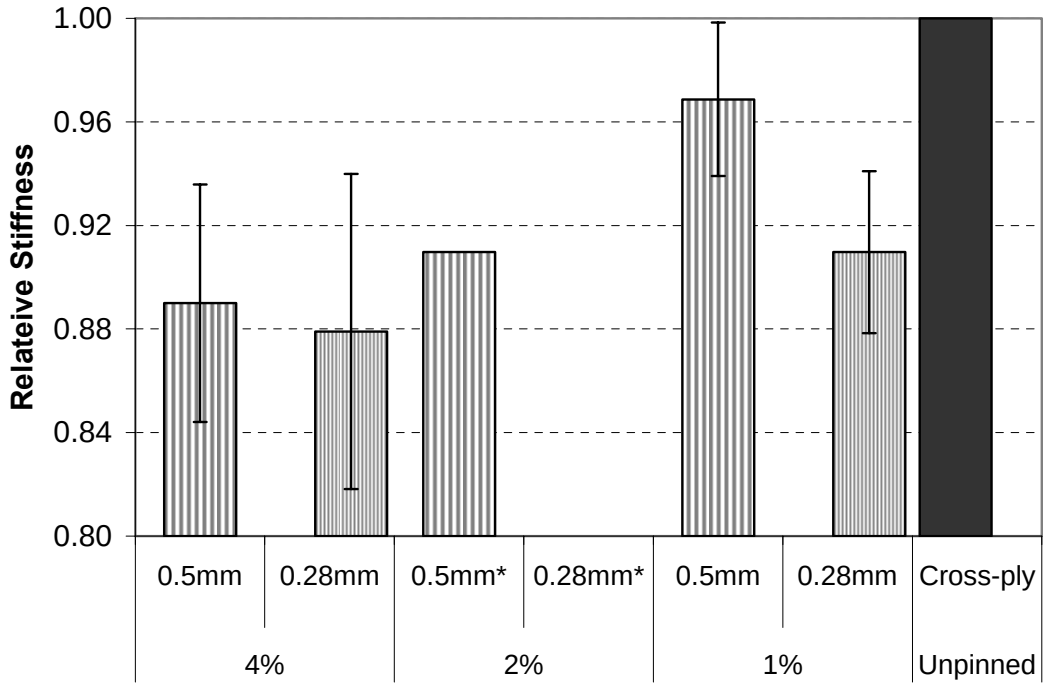

Figure 6-7*: Relative stiffness of Z-pinned Cross-ply IM7/M21 specimens; asterisk indicates only one specimen tested*

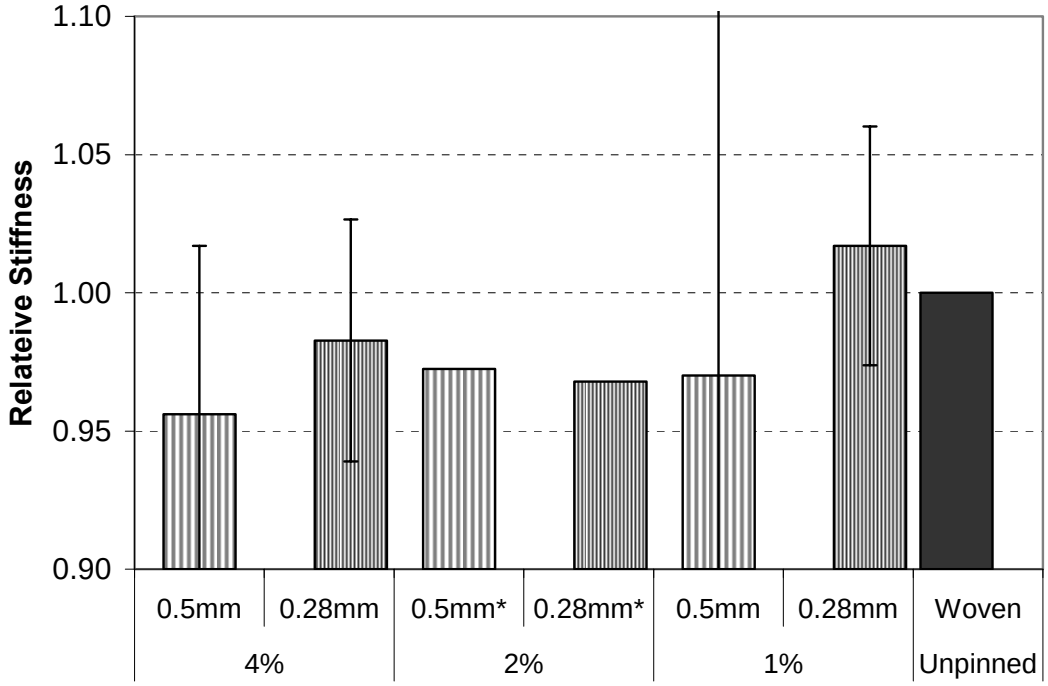

Figure 6-8: *Corrected relative stiffness of Z-pinned woven G986/M21; asterisk indicates only one specimen tested*

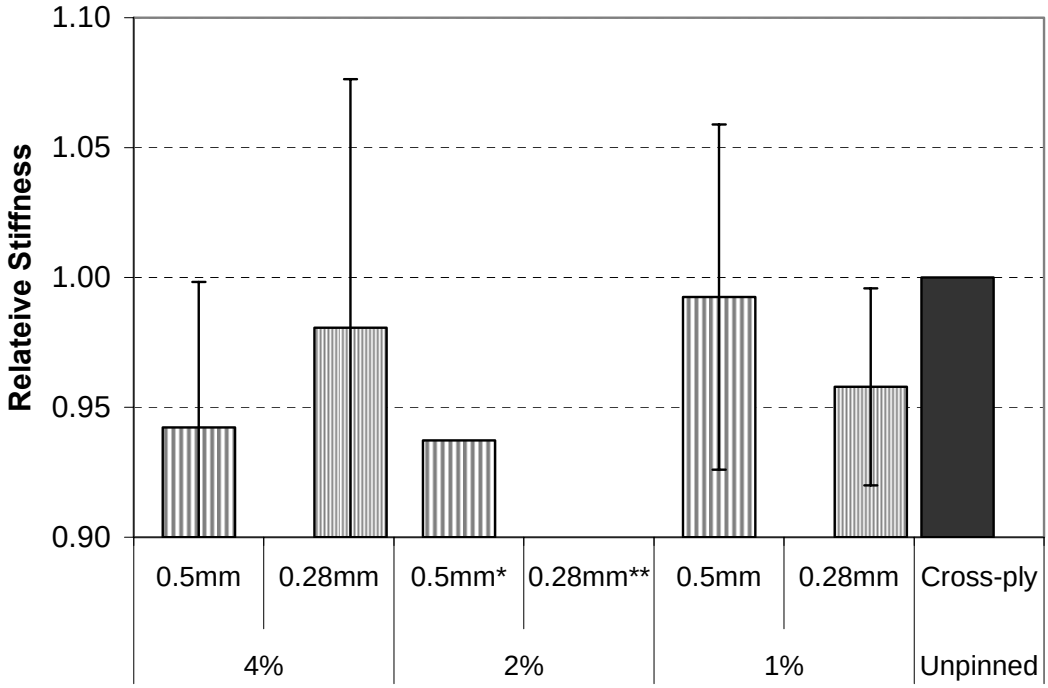

Figure 6-9: *Corrected relative stiffness of Z-pinned Cross-ply IM7/M21 specimens; asterisk indicates only one specimen tested*

6.4 Effect on Tensile strength

6.4.1 Failure behaviour

Failure occurred within the gauge length for most Tensile specimens. Failure in the grips occurred in only two out of a total of twelve woven specimens, eliminating them from the results; in both specimens failure actually occurred in both grips (Figure 6-10). UD specimens tested in the transverse direction behaved similarly, with one specimen out of a total of twenty failing at the grips. Failure occurred in a straight line across both types of specimens with minimal or no debris and was brittle in manner (Figure 6-11). Z-pinned specimens failed consistently at a single row of Z-pins.

Failure in UD specimens tested in the longitudinal direction was accompanied by intense audible signals before failure, with only minor visible splitting occurring at the edges. The specimens literally exploded into pieces at failure accompanied by the production of a considerable amount of dust. Values from all specimens were used in the results, since identification of the failure location relative to the gauge length is not possible (Figure 6-12).

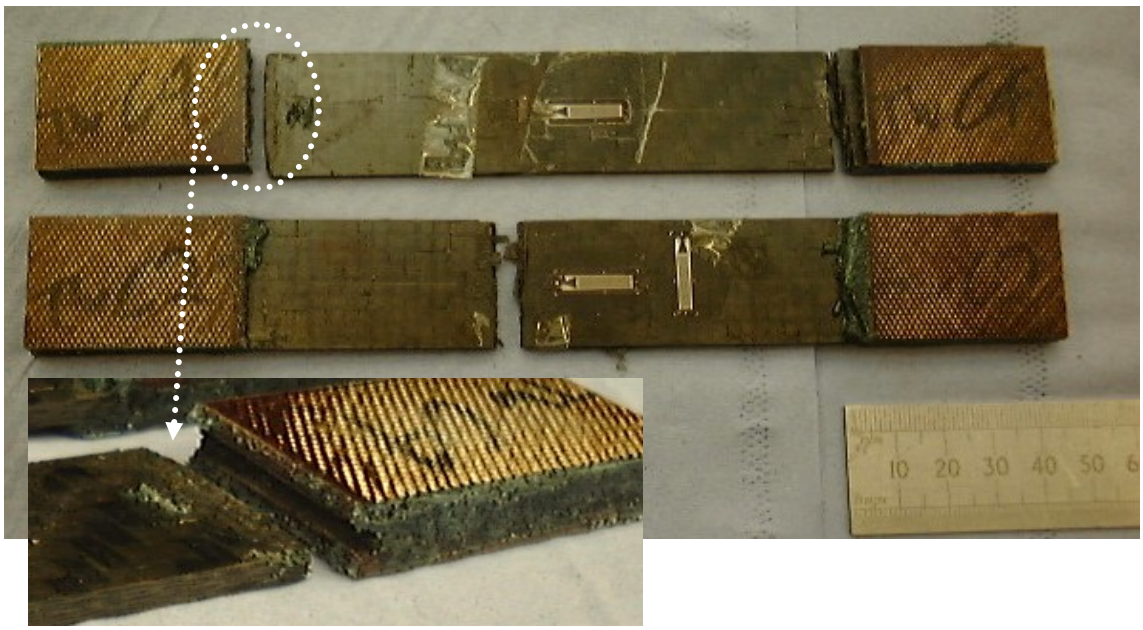

Figure 6-10: *Tensile failure of unpinned woven G986/M21 specimens at different failure locations.*

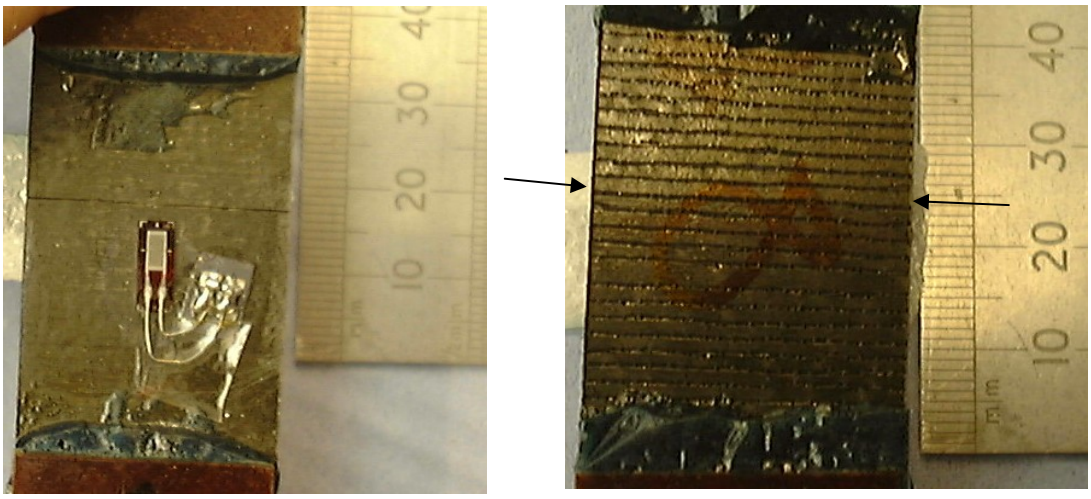

Figure 6-11: *Tensile failure of unpinned (left) and pinned (right) 90 UD IM7/M21 specimens; arrows denote failure line*

Figure 6-12: *Tensile failure of 0 UD IM7/M21 specimens*

OHT specimens are designed to fail at the hole (Figure 6-13). Failure initiates at the edges of the hole and propagates instantly throughout the cross section. Careful manufacturing of the Z-pinned specimens ensured symmetrical positioning of the Z-pin rows relative to the hole; a row of Z-pins was present in both axes of symmetry of the specimen. Z-pinning did not alter the failure behaviour, which is dominated by specimen geometry. Z-pins comprise flaws similar to the hole, only of a lesser magnitude. Z-pin presence provides an energetically favourable path for through-thickness crack propagation. Cross-ply specimens exhibited extensive fibre splitting, in contrast to woven specimens (Figure 6-14and Figure 6-15).

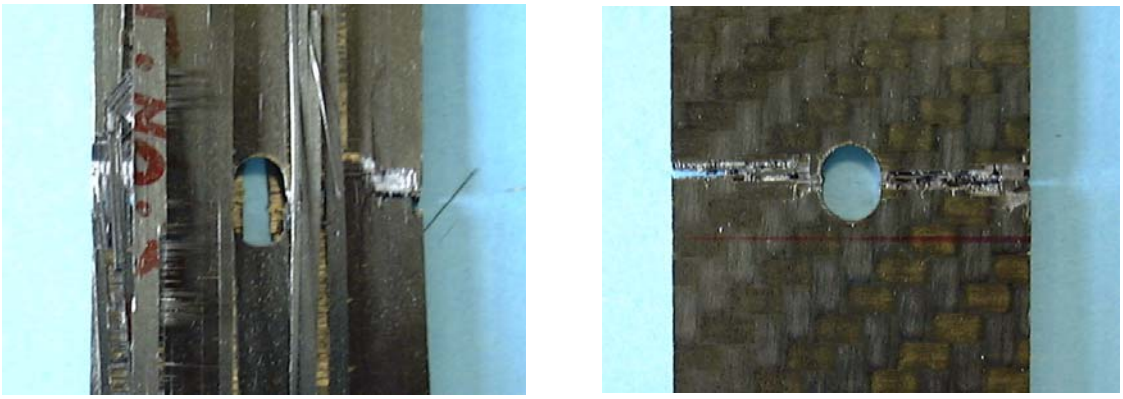

Figure 6-13: *Tensile failure of unpinned cross-ply IM7/M21 (left) and woven G986/M21 (right) notched specimens*

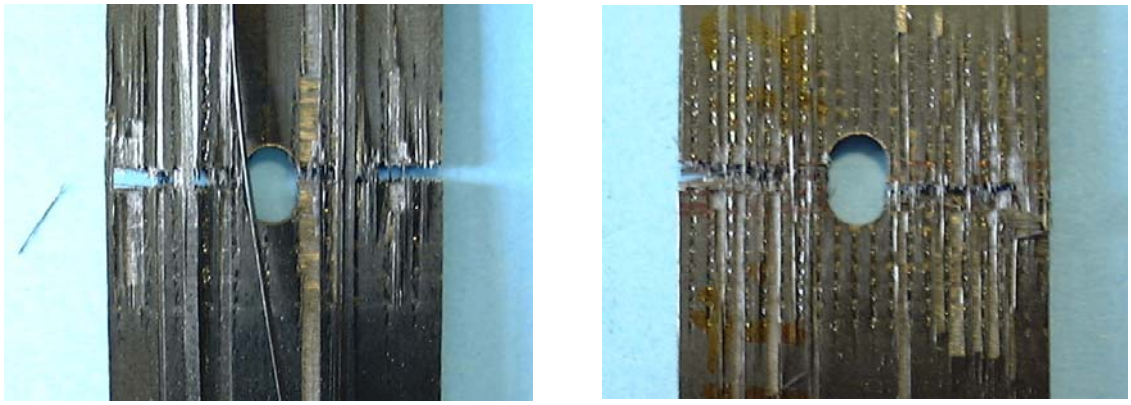

Figure 6-14: *Tensile failure of 2% pinned cross-ply IM7/M21notched specimens, using 0.5mm (left) and 0.28mm diameter (right) Z-pins.*

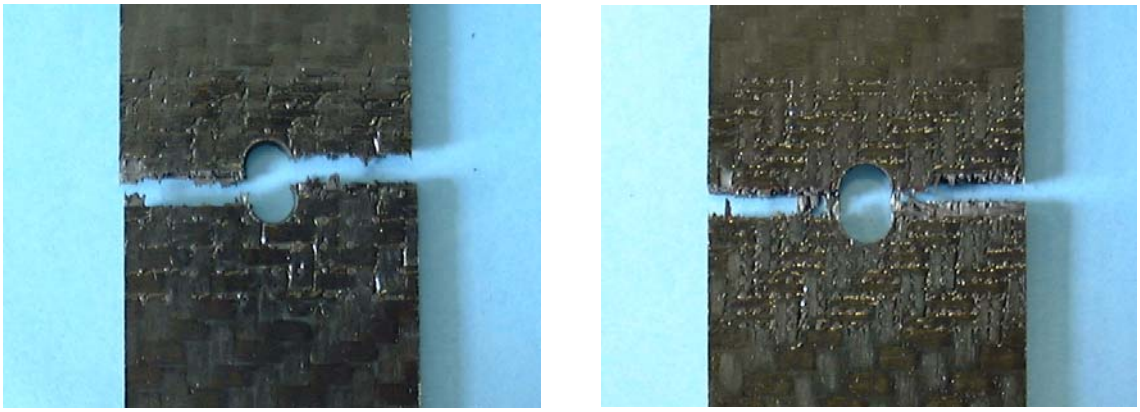

Figure 6-15: *Tensile failure of 2% pinned woven G986/M21notched specimens, using 0.5mm (left) and 0.28mm diameter (right) Z-pins*

Changes in the fibre volume fraction can influence tensile strength, as long as the loading is in the direction of laminate fibres. The complexity of the mechanisms of failure, which can increase in 3D composites [116], invalidate any attempts to "correct" strength values, as carried out in section *6.3.3*.

6.4.2 Unnotched strength

Ultimate tensile strength is affected considerably more than tensile stiffness by Z-pin presence. Without the presence of a notch, the reduction ranges from 35% to 50% in the transverse direction to the fibres in a UD material. Results are summarised in Table 6-4. Figure 6-16 and Figure 6-17 present the load versus displacement traces up to failure, as well as the measurement accuracy. The accuracy of the measurements is reduced for a 97.5% confidence level in a two sided normal distribution [93], similar to absolute stiffness values in section *6.3.1*. The accuracy is low for transverse strength, even for the unpinned material. This can be attributed partly to minor misalignment of the specimen during tightening of the grips. Z-pinned specimens exhibit a higher measurement scatter in all cases.

Material	Orientation	Density (%)	Diameter (mm)	UTS (MPa)	Reduction (%)
G986/M21	---		---	791	---
G986/M21	---	4%	0.28	514	35
IM7/M21	0		---	2488	---
IM7/M21	0	4%	0.28	1640	34
IM7/M21	90		---	46.3	---
IM7/M21	90	4%	0.28	23.4	49

Table 6-4: *Reduction in UTS in G986/M21 and IM7/M21 due to Z-pinning*

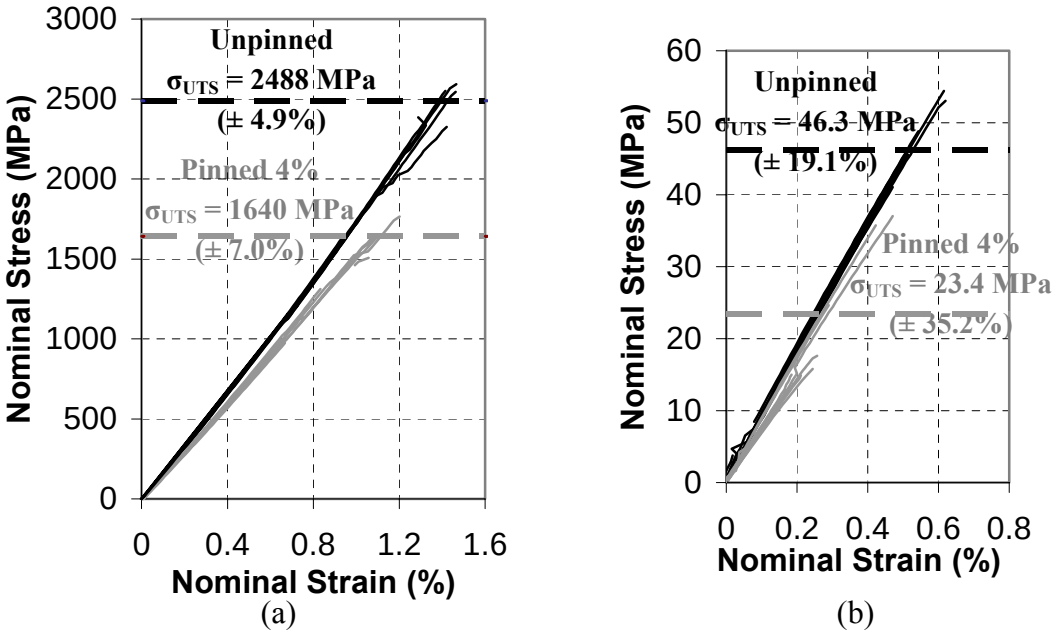

Figure 6-16: *Load vs. displacement traces and longitudinal (a) and transverse (b) tensile strength of UD IM7/M21*

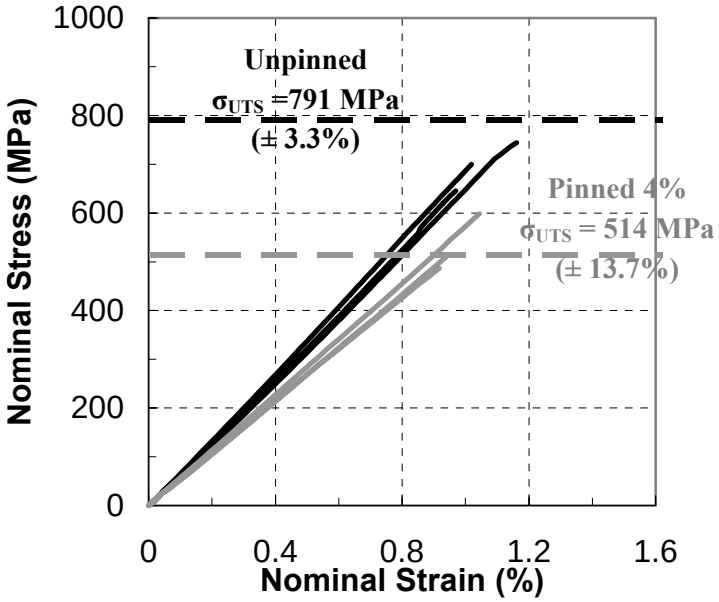

Figure 6-17: *Load vs. displacement traces and tensile strength of woven G986/M21*

Load versus displacement traces that stop short of the average stress failure line value indicate early gauge failure.

6.4.3 Notched strength

Notched tensile strength reduces with Z-pinning, although to a lesser extent compared to the unnotched strength reduction. The values obtained from the two different materials correspond to comparable fibre architecture. Woven material exhibits a slightly greater reduction in tensile strength than cross-ply. This can be attributed to the fibre volume fraction reduction, which is partly the cause of the strength reduction; woven specimens experienced a more significant fibre volume fraction reduction compared to cross-ply specimens. In that perspective, the reduction can be considered equivalent for both materials. Table 6-5 summarises obtained results.

Material	Density (%)	Diameter (mm)	Notched UTS (MPa)	Reduction (%)
G986/M21	---	---	496	---
G986/M21	1%	0.28	463	6.7
G986/M21	1%	0.5	451	9.1
G986/M21	2%	0.28	418	15.7
G986/M21	2%	0.5	429	13.5
G986/M21	4%	0.28	392	21.0
G986/M21	4%	0.5	426	14.1
IM7/M21	---	---	842	---
IM7/M21	1%	0.28	817	3
IM7/M21	1%	0.5	819	2.7
IM7/M21	2%	0.28	737	12.5
IM7/M21	2%	0.5	714	15.2
IM7/M21	4%	0.28	704	16.4
IM7/M21	4%	0.5	720	14.5

Table 6-5: *Reduction in notched UTS in G986/M21 and IM7/M21 due to Z-pinning*

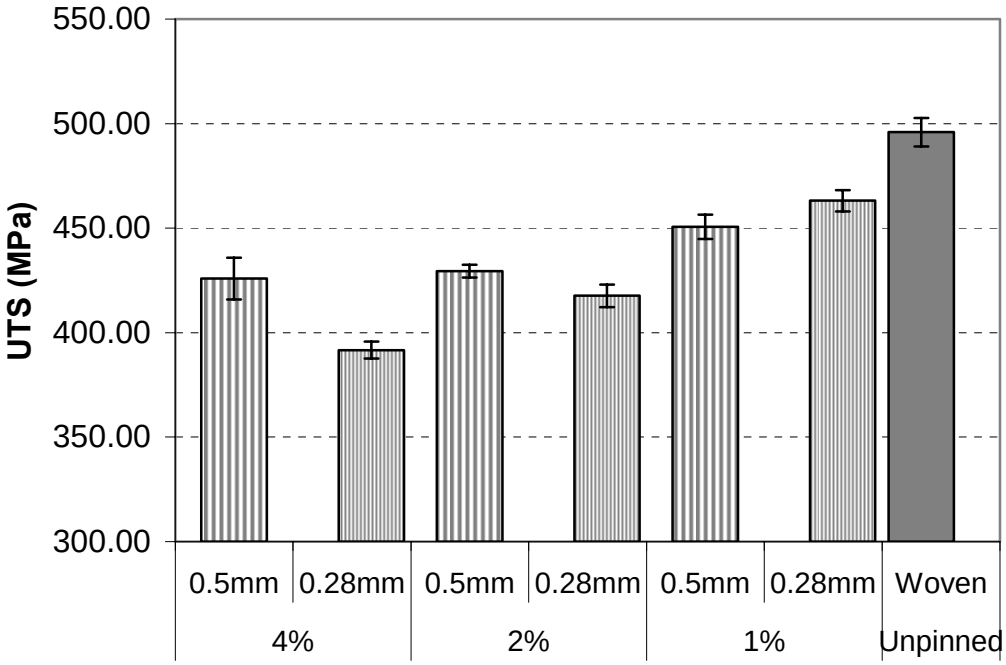

Figure 6-18: *Ultimate notched tensile strength of G986/M21*

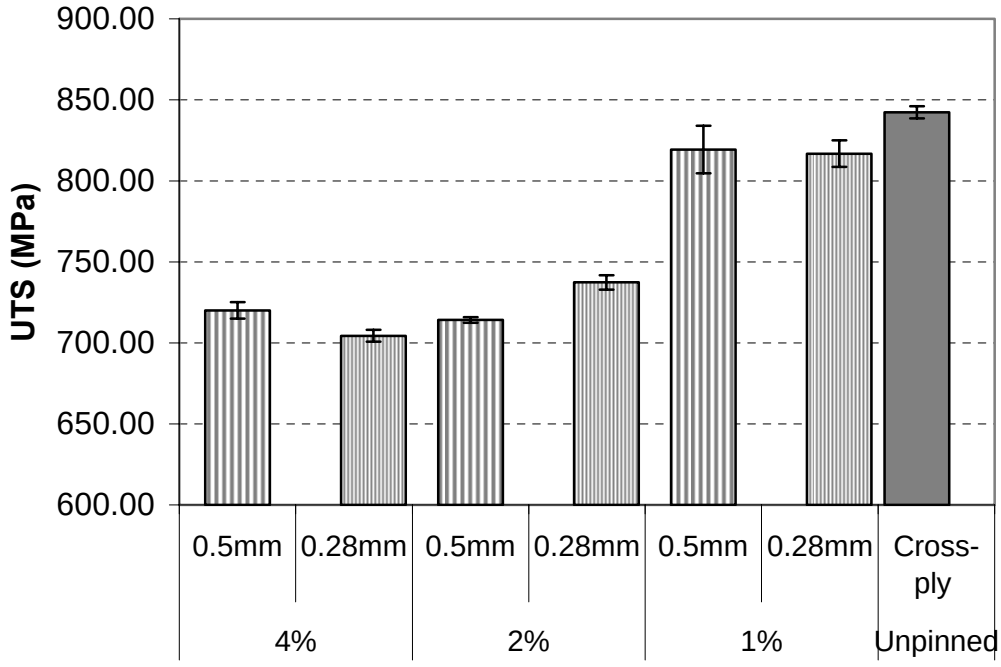

Figure 6-19: *Ultimate notched tensile strength of Cross-ply IM7/M21*

6.5 In-plane shear testing

Composites have a relatively low resistance to shear deformation, particularly in material planes dominated by matrix properties. However, it has been shown recently that those polymers used as matrices in fibre composites do not have a shear failure process; it can be argued that, for polymers at high strains, shear is a tensile process leading to chain alignment, where the local failure mechanism is tensile [117]. Nevertheless, in-plane shear for multidirectional laminates, which involve extensive fibre failure, is considered to be important. The alterations imposed to the laminate meso-structure by Z-pinning generate the need to investigate the in-plane shear response of Z-pinned laminates.

6.5.1 In-plane shear testing configurations

A number of methods are available for measuring the shear stiffness and strength of composite laminates. There is no universal method suitable for the accurate evaluation of the shear properties throughout the range of material architectures of composite materials. All methods have limitations. Six of the most commonly used methods include (a) the uniaxial tension of a ±45 laminate, (b) the uniaxial tension of a 10 off-axis laminate, (c) two-rail and three-rail shear tests, (d) twisting of a flat laminate, (e) torsion of a thin-walled tube and (f) the Iosipescu shear test, and are reviewed in detail in reference [82]. Only their predominant characteristics are reproduced here.

The ***±45 tension test*** is a straightforward test, from which both stiffness and strength can be obtained. Specimen preparation is moderately laborious, particularly when tabs are incorporated. The laminate is under a state of biaxial stress and not pure shear; however, the data reduction method takes this into account. On the other hand, a convention is necessary to nominate shear strength and is usually taken at a certain strain level. It is also influenced by laminate thickness.

The ***10 off-axis test*** entails a less laborious stacking sequence. It also exhibits uniformity of through thickness shear stresses and the absence of residual stresses. However, a three element rosette is required and the data reduction method is more complicated. Moreover, orientation errors can produce large measurement errors, although not critical when measuring shear strain at failure. Most importantly, it is not registered as a standard and significant non-uniformity of the stresses near the grips exists. In combination with the biaxial imposed stress state, ultimate shear strength tends to be underestimated. The use of oblique tabs, resulting in homogeneous stress in the specimen, improves the measurement, but gives only a lower bound for the in-plane shear strength [118].

Rail shear tests involve large specimens and extensive specimen preparation. Specimens are susceptible to machining defects and alternative failure modes due to errors in the laborious positioning procedure on the complicated testing fixture. Most importantly, they are only suitable for shear modulus determination.

The ***plate twist*** test imposes a pure shear stress state, involves easy specimen fabrication and is insensitive to variations in microstructure across the plate. It is, however, not suitable for obtaining strength data.

The ***torsion tube test*** is the most desirable method for shear characterisation from an applied mechanics viewpoint. A state of uniform pure shear stress along the whole length of the specimen is present, with a negligible through thickness shear gradient. Facility and fabrication costs are the major drawbacks.

6.5.2 The improved Iosipescu in-plane shear test

The ***Iosipescu*** shear test is favourable in terms of ease of manufacture, cost and accuracy. Both shear stiffness and shear strength can be obtained. It has potential for measuring shear properties in all three material planes [119]. A variety of types of

materials can be used, However the test is most accurate when testing UD materials with a longitudinal orientation [120]. The geometry and test procedure of the Iosipescu, or V-notch specimen, as it is referred, is described in the D5379-93 ASTM standard.

During the test a constant shear force is induced through the mid-section of the specimen. The failure behaviour of a UD 0 specimen is depicted in Figure 6-19. Cracks 1 and 2 initiate near the notch root, with crack 1 appearing systematically earlier. Propagation is instantaneous and stops at the highly compressed loading surfaces. Cracks 3 and 4 also grow slowly from the notch, but they cannot always be associated with load drops. Cracks 5 and beyond mark the end of the specimen life.

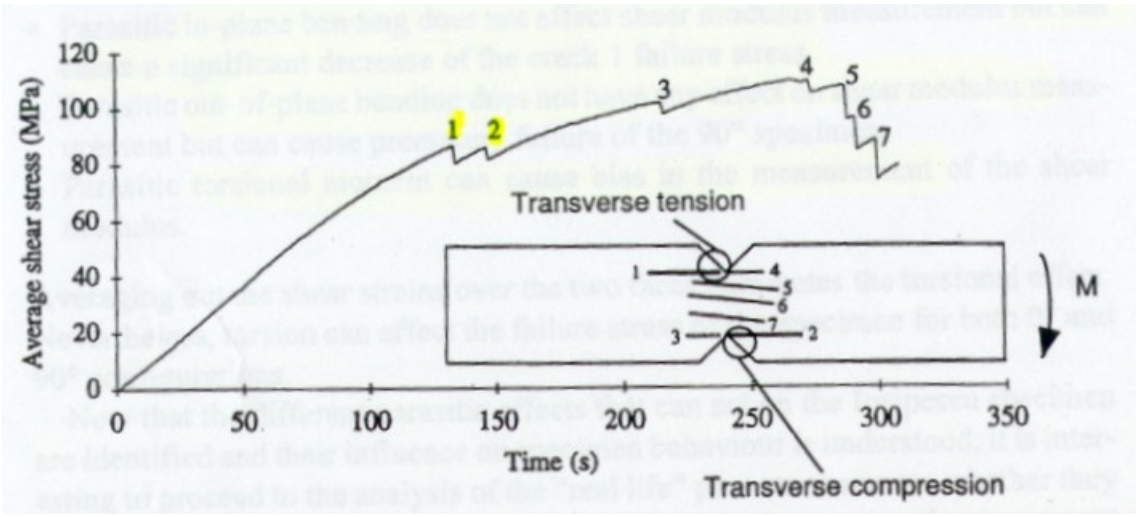

Figure 6-20: *Typical stress time curve for the 0 Iosipescu specimen with associated load drops and cracks, after [122]*

The rig commonly used to perform the Iosipescu test is known as the “Wyoming” rig. Recently an improved fixture, called the EMSE (Ecole des Mines de Saint-Etienne) rig, has been proposed; changes in the point of load application and in the guiding rail of the fixture have restricted the torsional and in-plane bending compliances of the Wyoming fixture. The occurrence of cracks 1 and 2 at significantly different stress values is one effect related to the parasitic in-plane bending of the Wyoming rig [121]. Parasitic out-of-plane bending can similarly affect the failure of a UD 90 Iosipescu specimen. Shear modulus can only affected by parasitic torsional moments [122]. The EMSE fixture was used throughout this study.

The proximity of the loading points to the gauge section of the specimen makes it susceptible to Saint-Venant effects. The through thickness stress uniformity assumption is invalidated due to parasitic specimen twisting. The effect of parasitic twisting moments on the shear modulus determination, imposed on the Iosipescu specimen due to parallelism defects of the loading surfaces, can be eliminated with averaging the strains of the two faces of the specimen. It is therefore essential to use strain gauges on both faces [122].

The state of stress in the notch area is not pure shear stress; stress and strain fields cannot be obtained through an analytical solution. The most important feature to achieve, in order to derive shear modulus and strength, is homogeneity, since the interpretation of failure under a complex state of stress concentrations is an unsolved problem [121]. Initial finite element modelling shows, that the occurrence of cracks 1 and 2 transform the stress distribution between the notches into a uniform state. Shear properties can be reduced with simple calculations. However, an explicitly defined stress correction factor, which depends solely on material properties, needs to be incorporated for the reduction of the shear modulus; still, the data reduction formula remains simple [122].

The transformation of the shear stress state into homogeneous state, due to the appearance of cracks 1 and 2, can be achieved by emulating the cracks during specimen manufacture. Figure 6-21 depicts the modified Iosipescu specimen configuration, where the cracks are emulated by the removal of the pertinent material. The final dimensions have been examined experimentally [123]. Finite element modelling indicates that the reduction of the shear modulus using this configuration requires no correction factors [122,124]. This is supported by a separate study, incorporating all non-linearities into the numerical modelling, such as specimen sliding, geometric non-linearity, frictional effects and most importantly non-linear material behaviour, which suggests that the experimental method of dividing the load by the cross-sectional area is an excellent approximation [120]. This method can be used subsequently to determine shear strength.

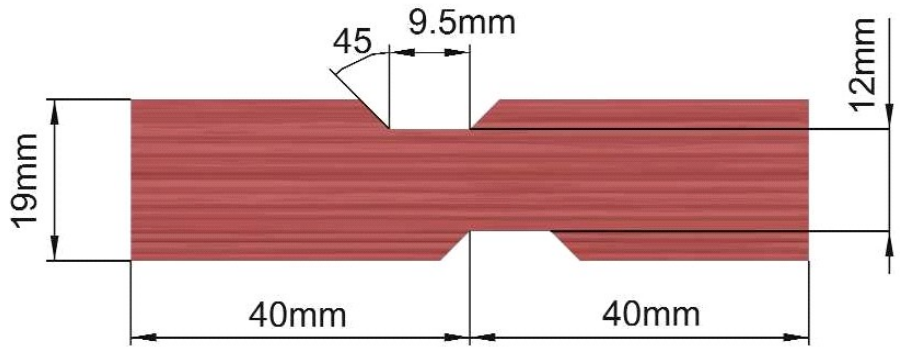

Figure 6-21: *Modified Iosipecu specimen geometry*

The initial finite element study [122,124] suggests that the implementation of a quadratic failure criterion is required to reduce shear strength; the influence of compressive stress needs to be taken into account. However, the approximations in the construction of this model, due to its linear approach, throw doubt on the validity of the latter proposition [120].

Concluding, the data reduction involved with the improved Iosipescu fixture and the improved specimen configuration is extremely simple, despite the complexity of the stress state at the gauge length. Shear modulus and shear strength can effectively be reduced from the experimental stress strain curve using the following simple formulas:

$$\varepsilon_{xy} = \varepsilon_{45} - \varepsilon_{-45} \tag{6-12}$$

$$\sigma_{xy} = \frac{P}{A} \tag{6-13}$$

Where:

$_{45}$ & $_{-45}$: strains directly measured by each strain gauge

$_{xy}$: shear strain

σ_{xy} : shear stress

P: applied load

A: specimen cross section

6.6 In-plane shear test cases

Table 6-6 lists the Iosipescu specimens used in this study. All specimens were instrumented with a rosette strain gauge on each side at ±45 . The foil strain gauge used has lead wires and was 3mm in length. The fixture and the instrumented specimen is depicted in Figure 6-22.

The width of the Z-pinned area is 10mm, covering the whole of the specimen gauge length. Low pining densities were not investigated due to the possibility of inconsistencies, considering the significant Z-pin spacing compared to the size of the specimen gauge length.

Material	Prepreg type	Lay-up	Density (%)	Z-pin diameter (mm)	No. of Specimens
IM7/M21	UD	$[0\ ]_{16}$	---	---	6
IM7/M21	UD	$[0\ ]_{16}$	4%	0.28	7
IM7/M21	UD	$[0\ ]_{16}$	4%	0.5	5
IM7/M21	UD	$[0\ ]_{16}$	2%	0.28	5
IM7/M21	UD	$[0\ ]_{16}$	2%	0.5	4

Table 6-6: *Iosipescu test cases*

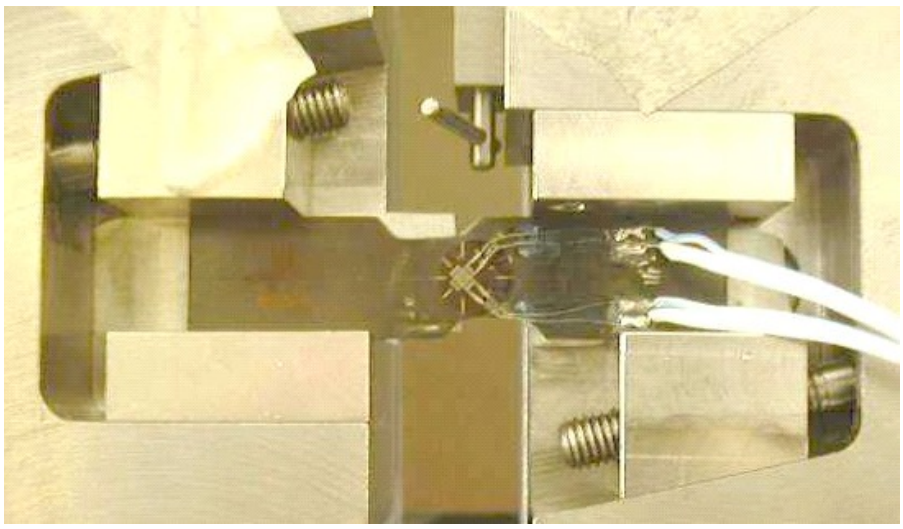

Figure 6-22: *The Iosipescu test fixture*

6.7 In-plane shear stiffness

Figure 6-23 presents the effect of Z-pinning on the shear modulus of UD IM7/M21 for two Z-pin densities and both Z-pin diameters. Error bars demonstrate the accuracy of the measurement with 97.5% confidence level for a two sided normal distribution [93].

Any changes in shear modulus are smaller than the accuracy of the measurement. The alteration of the modulus does not follow any trend. A reduction in stiffness can only be observed for 4%, 0.5mm diameter pins.

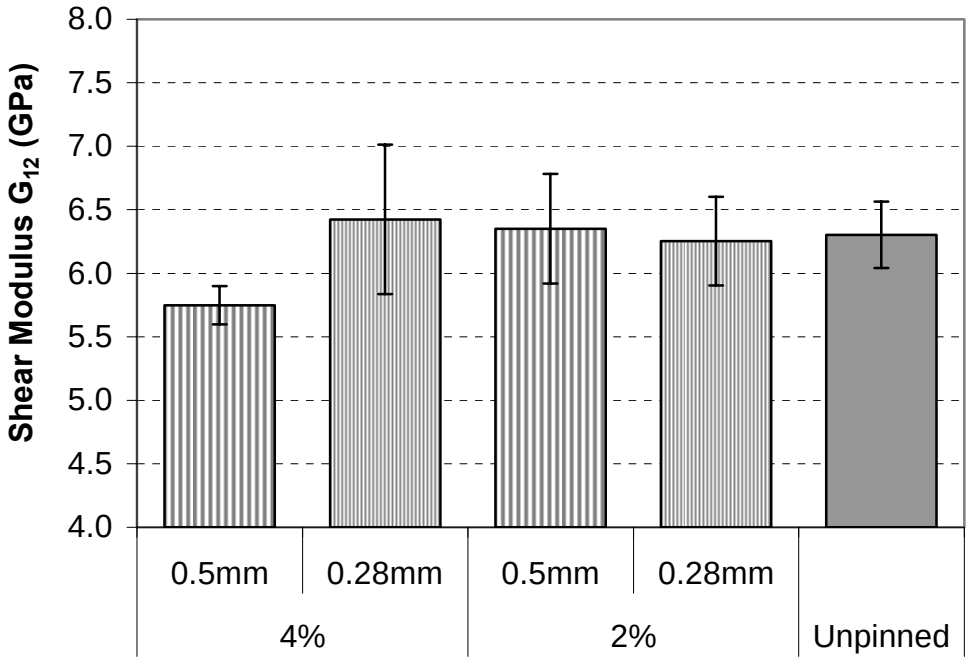

Figure 6-23: *Shear modulus of unpinned and pinned UD IM7/M2*

6.8 In-plane shear strength

In-plane shear strength was not measured, since crushing failure of the specimen edges against the stainless steel loading blocks preceded shear failure, despite the incorporation of a 5 angle to soften the load distribution near the loading edges (Figure 6-24). The most effective remedy for this occurrence would be the use of tapered tabs [82]. Time limitations prevented the addition of tabs, and no strength data is presented in this study.

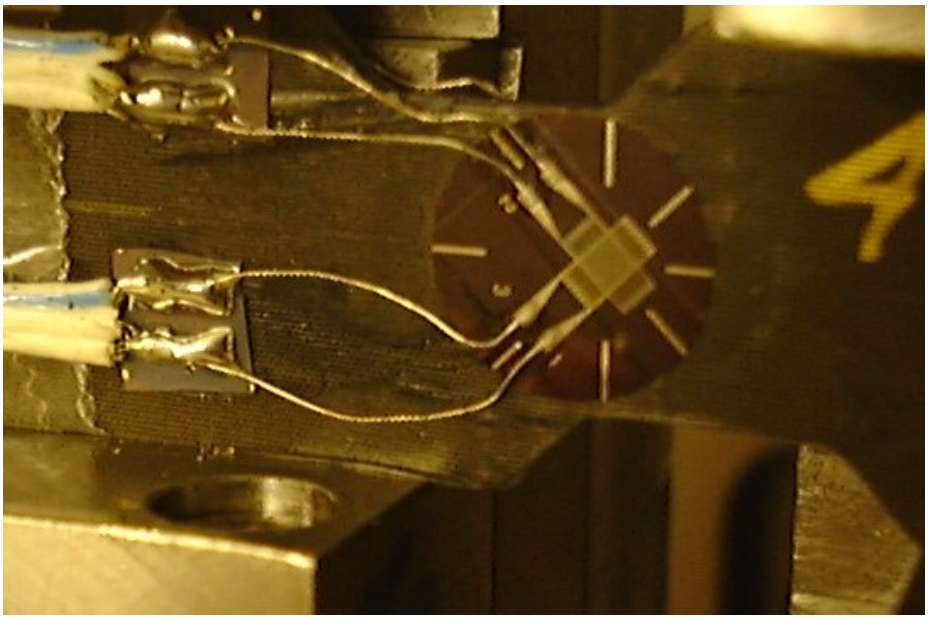

(a)

(b)

Figure 6-24: *Specimen edges crushing under high loads;(a) Specimen during test and (b) specimen edge*

6.9 Modelling the in-plane response of Z-pinned laminates

A recent publication has examined the effect of Z-pinning on laminate stiffness [125]. A micro-mechanical model is used to provide detailed interlaminar stress analysis near Z-pins and free edges and a macro-mechanical model, employing the unit cell method, is used for stiffness analysis. Curing stresses and any form of damage in the laminate during insertion are not taken into account. Among other properties and laminate configurations, the effect of Z-pinning on the tensile and shear modulus of both UD and cross-ply material is evaluated.

Table summarises results from the reference, contrasting them against the respective measurements in this study. To the defence of the numerical simulation, the current set of data was not available at the moment of the model construction. The geometry of the unit cell was based on early observations of resin pockets. The model does not incorporate any additional change in laminate fibre volume fraction, other than the change occurring with the introduction of the resin rich area around the Z-pin. The most significant influence on the longitudinal modulus is therefore laminate fibre misalignment. The effect of laminate fibre misalignment has been assessed in section *6.3.2*. The minimal effect of Z-pinning on the transverse stiffness according to the numerical model, indicates that more work is needed for an accurate simulation.

	E_{11}	E_{22}	G_{12}
Reduction (%) from FE model [125]	10.7	2.8	2.4
Reduction (%) from experiment	---	---	-0.75

Table 6-7: *Effect of 2% density, 0.5mm diameter Z-pins on the moduli of UD laminates*

	E_{11}	G_{12}
Reduction (%) from FE model [125]	7.6	2.0
Reduction (%) from experiment	9.0	---

Table 6-8: *Effect of 2% density, 0.5mm diameter Z-pins on the moduli of cross-ply laminates*

6.10 Summary

Z-pinning causes a reduction in tensile modulus and strength. The magnitude of reduction does not differ notably between woven laminates and laminates fabricated from UD prepreg, when an equivalent stacking sequence is maintained. Strength is influenced more severely than stiffness.

Larger diameter Z-pins at high densities impose additional reduction in the moduli of laminates fabricated from UD prepreg. In configurations of medium or low density or smaller Z-pins the shear modulus remains unaffected.

The reduction of in-plane properties is predominately attributed to the reduction in fibre volume fraction through the thickness increase imposed during manufacture.

7 Application of Z-Fiber pinning to T-stiffener structure

Z-pinning can be used selectively in locations prone to delamination in a structure. A common structural location exhibiting this type of failure is the T-joint of a stiffener to a laminate. Due to the local geometry, in-plane loads in the laminate generate out-of-plane loading at the joint in the stiffener area. As discussed in section *1.1*, out-of-plane loading can cause delamination failure. The effectiveness of Z-pinning the stiffener (stringer or web) to the laminate (skin) is examined in this chapter.

7.1 Stiffened structures

The design of lightweight structures involves the use of the correct amount of material in the most efficient way, so as to bear the loading the structure is subjected to. A common design is the space-frame type of structures, where certain members of the structure are aligned to the subjected loading and bear most of it. Despite the intrinsic advantage of composite materials to orientate their material properties through tailored stacking sequences thus improving material efficiency, the use of stiffened members, bearing the bulk of the load, is also widespread in composite structures. These members are either integrated in the manufacture of the structure or joined to the rest of the structure at a later stage. A common form implemented is that of I- or T-shape beams. A typical example is depicted in Figure 7-1.

The bonding of the stiffened members to the skin of the structure is of great importance. As long as the loads can be transferred to the stiffened members, the integrity of the structure is assured. Structures with stiffened members do not lose their load carrying capability when the skin is damaged by impact loads or even penetration [126]. On the other hand, impact loading directly on the stiffener bond line to the skin can be detrimental. The local geometry at the joint of the stiffener to the skin introduces out of

plane loading and these joints are a common location for the emergence of delaminations, most frequently through skin buckling under compressive loading [12].

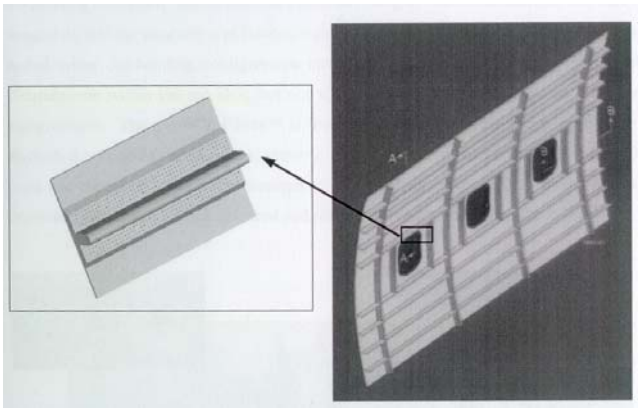

Figure 7-1: *Structural part implementing T-shaped stiffening beams*

Previous tests have indicated significant performance enhancement by the use of Z-pinning in T-stiffener sub-structures [64,72]. In this study the performance of Z-pins in a T-stiffener sub-structure, designed for use in a nacelle structure, is evaluated. This consists of a part of a collaboration programme aiming to certify the use of Z-pins in I- and T- shape joints for use in service within a short period of time (JOINTS). The most prominent difference from previous studies is the small thickness of the structure.

7.2 Manufacture and test cases

The material used for the manufacture of the test specimens was woven fabric G986/M36. Additionally, E-glass/914 UD prepreg was used for the manufacture of the tabs (±45 stacking sequence). The tabs were co-cured, as the cure cycles of the two resin systems used are similar. Specimen dimensions were decided by the programme collaborator responsible (QinetiQ). The stacking sequence is optimised according to the requirements of the complete structure by another collaborator (Hurel-Hispano). Specimen dimensions and the stacking sequence are depicted in Figure 7-2.

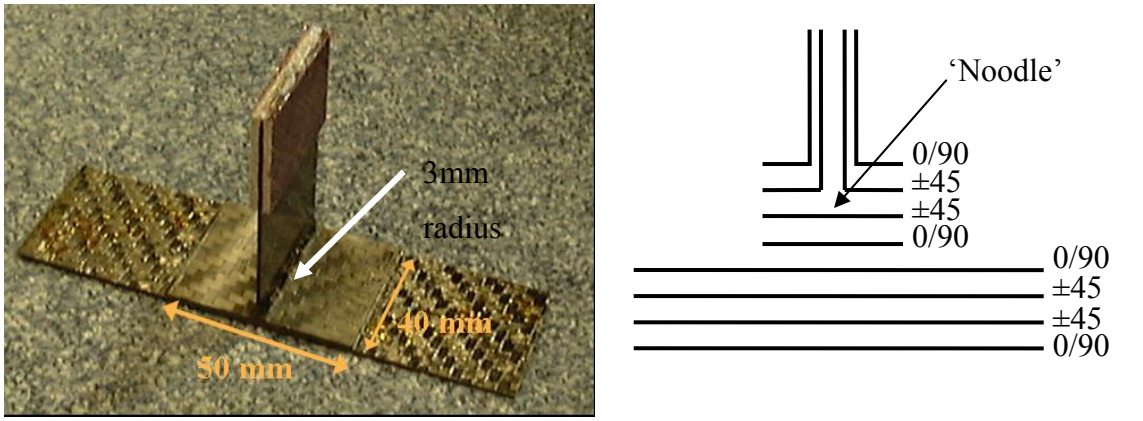

Figure 7-2: *Specimen dimensions and specimen stacking sequence (original design); material thickness is 1.1mm every 4 plies*

The insertion of Z-pins was performed using the hand held unit, as the size of the mould was too large too fit under the head of the gun within the available space in the gantry. Three combinations of Z-pin density and diameter were used. Additionally, the compaction procedure employed for the woven fabric materials in this study is only applicable for flat laminates; the standard vacuum hot de-bulking procedure was used for the manufacture of the T-stiffener. To compensate, de-bulking was performed for every ply. Figure 7-3 depicts intermediate stages of the lay-up and the de-bulking procedure. Z-pins were inserted from the skin side.

The triangular area at the bottom of the web of the T-stiffener, referred to as the 'noodle', is usually filled with additional material, as the existing material leaves space unoccupied due to the necessary radius of the mould. A strip of woven fabric prepreg was laid after the assembly of the two parts of the mould together, as illustrated in Figure 7-3c. No Z-pins were intentionally inserted into the noodle area.

(a)

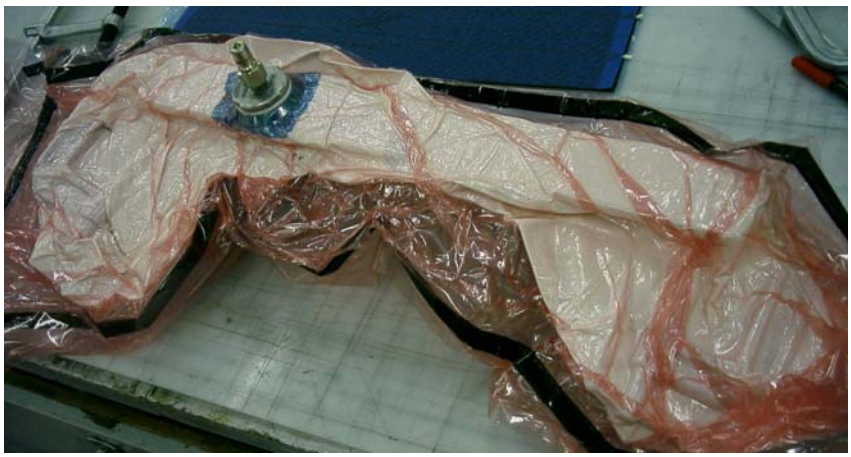

(b)

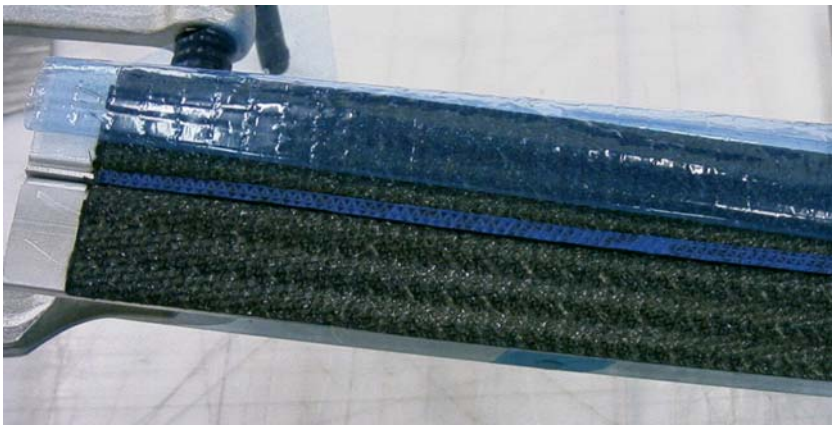

(c)

Figure 7-3: *Intermediate stages of manufacture; (a) lay-up, (b) de-bulking using an envelope type vacuum bag and (c) addition of a strip of self-same material in the noodle area.*

The mould was manufactured by modifying commercially available L-shaped aluminium beams (3 in × 1 in × 6mm). The mould has a length of 520mm usable for lay-up, which provides 12 specimens after each cure. A radius of 3mm was machined into the outside edge of the L-beams, according to design. Additional grooves, 1.5mm in depth, were introduced to accommodate the co-cured tabs. Holes were drilled to

accommodate aligning steel pins, and flanges were used to retain the necessary clearances, as well as retain the mould in an upright position. The design allows a variety of thicknesses of material to be manufactured by using sets of flanges of corresponding thickness. The mould is depicted in Figure 7-4. Additional caul plates are used to cover the remaining skin area of the T-stiffener.

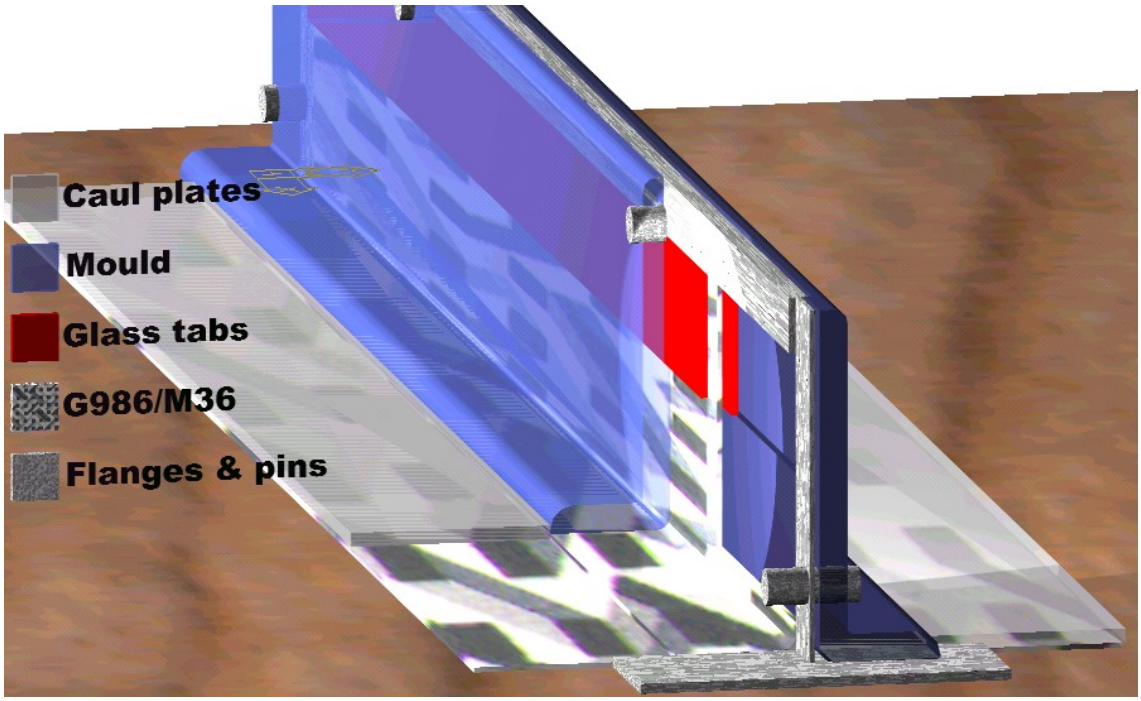

Figure 7-4: *View of a slice of the assembled mould containing the composite.*

An additional laminate of the same material (G986/M36) with a thickness of 1.1mm (4 plies) was also manufactured. The laminate was bonded, after cure, to a portion of the T-stiffener specimens, in order to provide stiffening to the skin. The lay-up of the complete stiffened design of the T-stiffener is depicted in Figure 7-5. Surfaces were abraded before bonding and the adhesive used was Redux 420. Strain gauges were also bonded to a portion of the specimens to aid later modelling of the structure by the collaborators (also depicted in Figure 7-5).

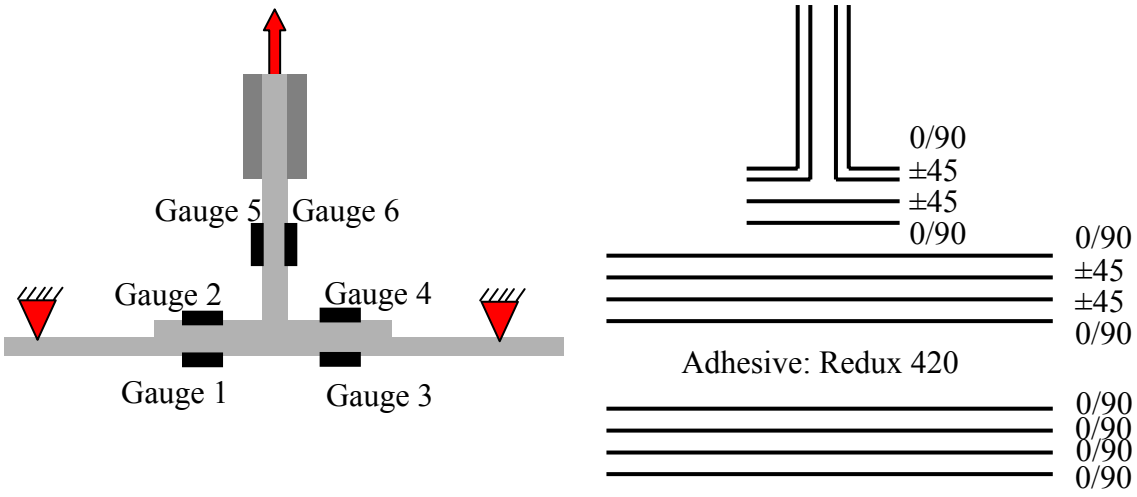

Figure 7-5: *Strain gauge positioning, stacking sequence of additional stiffening plate (stiffened design) and bonding adhesive; material thickness is 1.1mm every 4 plies.*

Specimens were cut using a dry diamond coated wheel and their sides were lightly polished; correction fluid was applied to one of the specimen sides to facilitate crack measurement during testing. All specimens are presented in Table 7-1.

Density (%)	Diameter (mm)	Type of design	No. of Specimens
---	---	Original	1
---	---	Stiffened	4
2%	0.28	Original	1
2%	0.28	Stiffened	4
2%	0.5	Original	1
2%	0.5	Stiffened	4
4%	*0.28*	*Stiffened*	3

Table 7-1: *T-stiffener test cases*

7.3 Description of test

The arrangement used was a pull-off test configuration. A pulling load is applied on the web of the T-stiffener, while the skin is fixed in the direction of load application with two supports. Movement in the lateral direction can also be fixed [127]. The distance between the supports determines the location of the initiation of failure [72]. A narrow configuration favours initiation at the noodle area, while a wide configuration favours initiation at the end of the foot of the T-stiffener.

The lay-out of the test is presented in Figure 7-6. Upward movement only is restricted by supports spaced at 80mm, while the tabbed portion of the specimen is clamped in grips connected to the load cell. The rig was designed and manufactured specially for the test with three objectives in mind; to facilitate an adjustable distance between support points, allow the T-stiffener foot-to-skin interface to be visually monitored during the test and accommodate an LVDT to obtain measurements of the displacement of the skin under the web of the T-stiffener, in order to aid later modeling of the structure. The same rig possesses a central channel and a side groove to accommodate additional parts used in the friction test as described in section *5.4.1*.

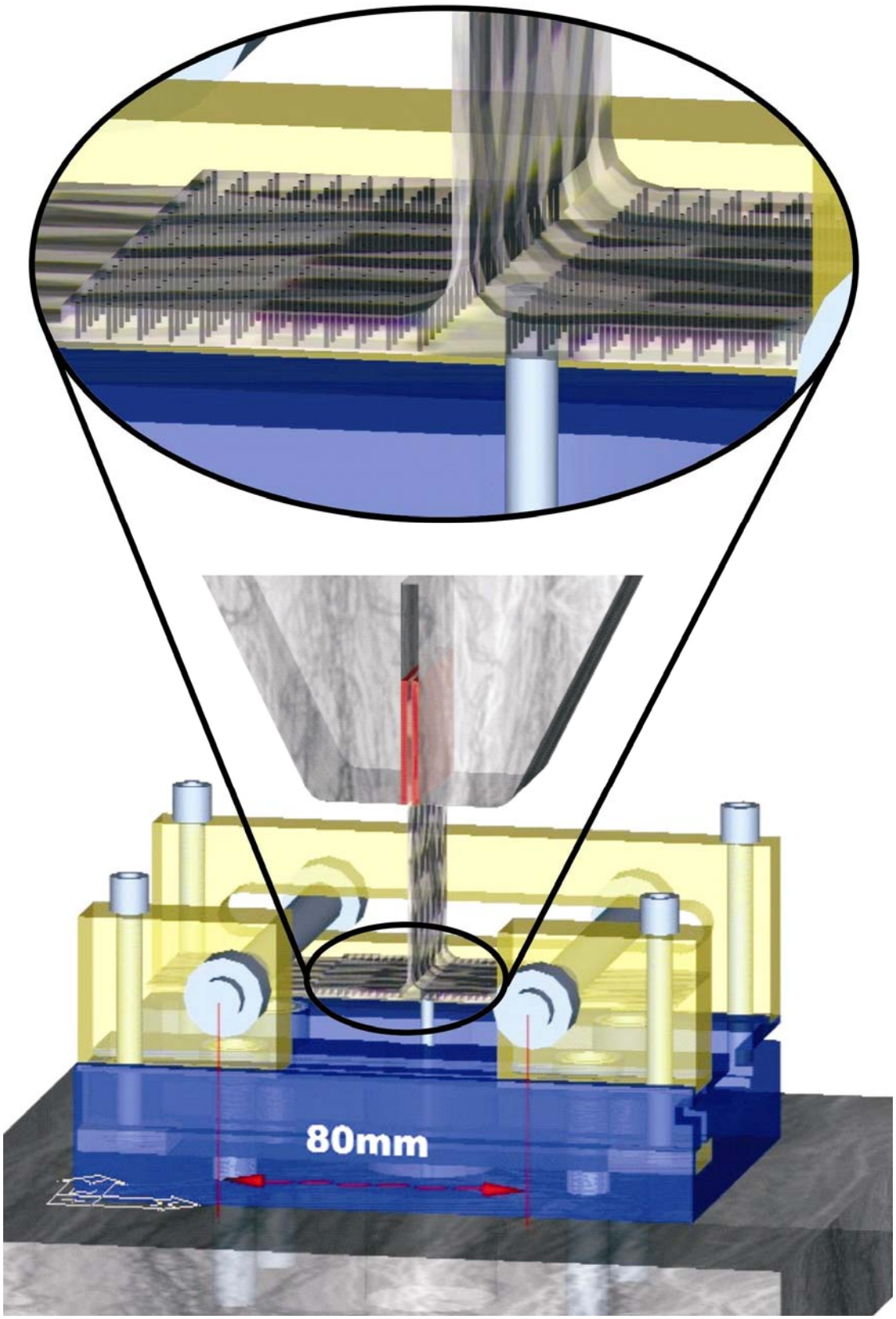

Figure 7-6: *Test configuration of the pull-off test; detail illustrates LVDT position and Z-pin location.*

7.4 Performance of original design

This section describes the performance of the T-stiffener before the addition of the stiffening plate (as in Figure 7-2). Only three such tests were performed (Table 7-1). Figure 7-7 depicts the load versus displacement trace of an unpinned sample. The load rises until delamination initiates on one side at the foot-to-skin interface. The maximum load reached is 450N. After propagating for 1.5mm, the crack jumps to 10mm. The specimen rotates after initial failure and the crack propagates further under the biased load distribution. The test was stopped before the crack reached the noodle area.

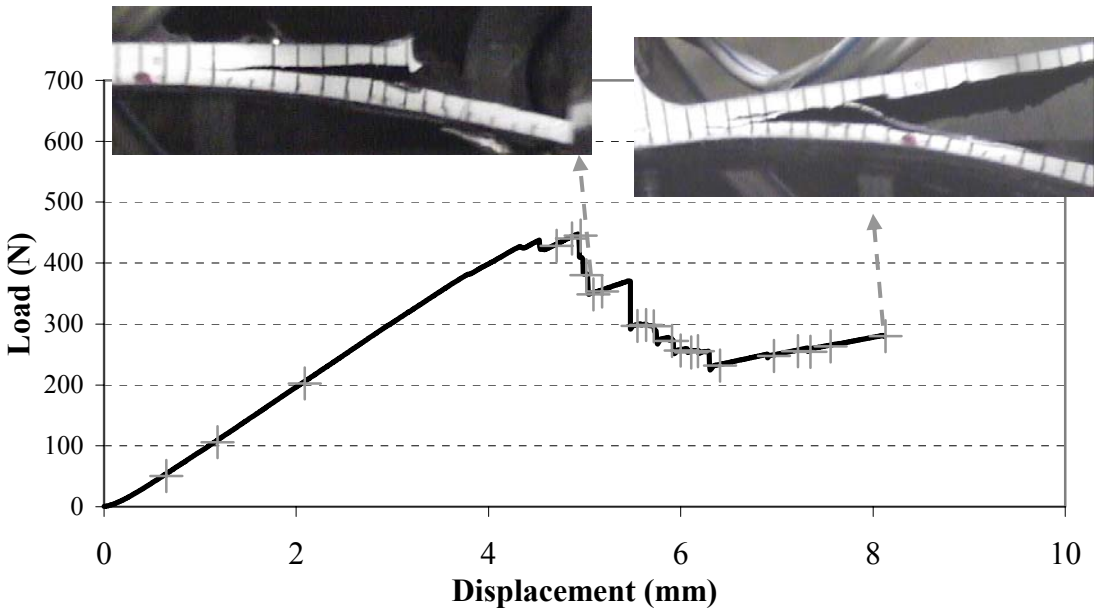

Figure 7-7: *Load versus displacement trace of an original unpinned sample; crosses indicate points of image capture.*

Figure 7-8 depicts the load versus displacement trace of a sample with 2% density, 0.5mm diameter Z-pins. At a load of 600N damage initiates in the skin area on the right side. At a larger displacement delamination initiates on the left side and is arrested at a crack length of 6mm. The skin under the cracked area delaminates and bending failure follows. The behaviour was similar in the second (2%, 0.28mm) pinned sample; although no delamination was observed, bending failure occurred in the skin. Post-mortem inspection revealed poor quality of the outside row of Z-pins in the first (2%,

0.5mm) pinned sample, where delamination occurred. The maximum value of the load is determined by the strength of the skin in bending.

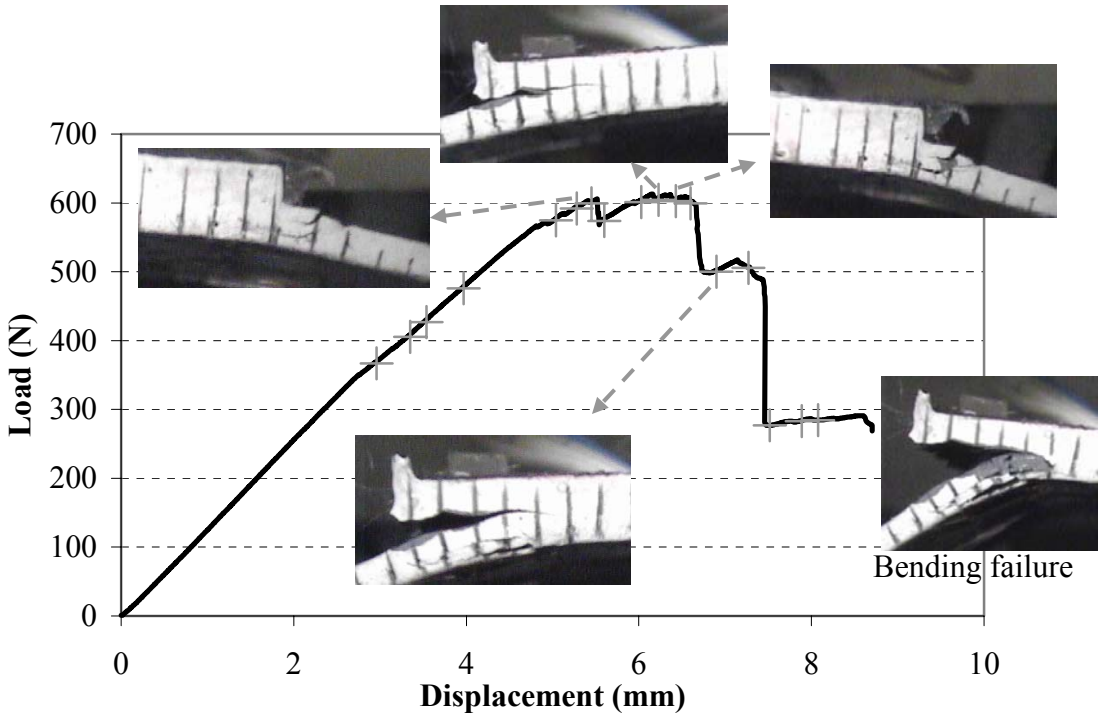

Figure 7-8: *Load versus displacement trace of an original sample with 2% density 0.5mm diameter Z-pins; crosses indicate points of image capture.*

7.5 Performance of stiffened design

The addition of the stiffening plate facilitates comparison between unpinned and pinned samples, as it prevents bending failure and allows delaminations to grow. At the same time there is a change in the location of failure of the specimen; failure initiates at the noodle area and propagates into the foot-to-skin interface as well as the web (Figure 7-9).

Two main differences can be observed between unpinned and pinned samples; firstly in the ultimate failure load and, secondly, in the capacity to sustain the load. These are discussed in the next two sections.

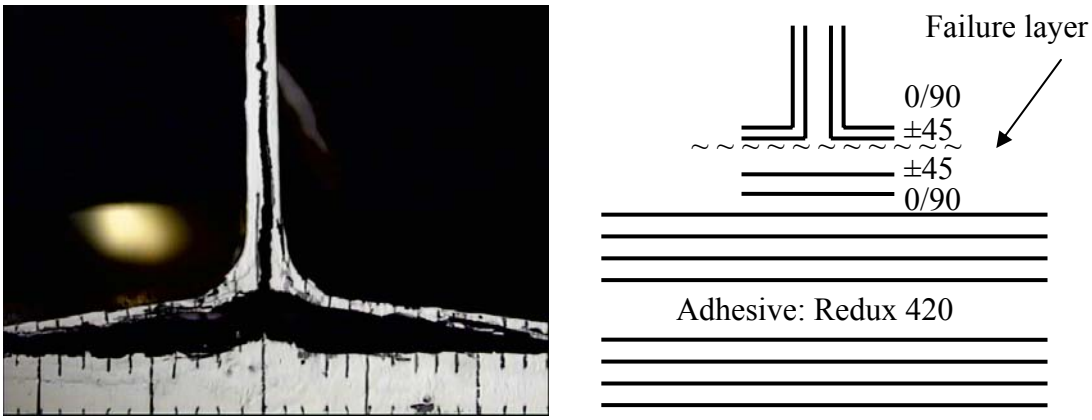

Figure 7-9: *Failure initiates from the 'noodle' area and propagates into the ±45 interfaces well as the web.*

7.5.1 Load carrying capacity

Figure 7-10 depicts the average value of the maximum load carried during the test for all test cases. Error bars represent one time the standard deviation. No distinction was made whether the maximum load was observed before or after the onset of failure.

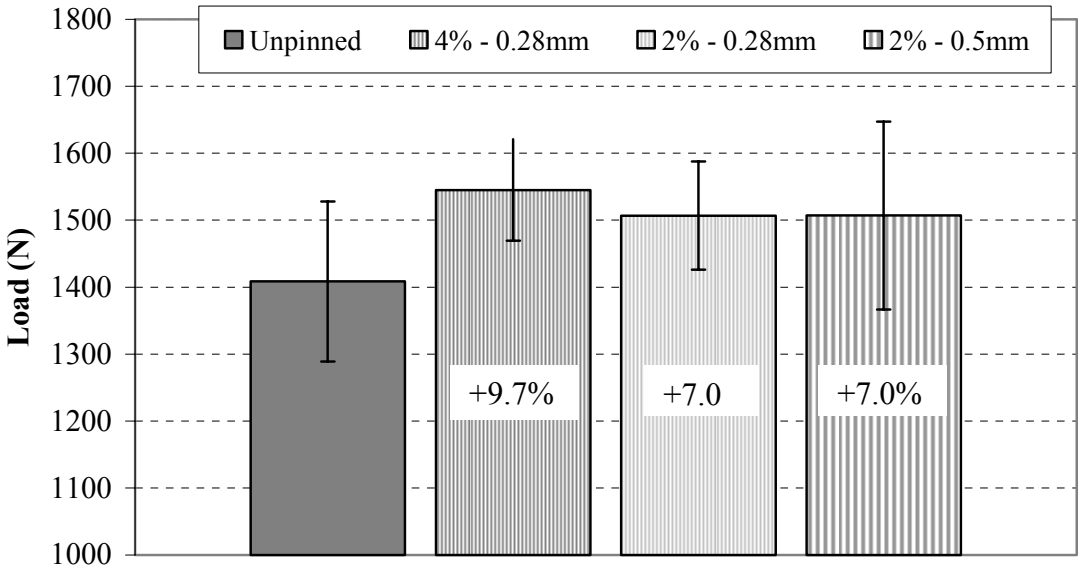

Figure 7-10: *Maximum load carried during the test of the stiffened sub-structure; average for each test case*

An increase of 7% to 10% is observed with the insertion of Z-pins. The scatter, however, is significant. Post-mortem inspection confirms the good pinning quality of all pinned specimens. Slight variation of the pinning location is responsible for the scatter in pinned samples, as will be discussed in the next section. The scatter of the unpinned samples is also significant and overlaps with the error bars of all test cases.

7.5.2 Damage tolerance

The failure of the unpinned specimens was catastrophic after the onset of delamination. Figure 7-11 presents the crack position in an unpinned sample in two instants separated by the amount of displacement denoted in the figure. No intermediate position exists; 0.1mm of displacement after a crack becomes visible, it propagates to a total length of over 20mm.

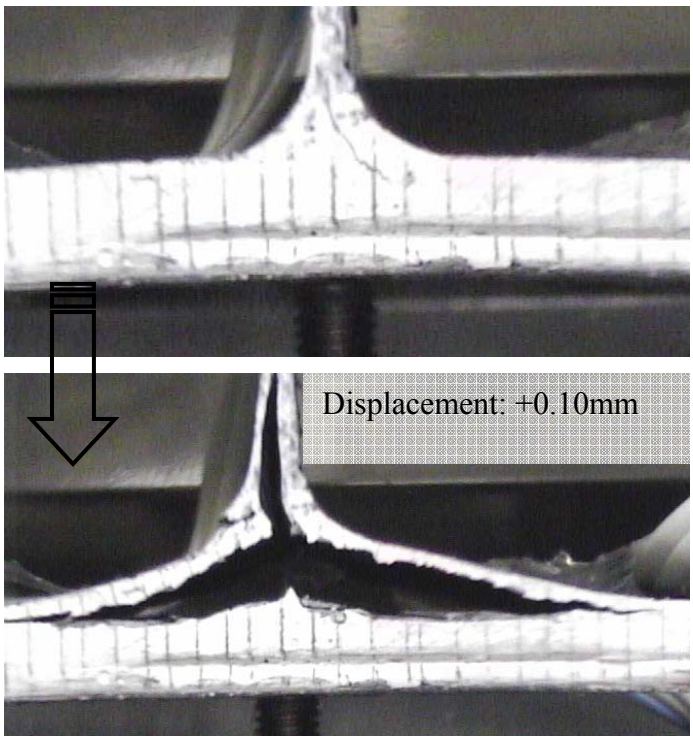

Figure 7-11: *Crack propagation in a stiffened unpinned sample at the illustrated crosshead displacement intervals*

Figure 7-12 and Figure 7-13 present the behaviour of pinned samples with a 2% density, 0.28mm diameter and 2% density, 0.5mm diameter pinning arrangement respectively. Failure is progressive in manner and significant crosshead displacement is required to propagate the crack. The crack propagates further in the web than in the foot-to-skin interfaces. More than one crack is present and, as the curvature changes substantially, it also delaminates. The delamination of the web introduces a high mode I component in the foot-to-skin interface and the small thickness of the delaminating material is subjected to a lot of bending locally close to the crack tip. Only one row of Z-pins on each side appears to work at a given crack length. Despite the substantial bending, mostly around the one working row of Z-pins, no bending failure is observed; the two horizontal cracks propagate until one reaches the end of one foot.

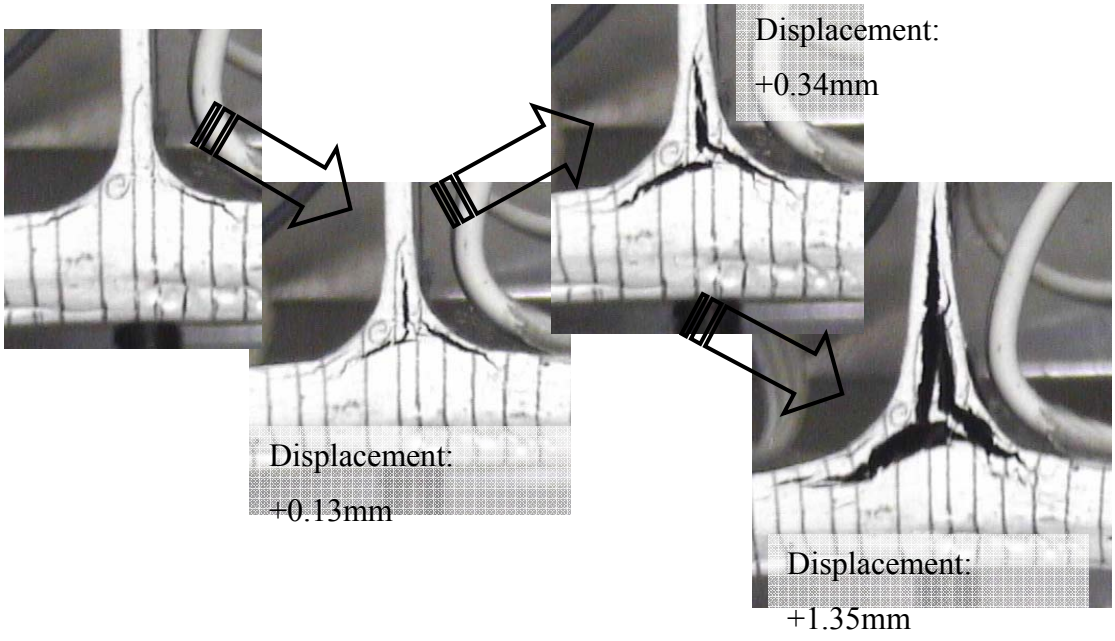

Figure 7-12: *Crack propagation in a stiffened sample with 2% density 0.28mm diameter Z-pins at the illustrated crosshead displacement intervals*

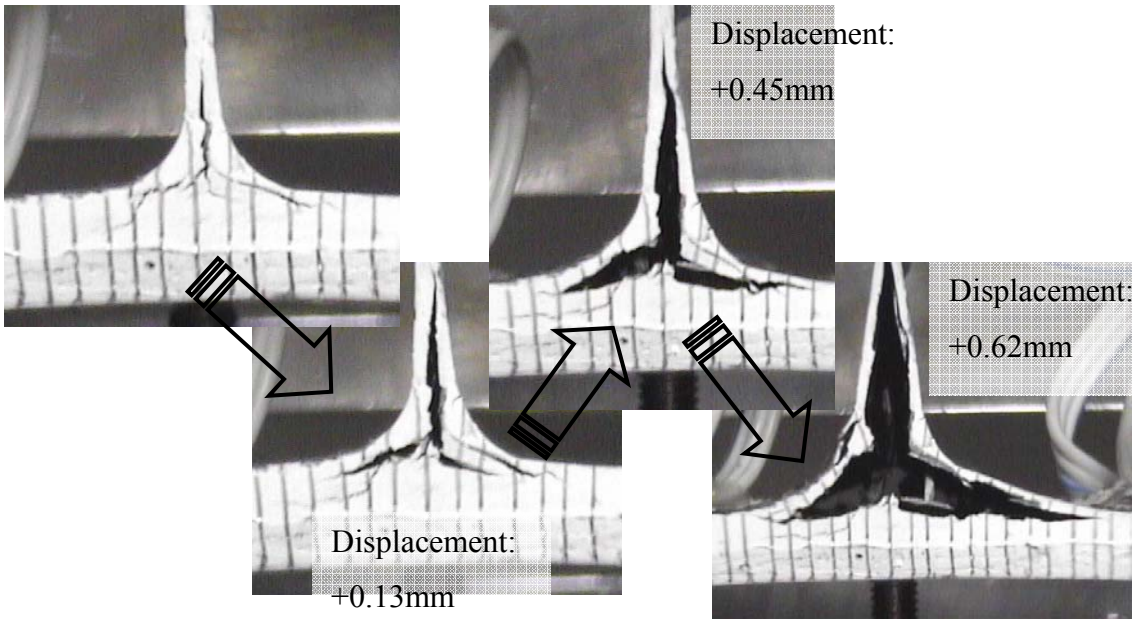

Figure 7-13: *Crack propagation in a stiffened sample with 2% density 0.5mm diameter*

The damage tolerant behaviour of the pinned samples is reflected in the load versus displacement curves. Figure 7-14 depicts four such curves, one from each type of specimen. All specimens exhibit failure, the point of the largest load drop, at a certain displacement, which indicates the strength of the joint. The strength of the joint is a property dominated by the failure interface, which is common for all specimens. The initial linear part of the curve, however, is a property dictated by specimen stiffness and, since the geometry is identical, it is dictated by the thickness of the foot and skin of each specimen. It is apparent that the slopes of the curves are significantly different and therefore specimen thickness is different. Table 7-2 illustrates the variation in the thickness of the specimens and the reflection on the slope of their curves. The surface preparation and the addition of the adhesive have affected the final thickness. The pinning density and Z-pin diameter vary and can affect the final thickness, despite the fact that curing in the same mould reduces the variability. The consolidation procedure and the use of the hand held unit for Z-pin insertion are not optimised for controlling the final cured thickness of pinned laminates. All these parameters resulted in the differences displayed in Table 7-2. The thickness of the web of all specimens is identical, which is indicative of the effect of the aforementioned parameters; none is applicable to the web of the specimens.

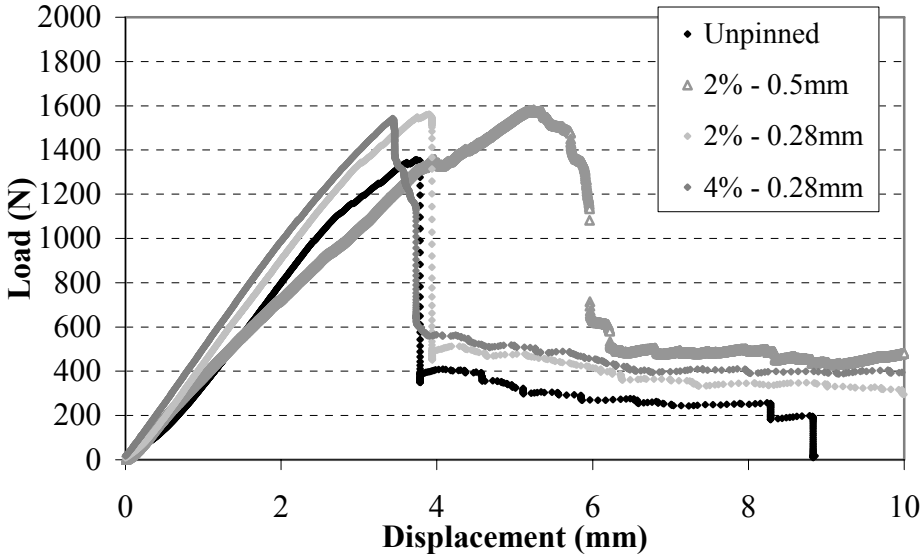

Figure 7-14: *Sample of load versus displacement traces with significantly different slopes*

	Variation in thickness compared to average sample thickness (%)	***Variation in slope compared to average slope (%)***
Minimum	-7.0	*-5.7*
Maximum	+10.9	+11.0

Table 7-2: *Effect of consolidation, Z-pinning and sample preparation on the load versus displacement curve.*

To eliminate the influence of the variability of specimen thickness, all curves are plotted against a corrected displacement. The procedure followed to correct the displacement relative to specimen thickness is simple. The original slope α of the linear part of each curve is given by the expression:

$$P = \alpha \cdot \delta \tag{7-1}$$

Where: P: load,

δ: displacement

If all specimens exhibited a slope equal to an artificial slope α', then the same expression would be:

$$P = \alpha' \cdot x \tag{7-2}$$

Where: P: load (same),

x: corresponding displacement

Thus, the corrected displacement can be calculated using the following formula, derived from combining (7-1) and (7-2):

$$x = \frac{\alpha}{\alpha'} \cdot \delta \tag{7-3}$$

Figure 7-15 displays all corrected curves; the uniformity of the slopes is apparent. The load values remain unaffected.

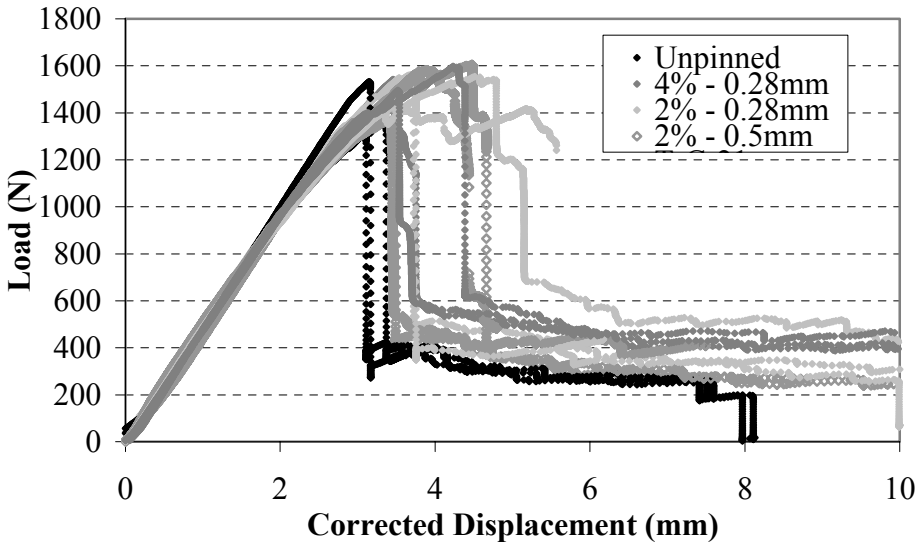

Figure 7-15: *All corrected experimental curves exhibiting identical slopes*

Figure 7-16 contrasts each pinned case to the unpinned specimens in the area of interest.

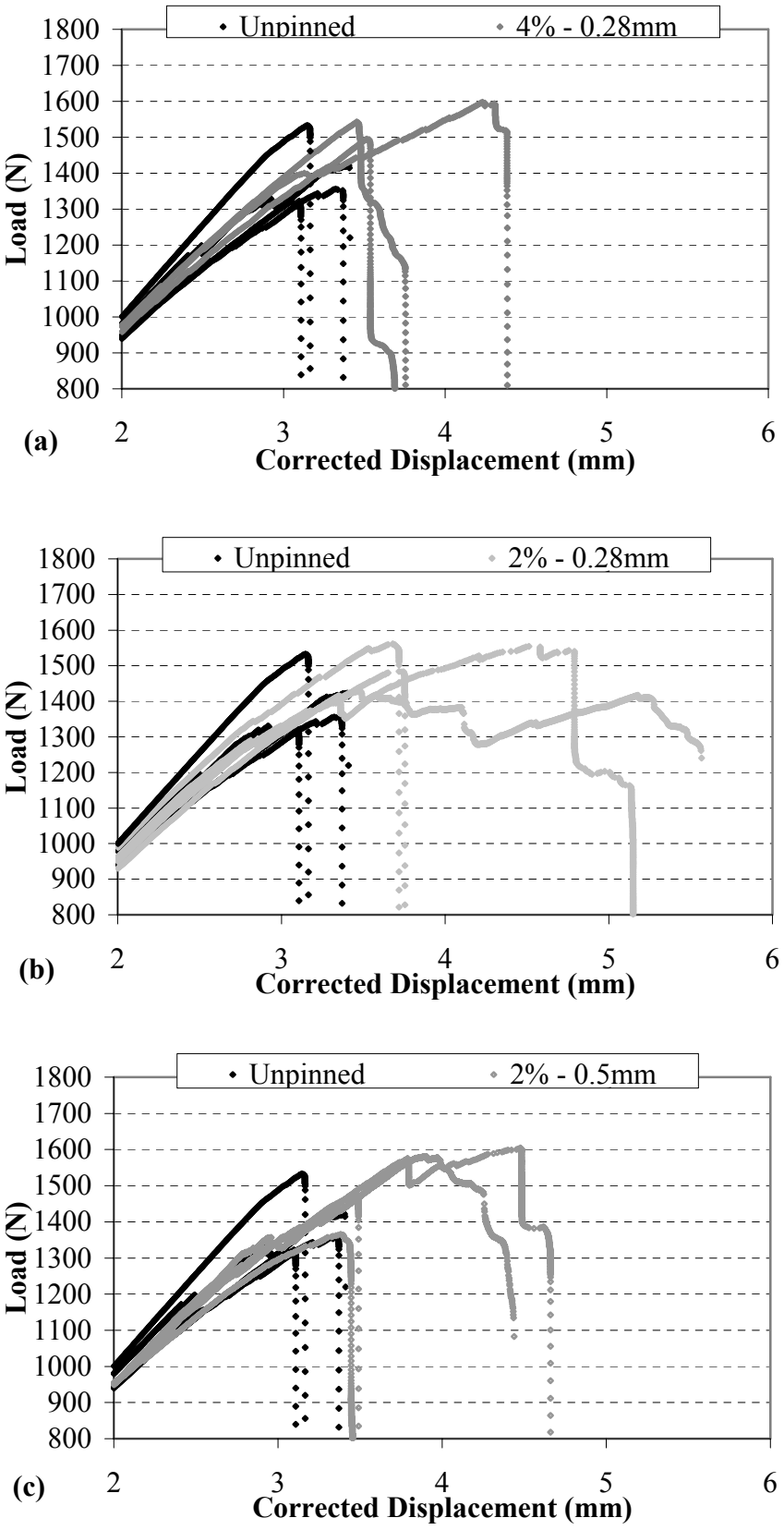

Figure 7-16: *Load versus corrected displacement curves for all pinned cases separately*

In all cases the corrected displacement required to reach ultimate failure is larger for the pinned specimens. More notably, certain specimens can retain the load for an additional 1mm to 2mm. After inspection, the location of the Z-pins in the failure interface of these specimens was slightly different. The noodle area was Z-pinned. This occurred by the emergence of a Z-pin angle during the insertion procedure. Furthermore, the initiation of failure in specimens pinned at the 'noodle' can shift from the 'noodle' to the curved section of the foot (Figure 7-12).

The beneficial effect of Z-pinning on the delamination damage tolerance of the T-stiffener is also apparent in Figure 7-17; the additional crosshead displacement required to grow a crack of total length of 20mm after initiation is depicted.

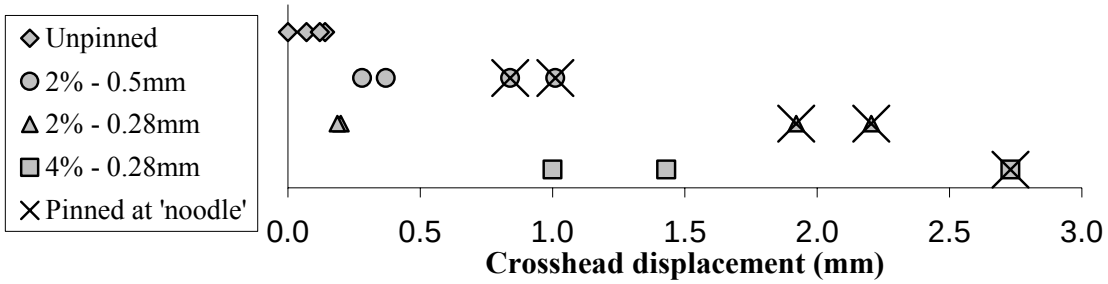

Figure 7-17: *Additional crosshead displacement required to grow a crack of total length of 20mm after its initiation for all test cases of the stiffened sub-structure; Specimens Z-pinned at the noodle area are denoted*

Z-pinning is beneficial to delamination resistance from the moment a crack advances past at least one row of Z-pins. As the failure initiates at the 'noodle' area, the presence of Z-pins just outside the 'noodle' area is not contributing to delamination resistance before the crack advances further. Furthermore, the bridging zone in a thin laminate delaminating under mixed mode loading is limited. With only two plies of material delaminating in the T-stiffener, very few rows of Z-pins resist delamination failure. According to Figure 7-17 delamination performance depends mostly on Z-pin spacing. Only in the 0.28mm-4% case does a second row of Z-pins provide sufficient resistance.

7.6 Summary

The performance of the T-stiffener in a pull off test is improved by Z-pinning. In the original thin skin configuration ***initiation*** of delamination at the edge of the foot was prevented with good quality Z-pinning close to the edge.

In the stiffened configuration no effect on the initiation of failure was observed with Z-pinning, whilst the ultimate load carrying capacity and damage tolerance are improved. Significant improvement in damage tolerance requires the insertion of Z-pins in the 'noodle' area.

Ultimate performance was affected by the fact that the design of the sub-structure did not incorporate the use of Z-pins. The low delaminating thickness limits both the length of the bridging zone and the available Z-pin length for pullout.

8 Overall discussion

Z-pinning is a recently developed through-the-thickness (TTR) reinforcing technique for composite materials. A number of beneficial attributes of the technique had been already identified before the completion of this study. The ease of use in pre-impregnated materials compared to other TTR techniques and the significant enhancement of delamination toughness are the most prominent. Testing with UD materials has demonstrated an increase of an order of magnitude in mode I delamination toughness. Mode II tests, using the ENF testing configuration, have suggested a notable increase in mode II delamination toughness as well; more importantly the stabilisation of crack propagation has been observed. Improvements in mixed mode delamination and CAI performance have been established. At the same time, the need for the development of rigorous data reduction methods specifically for Z-pinned composites has emerged, in order to accommodate the bridging effects introduced. Traction laws of a single Z-pin for mode I and mode II delamination in UD have been determined and considerable effort has been expended in the numerical modelling of mode I delamination, allowing parametric studies of the effects of Z-pinning. Analytical models describing the mechanics of Z-pin failure are also being developed. The mechanisms of the laminate ultimate failure can be changed by the presence of Z-pins.

The established state-of-the art has been summarised in a previous PhD thesis from this group [20] and in a recent review [19]. The work presented in this thesis has established the following new study areas:

Tests and analysis of delamination in woven fabric composites both under mode I and mode II loading conditions.

Identification and assessment of the effect of parameters influencing pinning quality, as well as new procedures facilitating improved pinning quality.

Effect of specimen geometry on the apparent toughness of UD and woven fabric composites both under mode I and mode II loading conditions.

Failure mechanisms involved in the delamination of Z-pinned laminates under mode II loading conditions, using a new Z-pin shear test.

Determination of the effect of friction in the measured delamination toughness and behaviour of composites under mode II loading conditions, using the 4ENF testing configuration, as well as a new basic friction testing configuration.

Tests and analysis of the effect of Z-pining on the in-plane properties of Z-pinned composites; namely tensile stiffness, unnotched and notched tensile strength and in-plane shear stiffness.

Performance of a Z-pinned sub-structural element with respect to delamination failure.

Some issues regarding the quality control, energy absorption, the influence of failure mechanisms on designing with Z-pins and modelling of Z-pinned composites are selected for further discussion here.

8.1 Manufacturing and quality control

The perception of need for pinning quality assessment has been increasing rapidly in recent years. A semi-automated insertion machine has been used throughout this study, providing reproducibility of good manufacturing quality. Accurately controlling the insertion depth is of paramount importance. Apart from the emergence of a Z-pin angle, the final thickness of the laminate can also affected by imprecision in the insertion depth. As Z-pinning is worthwhile mostly in pre-impregnated materials, the desired final thickness cannot be achieved without control on the insertion parameters. When using stitched dry fabric for instance, the final laminate thickness is controlled by the mould dimensions; despite any additional beneficial or unfavourable effects related to stitching the desired final laminate thickness will be achieved. Reproducibility of the desired thickness is a prerequisite for structural design, and is a critical area, if certification for service use is to be achieved.

Nevertheless, an increase in thickness will always occur with the insertion of Z-pins. The insertion of additional material cannot take place without an increase in total volume. The volume increase depends on the combination of Z-pin diameter and density. The percentage of increase is usually slightly higher than the percentage of the additional material inserted. The final fibre volume fraction of the laminate will be compromised proportionally. Increased yarn tension may have unfavourable effects on the meso-structure of a stitched laminate, but it results in an increase of the volume fraction. This does not necessarily suggest that a stitched laminate will have a higher fibre volume fraction. It does demonstrate, however, the need to normalise all measured laminate properties to the final volume fraction when providing data of both Z-pinned and stitched laminates, to aid the selection of material by the designer.

Satisfactory consolidation before Z-pin insertion is equally important. The designer must be aware of the potential of the selected material to achieve consolidation near the cured thickness with regard to the consolidation procedure applicable, considering stacking procedure, component size and component geometry. Moreover, material suppliers should provide such information and maybe take into account the importance of the potential of the material for sufficient consolidation when finalising prepreg properties.

Small variations of the Z-pin parameters can significantly influence the failure mechanisms involved. This influences the performance of the composite, as well as the location and type of failure. Apart from the emerging need to include Z-pin insertion in the design to ensure the integrity of the structure, if not to fully take advantage of the new technology, the ability to properly control and monitor the insertion procedure is essential to achieve certification.

Finally, in-plane misalignment of laminate fibres in UD material is comparable to that observed in stitched laminates; it ranges between 6 and 9 degrees in Z-pinned UD laminates, while the average value in stitched laminates is 10 . Contrary to high yarn loop tension stitching, out of plane misalignment is minor and is mostly observed with 0.5mm diameter Z-pins. The size of resin rich areas is correspondingly smaller on the

laminate surface, and complex stacking sequences result in a reduction in their size. Still, high quality surface finish requires the adoption of partial pinning.

8.2 Energy absorption mechanisms

Z-pin pullout characterises the failure mechanism involved in mode I delamination of a Z-pinned laminate. The frictional segment of the failure mechanism dissipates significant amounts of energy, reflected in the significantly increased apparent fracture toughness.

In mode II, failure type is a function of the crack opening constraint, material type, stacking sequence and insertion depth to Z-pin diameter ratio. An additional amount of variability is introduced with a change in the Z-pin angle. A combination of Z-pin pullout, Z-pin fracture and resin crushing comprises final failure. The aforementioned parameters can have contradictory effects on the balance of the mechanisms.

Even under mode II loading conditions, Z-pin pullout can be observed. If a significant amount of pullout is accommodated, the potential for energy absorption increases. A tailored insertion depth or Z-pin angle can favour Z-pin pullout. Energy dissipation at low displacements appears to be higher with Z-pin pullout; angled Z-pins pulling out of a woven laminate under shear loading exhibit steeper loading curves (see section *5.3.4*). With a higher ratio of tension to shear (or bending) striffness and strength, debonding and frictional resistance of the Z-pin seems to absorb more energy than when excess resin crushing or internal splitting of the Z-pin is present.

On the other hand, the maximum resistance load can be compromised, resulting in a lower amount of absorbed energy at large displacements. Accurate parameter selection is critical. Additionally, Z-pin pullout is accompanied by a higher opening to sliding displacement ratio. The introduction of significant opening displacement may

compromise the potential contribution of the resin under shear loading, as the mode II component decreases in favour of the mode I counterpart.

If the presence of an angle is deemed favourable, then implementation of both a negative and a positive Z-pin angle is necessary to provide appropriate resistance in both directions, as in [72].

Variations in thickness impose changes in both the opening constraint, and therefore to the mode ratio. Excessively thick laminates have displayed minor improvement in mode II delamination toughness with the use of Z-pinning [128]. This can be due to a change of the balance of the failure mechanisms, with Z-pins failing predominately in shear. Conversely, significantly small thicknesses, as in the T-stiffener, reduce the bridging zone length. After the appearance of a crack at the 'noodle' area, resistance to delamination was provided by very few rows of Z-pins. The enhancement of delamination resistance was a fraction of the potential of the Z-pins. The Z-pin chamfer further reduces the effective insertion depth up to 0.5mm for 0.5mm diameter Z-pins. This becomes important as laminate thickness decreases.

The presence of the Z-pin chamfer, and the subsequent reduced bridging force, prevented the in-plane failure of the delaminating foot during the test. The excessive bending in combination with the degraded properties of the pinned laminate in compression [65] should result in bending failure. A reduced laminate thickness can therefore further compromise the potential for energy absorption, by the initiation of alternative failure types, in the presence of significant crack bridging forces.

Resistance against mode I loading provided by the Z-pins is not compromised by the presence of significant mode II loading components. Figure 8-1 depicts a T-stiffener specimen under test, pinned at the 'noodle'. A significant mode II displacement is evident; however, the opening displacement is minimal.

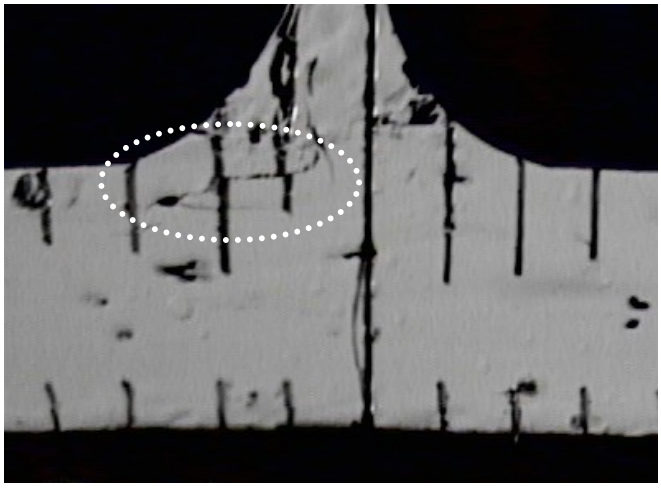

Figure 8-1: *Significant mode II component during the initiation of failure in the 'noodle' area of a T-stiffener specimen*

In stitched laminates, the yarn loop ensures the presence of high tensile loads (up to stitch failure) in the reinforcement. Although pure tensile Z-pin failure is not possible in a delaminating laminate, improved performance against delamination may be achieved, if imposed mode I components on the Z-pins are favoured by design.

Friction between the crack faces is an additional energy absorption mechanism involved in mode II delamination. Determination of the importance of the frictional effects can be aided by the determination of the friction coefficient between the fractured surfaces of a mode II delamination specimen. Literature on the subject is fairly sparse and values of friction coefficient hard to find. Most tests provide friction coefficients between composite and metallic surfaces. A new basic friction test has been implemented in this study. The curves obtained for the friction coefficient reflect the size of the microcracking and the occasional stick-slip behaviour observed in delamination testing.

Previous work has evaluated the effect of friction on the measurement of mode II delamination toughness in UD materials [99]. Frictional effects attributed to both the fibre architecture and the resin systems of the woven fabric materials used in this study have been observed. Despite the absence of an accurate determination of the effect of friction in this study, the level of increase in delamination toughness supports the scepticism revolving around the validity of mode II delamination toughness values.

Nevertheless, any increase in mode II delamination toughness as a result of Z-pinning alone is amplified, considering that an appreciable part of mode II delamination toughness in unpinned samples can be attributed to friction.

8.3 Designing with Z-pin reinforcement

The importance of incorporating Z-pin insertion in the design of structures and joints is demonstrated in a recent study performed by Ferrari [113], comparing the performance between the tension-tension fatigue strength of pinned and unpinned double lap joints. Loading mode and specimen geometry are depicted in Figure 8-2. The results showed no improvement in the fatigue life and the appearance of a crack at a lower number of cycles in the pinned specimen than in the unpinned one. The crack initiated from the tips of the joint (denoted with arrows), propagated a few millimetres and then catastrophic failure followed, both in the unpinned and pinned specimens.

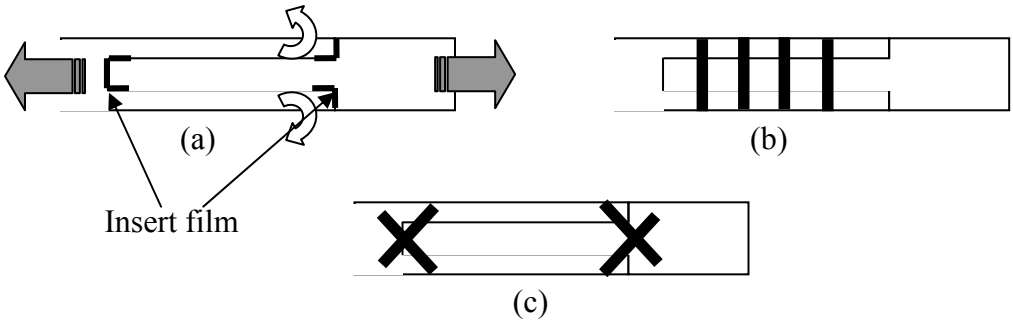

Figure 8-2: *Double lap specimen geometry and loading; (a) unpinned specimen, (b) pinned specimen (c) suggested specimen.*

Finite element modelling indicated a significant mode I component at the tips of the joint, up to 40%. The design of the pinned specimen emulates a bolted joint, or a riveted joint of metallic plates. In a bolted joint the friction between surfaces is enhanced through bolt tension, while metallic rivets constrain the opening by rivet tension and rely on high shear strength to bear the load. In both configurations the opening is completely constrained. In the Z-pinned specimen opening is not constrained before the crack propagates into the Z-pinned area. The appearance of a crack through part of the

bonded area compromises the ultimate strength of the bond, equally in unpinned and pinned specimens. Additional shear displacement results in the introduction of an opening displacement by Z-pin presence. The cracking resistance of the resin is compromised due to the increased mode I loading component and a crack appears at low cycles. Despite the reduced cracking resistance available in the resin under the altered mode ratio, the life of the specimens remains the same due to additional resistance provided by the Z-pins. The importance of constraining the opening displacement is emphasised by the fact that the use of titanium Z-pins, possessing higher shear strength, did not offer any improvement. At final failure both carbon and titanium Z-pins pull out.

It appears that when designing to optimise Z-pin reinforcement there are two important factors to be considered. Firstly, imposing a mode I component on the Z-pins by design and, secondly, allowing the presence of an artificial crack in order to maximise the effect of the presence of the Z-pins. Figure 8-2c and Figure 8-3 demonstrate designs where these factors are incorporated. The idea of creating an artificial crack using foam in the final structure is borrowed from the structure of X-Cor and K-Cor , a new product competing with established sandwich structure designs.

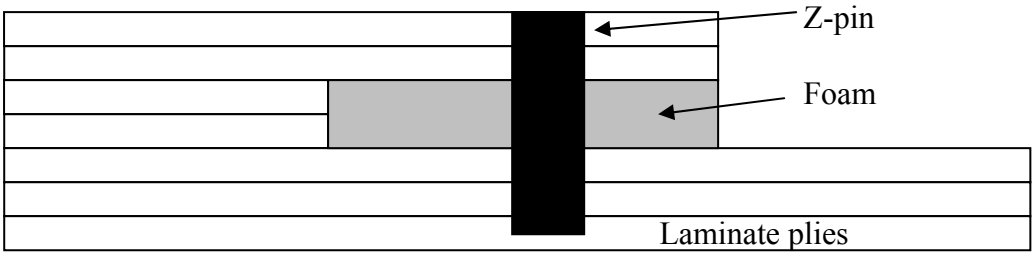

Figure 8-3: *Z-pinning suggestion for a stiffener foot-to-skin interface.*

8.4 Modelling mode II delamination with Z-pin reinforcement

The experimental data obtained in section *5.3*, concerning the performance of a single Z-pin under shear loading conditions, can be utilized as an experimental bridging law in the construction of an FE model, similar to [77], in order to study mode II delamination of Z-pinned laminates. However, parameters as the insertion depth, Z-pin angle, opening constraint and material type would have to be incorporated in the model, since they determine the balance of the failure mechanisms, as discussed in section *5.3.8*. A constitutive bridging law of the bridging ligaments would be required to avoid additional testing using the configuration described in section *5.3*, in order to obtain separate experimental bridging laws for each case. The model described in [34,74] is a constitutive model of through-thickness bridging ligaments.

Laminate material type and stacking sequence affects the type of constraint on the Z-pin, as well as the length of the Z-pin that is allowed to deform under the combined shear, bending and tension loads discussed in section *5.3.8*. The size of this critical length is not incorporated in the formulation of the constitutive bridging law, described in [34,74]. The development of a constitutive bridging law considering the Z-pin as an engineering beam subjected to the experimentally observed loading and boundary conditions may be the most appropriate model to study.

8.5 Potential applications

The potential of industrial application of Z-pinning revolves around structures, in which the principal mode of failure is delamination. The insertion of Z-pins in order to enhance delamination toughness can be combined with the potential of the method for component joining, with minimal changes in the manufacturing procedure. Z-pinning shows promise for use in structural subcomponents similar to the one described in chapter 8. The commercial aeronautical industry is a strong candidate for future use of Z-pins, considering the dominance of prepreg materials in the manufacture of

aeronautical components. The military sector is already using the Z-pinning technique (F18 E/F fighter) and can also benefit from the increased damage tolerance attributes of Z-pinned laminates in ballistic applications.

Figure 8-4: *Race accident, severely testing crash structure components in F1 (Melbourne 1996)*

The automotive industry, and in particular the motorsport sector, shows growing interest in Z-pinning. The use of Z-pins is currently extremely popular in crash structures. Sacrificial crash structures have recently become a standard feature in passenger and commercial vehicles. Although prepreg materials are not used in the manufacture of high volume vehicles, the niche car sector uses increasing amounts of high grade composites. A popular project (the Mercedes SLR) is a forthcoming example of the use of composite containing TTR in production, albeit incorporating stitching technology and not Z-pinning. Crash structures in heavy people carrier vehicles are another potential application, where increased damage tolerance and weight savings overcome the increased cost of manufacture related to prepreg materials.

Figure 8-5: *The stitched composite body of the SLR*

9 Conclusions and suggestions for further work

9.1 Conclusions

1. The insertion of Z-pins into prepreg materials results in an unavoidable increase in nominal cured laminate thickness.

2. Z-pinning introduces in-plane fibre misalignment, the magnitude of which depends on material type and stacking sequence, and minimal fibre damage; out-of-plane fibre misalignment is also present.

3. The insertion of excessive Z-pin length will result in the emergence of an angle. Sufficient consolidation prior to pinning and partial pinning are techniques to effectively restrict Z-pin angle presence.

4. Z-pinning greatly enhances mode I delamination resistance and provides stability during crack propagation in woven carbon composites.

5. Any increase of Z-pin density, insertion depth and laminate thickness, increases mode I delamination resistance in Z-pinned laminates; any increase of the Z-pin diameter has the contrary result.

6. The 4ENF testing configuration appears as an advantageous mode II configuration in the testing of Z-pinned laminates.

7. In order to achieve accurate data reduction of mode II delamination measurements with Z-pinned woven fabric materials, alternative methods are required; the introduction of a new specimen was implemented in this study to avoid the compliance calibration procedure, as used in the typical procedure of delamination testing with the ENF configuration.

8. Additional frictional effects between the crack faces have been observed in mode II delamination of woven Z-pinned laminates, attributed to the woven fibre architecture.

9. Z-pins fail under shear loading through a combination of resin crushing, laminate fibre breakage, pin shear, pin bending and pin pullout. The balance of the failure mechanisms of a Z-pin under shear loading is a function of the crack opening constraint, material type, stacking sequence, Z-pin angle and insertion depth to Z-pin diameter ratio.

10. An optimum insertion depth exists, depending on material type, where energy absorption under shear loading is at maximum.

11. Z-pins introduce a mode I component under shear loading.

12. The reduction in the fibre volume fraction is the single most important parameter affecting in-plane stiffness of Z-pinned laminates.

13. Any increase in Z-pin density or diameter results in a reduction of Z-pinned laminate strength. Any increase in the complexity of the stacking sequence diminishes this effect.

14. The effectiveness of Z-pinning is enhanced when mode I delamination conditions are favoured by design.

9.2 Suggestions for further work

The importance of pinning quality has been underlined throughout this study. Further development of the pinning quality metrics is the next stage; the development of a

database for the *insertion* parameters may decrease certification time if different materials are used. The upgrade of the current insertion equipment to collecting data of force as a function of displacement and temperature during insertion is possible.

The effect of Z-pin angle has not been fully investigated in mode II and not attempted in mode I. Mode I tests with angled Z-pins will help further evaluation of the performance of Z-pins under mode I loading with significant lateral deformations. Mode II tests will provide the design envelope available in terms of energy absorption, within which using angled Z-pins under mode II loading conditions is feasible. Moreover, as stressed in [20], no work has been done on strain rate effects of Z-pinned laminates.

The threshold force for damage initiation for an impact is reduced when the impact is located on a pinned region, probably due to the stress concentrations introduced by the Z-pins [20]. It would be interesting to investigate if partial pinning overcomes this problem.

The subsequent CAI performance of partially pinned laminates can be investigated further. The effect on the compression properties of woven fabric Z-pinned laminates in general is a totally unexplored area.

A first exploration of fatigue behaviour has been carried out recently [113]. Fatigue is probably the most important unexplored area yet. Sustaining the beneficial performance of Z-pinning under fatigue loading conditions will widen the application opportunities of Z-pinning.

A more accurate determination of the role of friction on the mode II failure resistance can be achieved by the implementation of a mechanism that control or measure the opening constraint in the pin shear test.

It would be interesting to measure the performance difference between delaminated (after impact for instance) unpinned and Z-pinned sub-structures similar to the one

described in chapter 8. Delamination damage is the main purpose, that Z-pinning was initially considered for.

In general, more experimental work on structural components can test the soundness of the design techniques proposed in the previous chapter and provide new design strategies with Z-pin reinforcement. Testing of the joints of Figure 8-2c and Figure 8-3 can provide useful information.

10 References

1. Pilato L.A. and Michno M.J. *'Advanced composite materials, Chapter 11: Applications'* Springer-Verlag, 1994
2. Gay D., Hoa S.V. and Tsai S.W. *'Composite materials: Design and applications'* CRC Press LLC, 2003
3. Kelly A., *'Concise Encyclopedia of Composite Materials'*, Pergamon Press,1989
4. Eckold G. *'Chapter 8: Examples of composite applications'* Design and Manufacture of Composite Structures, Woodhead publishing,1994
5. Niu M.C.Y. *'Composite airframe structures: Practical design information and data'* Conmilit Press Ltd., 1992
6. Jones R.M. *'Mechanics of composite materials'* Taylor & Francis 1999
7. Gibson R.F. *'Principles of composite materials mechanics'* McGraw-Hill, 1994
8. Bradley W.L. *'Chapter 5: Relantionship of matrix toughness to interlaminar fracture toughness'* Application of Fracture mechanics to Composite Materials, editor Friedrich K., Elsevier, 1989
9. Deo R.B.& Saff C.R., *'Composite materials: Testing and design'*, 12th Volume, ASTM STP, August 1996
10. Schulte K. and Stinchcomb W.W. *'Chapter 8: Damage mechanisms – including edge effects – in carbon fibre-reinforced composite materials'* Application of Fracture mechanics to Composite Materials, editor Friedrich K., Elsevier, 1989
11. Daniel I.M. and Ishai O. *'Chapter 7: Stress and failure analysis of multidirectional laminates'* Engineering mechanics of composite materials, Oxford University Press, 1994
12. Davies G.A.O., Hitchings D. and Zhang X. *'Damage tolerance to low velocity impact of laminated composites',* Paper presented at RTO meeting proceedings 24, Corfu, Greece, 21-22 April 1999
13. Davies G.A.O. and Zhang X. *'Predicting impact damage of composite stiffened panels',* The Aeronautical Journal, 97, February 2000

14. Fawcett A., Trostle J and Ward S. *'777 empennage certification approach',* ICCM-11, Australia, 14th-18th July, 1997
15. *'Guidance material for the design, maintenance, inspection and repair of thermosetting epoxy matrix composite aircraft structures'* IATA, May 1991
16. FAA AC 20-107A, Advisory circular, 1984
17. JAR 25.571
18. Cox B.N. and Flanagan G. *'Handbook of analytical methods for textile composites'* NASA contractor report 4750, March 1997
19. Partridge I.K., Cartié D.D.R and Bonnington T. *'Manufacture and Performance of Z-pinned Composites'* Advanced Polymeric Materials, eds S. Advani & G. Shonaike, CRC Press LLC, March 2003
20. Cartié D.D.R *'Effect of Z-fibres on the delamination behaviour of carbon-fibre/epoxy laminates'* PhD Thesis, Cranfield University, 2001
21. Williams J.G. *'Chapter 1: Fracture mechanics of anisotropic materials'* Application of Fracture mechanics to Composite Materials, editor Friedrich K., Elsevier, 1989
22. ISO, *Standard test method for Mode I interlaminar fracture toughness G_{IC}, of unidirectional fibre-reinforced polymer matrix composites*. **ISO 15024: 2001**
23. Turmel D.J-P. *'Effect of face separation in epoxy/PEI matrix on the mixed mode I/II delamination behaviour of unidirectional glass fibre composites'* PhD. Thesis, Cranfield University, 1995
24. Singh S. *'Mixed mode fracture of interleaved composites'* MSc. Thesis, Cranfield University, 1994
25. Jaussaud J.A.M *'Toughness transfer between unreinforced matrix and fibre composites'* PhD. Thesis, Cranfield University, 1992
26. Mai K., Mäder E. and Mühle M. *'Interphase characterisation in composites with new non-destructive methods'* Composites Part A, 29A, 1111-1119, 1998
27. Crews J.H., Shivakumar K.N., and Raju I.S. *'A fibre-resin micromechanics analysis of the delamination front in a DCB specimen'* NASA Technical Memorandum 1000540, NASA Langley Research center, Hampton, 1988

28. Sela N., Ishai O. and Banks-Sills L. *'The effect of adhesive thickness on interlaminar fracture toughness of interleaved CFRP specimens'* Composites, 20, No.3, 257-265, 1989
29. Ishai O., Rosenthal H., Sela N. and Drukker E. *'Effect of selective adhesive interleaving on interlaminar fracture toughness of graphite/epoxy composite laminates'* Composites, 19, No.1, 49-54, 1988
30. Aksoy A. and Carlsson L.A. *'Crack tip yield zone estimates in mode II interlaminar fracture of interleaved composites'* Engineering Fracture Mechanics, 39, No.3, 25-534, 1991
31. Ozdil F. and Carlsson L.A. *'Plastic zone estimates in mode I interlaminar fracture of interleaved composites'* Engineering Fracture Mechanics, 41, No.5, 645-658, 1992
32. Ozdil F. and Carlsson L.A. *'Finite element analysis of interleaved DCB specimen'* Engineering Fracture Mechanics, 41, No.4, 475-485, 1992
33. Massabò, R. and Cox, B. N. *'Interlaminar fracture of laminates with through-thickness reinforcement'* 5th Damage and Fracture Mechanics conference, Bologna, Italy, 1998
34. Cox B.N. *'Constitutive model for a fiber tow bridging a delamination crack'* Mechanics of Composite Materials and Structures 6, 117-138, 1999
35. Barrett D.J. *The mechanics of Z-fiber reinforcement'* Composite Structures, 36, No. 1/2, 23-32
36. Mouritz A.P. and Cox B.N. *'A mechanistic approach to the properties of stitched laminates'* Composites Part A, 31, 1-27, 2000
37. Dransfield K., Baillie C. and Mai Y,-W. *'Improving the delamination resistance of CFRP by stitching – a review'* Composites Science and Technology, 50, 305-317, 1994
38. Mouritz A.P., Leong K.H., Herszberg I. *'A review of the effect of stitching on the in-plane mechanical properties of fibre-reinforced polymer composites'*, Composites Part A, 28A (1999) 979-991
39. Dransfield K. A., Mai Y. –W. and Jain L. K. *'On the effects of stitching in CFRPs-I. Mode I delamination toughness'* Composites Science and Technology, 58, Issue 6, 815-827, 1998

40. Dransfield K. A., Mai Y. –W. and Jain L. K. *'On the effects of stitching in CFRPs-II. Mode II delamination toughness'* Composites Science and Technology, 58, Issue 6, 829-837, 1998
41. Sankar B.V and Sharma S.K. *'Mode II delamination toughness of stitched graphite/epoxy textile composites'* Composites Science and Technology, 57, 729-737, 1997
42. Sankar B.V. and Dharmapuri S.M. *'Analysis of a stitched double cantilever beam'* Journal of Composite Materials 32, No.24, 2203-2225, 1998
43. Larsson F. *'Damage tolerance of a stitched carbon/epoxy laminate'* Composites Part A 28A, 923-934, 1997
44. Aztex Inc., http://www.Aztex-z-fiber.com
45. Bitsianis N. *'The influence of Z-pinning on toughness and impact performance of carbon fibre polymer composite materials'* MSc Thesis, Cranfield University, 1999
46. Cartié D.D.R., Bitsianis N., Irving P.E. and Partridge I.K. *'Z-fiber reinforcement: effects on the compression after impact performance of T300/914 laminates'* Proceedings of JNC12, Cachan, Paris, France, 15-17 November 2000
47. Cartié D.D.R and Partridge I.K. *'Delamination behaviour of Z-pinned laminates'* Proceedings of 2nd ESIS TC4 conference, Les Diableret, Switzerland, 13-15 September 1999
48. Cartié D.D.R. and Partridge I.K. *'Delamination behaviour of Z-pinned laminates'* Keynote lecture in ICCM 12, 5-9 July 1999, Paris
49. Shi Y.B., and Hull D. *'Mode II fracture of +θ/-θ angled laminate interfaces'*, Composites Science and Technology, 47, 173-184, 1993
50. De Morais A.B., De Moura M.F., Marques A.T. and De Castro P.T., *'Mode-I interlaminar fracture of carbon/epoxy cross-ply composites'*, Composites Science and Technology 62, 679-686, 2002
51. Tohgo K., Hirako Y. and Ishii H. *'Mode I interlaminar fracture toughness and fracture mechanism of angle-ply carbon/nylon laminates'*, Journal of Composite Materials, 30, No.6, 650-661, 1996

52. Alif N, Carlsson L.A. and Boogh L., *'The effect of weave pattern and crack propagation direction on mode I delamination resistance of woven glass and carbon composites'* Composites Part B, 29B, 603-611, 1998

53. Shin S. and Jang J. *'Fractographical analysis on the mode II delamination in woven carbon fiber reinforced epoxy laminates'* Journal of Material Science, 34, 5299-5306, 1999

54. Farley G.L. and Dickinson L.C. *'Mechanical response of composite material with through-the-thickness reinforcement'* NASA conference publication, Issue 3176, 1992

55. Mouritz A.P. *'Flexural properties of stitched GRP laminates'* Composites Part A, 27A, 525-530, 1996

56. Cox B.N. and Dadkhah M.S. *'The macroscopic elasticity of 3D woven composites'* J. of Composite Materials, 29, No.6, 785-819, 1995

57. Brandt J., Drechsler K. and Arendts F.-J *'Mechanical performance of composites based on various three-dimansional woven-fibre preforms'* Composites Science and Technology 56, 381-386, 1996

58. Tanzawa Y., Watanabe N. and Ishikawa T. *'Interlaminar fracture toughness of 3D orthogonal interlocked fabric composites'* Composites Science and Technology 59, 1261-1270, 1999

59. Falconnet D., Bourdan P.-E., Pandita S., Månson J.-A.E., Verpoest I. *'Fracture toughness of weft-knitted fabric composites'* Composites Part B, 33, 579-588, 2002

60. Jain, L. K. and Mai, Y.-W. *'Determination of mode II delamination toughness of stitched laminated composites'* Composites Science and Technology 55, No.3, 241-253,1995

61. He M. and Cox B.N. *'Crack bridging by through-thickness reinforcement in delaminating curved structures'* Composites Part A, 29A, 377-393, 1998

62. Jain, L. K and Mai, Y.-W. *'On the effect of stitching on mode I delamination toughness of laminated composites'* Composites Science and Technology 51, No.3, 331-345, 1994

63. Jain L.K *'Effect of reinforcing tabs on the mode I delamination toughness of stitched CFRPs'* Journal of Composite Materials 32, No.22, 2016-2041, 1998

64. Aztex Inc., *'Preliminary lamina, laminate and sub-element test results for Z-Fiber reinforced IM7/977-3 unidirectional tape and fabric'* Released Version 1.3, 1998

65. Steeves G.A. and Fleck N.A., *'Z-pinned composite laminates: knockdown in compressive strength'* DFC5 Conference, London, UK, 18-19 March 1999

66. Cox B.N., Massabò R. and Rugg K.L. *'The science and engineering of delamination suppression'* DFC6 Conference, Manchester, UK, 4-5 April 2001

67. Mouritz A.P. and Jain L.K. *'Further validation of the Jain and Mai models for interlaminar fracture of stitched composites'* Composites Science and Technology, 59, 1653-1662, 1999

68. Cox B.N., Massabò R. and Kedward K.T. *'Suppression of delaminations in curved structures by stitching'* Composites Part A, 27A, 1133-1138, 1996

69. Massabò, R., Mumm D.R. and Cox B.N. '*Characterizing mode II delamination cracks in stitched composites'* International Journal of Fracture, 92, 1-38, 1998

70. Massabò, R. and Cox, B. N. *'Concepts for bridged mode II delamination cracks'* Journal of the Mechanics and Physics of Solids, 47, 1265-1300, 1999

71. Massabò, R. and Cox, B. N. *'Unusual characteristics of mixed-mode delamination fracture in the presence of large-scale bridging '* Mechanics of Composite Materials and Structures, 8, Part 1, 61-80, 2001

72. Rugg, K. L., Cox, B. N., Massabò, R. *'Mixed mode delamination of polymer composite laminates reinforced through the thickness by z-fibers'* Composites Part A, 33, No.2, 177-190, 2002

73. Mabson G.E. and Deobald L.R. *'Design curves for 3D reinforced composite laminated double cantilever beams'* presented at ASME meeting, Orlando Fl., November 2000

74. Cox, B. N. *'Snubbing effects in the pullout of a fibrous rod from a laminates'* to be submitted to Composites

75. Barrett D.J. *'A micromechanical model for the analysis of Z-fiber reinforcement'* AIAA-96-1329-CP

76. Barrett D.J. *'The analysis of a Z-fiber reinforced plate'* NAWCADWAR-95-12-TR, 1995

77. Cartié D.D.R and Partridge I.K. *'A Finite Element Tool for Parametric Studies of Delamination in Z-pinned Laminates'* DFC6 Conference, Manchester, UK, 4-5 April 2001
78. Liu, H.-Y. and Mai, Y.-W. *'Z-pin bridging stress in composite delamination'* Proceedings of 3rd ESIS TC4 conference, Les Diableret, Switzerland, 15-18 September 2002
79. Liu, H.-Y., Yan W. and Mai, Y.-W. *'Z-pin bridging stress in composite delamination'* Proceedings of 3rd ESIS TC4 conference, Les Diableret, Switzerland, 15-18 September 2002
80. Grassi M., PhD Thesis, to be submitted
81. Racecar Engineering, 12, No.12, December 2002
82. Hodgkinson J.M., *'Mechanical testing of advanced fibre composites'* CRC Press, Woodhead Publishing Ltd., 2000
83. October N., Hexcel Composites, Duxford UK, (personal communication)
84. Blackman B.R.K. and Williams J.G. *'Fracture from defects'*, ECF12, Sheffield, UK, 14-18 September 1998.
85. Turmel D. J.-P, Szpicak J.-A., Singh S. and Partridge I.K., *'Crack initiators and pre-cracking techniques for fracture testing of polymer matrix composites'*, DFC3, University of Surrey, Guilford, UK, 27-29 March 1995.
86. Polaha J.J., Davidson B.D. Hudson R.C. and Pieracci A. *'Effects of mode ratio, ply orientation and precracking on the delamination toughness of a laminated composite'* Journal of Reinforced Plastics and Composites, 15, 142-173, 1996
87. O'Brien T.K. *'Interlaminar fracture toughness the long and winding road to standardisation'* Composites Part B, 29B, 57-62, 1998
88. Davies P., Blackman B.R.K. and Brunner A.J. *'Standard test methods for delamination resistance of composite materials: current status'* Applied Composite Materials 5, 345-364, 1998
89. Cartié D.D.R and Partridge I.K. *'Increasing delamination resistance of composites by Zfibre pinning'* Proceedings of ACUN3 conference, Sydney, Australia, 6-9 February 2001

90. Brunner A.J. and Williams J.G. *'Deducing bridging stresses from G_{IC} tests on fibre composites'*, Proceedings of 3rd ESIS TC4 conference, Les Diableret, Switzerland, 15-18 September 2002
91. Tanner S., Excel worksheet for the data analysis of the DCB test, ©EMPA, CH-8600, Dübendorf, Switzerland, 1996
92. ISO*, Determination of fracture toughness (G_{IC} & K_{IC}) for plastics. An LEFM approach.* **ISO 13586-1**
93. http://www.itl.nist.gov/div898/handbook/, NIST/SEMATECH e-Handbook of Statistical Methods, section 2.5: Uncertainty Analysis
94. Barattoni L., MSc Thesis, Cranfield University, September 2001
95. Moore D.R., 2000. "*Fracture Mechanics Testing Methods for Polymers, Adhesives and Composites*". ISBN 008 0436897. Edited by Moore D.R., Pavan A., Williams J.G., Elsevier 2000
96. Martin R.H. and Davidson B.D. *'Mode II fracture toughness evaluation using a four point bend end notched flexure test'* Plastics Rubber and Composites 28, No.8, 401-408, 1999
97. Alessandrini A., MSc Thesis, Cranfield University, September 2003
98. O'Brien T.K. *'Composite interlaminar fracture toughness: shear measurement or sheer myth?'* Composite Materials Fatigue and Fracture, 7, 3-18, 1998
99. Blackman B.R.K. *'A review of mode II loading in laminates and joints' Presentation for ESIS TC4, October 2001*
100. Davies P., Moulin C. and Kausch H.H. *'Measurement of G_{Ic} and G_{IIc} in carbon/epoxy composites'* Composites Science and Technology 39, 193-205, 1990
101. Davies P. *'Summary of results from second VAMAS mode II round robin test exercise using the 4ENF specimen'* Draft summary for comments, July 1999
102. Davies P., Sims G.D., Blackman B.R.K., Brunner A.J., Kageyama K., Hojo M., Tanaka K., Murri G., Rousseau C., Gieseke B. ans Martin R.H. *'Comparison of test configurations for the determination of mode II interlaminar fracture toughness results from international collaborative programme'* Plastics, Rubber and Composites, 28, No.9, 432-437, 1999
103. Blackman B.R.K., (personal communication)

104. Carlsson L.A. and Gillespie J.W. *'Chapter 4: Mode-II interlaminar fracture of composites'* Application of Fracture mechanics to Composite Materials, editor Friedrich K., Elsevier, 1989
105. Blackman B.R.K., Kinloch A.J. and Paraschi M. *'On the mode II loading of adhesive joints'*, submitted for publication to Fracture of Polymers, Composites and Adhesives
106. Cartié D.D.R., confidential data, Cranfield University, UK
107. Schuecker C. and Davidson B. *'Evaluation of the accuracy of the four-point bend end-notched flexure test for mode II delamination toughness determination'* Composite Science and Technology, 60, 2137-2146, 2000
108. Davies, P., *'Influence of ENF Specimen Geometry and Friction on the Mode II Delamination Resistance of Carbon/PEEK'* Journal of Thermoplastic Composite Materials, 10, No.4, 353-361 , 1997
109. Carlsson L.A., Gillespie J.W. and Pipes R.B. *'On the analysis and design of the End Notched Flexure (ENF) Specmen for Mode II Testing'* Journal of Composite Materials 20, No. 6, 594-605, 1986
110. Kageyama K., Kimpara I., Suzuki T., Ohsawa I. and Kanai M. *'Four-point bend ENF test applied to mode II interlaminar fracture toughness characterization for composite laminates'* 6th SAMPE, Tokyo, 26-29 October 1999
111. Schön J. *'Coefficient of friction of composite delamination surfaces'* Wear, 237, 77-89, 2000
112. Wisnom M.R. and Jones M.I. *'Measurement of friction in mode II delamination with through thickness compression'* Proceedings of 7th European Conference on Composite Materials, London, 87-92, May 1996
113. Ferrari S., MSc Thesis, Cranfield University, September 2003
114. Wisnom M.R., *'Size effects in the testing of fibre-composite materials'* Composites Science and Technology, 59, 1937-1957, 1999
115. Lin H.J. and Tsai C.C. *'Failure analysis of bolted connections of composites with drilled and moulded-in hole'* Composite Structures 30, 159-168, 1995
116. Cox B.N., Dadkhah M.S. and Morri W.L. *'On the tensile failure of 3D woven composites'* Composites Part A, 27A, 447-458, 1996

117. Han L. and Piggott M.R. *'Tension-compression and Iosipescu tests on laminates'* Composites Part A, 33, 35-42, 2002

118. Pierron F. and Vautrin A. *'The 10 off-axix tensile test: a critical approach'* Composites Science and Technology, 56, 483-488, 1996

119. Zhou G., Green E.R. and Morrison C. *'In-plane and interlaminar shear properties of carbon/epoxy laminates'* Composites Science and Technology, 55, 187-193, 1995

120. Odegard G. and Kumosa M. *'Elasto-plastic analysis of the Iosipescu shear test'* J. of Composite Materials, 33, No.21, 1981-2001, 1999.

121. Pierron F. and Vautrin A. *'Measurement of the in-plane shear strengths of unidirectional composites with the Iosipescu test'* Composites Science and Technology, 57, 1653-1660, 1997

122. Pierron F. *'Saint-Venant effects in the Iosipescu specimen'* J. of Composite Materials, 32, No.22, 1986-2015, 1998

123. Adams D.F. and Lewis E.Q. *'Experimental strain analysis of the Iosipescu shear test specimen'* Experimental Mechanics, 35, No.4, 352-360, 1996

124. Pierron F. and Vautrin A. *'Discussion of the article, "Experimental strain analysis of the Iosipescu shear test specimen'* Experimental Mechanics, 37, No.1, 11-12, 1997

125. Grassi M., Zhang X., Meo M. *'Numerical prediction of stiffness and stresses in Z-fibre reinforced composite laminates'* DFC6 Conference, Manchester, 4-5 April 2001, UK

126. Greenhalgh E., *'DSIONS research programme results on stringers'*, MercuryM project meeting, Burnley, 6th September 2000 (personal communication)

127. Clarke A., JOINTS project meeting, Cranfield University, 28th April 2003 (personal communication)

128. O'Brien T.K, (personal communication)

129. Rugg K.L., Cox B.N., Ward K.E. and Sherrick G.O *'Damage mechanisms for angled through-thickness rod reinforcement in carbon-epoxy laminates'* Composites Part A, 29A, 1603-1613, 1998

Appendix A

A1. OHT model details

The FE model of the Open-Hole Tension test coupon, discussed in section *6.1.1*, was built using LUSAS software, version 13.4. The aim of the model was to obtain a strain map of the specimen under testing conditions, in order to aid strain gauge positioning.

A quarter plane stress model of the specimen was built, due to the two axes symmetry of the geometry. The boundary conditions are depicted in FigureA1. Lines 5 and 8 are fixed against translation in the horizontal axis, while line 2 is fixed against translation in the vertical axis. Line 6 is loaded with a distributed load. The size of the model – namely the length of the lines – is 18mm horizontally (line 6) and 62.5mm vertically (lines 3 and 7). Line 4 is placed at the end of the pinned area (line 3 is 12.5mm long).

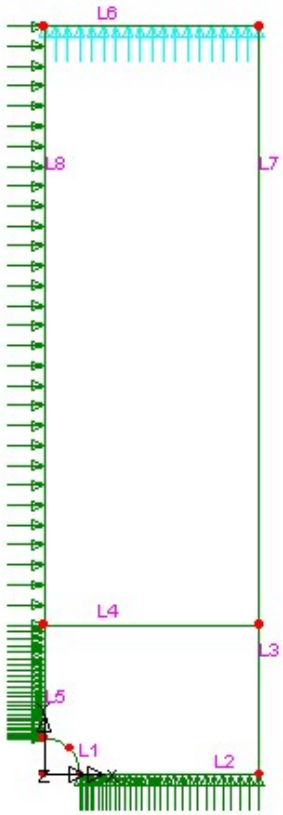

Figure A1: *Model boundary conditions*

The elements are linear quadrilateral. Effort was expended initially to create an economical mesh, in order to run the model using the student version of the software. Thus, a non-uniform mesh of the lower part of the model was constructed. Table A1 displays the final element divisions along each line. Figure A2 depicts a closer view of the undeformed mesh as well as the view of the full deformed model. The mesh was refined in steps by increasing the number of divisions (and therefore elements), until a further increase did not affect the strain contour results. The total number of elements required was higher than the allowable limit of the student version and a dongle key was acquired to

properly built and run the model. Subsequently, with no more limitations on the element number, no further effort was spent to create a non-uniform mesh of the upper part of the model. The model is simple and, therefore, not time consuming; less than 10 seconds are needed for acquiring a solution on a PIII-500MHz processor.

Line	No. of Divisions	Line	*No. of Divisions*
1	12	5	*25*
2	30	6	*18*
3	15	7	*30*
4	*18*	*8*	*30*

Table A1: *Number of mesh divisions per line*

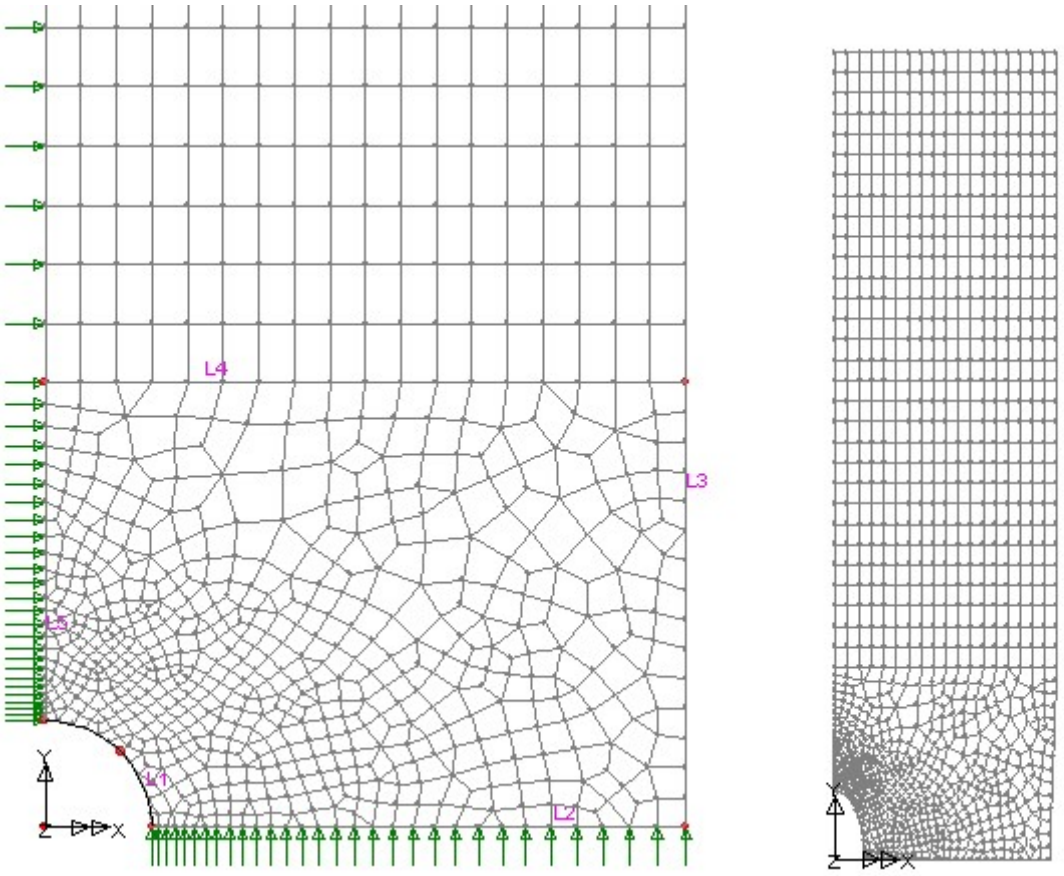

Figure A2: *Close-up of the undeformed mesh (left) and full view of the deformed mesh (right).*

The model was run twice for each case. The first case was the case of the unpinned specimen where the material properties were the same throughout the model. A solution

was run for each type of material (Cross-ply and woven). For the pinned case, the material properties of the lower part of the model (representing the pinned area) were changed accordingly and, again, two solutions for the two types of materials were run. The change in the properties of the woven material due to Z-pinning was measured in section *6.3.1*. For the cross-ply case, where no data were available, a similar percentile reduction for the tensile stiffness (13%) was initially assumed. The Poisson ratio was similarly assumed to be 0.08, as measured in the woven tensile specimen, while the shear modulus was assumed to remain unchanged with a value of 6GPa in both cases.

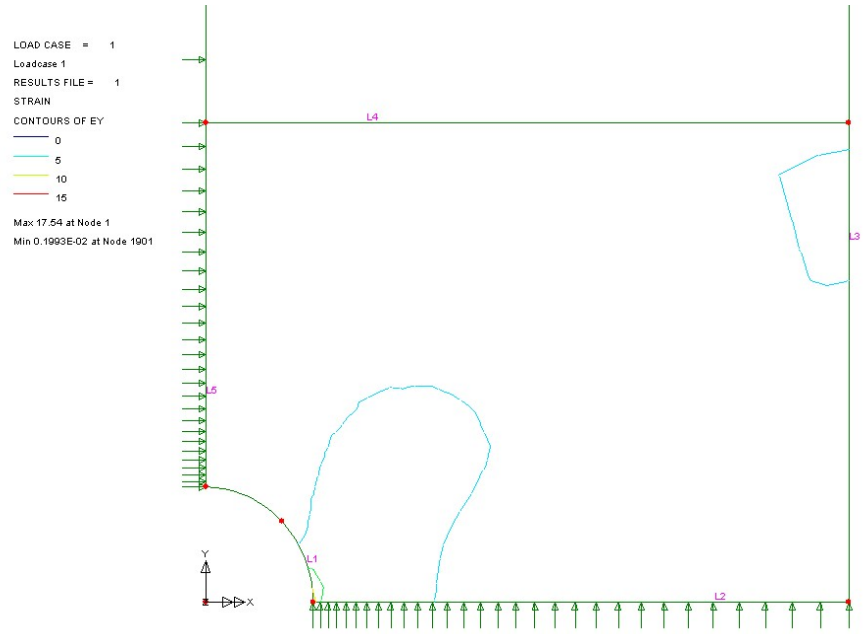

(a)

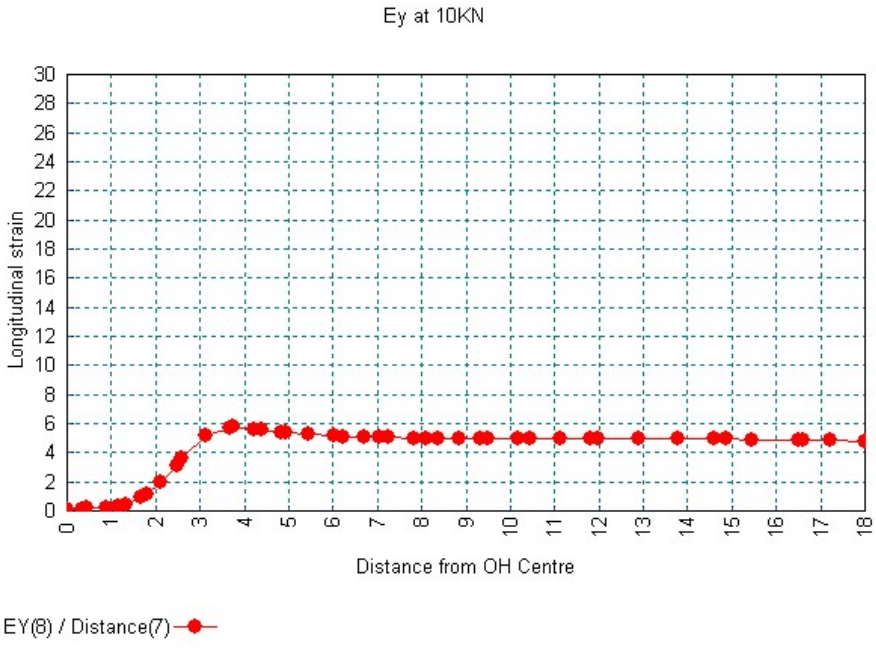

(b)

Figure A3: *Longitudinal strain contour (a) and strain distribution (b) at strain gauge position (horizontal slice) for a 10kN load.*

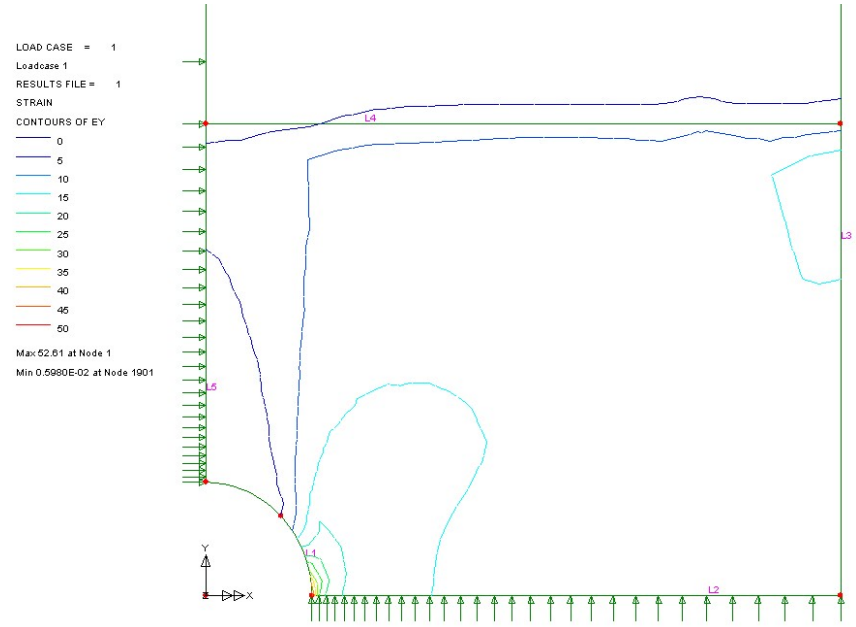

(a)

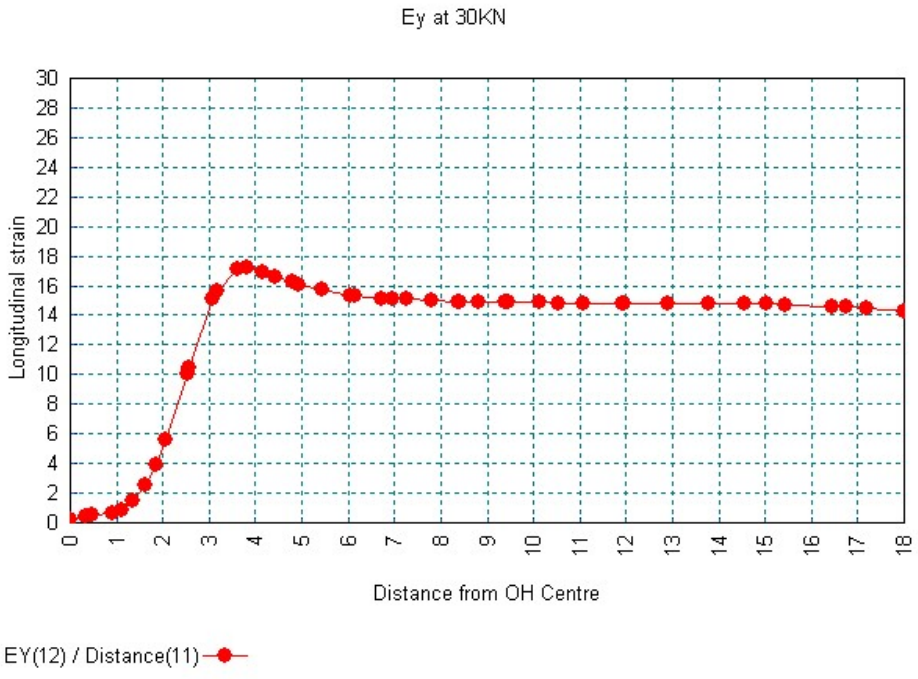

(b)

Figure A4: *Longitudinal strain contour (a) and strain distribution (b) at strain gauge position (horizontal slice) for a 30kN load.*

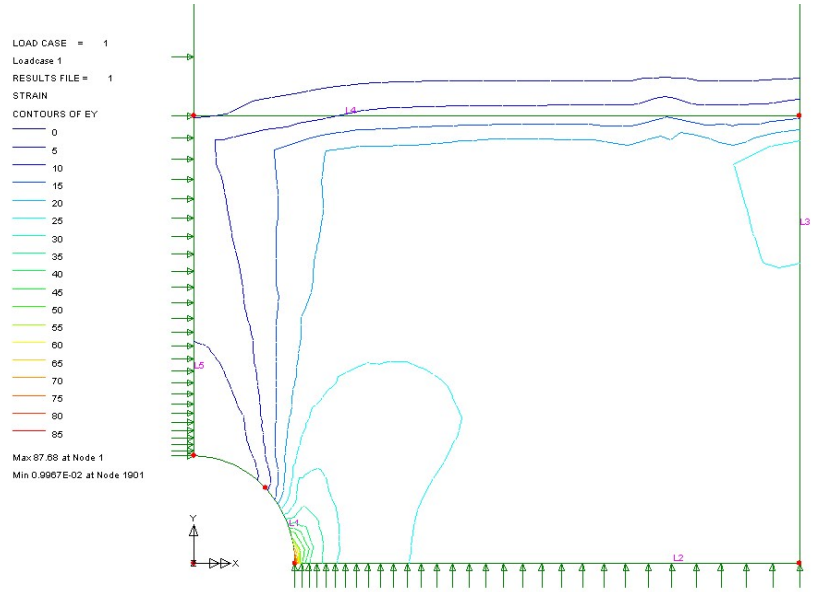

(a)

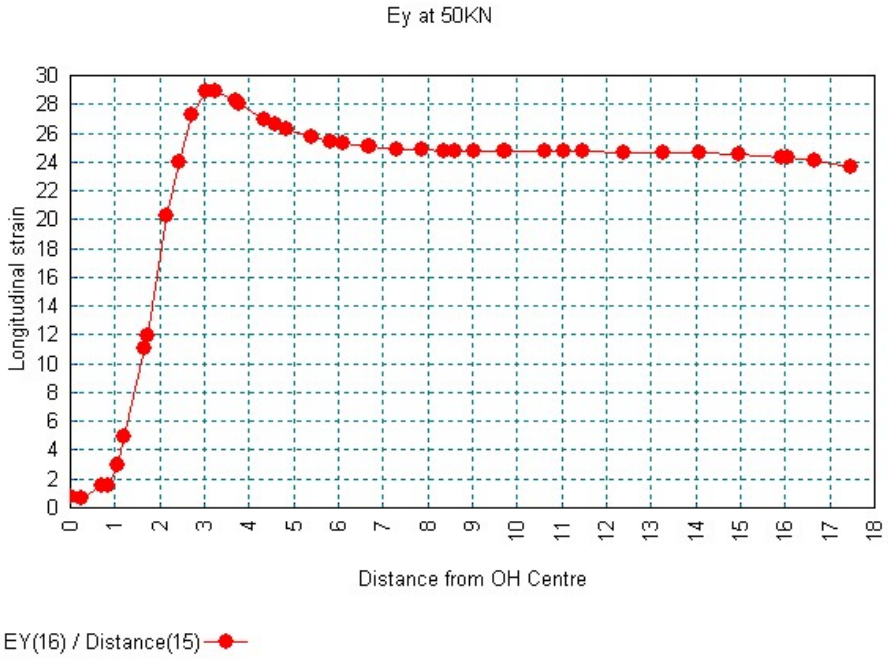

(b)

Figure A5: *Longitudinal strain contour (a) and strain distribution (b) at strain gauge position (horizontal slice) for a 50kN load.*